THE PETROGENESIS OF THE MESOZOIC MANINGOZA SUITE IGNEOUS COMPLEXES, CENTRAL WEST MADAGASCAR

Jarryd Finkelstein

Dissertation presented for the degree of Master of Science
Department of Geological Sciences
University of Cape Town
August 2010

DECLARATION

I hereby declare that all of the work presented in this thesis is my own, except where otherwise stated in the text.

Signed by candidate

Signature Removed

J. C. Finkelstein

TABLE OF CONTENTS

ABSTRACT

The Maningoza Suite is a set of Mesozoic igneous sub-volcanic to volcanic complexes situated in the Mahajanga sedimentary and volcanic basin in central-west Madagascar. The Maningoza Suite is exposed in an area roughly 50 x 80 km and consists of the Ambereny, Ambohitrosy, Ankibobozaka, Berevo, Fonjay and Maningoza Complexes. The Maningoza Complex also consists of the Ambolodia, Antanetilava and Sambao Formations.

The Maningoza Suite rocks are generally fine- to medium-grained with some rare coarse-grained rocks occurring in two of the six complexes. Typical minerals found in mafic samples are plagioclase, clinopyroxene, Fe-Ti oxides and to a lesser extent olivine. Minerals found in felsic samples tend be K-feldspar, plagioclase, Fe-Ti oxides, quartz and clinopyroxene. In almost all the rocks secondary minerals are observed with chlorite being the most common followed by epidote and calcite. Mineral chemistry of the Maningoza Suite shows a range in feldspar compositions from almost pure anorthite through albite to orthoclase for most of the complexes. Clinopyroxenes of the Maningoza Suite all have an augitic composition plotting below the field of diopside with little variation on the pyroxene quadrilateral. Olivine compositions for the Maningoza Suite are magnesium-rich with a range in composition from Fo_{74} to Fo_{64}. The olivine composition of the dyke swarm is slightly more iron-rich with a composition from Fo_{60} to Fo_{45}. Oxide compositions plot on the hematite-ilmenite solid solution series and range from 100% hematite to 17% hematite.

The rocks of the Maningoza Suite are classified as basalts, basaltic andesites, andesites, trachyandesites, dacites and rhyolites. Also one sample classifies as a basanite and one sample classifies as a picrobasalt. The rocks of the dyke swarm classify as basalts, basaltic andesites, basaltic trachyandesites, trachytes and rhyolites. The variation in chemical composition of these rocks is consistent with fractional crystallisation. The Maningoza Suite rocks have whole-rock $\delta^{18}O$ values that range from 2.3‰ to 12.1‰ with average of 6.3‰ (n = 42) and whole-rock δD values that range from -127‰ to -62‰ with an average of -89‰ (n = 25). The δD values can be explained by degassing effects and the low $\delta^{18}O$ values are either an effect of hydrothermal alteration after emplacement or an effect of assimilating a low $\delta^{18}O$ contaminant. On comparison of the $\delta^{18}O$ and δD values the fluid involved in the Maningoza Suite is magmatic in origin.

Ar-Ar geochronology of two samples from the Maningoza Suite gives an average age of 93.4 Ma. The Maningoza Suite rocks have ε_{Sr} values that range from -23.2 to 187.7 with an average of 41.5 (n = 14) and ε_{Nd} values that range from -11.4 to 10.0 with an average of -2.6

(n = 14). The low ε_{Nd} values and high ε_{Sr} values indicate fractional crystallisation with assimilation of a crustal component. Geochemical modelling of the Maningoza Suite revealed estimates of fractional crystallisation that range from 68% to 86% with mineral assemblages of 35% - 60% plagioclase, 35% - 50% augite and 5% - 20% Ti-Fe oxide (depending on the individual complex). Modelling via simple magma mixing using Sr and Nd isotopes estimate up to 35% mixing between a primitive and crustal end-member to fit the majority of the Maningoza Suite data. Comparison of mineral composition, bulk rock chemistry and radiogenic isotopes from the Maningoza Suite and other Cretaceous igneous complexes from Madagascar showed that the Maningoza Suite is similar to the Mailaka Complex, located 100 – 200 km SW of the Maningoza Suite, as both have a similar mantle source, crustal component with assimilation and signs of fractional crystallisation.

1. INTRODUCTION

The Maningoza Suite of Late Cretaceous sub-volcanic to volcanic rocks is situated in central-west Madagascar, in a geological survey area known to the Council for Geoscience of South Africa as Zone F (Figure 1.1). The Maningoza Suite gathers its name from the river that runs through the area and through some of the complexes and volcanic sequences of the Maningoza Suite. The aim of this thesis is to describe the petrography, bulk rock geochemistry, mineral chemistry and the isotopic compositions of the Maningoza Suite geology. The age of the Maningoza Suite suggests that its formation is possibly associated with Gondwana break-up and/or melts caused by hot spots, for example the Marion Hotspot to the south (Duncan 1981, Hartnady and Le Roux 1985 and Dostal et al. 1992).

The project was first given to the University of Cape Town by the Council for Geoscience in 2007 as an honours project for four students. The Council for Geoscience of South Africa had done a land survey of areas demarcated as Zone E and Zone F, shown in Figure 1, and wished to study the area further with an inclusion of petrographic and bulk rock geochemistry studies. The rock samples of area Zone E was allocated to the University of Stellenbosch and the rock samples of area Zone F was allocated to the University of Cape Town. The study has been enhanced by the addition of stable isotopes, radiogenic isotopes and mineral chemistry studies described in this project.

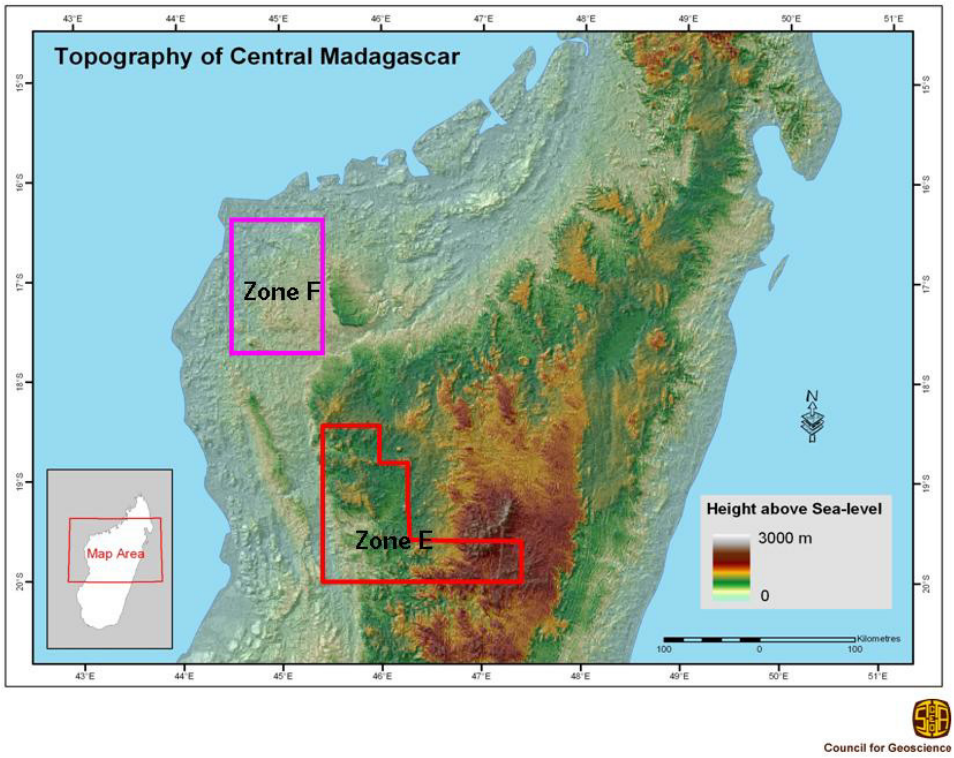

Figure 1.1: A topographical map of Central Madagascar showing the locations of Zone E and Zone F assigned to the Council for Geoscience for surveying. The area of Zone F is 80x40 kilometres. This map was supplied by the Council for Geoscience.

1.1 Geological Setting

1.1.1 Regional

Madagascar has a surface area of 627 000km^2 and a size similar to that of Spain (Torsvik et al. 1998). Madagascar has a length of 1600 km north to south as well as being 600km at its widest point. Madagascar stretches over 14° latitude roughly between 12°S and 26°S (Figure 1.2). The topography of Madagascar is asymmetric: along 22°S there is a quick rise to 2000m height over 100km from the Indian Ocean; there is a gradual drop back to sea level over 400km towards the Mozambique Channel in the West.

The Mozambique Channel runs at 2-3km below sea level but in the middle it is as shallow as 500-1000m below sea level. This ridge in the middle of the Mozambique Channel is known as the Davie Ridge and is said to be an extinct and deformed transform fault (de Wit 2003). This transform fault displaced Madagascar more than 1000km southward from East Africa (Southern Somalia, Kenya and Tanzania) between 160 to 117 Ma.

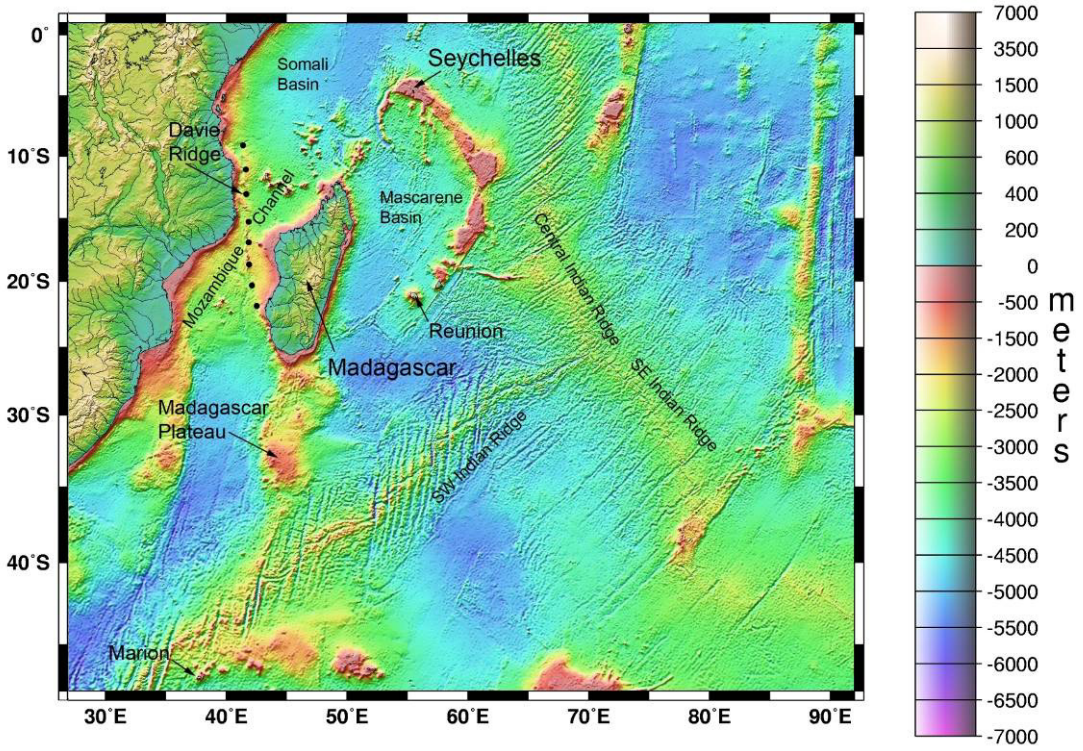

Figure 1.2: Indian Ocean topography from a global digital elevation model from Smith and Sandwell 1997, showing Madagascar and other relevant tectonic features.

The eastern two-thirds of Madagascar comprises of variably deformed and metamorphosed Precambrian granitoids and mafic rocks that are intruded by Cretaceous to Neogene basalts and rhyolites. The eastern two-thirds of Madagascar also contain Archaean rocks giving the eastern two-thirds of basement rocks ages that range from as old as 3.2 Ga to more recent 550 Ma (Torsvik et al. 1998 and Ashwal and Tucker 1999). The eastern third of Madagascar comprises of extensive, west-dipping Phanerozoic sedimentary and volcanic rocks including three basins (Ashwal and Tucker 1999).

As Madagascar broke away from East Africa at about 165 Ma it led to the formation of three basins on the west coast of Madagascar (Papini and Benvenuti 1998, Torsvik et al. 1998). The three basins contain sedimentary deposits which range in age from Late Palaeozoic to Cenozoic. The southern most basin is the Morondava basin and stretches over 1200km where it meets the central west basin named the Majunga basin with a length of 600km. The basin to the north of the west coast is known as the Diego-Suarez (Ambilobe) basin and has a range of 400km (Rakotosolofo et al. 1999).

Madagascar was part of a larger continent during the Neoproterozoic where the final collision between East and West Gondwana occurred (Bardintzeff et al. 2001). The Supercontinent Gondwana stayed complete until its break up during the Mesozoic (Bardintzeff et al. 2001

and de Wit 1999). During the Carboniferous to the Triassic, deposits equivalent to the Karoo Supergroup covered the central part of the Supercontinent. These deposits covered the western third of Madagascar and three groups have been recorded (Bardintzeff et al. 2001, Papini and Benvenuti 1998, and Rakotosolofo et al. 1999). The first group is the Sakao Group and was deposited during the Late Carboniferous to Early Permian and is 2000m thick with tillites, coals, sandstones and limestones. The second group is the Sakamena Group which is 2000-4000m thick and composed of detrital layers deposited during the Late Permian to Middle Triassic. The last group is the Isalo Group which was deposited during the Triassic to Early Jurassic and is 5000-6000m thick of conglomerates and sandstones.

The Gondwana Supercontinent break up occurred during two events: the first event occurred during the Middle Jurassic to the Middle Cretaceous; the second event occurred during the Early Cretaceous. The first event generated two continental blocks with the first consisting of Africa and South America and the second consisting of Antarctica, Australia, Madagascar and Greater India. Madagascar disconnected from Kenya and Somalia and displaced laterally along the Davie Ridge within the Mozambique Channel. Madagascar and Greater India broke away from each other during the second event and during this there were episodes of extensive magmatism within Madagascar. Remnants of these volcanic formations are exposed along the Eastern, Southern and Western coasts of Madagascar (Melluso et al. 2001 and Bardintzeff et al. 2001).

Outcrops of Cretaceous volcanism and magmatism can be seen all over the island of Madagascar as mentioned previously (Figure 1.3). The ages of this magmatism is constrained to a relatively short period of time of roughly 6 Ma. The magmatism roughly began at 92 Ma and ended at 86 Ma (Storey et al. 1995 and Torsvik et al. 1998). Around 88 Ma the southern end of Madagascar was the focal point of the Marion Hotspot which is believed to be an influence in causing continental break up (Storey et al. 1995).

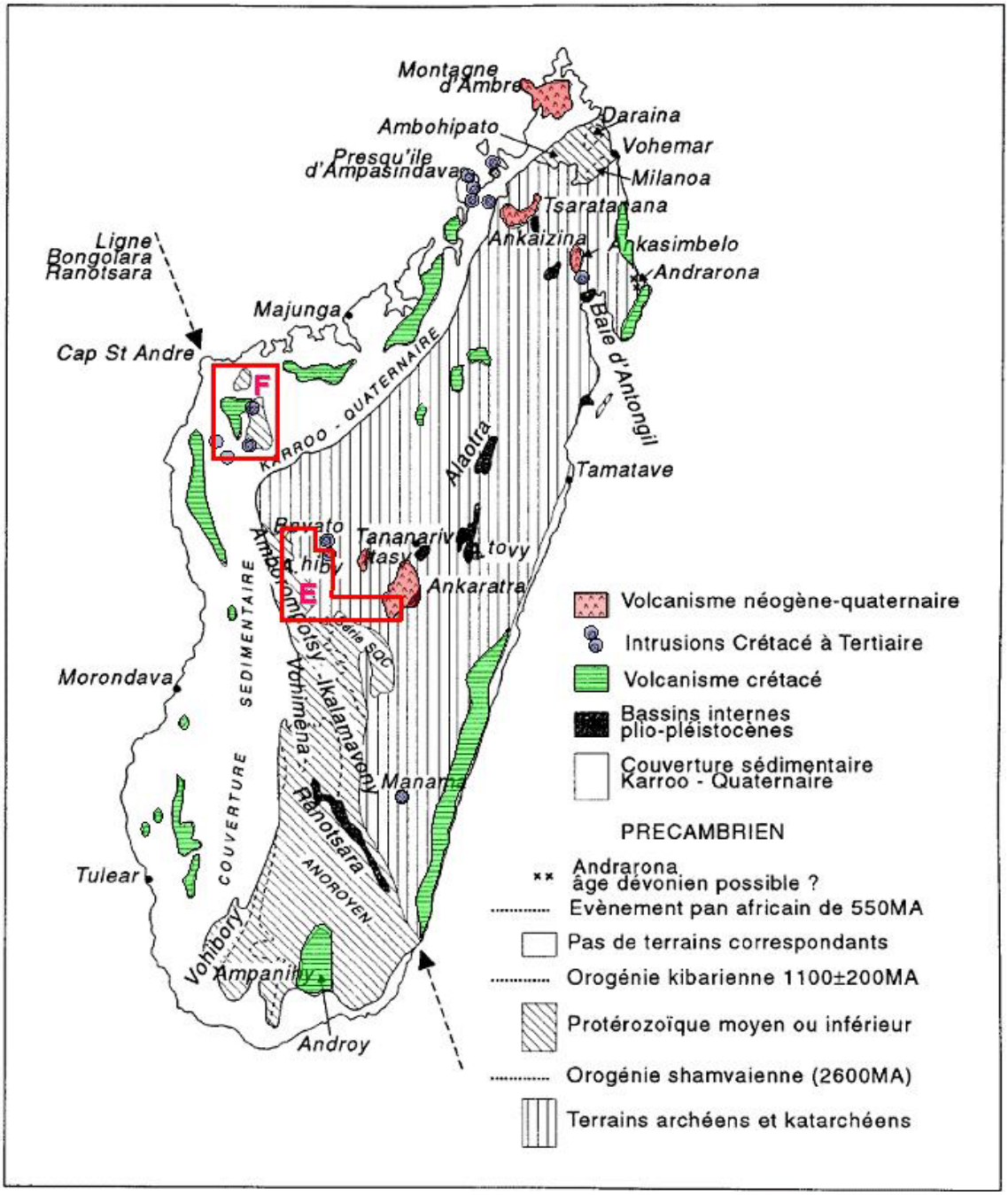

Figure 1.3: Map of Madagascar highlighting Cretaceous volcanism and ring complexes as well as the location of Zone E and Zone F. After Hottin 1976.

1.1.2 Local Geology

The local geology of Zone F contains two inliers named Bekodoka and Ambohipaky (Figure 1.4). The Bekodoka and Ambohipaky inliers are Neoarchaean – Proterozoic and are amphibole gneisses and amphibole, marble, quartz gneisses (Macey et al. 2007). The inliers are unconformably overlain by, and faulted against, Triassic-Cretaceous sedimentary and volcanic rocks. This is followed by intrusions of late Cretaceous subvolcanic ring complexes,

volcanic flows and associated dyke swarms. The youngest rocks in the area are Miocene limestones and Quaternary alluvium (Macey et al. 2007).

The Bekodoka inlier is located in the eastern part of Zone F (Figure 1.4) and the southern part of the Bekodoka inlier consists of the Miako Gneiss. The Miako Gneiss (2529 Ma) is of the Neoarchaean Betsiboka Suite (Antananarivo domain) and is migmatitic granodioritic orthogneisses. The northern two-thirds of the Bekodoka inlier contain the Neoarchaean Ambohipaky Group of the Tsaratanana sheet. The Ambohipaky Group consists of metagreenstones (amphibolite-facies). A small section in the southwest of the Bekodoka inlier has exposed rocks of the Proterozoic Itremo-Ikalamavoney belt. Rock types include marble, quartzite and amphibole from the Itremo (855 - 1700 Ma) and Ikalamavoney Group (1020 - 1070 Ma) (Macey et al. 2007).

The Ambohipaky inlier is located in the central northern parts of Zone F and contains the Andranojongy and Ambohipaky components. The Andranojongy component is about 5 square kilometres in size and is located 6km west-southwest of the main Ambohipaky inlier and is separated by overlying sedimentary rocks. The Ambohipaky component is about 20km by 30km in size and is largely faulted. The Ambohipaky inlier is split into north-western and south-eastern parts by a southwest-northeast trending fault graben. The Ambohipaky inlier geology consists of metagreenstones and is seen as a continuation of the Ambohipaky Group from north of the Bekodoka inlier (Macey et al. 2007).

During the Upper Carboniferous to Middle Jurassic rocks equivalent to the Karoo Supergroup where deposited on Madagascar as mentioned previously. The mudrocks of the middle of the Sakamena Formation form the oldest sedimentary rocks in Zone F. The Sakamena Formation is overlain by the sandstones of the Isalo Formation (Isalo I and Isalo II). The Andafia Formation is found next with calcareous sandstones and dolomitic limestones representing the onset of marine transgression. The Karoo sedimentary rocks are overlain by the Bemaraha Formation (limestones) and were deposited during the Upper Jurassic as Madagascar moved from Africa (Macey et al. 2007).

The Maningoza Suite is composed of six complexes namely the Ankibobozaka, Ambereny, Ambohitrosy, Berevo, Fonjay and Maningoza Complexes with locations shown in Figure 1.4. The Maningoza Complex is further subdivided into the Sambao Formation, Ambolodia Formation and Antanetilava Formation.

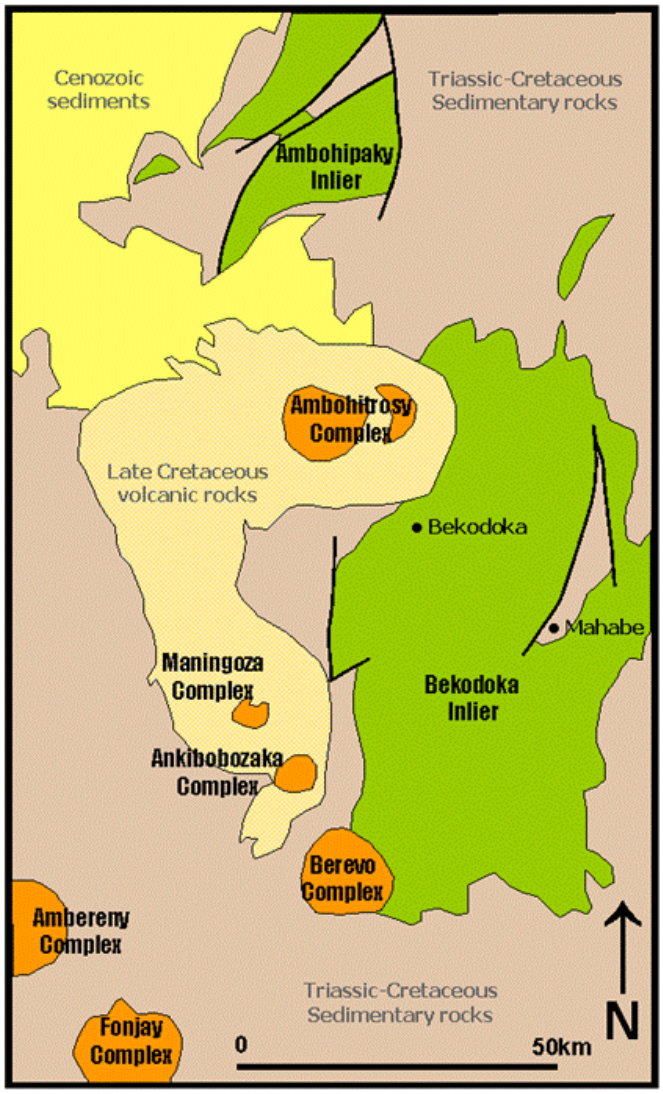

Figure 1.4: Map of Zone F showing the locations of the Cretaceous volcanism and complexes of the Maningoza Suite. This map was supplied by the Council for Geoscience.

1.2 Aims of Project

The aim of this study is to document the petrography and chemical analyses of the samples of the Maningoza Suite to gain further insight into processes that led to the rifting of the Indian Ocean. The aims for achieving this goal are listed below:

- The samples of Maningoza Suite will be studied using thin-section petrography to gain insight into the type of rocks and their minerals present.

- Mineral chemistry of selected samples will be used to gain data on the composition of minerals. These rock samples will be chosen on the basis that they are the best representation of mafic and felsic samples from each complex.

- All samples of the Maningoza Suite will be analysed for major and trace element data. The data will be used for classification, variation diagrams and rare earth element diagrams.

- Oxygen stable isotopes will be used to model the source and evolution of magmas in terms of crustal contamination. Hydrogen isotopes will be used to give further insight into fluid-rock interaction when combined with oxygen isotopes.

- Radiogenic isotopes strontium and neodymium will allow further modelling of crustal contamination. Once contamination processes are understood, it should be possible to use the composition of the least contaminated rocks to determine the composition of the mantle component in the parental magmas.

- The thin-section petrography, mineral chemistry, major and trace element data as well as the isotope data will be used to compare the complexes of the Maningoza Suite to one another. Modelling of the evolution of the complexes of the Maningoza Suite will be attempted to gain further insights into the processes taking place.

- Comparison with other Madagascan igneous complexes of the same age will be examined for similarities and differences. This will help in understanding the extent of Cretaceous magmatism in Madagascar. This will be followed up by the comparison of the Maningoza Suite with Cretaceous igneous complexes that are found nearby to get a better idea of the constraints on processes of Gondwana break-up.

1.3 Previous Studies

The earliest geological work on north-western Madagascar includes the exploration studies of Baron and Mouneyres (1904), Dumas (1923), Barrabe (1929), and Hourcq (1949). Studies on the basement, sedimentary and subvolcanic complexes are covered by Koenig and Tortochaux (1949), Tortochaux (1950), Heilammer (1958), and Boulanger and Riedel (1959). Zone F has been covered by geological maps done by Bauer (1958, 1959, 1960, 1961), Bauer et al. (1958, 1959), Heilammer (1959), Heilammer and Bauer (1959), Hindermeyer

and Hourcq (1960), Rasoamahenina et al. (1967, 1968) and Razafimanantsoa (1969). All the findings before 1970 were summarised in a textbook by Besairie (1972) and the geological map by Besairie (1969). Two PhD thesis were also done on the area, with the first focussing on the geology of the Archaean Soalala ironstones (Ranaivoarivelo, 1997) and the second on the Ambohitrosy Complex (Rasolofomanana, 1998).

2 SAMPLING AND METHODOLOGY

2.1 Sampling of the Maningoza Suite

Sampling of the Maningoza Suite was done by the Council for Geoscience of South Africa in April – May 2007. They supplied this project with 6 samples from the Ankibobozaka Complex, 22 from the Berevo Complex, 15 from the Ambolodia Formation, 20 from the Antanetilava Formation, 14 from the Sambao Formation, 6 from each of the Fonjay and Ambereny Complexes, and 9 from the Ambohitrosy Complex. Each sample was of large size, roughly 10 x 10 x 10 cm, enough to be representative of the outcrop.

2.1.1 Sampling of the Ambohitrosy Complex

The 9 samples from the Ambohitrosy Complex were only analysed in thin-section petrography. Data was taken from Rasolofomanana's PhD thesis to add major and rare earth element data as well as mineral chemistry data to the Ambohitrosy Complex dataset.

2.1.2 Locations and GPS Coordinates of the Maningoza Suite

Figure 2.1 shows a simplified geological map of Zone F and three areas marked A, B and C. These areas are expanded in Figure 2.2 (Area A), Figure 2.3 (Area B) and Figure 2.4 (Area C) and show the locations of the samples from the Maningoza Suite. The exact GPS coordinates are given in Table 2.1.

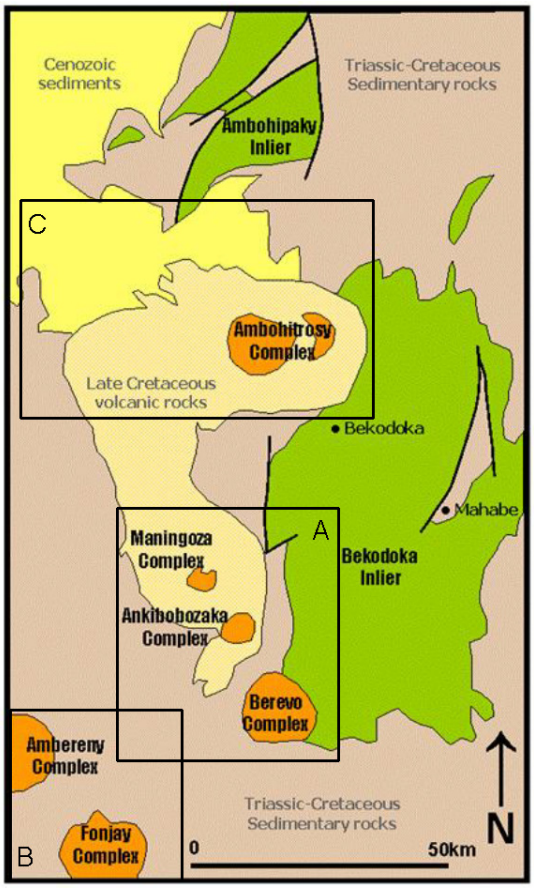

Figure 2.1: Map of Zone F showing simplified geology and the locations of Maps A, B and C containing the GPS locations of the samples of the Maningoza Suite.

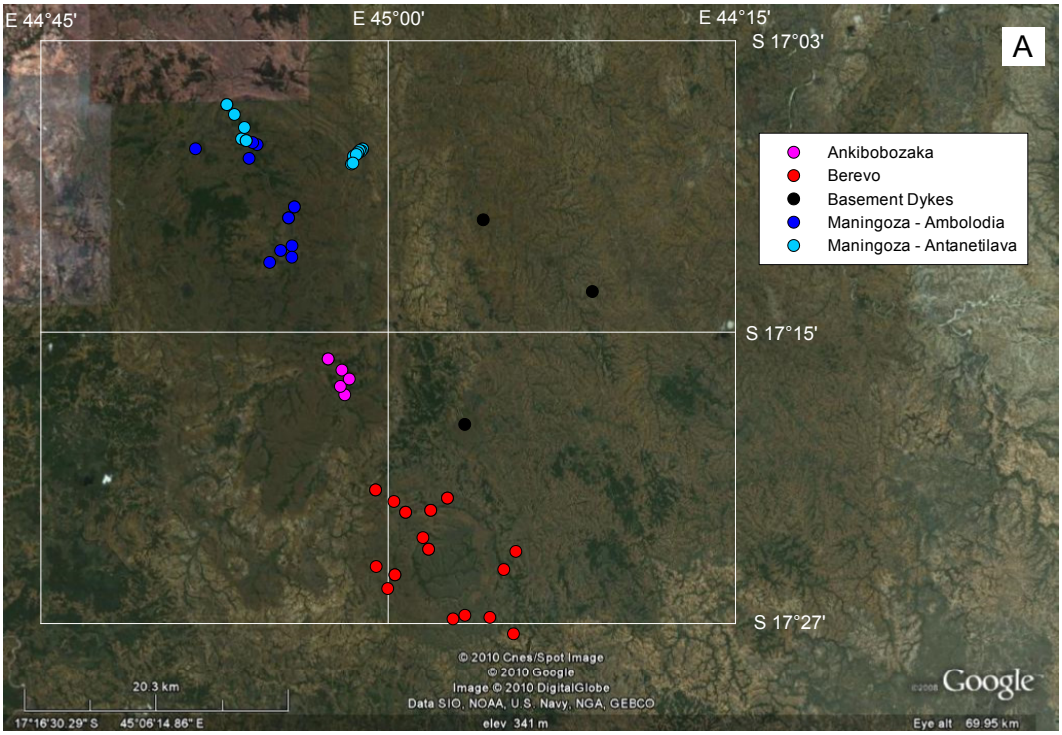

Figure 2.2: Area A showing the GPS locations for the Ankibobozaka Complex, Berevo Complex, Ambolodia Formation, Antanetilava Formation and the basement dykes.

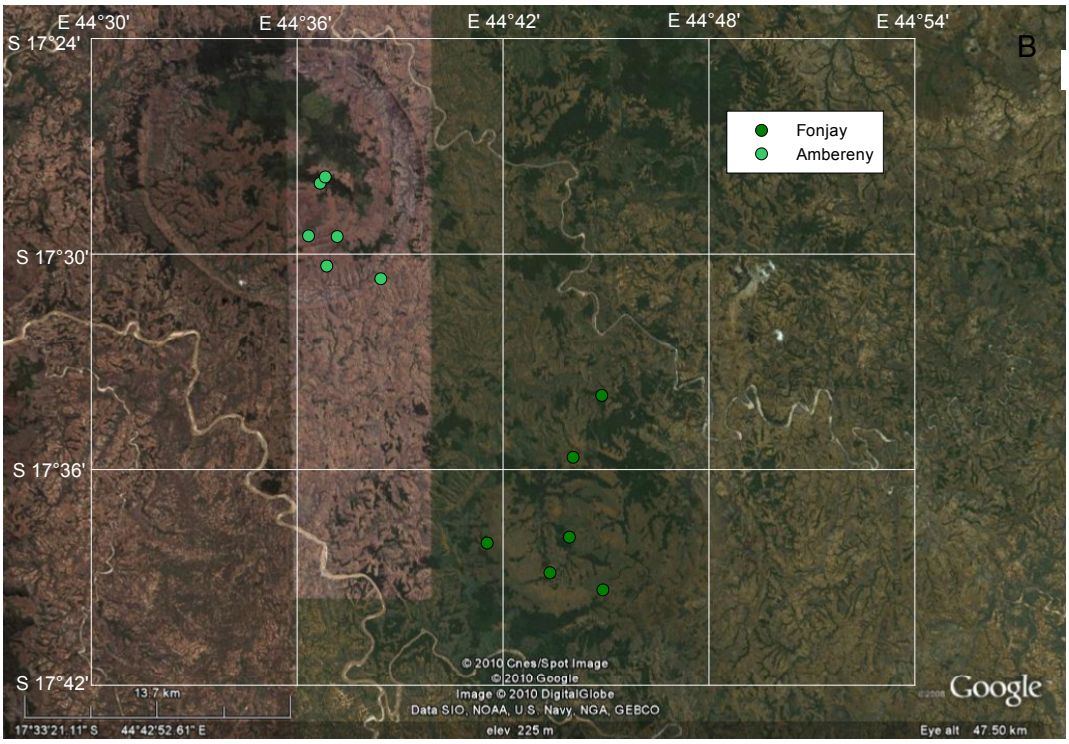

Figure 2.3: Area B showing the GPS locations for the Fonjay and Ambereny Complexes.

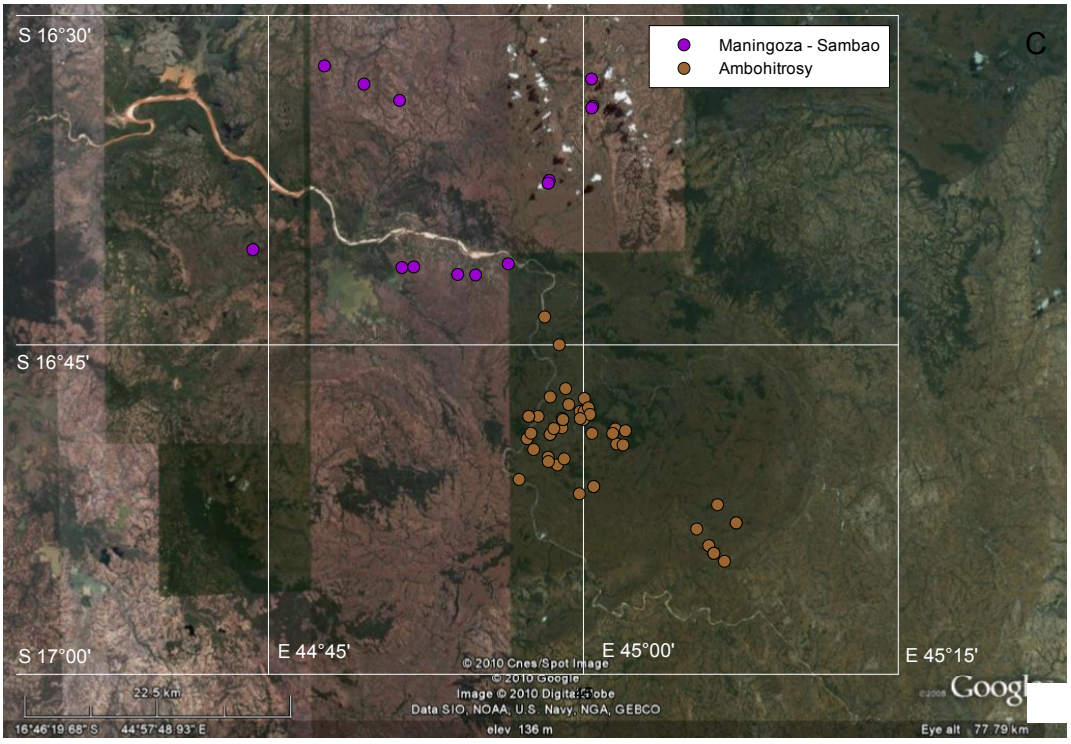

Figure 2.4: Area C showing the GPS location for the Sambao Formation and the Ambohitrosy Complex.

Sample	Latitude	Longitude	Sample	Latitude	Longitude	Sample	Latitude	Longitude
ANKIBOBOZAKA			**MANINGOZA - SAMBAO**			**AMBOHITROSY**		
PF06-004	-17.26838	44.95680	BYF6-107	-16.69128	44.85587	95-15	-16.85755	45.00808
PF06-001	-17.29299	44.96874	BY6F-086	-16.54816	45.00637	AB-26b	-16.80425	44.96398
PF06-002	-17.28723	44.96559	BY6F-090	-16.56893	45.00739	AB-07	-16.79532	44.98833
PF06-003	-17.26838	44.95680	BY6F-098	-16.62522	44.97283	95-16	-16.85755	45.00808
PF06-005	-17.27603	44.96669	BY6F-101	-16.68847	44.94025	95-13b	-16.80670	45.00007
PF06-006	-17.28214	44.97201	BY6F-113	-16.67770	44.73756	95-01a	-16.90818	45.10350
BEREVO			BY6F-154	-16.53827	44.79432	AB-06	-16.78323	44.98578
PF06-008	-17.35827	44.99089	BY6F-091	-16.57016	45.00651	AB-17	-16.83530	44.97192
PF06-011	-17.37362	45.01256	BY6F-102	-16.69691	44.91433	AB-16	-16.82943	44.96042
PF06-024	-17.44680	45.04666	BY6F-103	-16.69654	44.90012	95-05	-16.87135	45.10642
PF06-030	-17.41292	45.08321	BY6F-151	-16.55208	44.82571	AB-26a	-16.80425	44.95648
PF06-013	-17.37228	45.03062	BY6F-098B	-16.62727	44.97200	95-02	-16.91425	45.11188
PF06-017	-17.39103	45.02502	BY6F-148	-16.56447	44.85400	AB-15	-16.81295	44.98292
PF06-020	-17.41653	45.00487	BY6F-106	-16.69082	44.86526	AB-26n	-16.80425	44.95648
PF06-021	-17.41653	45.00487	**MANINGOZA - ANTANETILAVA**			AB-12	-16.81722	45.00670
PF06-027	-17.44576	45.07319	PF06-131	-17.11736	44.89446	95-03	-16.90235	45.09945
PF06-032	-17.40049	45.09191	PF06-133	-17.10060	44.88929	95-01b	-16.90818	45.10350
PF06-022	-17.39898	45.02910	PF06-134	-17.09382	44.88386	95-05b	-16.88512	45.12123
PF06-018	-17.42599	44.99967	PF06-142	-17.12428	44.98161	95-06	-16.88512	45.12123
PF06-019	-17.41086	44.99135	PF06-143	-17.12428	44.98161	AB-05	-16.74990	44.98075
PF06-026	-17.44434	45.05524	PF06-144	-17.12567	44.98059	AB-10	-16.80047	44.99732
PF06-015	-17.36387	45.04268	PF06-147	-17.12681	44.97862	AB-19	-16.84115	44.97933
PF06-016	-17.36387	45.04268	PF06-149	-17.12754	44.97731	95-20b	-16.81798	44.97350
PF06-023	-17.39898	45.02910	PF06-151	-17.12922	44.97502	AB-14	-16.80577	44.98297
PF06-028	-17.45706	45.09019	PF06-154	-17.13456	44.97353	95-20a	-16.81798	44.97350
PF06-009	-17.35827	44.99094	PF06-152	-17.12922	44.97502	AB-13	-16.80670	44.98368
PF06-012	-17.37362	45.01256	PF06-130	-17.11853	44.89778	95-14	-16.86305	44.99673
PF06-014	-17.37228	45.03062	PF06-135	-17.09382	44.88386	AB-18	-16.83855	44.97213
PF06-010	-17.36622	45.00414	PF06-145	-17.12536	44.97936	AB-9	-16.80033	45.00057
MANINGOZA - AMBOLODIA			PF06-148	-17.12679	44.97816	AB-13a	-16.80670	44.98368
PF06-115	-17.20212	44.91471	PF06-150	-17.12807	44.97704	AB-27	-16.79077	45.00065
PF06-116	-17.19395	44.92258	PF06-153	-17.13395	44.97460	AB-08	-16.79773	45.00392
PF06-118	-17.19075	44.93075	PF06-129	-17.11853	44.89778	AB-24	-16.81387	45.02525
PF06-117	-17.19853	44.93066	PF06-132	-17.10953	44.89652	AB-20	-16.82523	45.02637
PF06-119	-17.17156	44.92830	**FONJAY**			95-18	-16.83653	44.98467
PF06-120	-17.17156	44.92830	MI06-004	-17.56559	44.74793	AB-22	-16.82597	45.03142
PF06-121	-17.16403	44.93248	MI06-006	-17.59428	44.73402	ABF079	-16.81517	45.03333
PF06-122	-17.16403	44.93248	MI06-008	-17.63134	44.73222	95-1	-16.90818	45.10350
PF06-126	-17.13073	44.89986	MI06-010	-17.65581	44.74852	95-04	-16.88978	45.08992
PF06-127	-17.12130	44.90564	MI06-011	-17.64783	44.72278	ABF052	-16.85212	44.94890
PF06-128	-17.11990	44.90248	MI06-013	-17.63404	44.69227	ABF057	-16.82117	44.95522
PF06-136	-17.12415	44.86129	**AMBERENY**			ABF058	-16.81708	44.95832
PF06-123	-17.14178	44.91461	MI06-014	-17.49155	44.60553	ABF060	-16.81357	44.97647
PF06-124	-17.14178	44.91461	MI06-017	-17.46712	44.61120	ABF063	-16.78948	44.97362
PF06-125	-17.13822	44.90675	MI06-018	-17.49187	44.61944	ABF066	-16.72882	44.96918
DYKES INTRUDING BASEMENT			MI06-019	-17.50555	44.61437	ABF074	-16.80278	45.00512
PF06-071	-17.31332	45.05513	MI06-021	-17.51144	44.64063	ABF075	-16.80597	44.99738
PF06-138	-17.17289	45.06841	MI06-016	-17.46421	44.61365	ABF076	-16.81723	45.02318
MI06-034	-17.22212	45.14698						

Table 2.1: Latitude and longitude coordinates for the samples of the Maningoza Suite. Coordinates for the Ambohitrosy Complex include the thin-section samples and data from Rasolofomanana (1998).

2.2 Analytical Techniques

2.2.1 Sample Preparation

The samples were split into smaller 3-4cm size pieces using a hydraulic splitter. Weathered edges of the samples were discarded to prevent surface contamination. The smaller pieces of sample were further reduced using a jaw crusher. Once the sample pieces were crushed they were ground into a fine 300 mesh powder using a carbon-steel swing-mill for 2-3 minutes.

2.2.2 Microprobe

Mineral analyses were obtained using the Jeol JXA 8100 Electron Microprobe Microanalyzer at the University of Cape Town. The electron microprobe is equipped with four wavelength dispersive spectrometers and a range of crystals (LDE1, LDE2, PETJ, PETH, TAP, LIF, LIFH). The instrument is also fitted with two gas-flow proportional detectors and two sealed xenon detectors as well a backscattered electron detector and a cathode luminescence detector. The acceleration voltage used was 15kV and the data was corrected using the XAF method. A selection of natural and synthetic minerals was used as standards. All standards used were appropriate to the mineral being analysed.

2.2.3 Major Element and Selected Trace Element Analysis by XRF

Major elements and selected trace elements (Zr, Sr, Rb, Y and Nb) were analysed using wavelength dispersive X-Ray Fluorescence Spectrometry (WDXRFS). The analyses were carried out using a Phillips X'Unique wavelength spectrometer at the department for Geological Sciences, University of Cape Town. Powder briquettes and fusion discs were generated for analysis using a XRF spectrometer using the method described by Willis 1999. The powder briquettes were made from 6g of sample and a coating of 4g of boric acid. The sample and boric acid coating were then compressed with 10 tonnes of pressure to create the powder briquette. The fusion discs were generated by weighing out 2g of sample into a crucible. The crucible was then placed in an oven at 110 °C for 4 hours and then roasted overnight at 850 °C to determine loss on ignition (LOI) and to oxidise all Fe to Fe^{3+}. The crucibles of sample were then removed and 0.7g of the sample was added to 6g of LiT-LiM flux that was in the proportion 57:43, with LiBr as the releasing agent. The mixture was then melted to form a fusion disc. Analytical errors and detection limits are 95% and 99% (ppm), respectively and are given by le Roex et al. (1981), Duncan et al. (1984), and le Roex (1985).

The analysis of selected trace elements by XRF was required as zirconium data obtained by ICP-MS is unreliable. Figure 2.5 shows variation diagrams of XRF analyses plotted against ICP-MS analyses for zirconium. If both analytical methods yielded the same results a straight line would occur, such as for Sr. The zirconium variation diagram shows a number of analyses that do not plot to form a straight line. This is due to the fact that zirconium doesn't readily dissolve during the acid digestion process leaving zirconium behind before the ICP-MS analysis. The XRF data for Zr is then more reliable than the ICP-MS data. The XRF data for Nb has an offset of ±5ppm compared to the ICP-MS data. The XRF data for Sr, Rb, Y, Nb and Zr as opposed to the ICP-MS data is used in further discussions.

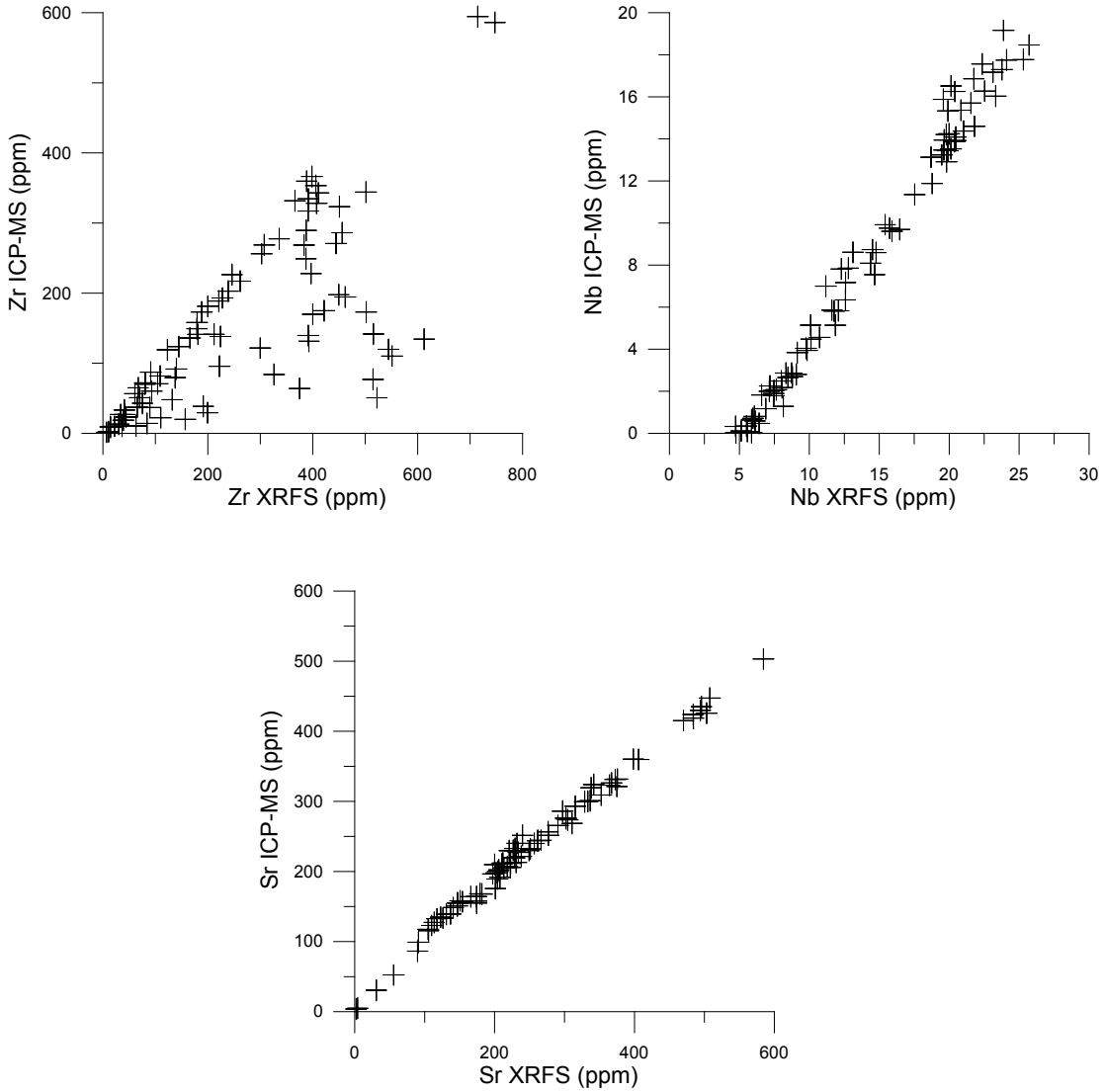

Figure 2.5: Variation diagrams of ICP-MS against XRFS analyses for trace elements Zr, Nb and Sr.

2.2.4 Trace Element Analysis by ICP-MS

Trace elements including rare earth elements (REE) were analysed by Inductively Coupled Plasma – Mass Spectrometry (ICP-MS) using a Perkin-Elmer ELAN 6000. A three-step HNO_3 acid digestion method following that of Le Roex et al. (2001) was used to obtain solutions. Approximately 50 milligrams of sample were weighed out into Teflon containers (Savilex beakers) and 4 ml of a 3:1 HF/HNO_3 was added. The container was then placed on a hot plate for 48 hours for digestion. Once the samples were dry another 2 ml of concentrated nitric acid (HNO_3) was added and reheated on a hot plate till dry. This procedure was repeated once more with 2 ml of concentrated nitric acid. Once the sample was dry a final addition of 5% nitric acid was added and the container was moved to a centrifuge tube and placed into an ultrasonic bath for dissolution. Once the sample was dissolved it was ready for use in the ICP Mass spectrometer. Errors were better than 3%, relative, and detection limits were in the lower ppb range.

2.2.5 Ar-Ar Isotopes

Two samples were sent by the CGS to the United States Geological Survey (USGS) for Ar-Ar geochronology. The samples were prepared by placing 50mg of whole-rock powder in copper capsules and sealed under vacuum in fused quartz tubes. The samples were then irradiated in the central thimble facility at the Training Reactor Isotopes General Atomics (TRIGA) reactor at the USGS in Denver, Colorado (Kunk and McAleer 2008). As per Kunk and McAleer (2008), the samples were analysed at the USGS in Denver on a VG Isotopes, Ltd. model 1200B mass spectrometer fitted with an electron multiplier using the $^{40}Ar/^{39}Ar$ step heating method of dating. Heating for 10 minutes per step followed a schedule of 5 steps. The sample was heated in a molybdenum-lined, tantalum furnace similar to that described by Staudacher et al. (1978). The isotopic data was then reduced using a computer program of Haugerud and Kunk (1988), and using the decay constants of Steiger and Jäger (1977).

2.2.6 Sr and Nd Isotopes

Fourteen samples were selected for radiogenic isotope analysis (Sr and Nd) and it was decided to analyse at least one mafic and one felsic version of each complex. The chemical separation procedure was done following that of Miková and Denková (2007). A standard BHVO-2 was also analysed with the samples as well as a blank. The samples were weighed out into 7ml Teflon beakers. Approximately 50mg of each powdered sample was used except for the Fonjay sample (MI06011) where two sets of approximately 70mg of sample powder

was used due to low Nd concentrations. The sample powders were then digested in 4ml of 4:1 HF:HNO_3. The beaker was then closed and left on a hot plate (90°C) for 72 hours. The beakers were then opened to dry down the samples and converted to a nitrate by adding 4ml of concentrated HNO_3 and dried down again. Lastly the samples were redissolved in 1ml of 2.0M HNO_3 and transferred to 1.5ml centrifuge tubes and spun at 4000rpm for 20 minutes.

The supernatant liquids were run through a 200µl Eichrome Sr spec resin bed in polypropene columns to collect Sr. There was also REE fraction collection that was later used for REE separation and to elute Nd. The Sr fraction was dried down on a hot plate and then 0.2% HNO_3 was added. It was then run through the Multi-collector ICP-MS machine for Sr isotope analysis. The REE fraction was dried down on a hot plate and converted to a chloride first by cooling, then adding 2ml of 6M HCl and then drying down. This procedure was done twice and then 1ml of 0.5M HCl was added. The samples were then transferred to a 1.5ml centrifuge tube and spun at 4000 rpm or 20 minutes.

The samples were then run through an AG 50W cation resin (200 – 400 mesh) in polypropene columns to separate REE. The REE separation was collected and dried on a hot plate overnight, cooled and then converted to a nitrate by adding 2mls of concentrated HNO_3 and drying down twice. The samples were then cooled and 1.75ml 0.05M HNO_3 was added. The samples were then run through 2ml Ln spec resin columns to collect Nd. The Nd fraction was then dried down on a hot plate overnight and then cooled. 2% HNO_3 was then added to the Nd fraction and the Nd fraction was run through the Multi-collector ICP-MS machine for Nd isotope analysis. The Fonjay samples were first combined before they were run through the ICP-MS machine.

The ICP-Ms machine used was a Nu instruments NuPlasma HR mass spectrometer in AEON EarthLAB at UCT. The standard used in the $^{87}Sr/^{86}Sr$ isotope analyses was NIST SRM987 and had an average value of 0.710248 ± 0.000035 (2σ, n = 5) of and the standard used in the $^{143}Nd/^{144}Nd$ isotope analyses was JNdi-1 and had an average value of 0.512088 ± 0.000016 (2σ, n = 5). A DSN-100 desolvating nebuliser was used to introduce the samples into the MC-ICP-MS. Each analysis took 10 minutes and the internal standard was run after every 5 samples. Instrumental mass fractionation was corrected using the exponential law with a $^{86}Sr/^{88}Sr$ ratio of 0.1194 and a $^{146}Nd/^{144}Nd$ ratio of 0.7219.

2.2.7 Stable Isotopes

Oxygen isotopes for whole rock samples were determined using the conventional silicate line method and oxygen isotopes for separate minerals were determined using the laser fluorination method. Hydrogen isotope analyses of bulk-rock powders were carried out using techniques described by Harris et al. (2000).

The oxygen silicate line samples were crushed to powders and then dried in an oven at 50°C overnight. Approximately 10mg was weighed out using a balance. The weighed out samples were then transferred into the Ni reaction vessels where eight samples and two standards were run at the same time. The quartz standard NBS-28 was used. The samples were then degassed under vacuum at 200°C for 2 hours.

The silicate minerals were then reacted with ClF_3 (Borthwick and Harmon 1982) on a conventional silicate line and the O_2 converted to CO_2 using a hot platinized carbon rod. Further details of the methods employed for the extraction of oxygen from silicates at UCT is given by Vennemann and Smith (1990), and Harris and Erlank (1992).

The isotope ratios of CO_2 were measured using a Finnigan MAT-252 mass spectrometer at the University of Cape Town. The data is reported in the δ notation where $\delta = 1\,000 \times [(R_{sample} - R_{standard})/R_{standard}]$ and $R = {}^{18}O/{}^{16}O$. Assuming a $\delta^{18}O$ value of 9.64‰ for NBS-28 there is less than 0.32‰ difference between the normalised and un-normalised data. The average difference between the NBS-28 data was 0.13‰ during the course of these analyses and this corresponds to a 1σ value of 0.1‰.

The oxygen laser fluorination samples were crushed and then sieved using a 600 micron mesh sieve. The mineral grains were then collected for washings with water and ethanol. They were then dried over night in an oven at 50°C and separated by hand picking using a binocular microscope and tweezers. The grains were cleaned again in ethanol and dried in an oven at 110°C and were then ready for laser fluorination. 1-3mg of sample was weighed out (one or two grains) for each analysis.

The sample grains were examined for impurities under the binocular microscope and then placed in a nickel sample tray. The sample holder holds twelve samples, including two monastery garnet grains as standards. The nickel tray was placed onto a stainless steel column and placed in the oven at 110°C for at least an hour. The nickel tray and stainless steel column were always handled with gloves to avoid contamination. The nickel tray and

stainless column were then placed in a reaction chamber and sealed while hot. The top metal plate was replaced and the nuts tightened and the whole sample chamber placed on the base plate and clamped together.

The sample chamber was then pumped out for at least an hour and then filled with ~10kPa BrF_5 to remove any remaining moisture. The BrF_5 was replaced after 30 seconds and then left in the sample chamber overnight. The KCl furnace was then turned on and the entire contents of the line frozen in metal U-traps using liquid nitrogen (N_2) for 5 minutes. After pumping out the sample chamber it was prefluorinated again for 5 minutes. A blank measurement was taken and the pressure was recorded.

The sample in the chamber was then lased and O_2 was moved through the line using liquid nitrogen, a KCl trap and a 5 micron molecular sieve. The O_2 from the samples were collected in glass bottles which were then transferred over to the Archaeology Department at the University of Cape Town where a Finnigan MAT-252 mass spectrometer analysed the O_2 gas. The data is reported in the δ notation as above. The pressure of the gas was used to calculate yield. The difference between the normalised and un-normalised data is 0.61‰ with the assumption that the $\delta^{18}O$ value for monastery garnet is 5.39‰. The average difference between the two monastery garnets was 0.04‰ during the course of this work.

For hydrogen analysis 50-200mg of powdered samples were weighed out according to loss on ignition values and were loaded into 6mm quartz tubes (oven dried at 800°C). Decrepitated gravel-size quartz chips and quartz wool was loaded on top of the sample in order to prevent the neck of the tube from collapsing during pyrolysis, and to prevent the sample powder from being pumped into the vacuum line. The quartz tube with the sample was oven dried overnight at 110°C and afterwards placed on a hot plate at 190°C for an hour. The quartz tube was attached to the vacuum line and further degassed for 15 minutes at 190°C by using a heated aluminium block from a hot plate. The structural H_2O within the sample was released by heat (pyrolysis) using a propane-oxygen torch (>1200°C) for 3-5 minutes until the whole sample had fused.

The released H_2O was collected in a liquid nitrogen trap and any organic or molecular hydrogen was oxidised to H_2O using a copper-oxide furnace at 700°C. The liquid nitrogen trap was replaced by an alcohol trap (isopropanol mixed with liquid nitrogen) and all non-condensable gases were pumped out. The H_2O from the sample was then trapped in a glass break-seal tube containing zinc shavings (low blank 'Indiana Zinc' batch 569B) using liquid nitrogen. Excess Zn was used to prevent poisoning from fluorine present in the samples. The

glass break-seal tube was then placed in a furnace for 30 minutes at 450°C to reduce the H_2O to elemental hydrogen.

The hydrogen isotope composition of the sample was measured using a Finnigan MAT-252 mass spectrometer at the University of Cape Town. The instrumental hydrogen isotope ratios were normalised and standardised relative to SMOW using the equations of Coplen (1988). The analytical errors for δD and H_2O^+ are ±2‰ (1σ) and 0.10 wt%, respectively. The error of δD increases as the amount of water extracted decreases as there is insufficient gas to measure δD accurately. It is also possible that the very negative values in samples represent a proportionally higher component from the blank as the blank has an extremely negative δD value.

3 PETROGRAPHY OF THE MANINGOZA SUITE

The petrography of the Maningoza Suite is described below and is divided into sections by each complex. The Maningoza Complex is further divided into the Ambolodia Formation, Antanetilava Formation, Sambao Formation and dykes. Descriptions for each sample analysed are given in the appendix. The samples were classified using mineral proportions observed in thin-section. Descriptions of the samples of the Fonjay and Ambereny Complexes were completed previously by the Council for Geoscience of South Africa and have been summarised in sections 3.9 and 3.10 below.

3.1 Ankibobozaka Complex

The mafic rocks of the Ankibobozaka Complex belong to two main rock types. The first rock type is fine-grained (≤0.5mm) suggesting it is extrusive. The fine-grained rocks contain 60% plagioclase, 10% clinopyroxene with magnetite and secondary mineral chlorite. These rocks are classified as basalts and have an equigranular texture. The second rock type is fine- to medium-grained (0.5-2.0mm) suggesting it crystallised at shallow depths. This fine- to medium-grained rock contains 40% plagioclase, 50% clinopyroxene, magnetite and secondary mineral chlorite (Figure 3.2). The secondary mineral chlorite suggests that alteration has occurred. These rocks have a subophitic texture where the plagioclase grains penetrate the clinopyroxene grains. The fine- to medium-grained rocks are classified as microgabbros.

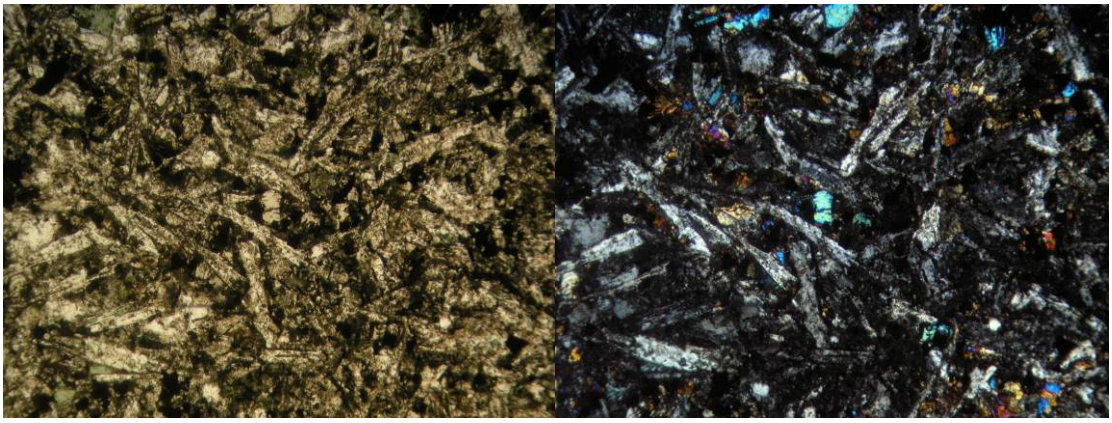

Figure 3.2: Sample PF06001 with PPL and XPL showing plagioclase laths and secondary alteration. Scale = 5mm across horizontal.

The felsic rocks of the Ankibobozaka Complex have alkali-feldspar that ranges from 55 to 70% volume with approximately 20% quartz. The alkali-feldspar and quartz show angular

intergrowths giving a granophyric texture (Figure 3.1). The overall grain size is fine- to medium-grained (0.5-2.0mm) suggesting crystallisation occurred at shallow depths. The remaining minerals consist of plagioclase, Fe-Ti opaques, traces of amphibole and in some samples secondary minerals such as calcite and biotite. These rocks are classified as granophyres.

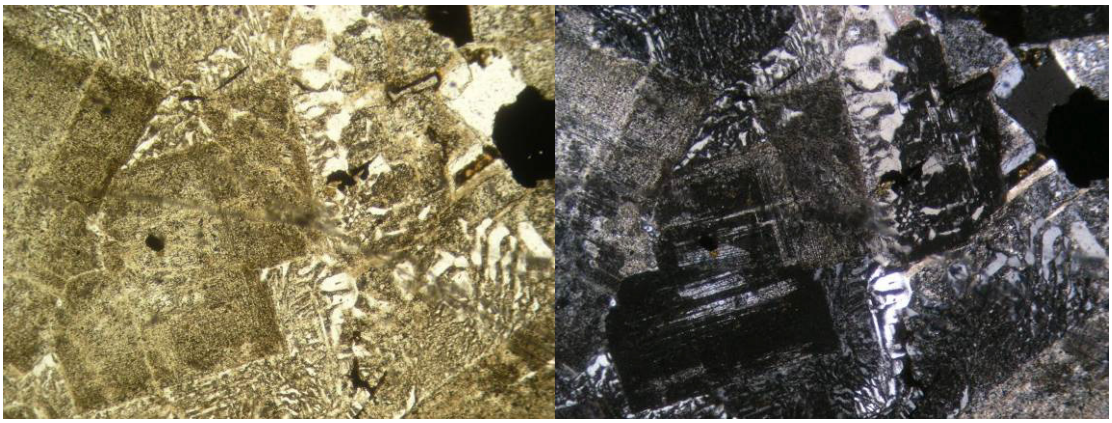

Figure 3.1: Sample PF06005 with plane polarised light (PPL) and crossed polarised light (XPL) showing a granophyric texture. Scale = 5mm across horizontal.

3.2 Berevo Complex

The mafic rocks of the Berevo Complex can be divided into two rock types based on grain size. The fine- to medium-grained rocks (0.5-1.5mm) contain 45%-68% plagioclase and 25%-35% clinopyroxene with Fe-Ti oxides and secondary mineral chlorite (Figure 3.3). The fine- to medium-grained rocks have an inequigranular texture and are classified as microgabbros. The coarse-grained rocks (2.0-4.0mm) have plagioclase, clinopyroxene, Fe-Ti oxides and secondary minerals chlorite, epidote, serpentine and calcite. Samples PF06017 and PF06027 also contain olivine as main mineral. The coarse-grained rocks have a porphyritic texture and are classified as gabbros. These rocks also show an ophitic and subophitic texture with plagioclase embedded in clinopyroxene, except in samples PF06013 and PF06017 (Figure 3.3).

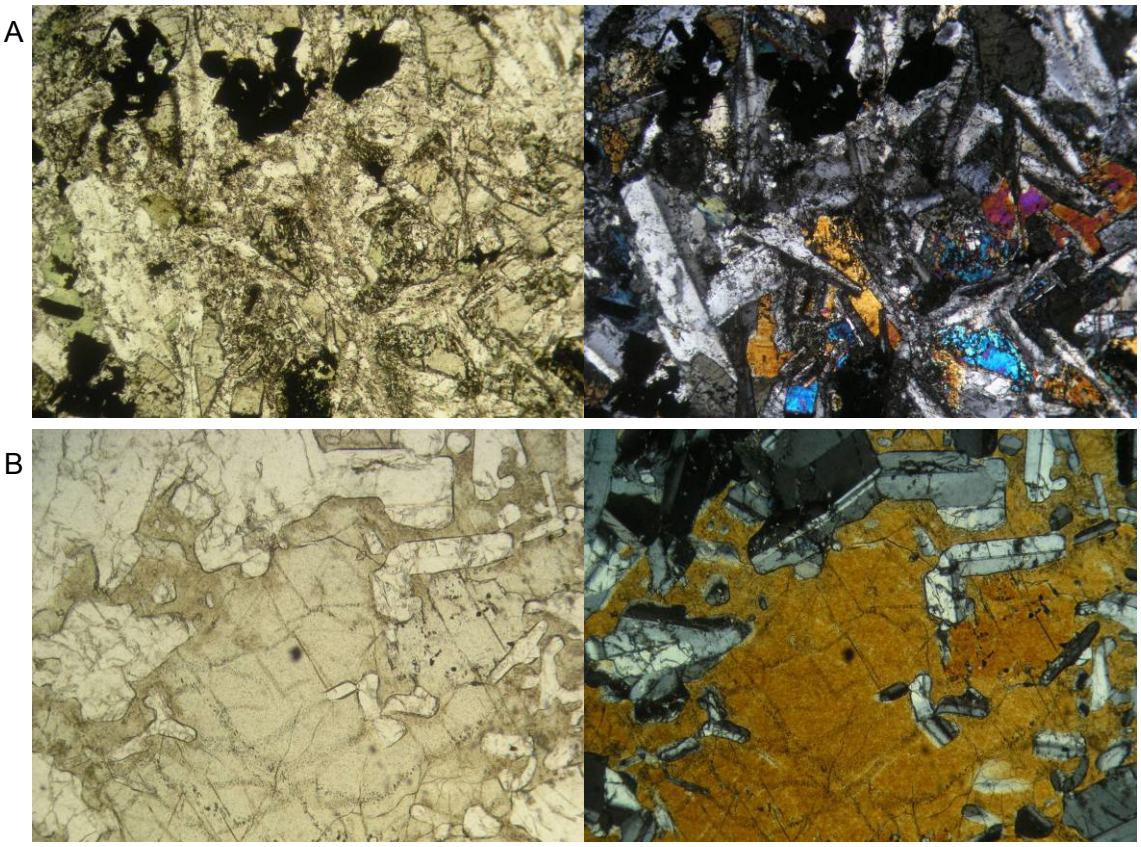

Figure 3.3: Samples PF06030 (A) and PF06021 (B) with PPL and XPL. Sample PF06030 shows plagioclase laths and green secondary minerals (chlorite) as well as Fe-Ti oxides. Sample PF06021 shows plagioclase laths enclosed within large clinopyroxene grains (ophitic texture). Scale = 5mm across horizontal.

The felsic rocks of the Berevo Complex are fine- to medium-grained (0.5-2.0mm) and contain alkali-feldspar, plagioclase, Fe-Ti oxides and the secondary minerals epidote, calcite and chlorite. The alkali-feldspar and quartz show angular intergrowths giving a granophyric texture (Figure 3.4). The medium grain size suggests that these rocks crystallised at shallow depth. These rocks are classified as granophyres.

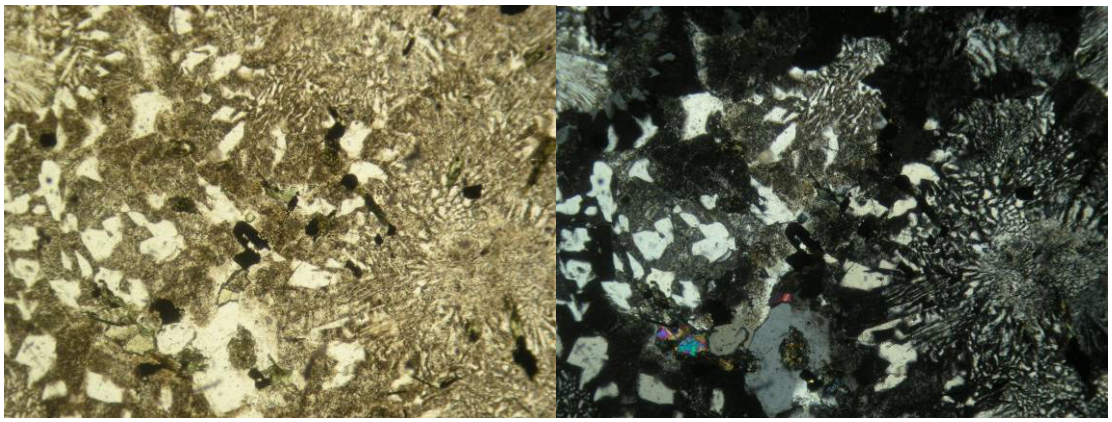

Figure 3.4: Sample PF06015 with PPL and XPL showing a granophyric texture. Scale = 5mm across horizontal.

The mafic dykes of the Berevo Complex can be divided into two types depending on grain size. The first rock type is fine- to medium-grained (0.2-1.5mm) with an equigranular texture (Figure 3.5). This rock type consists of plagioclase, clinopyroxene, Fe-Ti oxides and secondary mineral chlorite. These rocks are classified as dolerites. The second type is fine-grained (0.2mm) has 60% plagioclase, 40% opaque minerals (magnetite) and is holocrystalline and aphanitic with an equigranular texture. These rocks are classified as basalts. The felsic dykes of the Berevo Complex are fine-grained (0.2mm) and have an equigranular texture. The main crystallising minerals are plagioclase, quartz and Fe-Ti oxides. The felsic dykes are classified as trachytes.

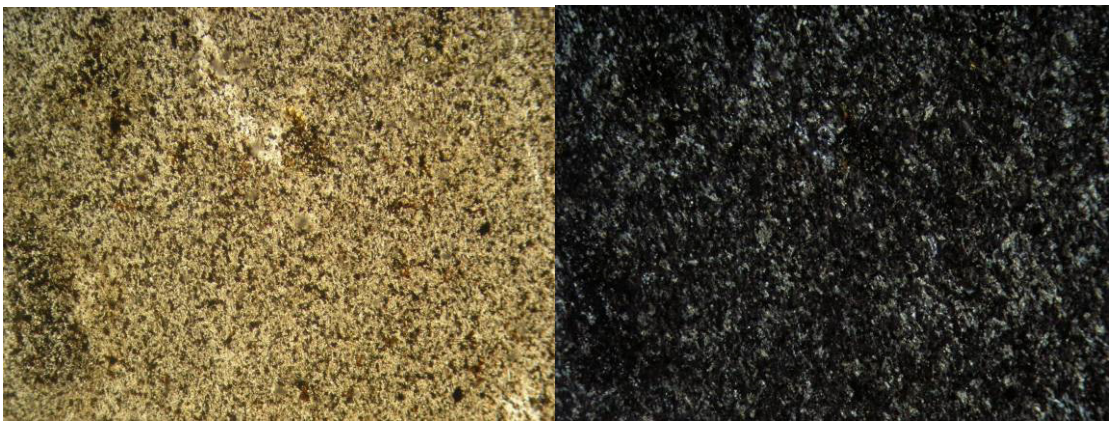

Figure 3.5: Sample PF06009 with PPL and XPL showing a fine-grained and equigranular texture. Scale = 5mm across horizontal.

3.3 Maningoza – Ambolodia Formation

The mafic rocks of the Ambolodia Formation contain plagioclase, clinopyroxene, magnetite and secondary minerals such as chlorite and epidote (Figure 3.6). The mafic rocks are fine-grained (0.2-0.5mm) and are equigranular in texture suggesting an extrusive origin. The mafic rocks are classified as basalts with the exception of sample PF06120 which is classified as a basaltic-andesite and contains some quartz.

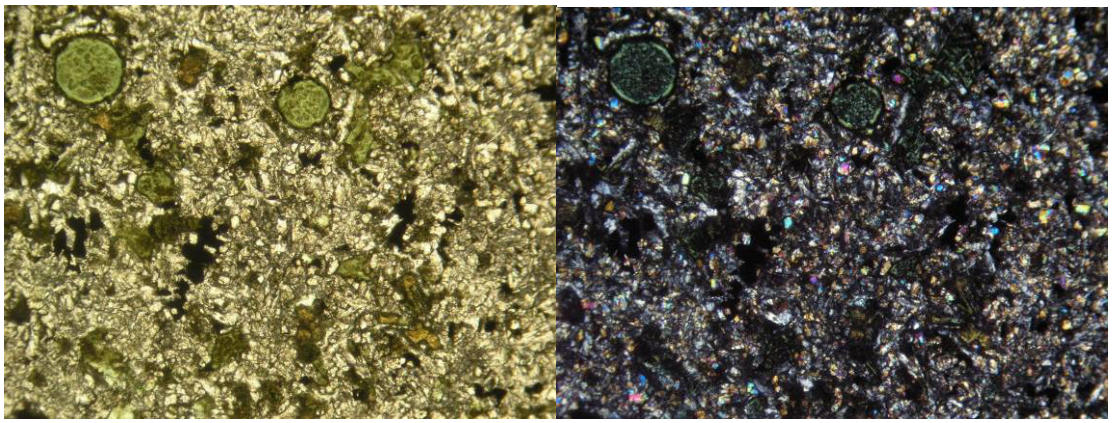

Figure 3.6: Sample PF06127 with PPL and XPL showing secondary alteration to green chlorite as well as amygdales. Scale = 5mm across horizontal.

The intermediate rocks of Ambolodia have plagioclase, clinopyroxene, Fe-Ti oxides and secondary minerals such as chlorite and epidote with the exception of PF06126 which also contains traces of amphibole. The intermediate rocks are fine-grained (0.2-0.8mm) and two samples classify as andesite (PF06126 and PF06128) and one sample classifies as a trachy-andesite (PF06119).

The felsic rocks of Ambolodia are sampled from a plug named the Ambohibeory Formation and contain plagioclase, quartz, magnetite and secondary minerals such as epidote, calcite and chlorite except for PF06115 which also contains alkali-feldspar and amphibole. The felsic rocks are fine-grained (0.2-1.0mm), are inequigranular in texture and are classified as dacites (Figure 3.7). Sample PF06115 is classified as a trachyte with the addition of alkali-feldspar.

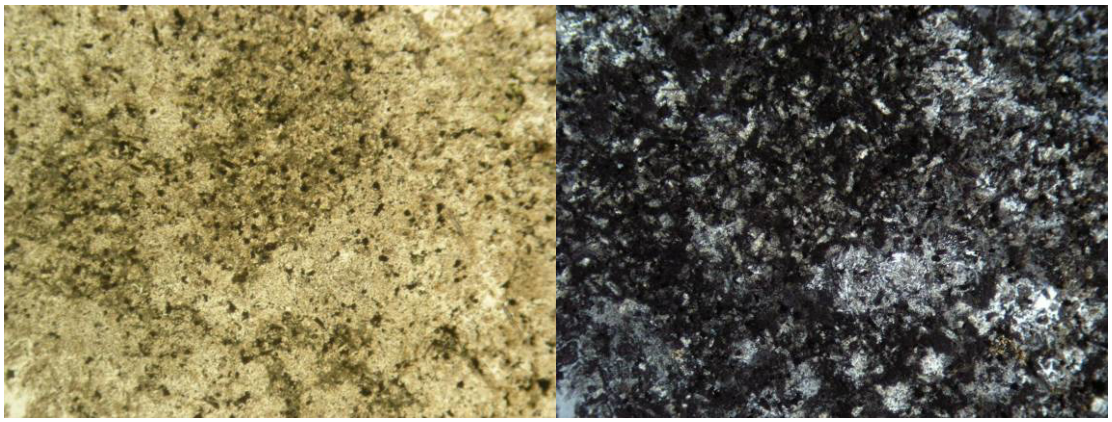

Figure 3.7: Sample PF06115 with PPL and XPL showing a fine-grained end equigranular texture. Scale = 5mm across horizontal.

3.4 Maningoza – Antanetilava Formation

The mafic rocks of Antanetilava have plagioclase, clinopyroxene, Fe-Ti oxide and secondary mineral chlorite. The clinopyroxene is light brown to brown in colour and has an augite composition. Sample PF06145 has olivine in place of secondary minerals. The mafic rocks are fine-grained (0.2-1.0mm) and have an equigranular texture except samples PF06130, PF06148 and PF06153 which are medium-grained (1.0-2.0mm) and have a porphyritic texture (Figure 3.8). The fine-grained mafic rocks are classified as basalts and the medium-grained mafic rocks are classified as dolerites. Two samples (PF06129 and PF06132) have a fine-grain groundmass with porphyritic feldspar and are classified as feldspar porphyry basalts.

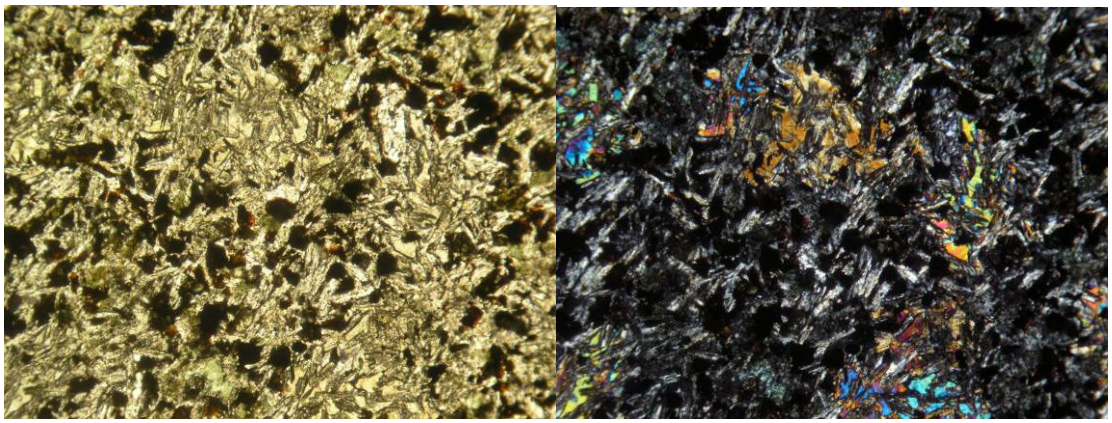

Figure 3.8: Sample PF06135 with PPL and XPL showing porphyritic pyroxene with feldspar intergrowths. Also present is Fe-Ti oxides and evidence of secondary alteration. Scale = 5mm across horizontal.

The felsic rocks of the Antanetilava Formation are fine-grained (0.5-1.0mm) suggesting they formed by extrusive crystallisation. The main minerals in the felsic rocks are plagioclase, alkali-feldspar, quartz, magnetite and secondary minerals such as chlorite and epidote. The presence of secondary minerals suggests alteration. The felsic rocks are classified as rhyolites except for three samples: sample PF06131 has no alkali-feldspar and is classified a dacite; sample PF06142 has larger amounts of alkali-feldspar and is classified as a trachyte; sample PF06143 has no quartz or alkali-feldspar and is classified as a dacite. Sample PF06144 also shows a quenched texture (Figure 3.9).

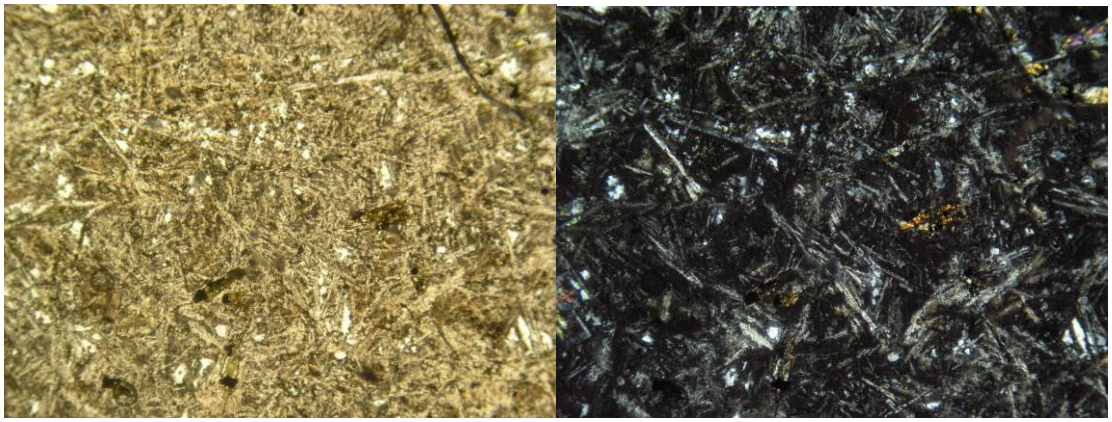

Figure 3.9: Sample PF06144 with PPL and XPL showing a quenched texture. Scale = 5mm across horizontal.

3.5 Maningoza – Sambao Formation

The mafic rocks of the Sambao Formation are fine-grained (0.2-1.0mm) suggesting an extrusive origin. The mafic rocks consist of plagioclase, clinopyroxene, magnetite, olivine and secondary minerals such as chlorite. Sample BY6F103 has 29% volume of secondary minerals present making it a largely altered sample. The fine-grained mafic rocks are classified as basalts and are typically porphyritic in texture (Figure 3.10). The felsic rocks of the Sambao Formation are fine-grained (0.2mm) and consist of alkali-feldspar, plagioclase, quartz, Fe-Ti oxides and secondary mineral chlorite. The fine-grained felsic rocks are classified as rhyolites and have a porphyritic texture (3.0mm).

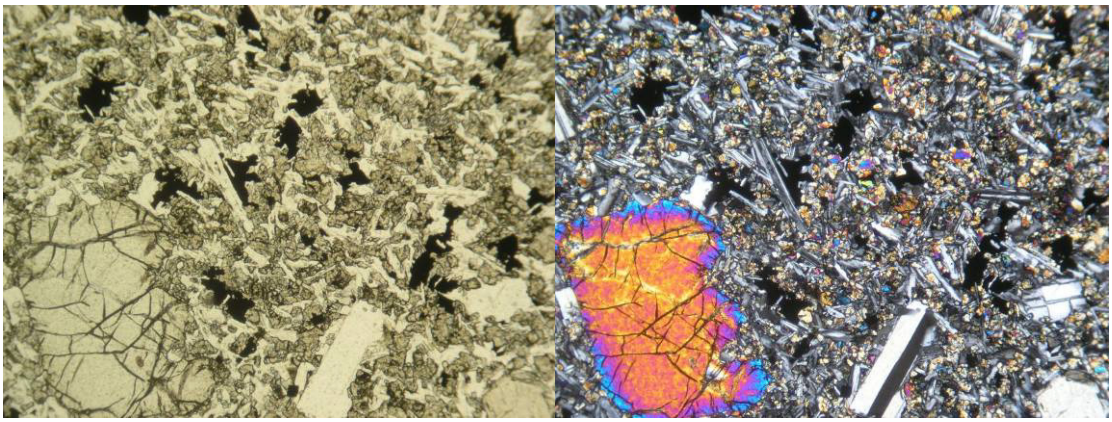

Figure 3.10: Sample BY6F091 with PPL and XPL showing phenocrysts of olivine and plagioclase. Scale = 5mm across horizontal.

3.6 Maningoza – Dyke Swarm

The mafic dykes of the Maningoza Suite are fine- to medium-grained (0.2-2.5mm) and consist of plagioclase, clinopyroxene, magnetite and secondary minerals such as chlorite and epidote (Figure 3.11). The mafic dykes are equigranular and are classified as dolerites. The felsic dykes of the Maningoza Suite are fine-grained (0.2-1.0mm) with porphyritic feldspars. The felsic dykes consist of feldspar, quartz, magnetite and secondary mineral epidote. The felsic dykes are classified as porphyritic rhyolites.

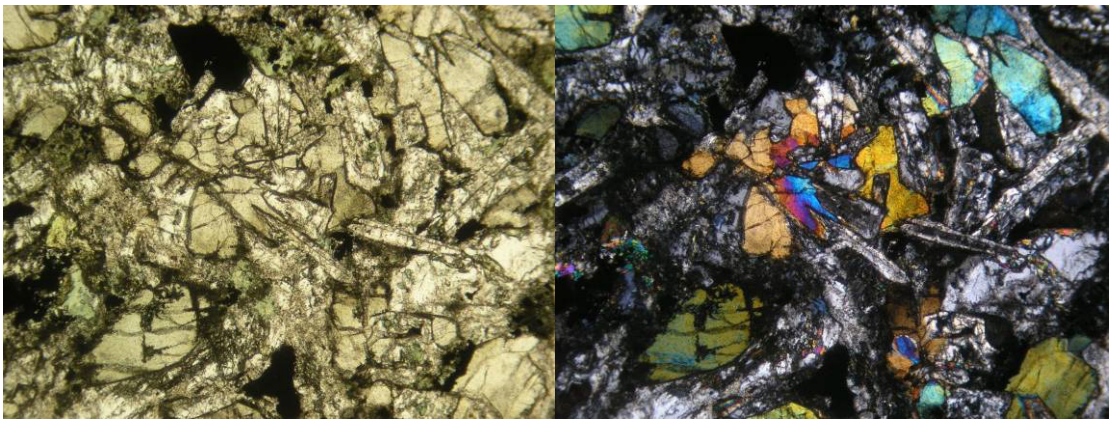

Figure 3.11: Sample PF06124 with PPL and XPL showing plagioclase laths and clinopyroxene. Also present are Fe-Ti oxides and evidence of secondary alteration. Scale = 5mm across horizontal.

3.7 Basement Dykes

The mafic dykes which intrude the basement rocks consist of plagioclase, clinopyroxene, magnetite and secondary minerals such as chlorite with the exception of PF06138 which also contains a small amount of olivine (Figure 3.12). The dykes are fine- to medium-grained (0.5-2.0mm) and have an equigranular texture. The felsic dykes are fine-grained (0.1-0.4mm) and have a porphyritic texture. The main crystallising minerals are feldspar, quartz, Fe-Ti oxides and secondary mineral epidote. The felsic dykes are classified as rhyolites

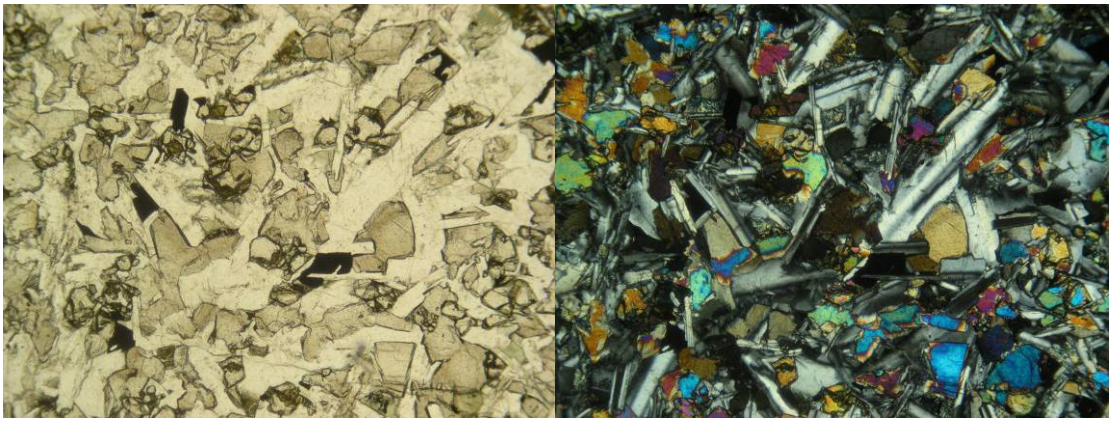

Figure 3.12: Sample PF06138 with PPL and XPL showing plagioclase laths in clinopyroxene and olivine. Scale = 5mm across horizontal.

3.8 Ambohitrosy Complex

The mafic rocks of the Ambohitrosy Complex can be divided into two types based on grain size. The first type has a fine grain size (0.2-1.0mm) and consists of plagioclase, clinopyroxene, magnetite and secondary mineral chlorite (Figure 3.13). ABF052 has undergone a large amount of alteration to secondary minerals such as chlorite and epidote. The fine-grained mafic rocks are classified as basalts. The second type of mafic rocks are coarse grained (1.0-5.0mm) and consists of plagioclase, clinopyroxene, magnetite and secondary minerals such as chlorite. The coarse-grained mafic rocks are porphyritic in texture and are classified as gabbros.

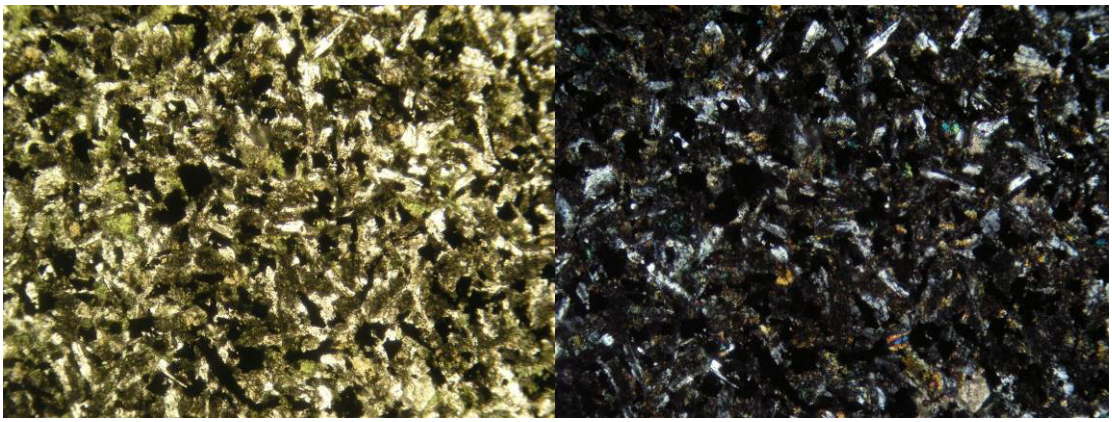

Figure 3.13: Sample ABF063 with PPL and XPL showing a fine-grained texture with secondary minerals as evidence for secondary alteration. Scale = 5mm across horizontal.

The felsic rocks of the Ambohitrosy Complex can also be divided into two types based on grain size. The first type is fine-grained (0.2-1.0mm) and has a composition of plagioclase, quartz, alkali-feldspar and magnetite. The fine-grained felsic rock has a porphyritic texture and is classified as a rhyolite. The second type of felsic rock is coarse-grained (1.0-4.0mm) and consists of plagioclase, alkali-feldspar, quartz, amphibole, magnetite and secondary mineral chlorite (Figure 3.14). The coarse-grained felsic rocks are classified as granites except sample ABF060 which is classified as a syenite with alkali-feldspar volume of 80%.

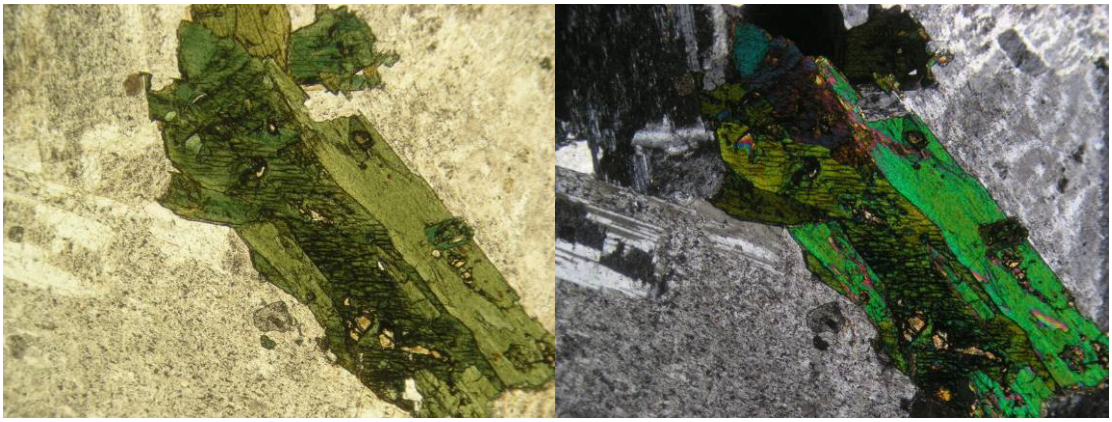

Figure 3.14: Sample ABF074 with PPL and XPL showing large grains of feldspar and amphibole. Scale = 5mm across horizontal.

3.9 Fonjay Complex

The mafic rocks of the Fonjay Complex can be divided into two types based on grain size. The first type is fine-grained (0.2-0.4mm) and consists of plagioclase, clinopyroxene, olivine, Fe-Ti oxides and trace amounts of biotite. The fine-grained samples have been classified as

microgabbros and have an inequigranular texture. The second type of mafic sample is medium-grained (1.0-2.0mm) and consists of plagioclase, clinopyroxene, Fe-Ti oxides and secondary minerals such as chlorite and calcite. Samples MI06007A and MI06010 also contain olivine and samples MI06008, MI06012 and MI06013 contain orthopyroxene. The medium-grained samples have been classified as gabbros and have a porphyroblastic texture.

The Fonjay Complex also has three samples which are exceptions to the above. The first sample have been classified as a gabbronorite and consists of plagioclase, orthopyroxene, Fe-Ti oxides, clinopyroxene, biotite and secondary mineral chlorite. The gabbronorite is medium-grained (1.0-1.5mm) and has an inequigranular texture. The second sample have been classified as a dolerite and consists of plagioclase, clinopyroxene, secondary mineral calcite, Fe-Ti oxides and trace amounts of quartz. The dolerite is fine-grained (0.2-0.4mm) and has an inequigranular texture. The third sample has been classified as a meta-mudstone and consists of quartz, muscovite, Fe-Ti oxides and trace amounts of zircon. The meta-mudstone is very fine-grained (aphanitic) and has vague laminations.

3.10 Ambereny Complex

The mafic rocks of the Ambereny Complex can be divided in two types based on the presence of orthopyroxene. The first type is fine- to medium-grained (0.1-1.5mm) and consists of plagioclase phenocrysts, clinopyroxene, orthopyroxene, Fe-Ti oxides, secondary mineral chlorite and trace amounts of biotite. These samples have been classified as gabbronorite and are inequigranular in texture. The second type is also fine- to medium-grained (0.2-1.5mm) and consists of plagioclase, clinopyroxene, Fe-Ti oxides, and trace amounts of quartz, chlorite and biotite. These samples have been classified as microgabbros and have an inequigranular texture. One mafic sample is an exception as it consists of plagioclase (50%) and olivine (40%) with trace amounts of pyroxene, chlorite and Fe-Ti oxides. This fine- to medium-grained (0.5-2.0mm) sample has been classified as a troctolite and has an inequigranular texture.

The felsic rocks of the Ambereny Complex are fine- to medium-grained (0.2-1.5mm) and consist of plagioclase, quartz, amphibole, K-feldspar, Fe-Ti oxides and trace amounts of biotite. These rocks have been classified as tonalities and have a granophyric texture. There is also a mafic dyke that has been sampled near the Ambereny Complex. The mafic dyke is fine- to medium grained (0.3-1.5mm) and consists of plagioclase, clinopyroxene, Fe-Ti

oxides, quartz and secondary mineral chlorite. The mafic dyke has been classified as a dolerite and has a porphyritic texture.

3.11 Summary

The mafic rocks in general consist mainly of plagioclase, clinopyroxene and Fe-Ti oxides. Olivine is observed in only in 11 out of 103 samples described and orthopyroxene is observed only in the Fonjay and Ambereny Complexes. The felsic rocks are dominated by K-feldspar, plagioclase, clinopyroxene, quartz and Fe-Ti oxides. Minerals such as amphibole and biotite are rare and mostly occur in trace amounts. The minerals feldspar, pyroxene, olivine and the Fe-Ti oxides are analysed for chemical composition in the following chapter. The felsic and mafic samples are described as either fine-grained or medium-grained rocks and rocks described as coarse-grained only occur in the Berevo and Ambohitrosy Complexes. In almost all samples secondary minerals are described with epidote and chlorite (chlorite being the major presence). Chlorite is indicative of surface alteration where as epidote suggests hydrothermal alteration has occurred. The effects of hydrothermal alteration will be investigated in Chapter 6.

4 MINERAL CHEMISTRY

The minerals analysed for the Maningoza Suite were feldspar, clinopyroxene, olivine and opaques. Since there were so many analyses this chapter is broken down into each mineral analysed and then further broken down into sample category (e.g. volcanic, complex or dyke in the Maningoza Suite). A sample from each complex was chosen on the basis that it represented either a felsic or mafic end-member. An attempt was made to analyse at least one mafic and one felsic end-member for each complex. Samples were also chosen on the basis that they had very little or no alteration observed in hand-specimen and thin-section, as alteration would effect the chemical composition of groundmass and minerals.

4.1 Feldspar

The Sambao Formation basalts have plagioclase that ranges from labradorite to albite (Figure 4.1). The chemical composition of the feldspars ranges from $An_{51}Ab_{47}Or_2$ to $An_4Ab_{96}Or_0$. The Antanetilava Formation basalts have feldspars that range from bytownite to oligoclase and in some cases sanidine. The chemical composition of these feldspars ranges from $An_{89}Ab_{11}Or_0$ to $An_{11}Ab_{86}Or_3$ as well as $An_0Ab_3Or_{97}$. The Ankibobozaka Complex microgabbros have plagioclase with a labradorite composition where as the granophyres have feldspars that range from albite to sanidine compositions. The chemical composition for the microgabbros range from $An_{68}Ab_{32}Or_0$ to $An_{61}Ab_{38}Or_1$ and the chemical composition for the granophyres range from $An_0Ab_{99}Or_1$ to $An_0Ab_{68}Or_{32}$. The Berevo Complex gabbros have plagioclase that ranges from anorthite to labradorite. The granites of the Berevo Complex have feldspars that range from albite to orthoclase. The chemical composition of the gabbro plagioclase ranges from $An_{92}Ab_8Or_0$ to $An_{65}Ab_{34}Or_1$ and the granite feldspar ranges from $An_6Ab_{94}Or_0$ as well as $An_0Ab_{12}Or_{88}$.

The Fonjay Complex gabbros have plagioclase that range from bytownite to labradorite. The chemical composition of the gabbros feldspars ranges from $An_{88}Ab_{12}Or_0$ to $An_{59}Ab_{39}Or_2$. The Ambereny Complex gabbros have plagioclase that ranges from bytownite to labradorite. The granites of the Ambereny Complex have feldspars that range from andesine to albite and also albite to orthoclase. The chemical composition of the gabbro plagioclase ranges from $An_{81}Ab_{19}Or_0$ to $An_{57}Ab_{42}Or_1$ and the granite feldspars range from $An_{31}Ab_{66}Or_3$ to $An_5Ab_{95}Or_0$ as well as $An_0Ab_3Or_{97}$. The Ambohitrosy Complex gabbros have plagioclase that ranges from anorthite to albite and the syenite feldspars range from albite to orthoclase. The chemical composition of the feldspars ranges from $An_{95}Ab_3Or_2$ to $An_0Ab_{99}Or_1$ as well as $An_0Ab_2Or_{98}$. The basement dykes has plagioclase that ranges from bytownite to andesine in composition.

The chemical composition of the plagioclase ranges from $An_{85}Ab_{15}Or_0$ to $An_{40}Ab_{58}Or_2$. The Berevo Complex trachytic dykes have feldspars that range from albite to orthoclase. The chemical composition of the feldspars ranges from $An_3Ab_{96}Or_1$ to $An_0Ab_7Or_{93}$.

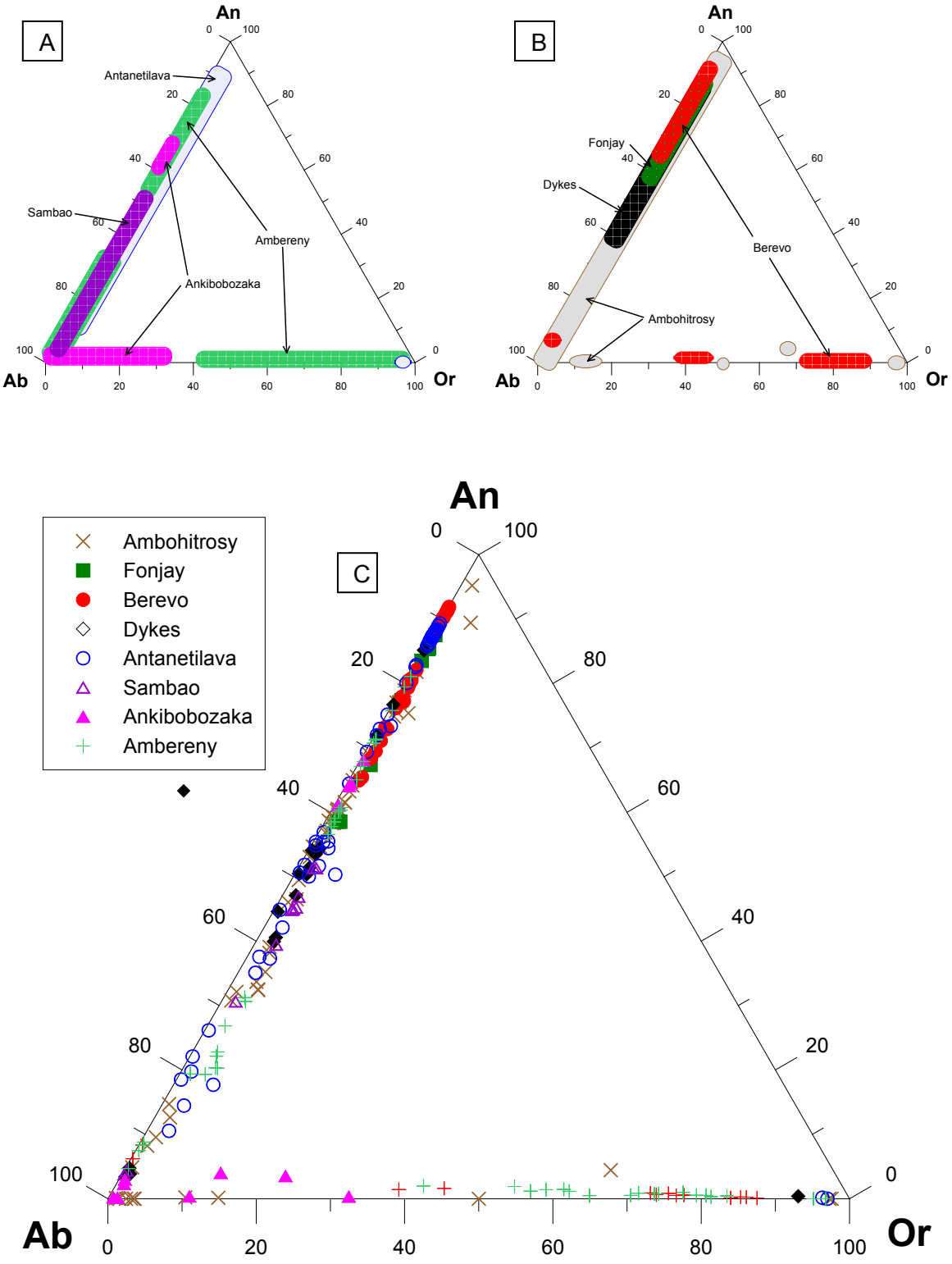

Figure 4.1: The feldspar triangle (C) showing the compositions of the feldspar minerals analysed by the Electron Microprobe. Compositions are in molecular percent. (Symbols: An = anorthite, Ab = albite and Or = orthoclase). Triangles (A) and (B) show the fields of each complex and are separated into three by sample category.

	Antanetilava		Sambao	Ankibobozaka		Berevo		Ambereny		Fonjay	Dyke	Ambohitrosy	
Sample	PF06130	PF06148	BY6F103	PF06002	PF06004	PF06018	PF06020	MI06016	MI06014	MI06010	PF06071	AB-07	AB-10
SiO_2	46.97	55.86	56.11	67.42	51.31	64.56	49.00	65.55	51.15	47.90	55.24	53.65	64.96
Al_2O_3	34.69	24.93	26.34	20.50	30.80	18.33	32.19	19.06	31.38	34.58	28.12	29.29	19.49
Fe_2O_3	0.38	3.72	1.39	0.33	0.91	0.17	0.66	0.14	0.48	0.40	0.87	0.36	0.08
CaO	16.10	6.67	9.49	0.08	12.86	0.05	15.69	0.09	14.06	16.95	10.85	12.36	0.93
Na_2O	2.19	5.88	5.68	10.33	3.93	1.53	2.38	3.75	3.75	1.79	5.49	4.72	3.47
K_2O	0.04	0.48	0.38	1.91	0.08	14.49	0.11	10.59	0.09	0.09	0.26	0.23	11.54
Total	100.51	99.60	99.64	100.61	100.11	99.19	100.13	99.24	101.02	101.78	101.10	100.72	100.53
Si^{4+}	2.145	2.552	2.547	2.951	2.335	2.994	2.243	2.989	2.310	2.161	2.477	2.418	2.948
Al^{3+}	1.867	1.343	1.410	1.058	1.652	1.002	1.737	1.024	1.671	1.839	1.486	1.556	1.043
Fe^{3+}	0.014	0.142	0.053	0.012	0.035	0.007	0.025	0.005	0.018	0.015	0.033	0.014	0.003
Ca^{2+}	0.788	0.327	0.462	0.004	0.627	0.002	0.769	0.005	0.681	0.819	0.521	0.597	0.045
Na^{+}	0.194	0.521	0.500	0.877	0.347	0.138	0.211	0.332	0.328	0.157	0.477	0.412	0.305
K^{+}	0.002	0.028	0.022	0.107	0.005	0.857	0.007	0.616	0.005	0.005	0.015	0.013	0.668
Sum	5.019	5.049	5.006	5.011	5.013	5.002	4.996	4.973	5.019	5.000	5.024	5.016	5.015
An	80.1	37.3	46.9	0.4	64.1	0.2	77.9	0.5	67.1	83.5	51.4	58.4	4.4
Ab	19.7	59.5	50.8	88.8	35.4	13.8	21.4	34.8	32.4	16.0	47.1	40.3	30.0
Or	0.2	3.2	2.2	10.8	0.5	86.0	0.7	64.7	0.5	0.5	1.5	1.3	65.6

Table 4.1: Selected feldspar analyses of the Maningoza Suite. See Tables A1.1 to A1.6 in the Appendix for all feldspar analyses.

4.2 Clinopyroxene

The Antanetilava Formation basalts have clinopyroxenes that have a composition of augite and the chemical composition ranges from $En_{46}Fs_{15}Wo_{39}$ to $En_{35}Fs_{28}Wo_{37}$ as well as $En_{41}Fs_{14}Wo_{45}$. The Ankibobozaka Complex microgabbros have clinopyroxenes that are augitic in composition. The chemical composition of the clinopyroxenes ranges from $En_{45}Fs_{13}Wo_{42}$ to $En_{43}Fs_{15}Wo_{42}$ and also $En_{44}Fs_{13}Wo_{43}$. The Berevo Complex gabbros have clinopyroxenes that are augitic in composition. The chemical composition of these clinopyroxenes ranges from $En_{39}Fs_{23}Wo_{38}$ to $En_{46}Fs_{10}Wo_{44}$. The Fonjay Complex gabbros have clinopyroxenes that are also augitic in composition. The chemical composition ranges from $En_{42}Fs_{14}Wo_{44}$ to $En_{42}Fs_{17}Wo_{41}$. The Ambereny Complex gabbros have clinopyroxenes that are augitic in composition and the chemical composition ranges from $En_{44}Fs_{13}Wo_{43}$ to $En_{44}Fs_{16}Wo_{40}$. The Ambohitrosy Complex gabbros have clinopyroxenes that are augitic in composition. The chemical composition of these clinopyroxenes ranges from $En_{48}Fs_{19}Wo_{33}$ to $En_{28}Fs_{33}Wo_{39}$ as well as $En_{38}Fs_{16}Wo_{46}$. The basement dykes have clinopyroxenes that are augitic in composition. The chemical composition ranges from $En_{47}Fs_{10}Wo_{43}$ to $En_{39}Fs_{32}Wo_{29}$.

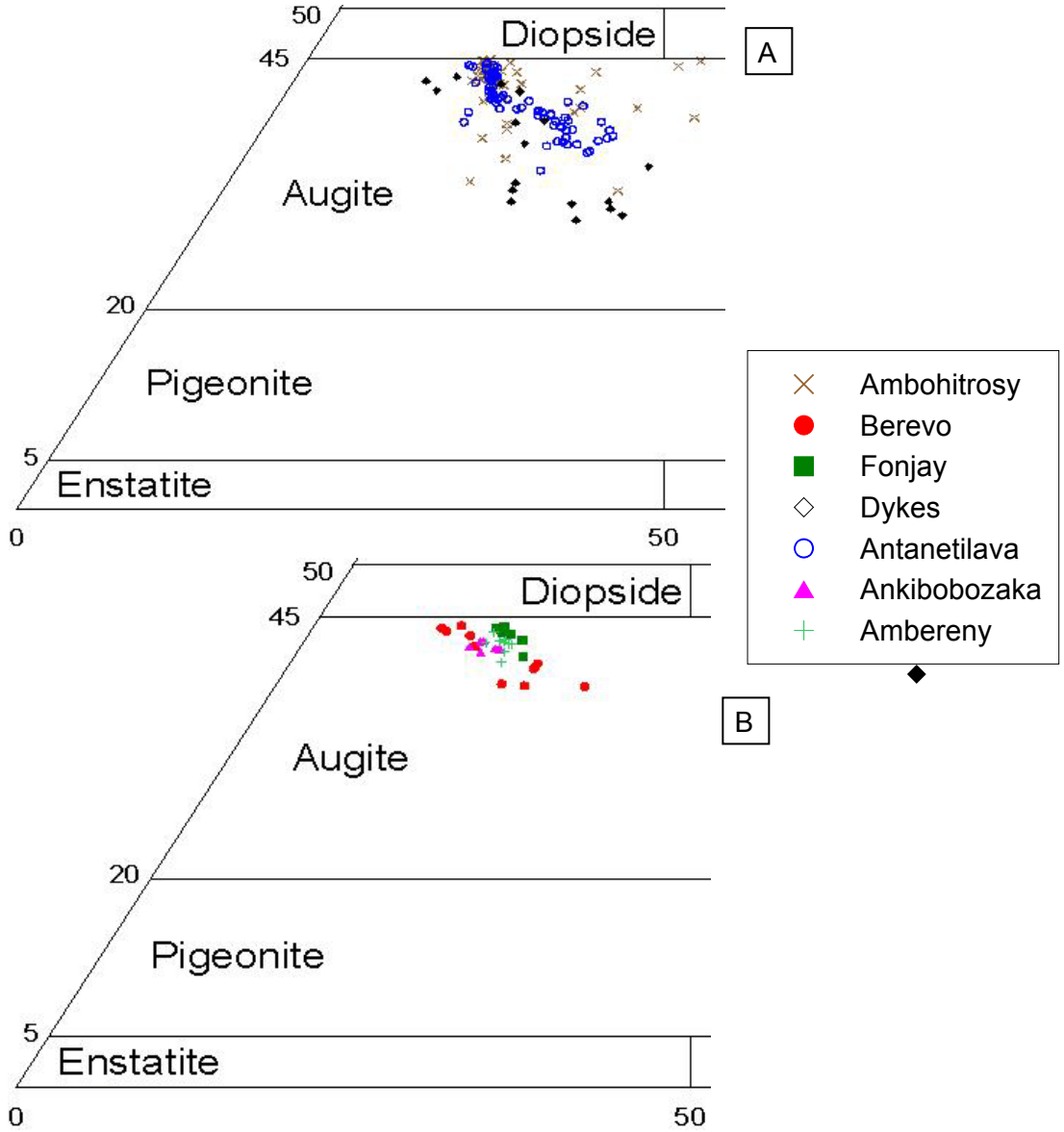

Figure 4.2: Portion of the clinopyroxene quadrilateral showing the compositions of the clinopyroxene minerals analysed by the electron microprobe. Quadrilateral (A) shows clinopyroxene compositions for the Ambohitrosy Complex, Antanetilava Formation and dyke swarm. Quadrilateral (B) shows clinopyroxene compositions for the Ambereny, Ankibobozaka, Berevo and Fonjay Complexes. All of the samples have an augitic composition. Compositions are in molecular percent.

	Antanetilava		Ankibobozaka		Berevo		Ambereny		Fonjay		Dyke	Ambohitrosy	
Sample	PF06130	PF06153	PF06004	PF06004	PF06027	PF06020	MI06014	MI06019	MI06010	MI06010	PF06071	AB07	95-14
SiO_2	50.32	49.89	50.01	50.17	51.09	51.98	52.65	53.86	50.68	50.63	51.96	51.39	50.97
TiO_2	0.80	1.13	0.80	0.89	0.57	0.47	0.69	0.42	0.97	1.10	1.00	0.96	0.30
Al_2O_3	5.44	2.88	4.73	4.33	3.45	3.10	2.60	1.74	4.01	5.29	2.57	2.82	0.27
FeO	7.79	14.41	8.20	8.01	7.92	5.83	8.22	8.36	9.86	8.10	12.71	8.21	28.26
MnO	0.24	0.27	0.17	0.15	0.24	0.15	0.23	0.25	0.36	0.20	0.39	0.29	0.92
MgO	13.94	14.05	15.40	15.12	15.86	16.35	14.93	15.66	14.11	14.45	14.88	14.43	0.43
CaO	21.27	19.27	19.96	20.49	20.78	21.54	21.15	21.12	19.40	20.84	17.84	21.68	12.95
Na_2O	0.48	0.39	0.25	0.24	0.25	0.25	0.30	0.33	0.40	0.31	0.32	0.39	5.55
Total	100.56	102.46	99.92	99.62	100.57	100.54	100.93	101.76	99.84	101.14	101.69	100.36	100.89
Si^{4+}	1.861	1.861	1.862	1.871	1.891	1.915	1.936	1.959	1.892	1.859	1.918	1.910	2.078
Ti^{4+}	0.027	0.038	0.027	0.030	0.019	0.016	0.023	0.014	0.032	0.037	0.034	0.032	0.009
Al^{3+}	0.237	0.127	0.208	0.190	0.151	0.135	0.113	0.075	0.177	0.229	0.112	0.124	0.013
Fe^{2+}	0.241	0.450	0.255	0.250	0.245	0.180	0.253	0.254	0.308	0.249	0.392	0.255	0.963
Mn^{2+}	0.008	0.009	0.005	0.005	0.007	0.005	0.007	0.008	0.012	0.006	0.012	0.009	0.032
Mg^{2+}	0.768	0.781	0.854	0.840	0.875	0.898	0.818	0.849	0.785	0.791	0.819	0.799	0.026
Ca^{2+}	0.843	0.770	0.796	0.819	0.824	0.850	0.833	0.823	0.776	0.820	0.706	0.863	0.566
Na^{+}	0.034	0.028	0.018	0.017	0.018	0.018	0.021	0.023	0.029	0.022	0.023	0.028	0.439
Sum	4.021	4.064	4.025	4.022	4.031	4.016	4.004	4.006	4.012	4.014	4.016	4.022	4.126
En	41.3	38.9	44.7	43.9	44.8	46.5	42.8	43.9	41.7	42.4	42.4	41.5	1.6
Fs	13.4	22.8	13.6	13.3	12.9	9.5	13.6	13.5	17.0	13.7	21.0	13.7	62.7
Wo	45.3	38.3	41.7	42.8	42.2	44.0	43.6	42.6	41.3	44.0	36.6	44.8	35.6

Table 4.2: Selected clinopyroxene analyses from the Maningoza Suite. See Tables A2.1 to A2.4 in the Appendix for all pyroxene analyses.

4.3 Olivine

The Berevo Complex gabbros have olivines that are much richer in magnesium than in iron (molecular percentage). The chemical composition of the olivines ranges from $Fo_{74}Fa_{26}$ to $Fo_{70}Fa_{30}$. The Ambereny Complex gabbros have olivines that have higher magnesium content as opposed to iron. The chemical composition of the olivines ranges from $Fo_{70}Fa_{30}$ to $Fo_{67}Fa_{33}$. The Ambohitrosy Complex has olivines with a chemical composition that ranges from $Fo_{73}Fa_{27}$ to $Fo_{64}Fa_{36}$.The basement dykes have olivines that generally have an equal mix of magnesium and iron. The chemical composition of the olivines ranges from $Fo_{60}Fa_{40}$ to $Fo_{45}Fa_{55}$.

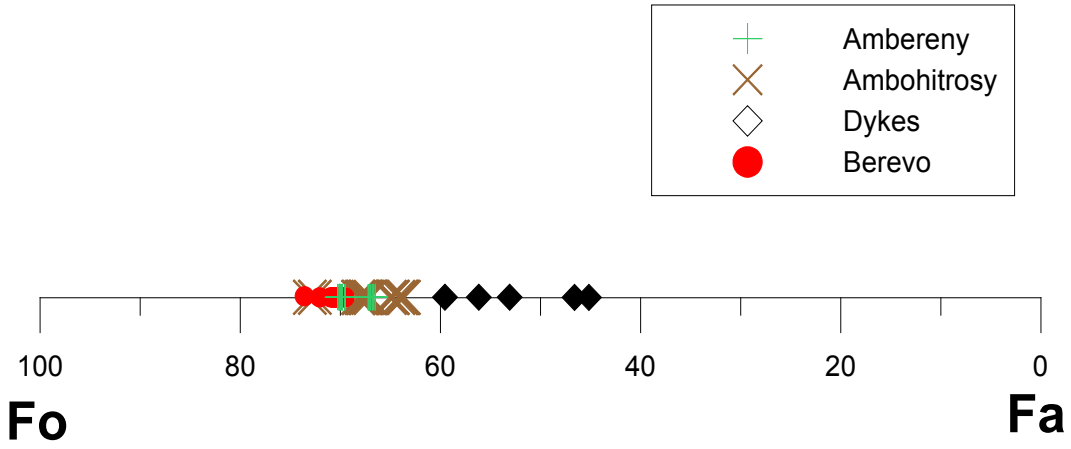

Figure 4.3: The olivine compositions obtained from the electron microprobe are plotted on a Fo/Fa line. The olivine samples all fall within Fo_{74} and Fo_{45} with the Berevo and Ambereny complexes having much higher amounts of forsterite than the dykes. The compositions are expressed in molecular weight percent. (Symbols: Fo = forsterite and Fa = fayalite).

	Ambereny			Dyke		Berevo				Ambohitrosy			
Sample	MI06014	MI06014	MI06019	PF06138	PF06138	PF06017	PF06017	PF06020	PF06020	AB-26A	AB-26A	AB-07	AB-07
SiO_2	38.26	40.67	40.12	38.93	38.85	37.40	37.75	37.21	37.60	37.05	37.36	37.53	37.44
FeO	28.80	28.07	26.09	36.68	34.28	26.61	26.69	25.84	26.17	31.15	30.75	28.22	28.88
MnO	0.45	0.44	0.44	0.61	0.59	0.46	0.46	0.47	0.48	0.50	0.64	0.55	0.48
MgO	33.57	31.78	34.93	26.83	28.81	35.83	35.79	35.85	35.73	31.10	31.60	33.59	33.43
CaO	0.04	0.30	0.04	0.39	0.36	0.07	0.10	0.08	0.07	0.18	0.12	0.10	0.05
Total	101.29	101.58	101.78	103.60	103.06	100.44	100.86	99.51	100.07	100.37	100.71	100.37	100.50
Si^{4+}	1.012	1.062	1.038	1.041	1.034	0.991	0.995	0.992	0.997	1.005	1.007	1.003	1.002
Fe^{2+}	0.637	0.613	0.564	0.820	0.763	0.589	0.589	0.576	0.580	0.707	0.693	0.631	0.647
Mn^{2+}	0.010	0.010	0.010	0.014	0.013	0.010	0.010	0.011	0.011	0.011	0.015	0.012	0.011
Mg^{2+}	1.324	1.236	1.347	1.069	1.143	1.414	1.406	1.425	1.412	1.258	1.269	1.339	1.334
Ca^{2+}	0.001	0.008	0.001	0.011	0.010	0.002	0.003	0.002	0.002	0.005	0.003	0.003	0.001
Sum	2.987	2.935	2.961	2.958	2.965	3.009	3.004	3.007	3.003	2.995	2.997	2.996	2.998
Fo	67.2	66.5	70.1	56.2	59.5	70.2	70.1	70.8	70.5	63.6	64.2	67.5	67.0

Table 4.3: Selected olivine analyses from the Maningoza Suite. See Table A3.1 in the Appendix for all olvine analyses.

4.4 Opaque Minerals

The values of FeO and Fe_2O_3 were recalculated according to the method described by Carmichael (1967). The recalculation was done after the analyses were completed because the electron microprobe cannot distinguish between the different oxidation states of iron. All of the Complexes fall onto the magnetite – ulvöspinel solid solution series except for one analysis from the Fonjay Complex which falls on the ilmenite – Fe_2O_3 solid solution series (Figure 4.4).

Figure 4.4 shows a triangular diagram of FeO, Fe_2O_3 and TiO_2 and all percentages are in molecular percent. The Antanetilava Formation basalts have a composition from 50% Fe_2O_3, 49% FeO and 1% TiO_2 (magnetite) to 15% Fe_2O_3, 60% FeO and 25% TiO_2 (ulvöspinel). The Berevo Complex gabbros have magnetite compositions and the Berevo Complex granites have an oxide composition that ranges from 45% Fe_2O_3, 51% FeO and 4% TiO_2 to 16% Fe_2O_3, 60% FeO and 24% TiO_2. The Ankibobozaka Complex microgabbros have an oxide composition that ranges from 45% Fe_2O_3, 52% FeO and 3% TiO_2 to 27% Fe_2O_3, 57% FeO and 16% TiO_2. The Ambereny Complex gabbros and granites have an oxide composition that ranges from 42% Fe_2O_3, 53% FeO and 5% TiO_2 to 2% Fe_2O_3, 67% FeO and 31% TiO_2. The basement dyke composition ranges from 13% Fe_2O_3, 62% FeO and 25% TiO_2 to 8% Fe_2O_3, 64% FeO and 28% TiO_2. The Fonjay Complex gabbros have one sample that is on the magnetite – ulvöspinel solid solution series and one on the the ilmenite – Fe_2O_3 solid solution series. Their compositions are 28% Fe_2O_3, 59% FeO and 13% TiO_2 (magnetite – ulvöspinel) and 9% Fe_2O_3, 42% FeO and 48% TiO_2 (ilmenite).

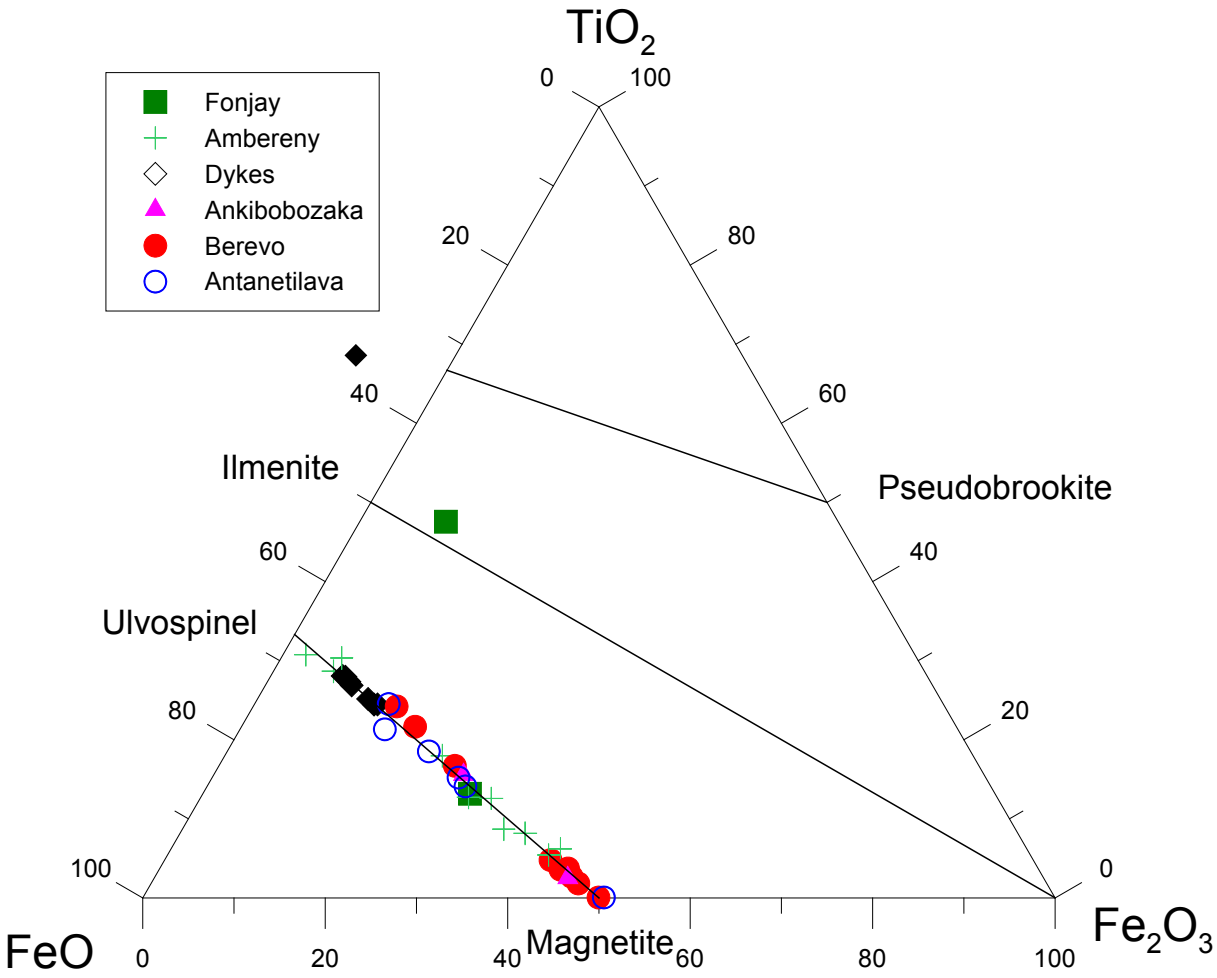

Fig 4.4: Triangular diagram of FeO, TiO_2 and Fe_2O_3 in molecular percentages showing the composition of oxides. The lines indicate solid-solution series.

Complex	Ankibobozaka	Berevo		Fonjay	Ambereny		Antanetilava		Dyke
Sample	PF06004	PF06020	PF06018	MI06010	MI06019	MI06016	PF06132	PF06153	PF06138
Rock type	Microgabbro	Gabbro	Granite	Gabbro	Gabbro	Granite	Basalt	Basalt	Dolerite
TiO_2	1.77	3.35	2.68	10.24	26.55	28.17	18.07	20.49	22.85
Al_2O_3	1.74	2.97	0.27	5.73	5.28	0.40	5.05	1.16	2.70
FeO (T)	89.65	86.51	91.36	81.21	64.90	63.75	72.10	67.80	71.04
MnO	0.05	0.21	0.49	0.46	1.93	3.78	0.23	2.95	1.22
MgO	0.04	0.69	0.07	1.25	0.60	0.02	0.03	0.03	0.25
Total	93.25	93.73	94.87	98.89	99.25	96.12	95.48	92.43	98.06
Ti^{4+}	0.051	0.095	0.076	0.273	0.722	0.813	0.509	0.608	0.635
Al^{3+}	0.078	0.132	0.012	0.239	0.225	0.018	0.223	0.054	0.118
Fe^{3+}	1.820	1.678	1.835	1.214	0.331	0.356	0.759	0.730	0.612
Fe^{2+}	1.047	1.050	1.057	1.193	1.631	1.689	1.500	1.508	1.583
Mn^{2+}	0.002	0.007	0.016	0.014	0.059	0.123	0.007	0.099	0.038
Mg^{2+}	0.002	0.039	0.004	0.066	0.032	0.001	0.002	0.002	0.014
sum	3.000	3.000	3.000	3.000	3.000	3.000	3.000	3.000	3.000
Fe_2O_3	45.3	42.3	44.8	29.3	6.6	6.6	15.9	14.7	12.1
FeO	52.1	52.9	51.5	57.5	64.8	63.0	62.8	60.8	62.7
TiO_2	2.5	4.8	3.7	13.2	28.7	30.3	21.3	24.5	25.2

Table 4.4: Selected opaque analyses from the Maningoza Suite. See Table A4.1 in the Appendix for all opaque mineral analyses.

4.5 Summary

The compositions of the feldspars range from anorthite through albite to orthoclase for the Antanetilava Formation, the Ankibobozaka Complex, the Berevo Complex, the Ambereny Complex, and the Ambohitrosy Complex. The gabbros of the Fonjay Complex have feldspars that are mostly calcium-rich ($An_{88}Ab_{12}Or_0$ to $An_{59}Ab_{39}Or_2$) and the basalts of the Sambao Formation have feldspars that only range from $An_{51}Ab_{47}Or_2$ to $An_4Ab_{96}Or_0$. The compositions of the clinopyroxene are augitic for all complexes with the Ankibobozaka, Berevo, Fonjay and Ambereny Complexes having the least amount of variation. The Ambohitrosy Complex and dyke swarm have the most variation with the compositions of $En_{28}Fs_{33}Wo_{39}$ (Ambohitrosy), $En_{47}Fs_{10}Wo_{43}$ (dyke swarm) and $En_{39}Fs_{32}Wo_{42}$ (dyke swarm). Olivine compositions range from Fo_{74} to Fo_{70} for the Berevo Complex, Fo_{70} to Fo_{67} for the Ambereny Complex and Fo_{73} to Fo_{64} for the Ambohitrosy Complex. The dyke swarm has more iron-rich olivines with compositions of Fo_{60} to Fo_{45}. The opaque minerals have compositions that range from pure hematite compositions (Berevo Complex and Antanetilava Formation) to 83% ilmenite (Fonjay Complex). The Ankibobozaka and Ambereny complexes range from high percentages of hematite to roughly 50% hematite while the Antanetilava Formation ranges to 35% hematite and the Berevo Complex range to 62% hematite. The dyke swarm has a small range in oxide composition from 58% to 48% hematite. Comparison of the mineral chemistry of the Maningoza Suite and other igneous complexes from Madagascar is covered in Chapter 7.

5 GEOCHEMISTRY OF THE MANINGOZA SUITE

The Maningoza Suite is grouped into three sections in this chapter, namely the Maningoza Volcanic Field, the Ring Complexes and the Dykes of the Maningoza Suite in this chapter. The Maningoza Volcanic Field consists of the Maningoza Complex divided into the Ambolodia Formation, Antanetilava Formation and Sambao Formation. The Ring Complexes consist of the Ankibobozaka, Berevo, Fonjay, Ambereny and Ambohitrosy Complexes. The Dykes of the Maningoza Suite consist of the samples from dykes throughout the Maningoza Suite. All three sections begin with classification using a total alkalis vs. silica diagram (TAS diagram, le Bas et al. 1986), followed by descriptions of variations of major and trace elements. Finally, rare-earth element (REE) patterns are described at the end of each section.

5.1 The Maningoza Volcanic Field

5.1.1 Classification

As shown in the total alkalis vs. silica diagram (Figure 5.1) five samples of the Sambao Formation classify as basalts, three samples classify as basaltic andesite, one sample classifies as an andesite and three samples classify as rhyolite. For the Antanetilava Formation seven samples classify as basalts, one classifies as an andesite, one sample classifies as trachyte, one classifies as a dacite and eight samples classify as rhyolite. For the Ambolodia Formation, four samples classify as basalts, one classifies as a basaltic andesite, two classify as trachy-andesite, one classifies as an andesite, one sample classifies as a dacite and three classify as a rhyolite.

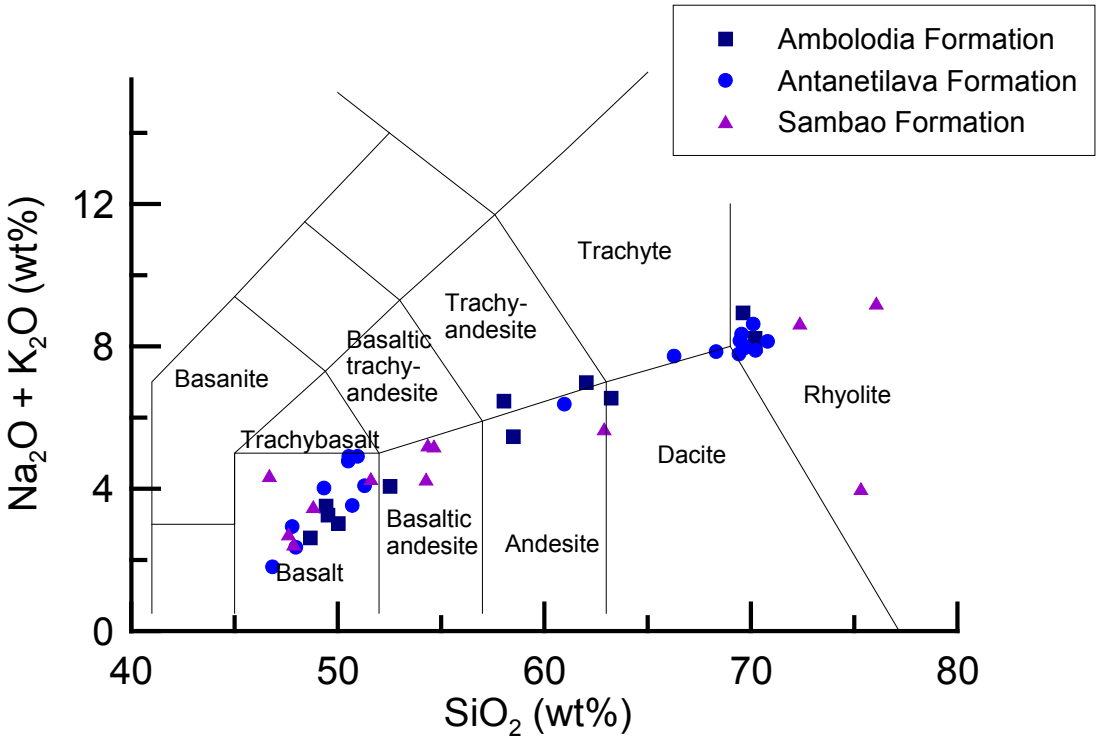

Figure 5.1: Plots of the Maningoza Volcanic Field samples on the TAS Diagram.

5.1.2 Major Elements vs. SiO_2

Figure 5.2 shows diagrams of SiO_2 versus major elements for the Ambolodia, Antanetilava and Sambao Formations. The Ambolodia Formation shows strong negative correlations for SiO_2 versus CaO (r = -0.97) and FeO (r = -0.93). The Antanetilava Formation shows similar strong negative correlations with an r value for CaO against SiO_2 of -0.94 and an r value for FeO against SiO_2 of -0.81. The Sambao Formation follows suit by having an r value for CaO against SiO_2 of -0.88 and an r value for FeO against SiO_2 of -0.93. For SiO_2 versus TiO_2 the Ambolodia Formations shows a strong negative correlation (r = -0.78) as well as for SiO_2 versus Al_2O_3 (r = -0.72). The Antanetilava Formation shows a strong negative correlation with SiO_2 against Al_2O_3 (r = -0.70) but a weak negative correlation for SiO_2 against TiO_2 (r = -0.45). The Sambao Formation shows strong negative correlations for SiO_2 against Al_2O_3 (r = -0.67) and SiO_2 against TiO_2 (r = -0.84).

The Ambolodia Formation shows a strong positive correlation (Figure 5.2) between SiO_2 and K_2O (r = 0.98) which is similar to the Antanetilava Formation (r = 0.98) and the Sambao Formation (r = 0.77). For Na_2O against SiO_2 the Ambolodia Formation shows a strong positive correlation (r = 0.79) which is similar to the Antanetilava Formation (r = 0.64) but the Sambao Formation shows very little correlation (r = 0.12).

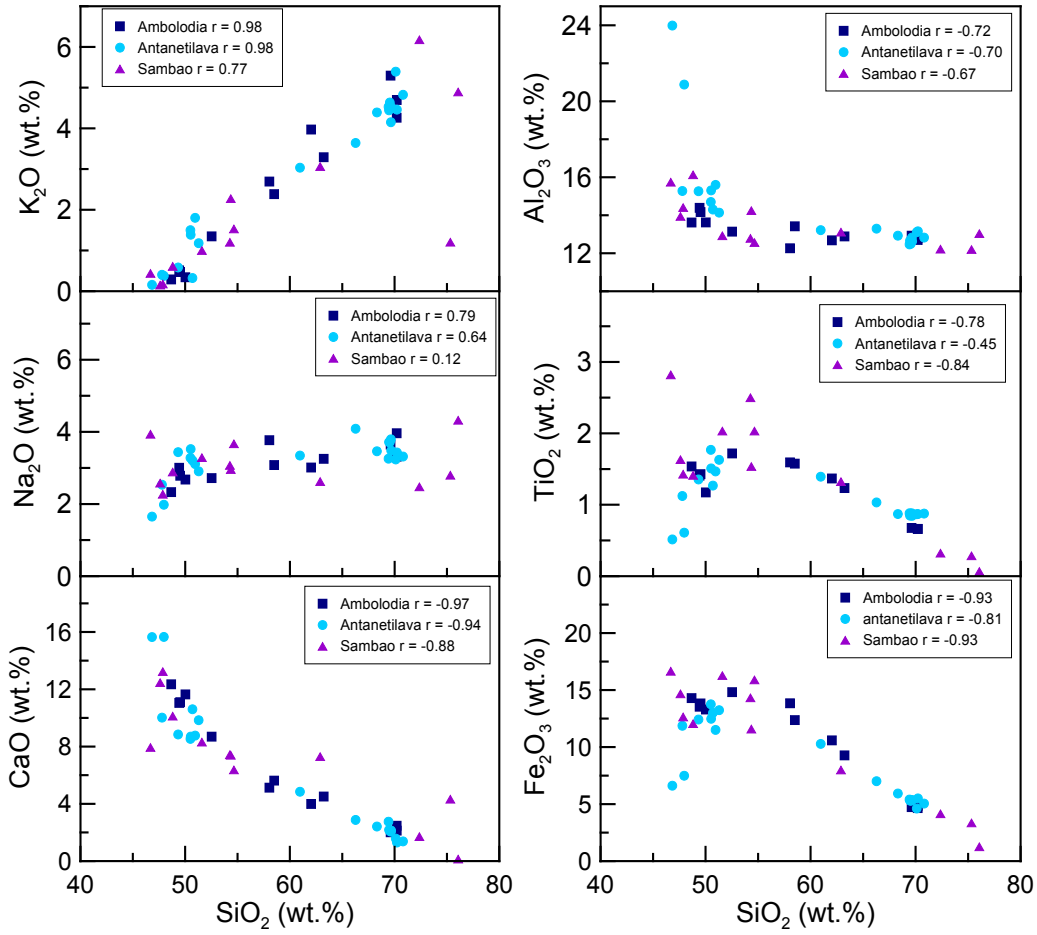

Figure 5.2: Plots of major and minor elements versus SiO_2 (wt. %) for the Ambolodia, Antanetilava and Sambao Formations.

5.1.3 Major Elements vs. MgO

Figure 5.3 shows diagrams of major elements versus MgO for the Ambolodia, Antanetilava and Sambao Formations. The Ambolodia Formation shows strong negative correlation for MgO against SiO_2 (r = -0.95) and MgO against K_2O (r = -0.96). The Antanetilava Formation shows similar correlations with an r value of -0.91 for MgO against SiO_2 and an r value of -0.89 for MgO against K_2O. The Sambao Formation has slightly lower r values than the previous two formations but are still strong and negative for MgO against SiO_2 (r = -0.89) and K_2O (r = -0.73). For MgO against Na_2O the Ambolodia Formation has a strong negative correlation (r = -0.81) but the Antanetilava and Sambao Formations both have a weak negative correlation with an r value of -0.29.

There is a strong positive correlation between MgO and CaO (Figure 5.3) for the Ambolodia (r = 0.99), Antanetilava (r = 0.76) and the Sambao Formations (r = 0.89). MgO against Al_2O_3 shows a strong positive correlation for the Ambolodia Formation (r = 0.83) and Sambao

Formation (r = 0.79) but a weak positive correlation for the Antanetilava Formation (r = 0.45). MgO versus Fe_2O_3 shows strong positive correlations for the Ambolodia (r = 0.77), Antanetilava Formations (r = 0.84) and the Sambao Formation (r = 0.68). MgO against TiO_2 shows weak positive correlations for the Antanetilava (r = 0.51), Ambolodia Formation (r = 0.54) and Sambao Formations (r = 0.53).

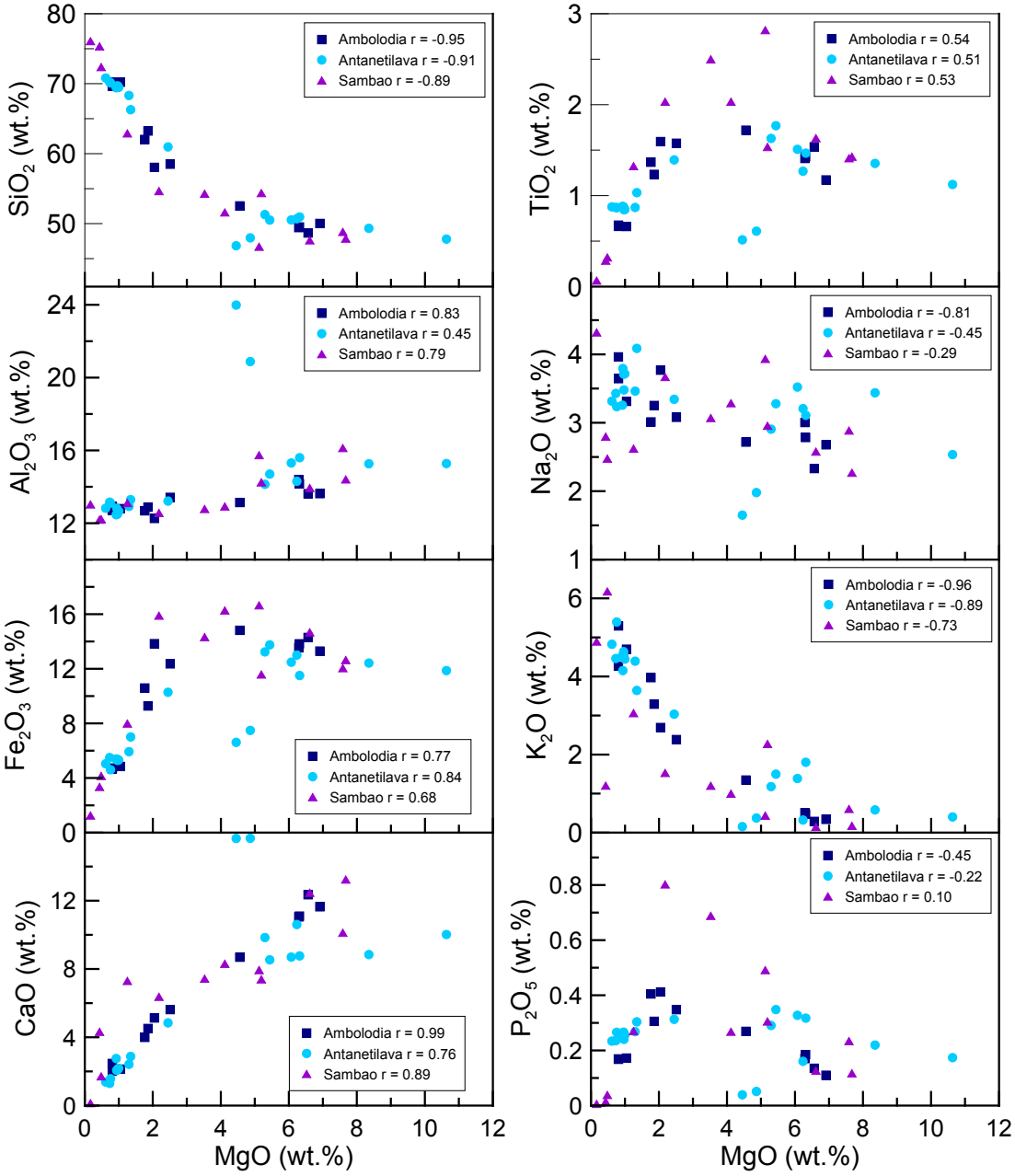

Figure 5.3: Plots of major and minor elements versus MgO (wt. %) for the Ambolodia, Antanetilava and Sambao Formations.

5.1.4 Trace Elements vs. SiO_2

Figure 5.4 shows plots of SiO_2 (wt. %) versus trace elements for the Ambolodia, Antanetilava and Sambao Formations. The Ambolodia Formation shows strong positive correlations for SiO_2 plotted against Rb (r = 0.98) and Nb (r = 0.98). The Antanetilava Formation also shows a strong positive correlation for SiO_2 plotted against Rb (r = 0.96) and Nb (r = 0.94). The Sambao Formation follows suit with r values of 0.73 for SiO_2 versus Rb and 0.75 for SiO_2 versus Nb. SiO_2 (wt.%) plotted against Zr shows strong positive correlations for the Ambolodia (r = 0.99) and Antanetilava Formations (r = 0.96) but the Sambao Formation shows a weak positive correlation (r = 0.53). SiO_2 (wt.%) plotted against Y shows a similar correlation with r values of 0.86 for the Ambolodia Formation, 0.94 for the Antanetilava Formation and 0.46 for the Sambao Formation.

There is a weak negative correlation between Sr and SiO_2 (Figure 5.4) for the Sambao Formation (r = -0.53), but a strong negative correlation for the Ambolodia Formation (r = -0.72) and the Antanetilava Formation (r = -0.76). SiO_2 plotted against Ni shows a strong negative for the Ambolodia Formation (r = -0.88), the Antanetilava Formation (r = -0.74) and the Sambao Formation (r = -0.63). The felsic samples of the Sambao Formation are generally inconsistent with the rest of the samples from the Sambao Formation especially in the case of Nb where they have a much higher concentrations than the other samples, and lie off the strongly correlated array.

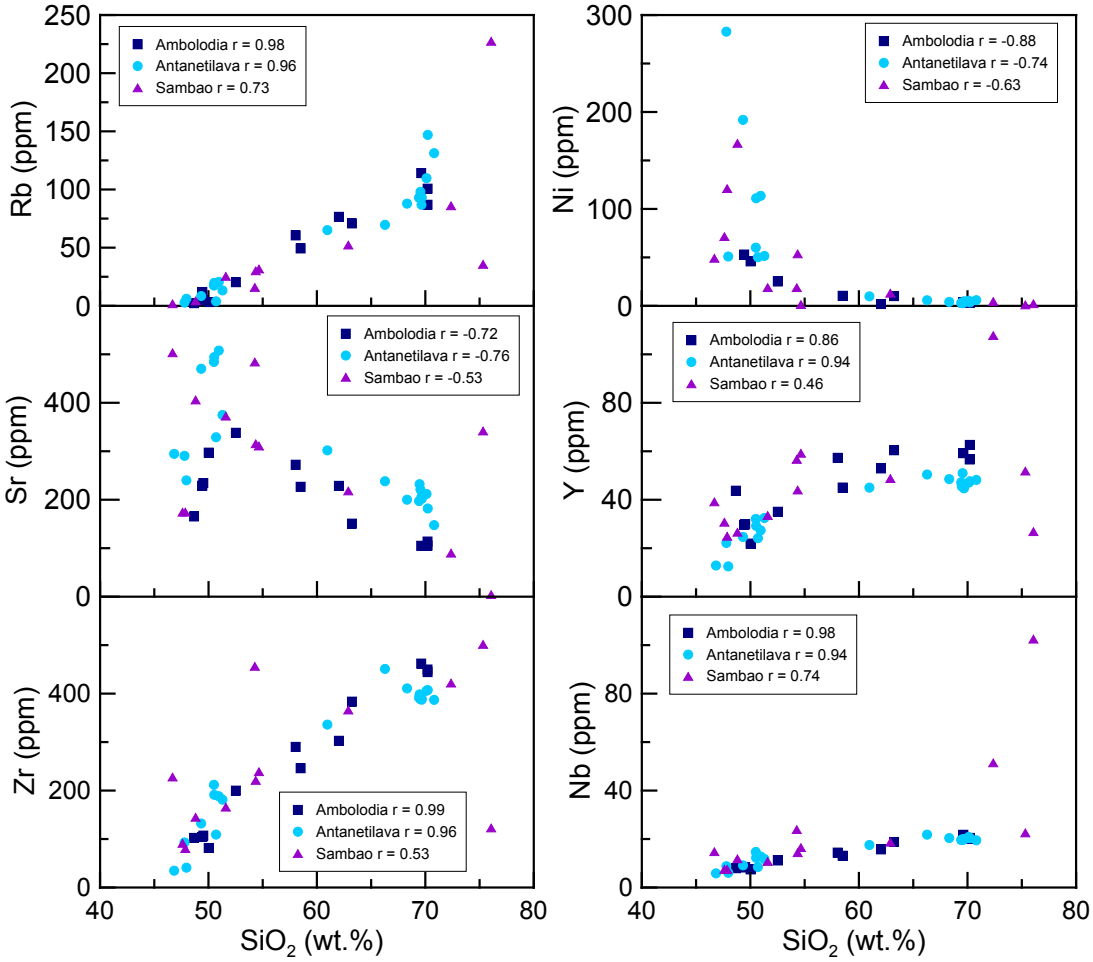

Figure 5.4: Plots of trace elements against SiO_2 for the Ambolodia, Antanetilava and Sambao Formations.

5.1.5 Trace Elements vs. Zr

Figure 5.5 shows plots of Zr (ppm) against trace elements for the Ambolodia, Antanetilava and Sambao Formations. Zr plotted against Y shows a strong positive correlation for all three formations with r values of 0.90 for the Ambolodia Formation, 0.99 for the Antanetilava Formation and 0.71 for the Sambao Formation. Zr plotted against Th shows a strong positive correlation for the Ambolodia Formation (r = 0.97) and the Antanetilava Formation (r = 0.96) as well as the Sambao Formation (r = 0.61). Zr against Sr shows a strong negative correlation for the Ambolodia (r = -0.69) and Antanetilava Formations (r = -0.59) where as the Sambao Formation shows a weak positive correlation (r = 0.24).

There are extremely strong correlations between Nb and Zr (Figure 5.5) for the Ambolodia (r = 1.00) and Antanetilava Formations (r = 1.00) but the Sambao Formation shows little correlation (r = 0.05). Zr against Rb shows strong positive correlations for the Ambolodia

(r = 0.97) and Antanetilava Formations (r = 0.90) where as the Sambao Formation shows a weak negative correlation (r = -0.22). Zr plotted against Ba shows a strong positive correlation for all three of the formations with r values of 0.92 for the Ambolodia Formation, 0.97 for the Antanetilava Formation and 0.96 for the Sambao Formation.

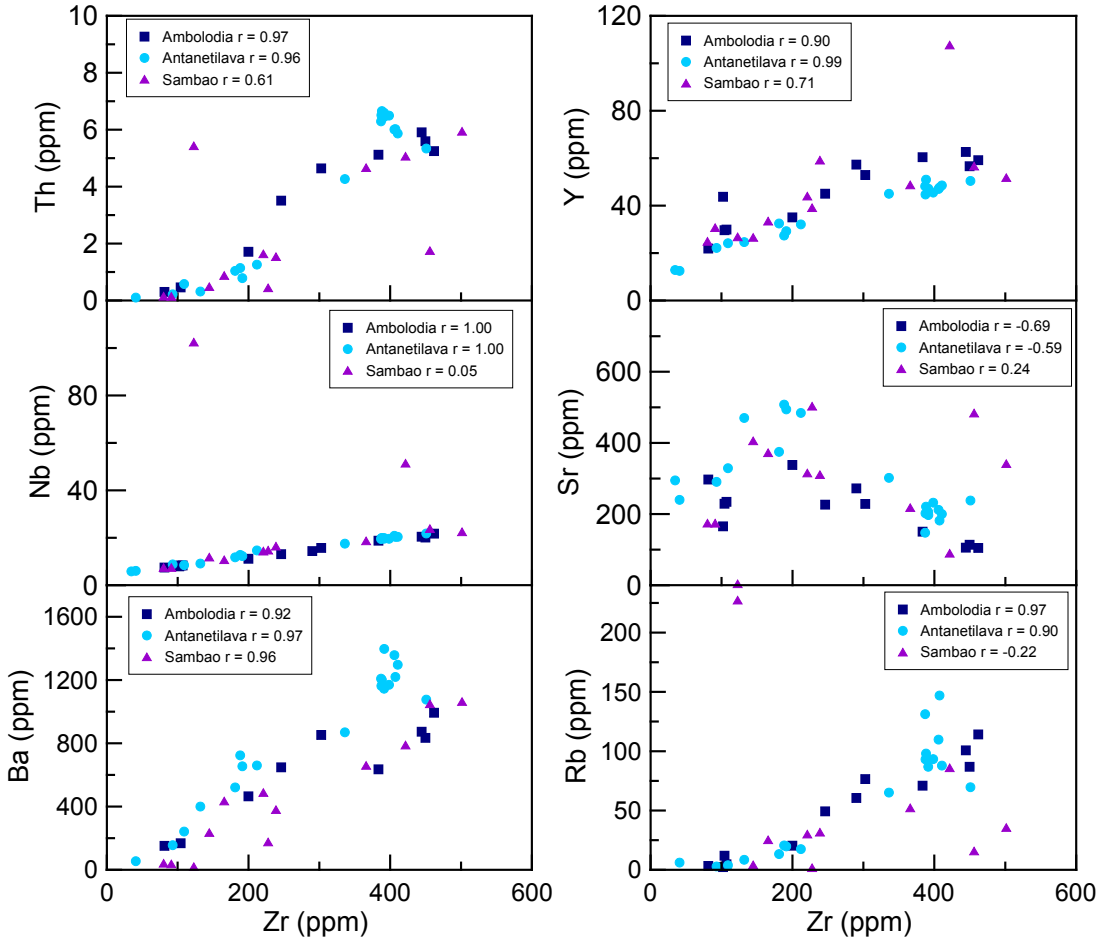

Figure 5.5: Plots of trace elements versus Zr (ppm) for the Ambolodia, Antanetilava and Sambao Formations.

5.1.6 Rare Earth Element Patterns

Chondrite-normalised REE (rare earth elements) patterns are shown in Figure 5.6 and have been calculated using the normalising factors given by Nakamura (1974). The Ambolodia, Antanetilava and Sambao Formations have similar REE patterns in that they have low concentrations of heavy rare earth elements (HREE) and comparatively high concentrations of light rare earth elements (LREE) so that the slope of the curve increases towards the LREE side. Samples PF06121, PF06127, PF06129, BY6F090 and BY6F090 are exceptions in that the curve slopes down towards the LREE. Sample BY6F098b also has a much higher concentration of REE and sample BY6F148 has a much lower concentration of REE when

compared to the rest of the Sambao Formation. The Eu anomalies are generally low for the felsic samples and only slightly high for more mafic samples for each of the formations. Average Eu/Eu* are 0.81 for the Ambolodia Formation, 0.87 for the Antanetilava Formation and 0.84 for the Sambao Formation. The Antanetilava Formation sample PF06129 which is a feldspar porphyry basalt has lower concentrations of REE in comparison with other mafic samples. Two felsic samples of the Sambao Formation (BY6F148 and BY6F098b) have very low Eu anomalies (Eu/Eu* = 0.29 and 0.32, respectively).

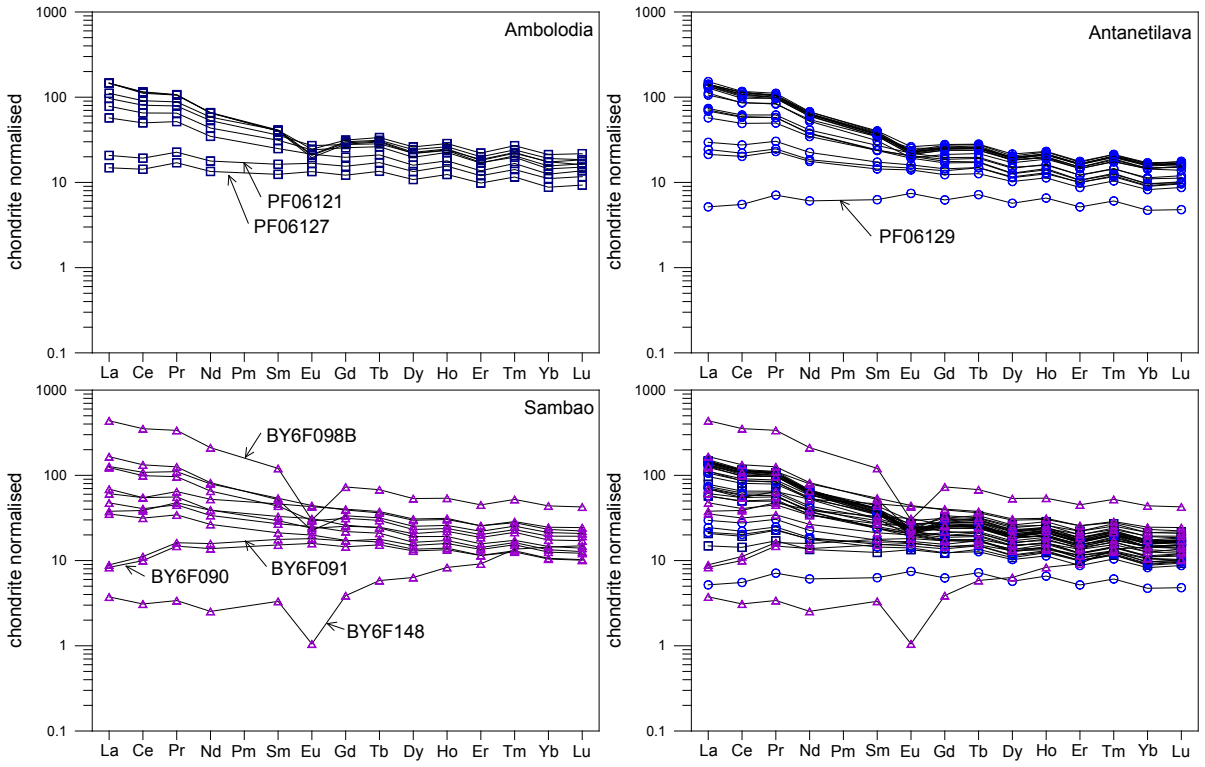

Figure 5.6: REE patterns for the Ambolodia, Antanetilava and Sambao Formations.

5.2 The Ring Complexes

Major and REE data for the Ambohitrosy Complex was taken from the thesis of Rasolofomanana (1998) but lacked trace element data required here. The Ambohitrosy Complex, therefore, does not feature in the variations with trace elements section.

5.2.1 Classification

From the total alkalis vs. silica diagram (Figure 5.7) the Berevo Complex has eight samples that classify as basalt, two samples that classify as basaltic andesite, one sample that classifies as a trachyte and five samples that classify as rhyolite. The Ankibobozaka Complex has one sample which classifies as a basalt, one as a basaltic andesite and four

samples which classify as rhyolites. The Fonjay Complex has five samples which classify as basalt and one sample which classifies as a trachyandesite. The Ambereny Complex has five samples that classify as basalt and one sample that classifies as a rhyolite. The Ambohitrosy Complex has one sample that classifies as a basanite, another sample that classifies as a picrobasalt and thirteen samples that classify as basalt. The Ambohitrosy Complex also has six samples that classify as basaltic andesite, two samples that classify as trachyandesite, two samples that classify as dacite, ten samples that classify as trachyte and six samples that classify as rhyolite.

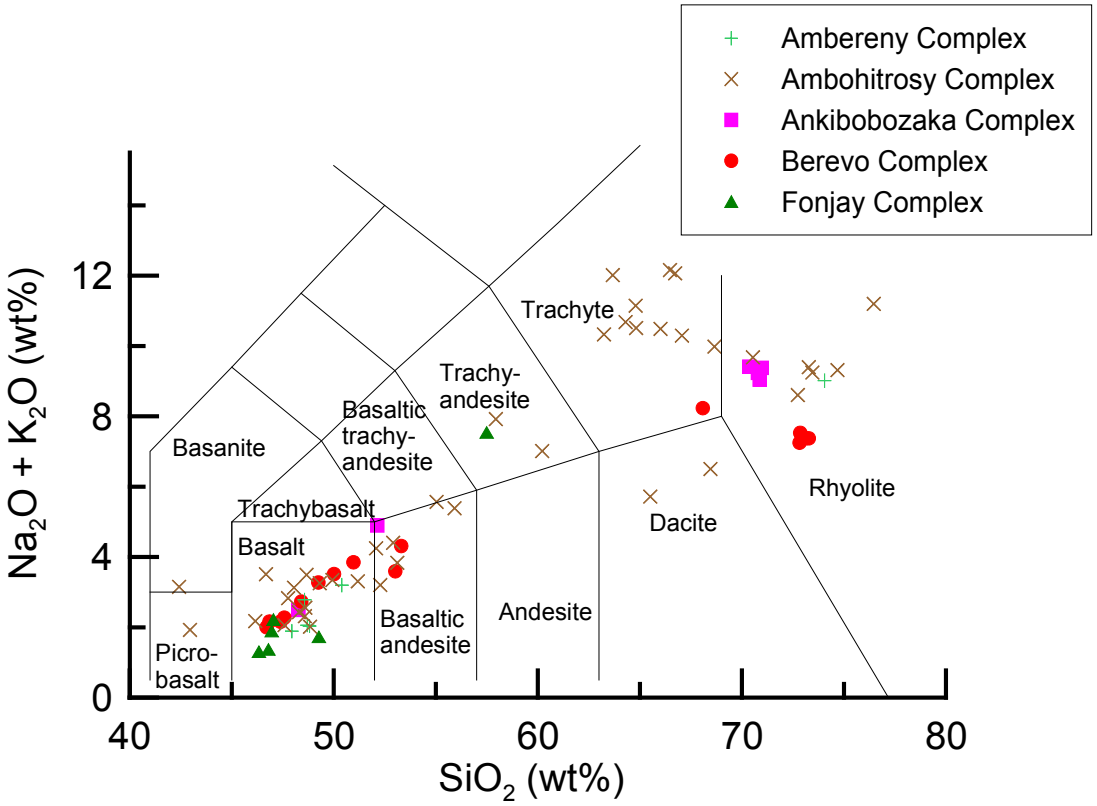

Figure 5.7: Plots of the Maningoza Ring Complexes on the TAS Diagram.

5.2.2 Major Elements vs. SiO_2

Figure 5.8 shows diagrams of SiO_2 versus major elements for the Ankibobozaka, Berevo, Fonjay, Ambereny and Ambohitrosy Complexes. All of the complexes show a strong negative correlation for SiO_2 versus CaO with r values of -0.99 for the Ankibobozaka Complex, -0.95 for the Berevo Complex, -0.97 for the Fonjay Complex, -0.91 for the Ambereny Complex and -0.93 for the Ambohitrosy Complex. For SiO_2 versus K_2O there is a strong positive correlation for all the complexes with r values of 1.00 for the Ankibobozaka Complex, 0.99 for the Berevo Complex, 0.93 for the Fonjay Complex, 1.00 for the Ambereny

Complex and 0.95 for the Ambohitrosy Complex. SiO_2 against Na_2O shows strong positive correlations for the Ankibobozaka (r = 0.96), Fonjay (r = 0.97), Ambereny (r = 0.84) and Ambohitrosy Complexes (r = 0.74) but the Berevo Complex shows a weak positive correlation for SiO_2 against Na_2O (r = 0.55).

There is a strong negative correlation between SiO_2 and Al_2O_3 (Figure 5.8) for the Ankibobozaka (r = -0.94), Berevo (r = -0.68) and Ambereny Complexes (r = -0.78) where as the Fonjay and Ambohitrosy Complexes show weak negative correlations (r = -0.53 and r = -0.35 respectively). SiO_2 plotted against Fe_2O_3 shows strong negative correlations for the Ankibobozaka Complex (r = -0.99), Berevo Complex (r = -0.70) and the Ambohitrosy Complex (r = -0.80). SiO_2 plotted against Fe_2O_3 shows weak negative correlations for the Ambereny Complex (r = -0.58) where as the Fonjay Complex shows a weak positive correlation (r = 0.46). SiO_2 plotted against TiO_2 also shows strong negative correlations for the Ankibobozaka Complex (r = -0.91) and the Ambohitrosy Complex (r = -0.70), weak negative correlations for the Berevo (r = -0.28) and Ambereny Complexes (r = -0.22), and a weak positive correlation for the Fonjay Complex (r = 0.32).

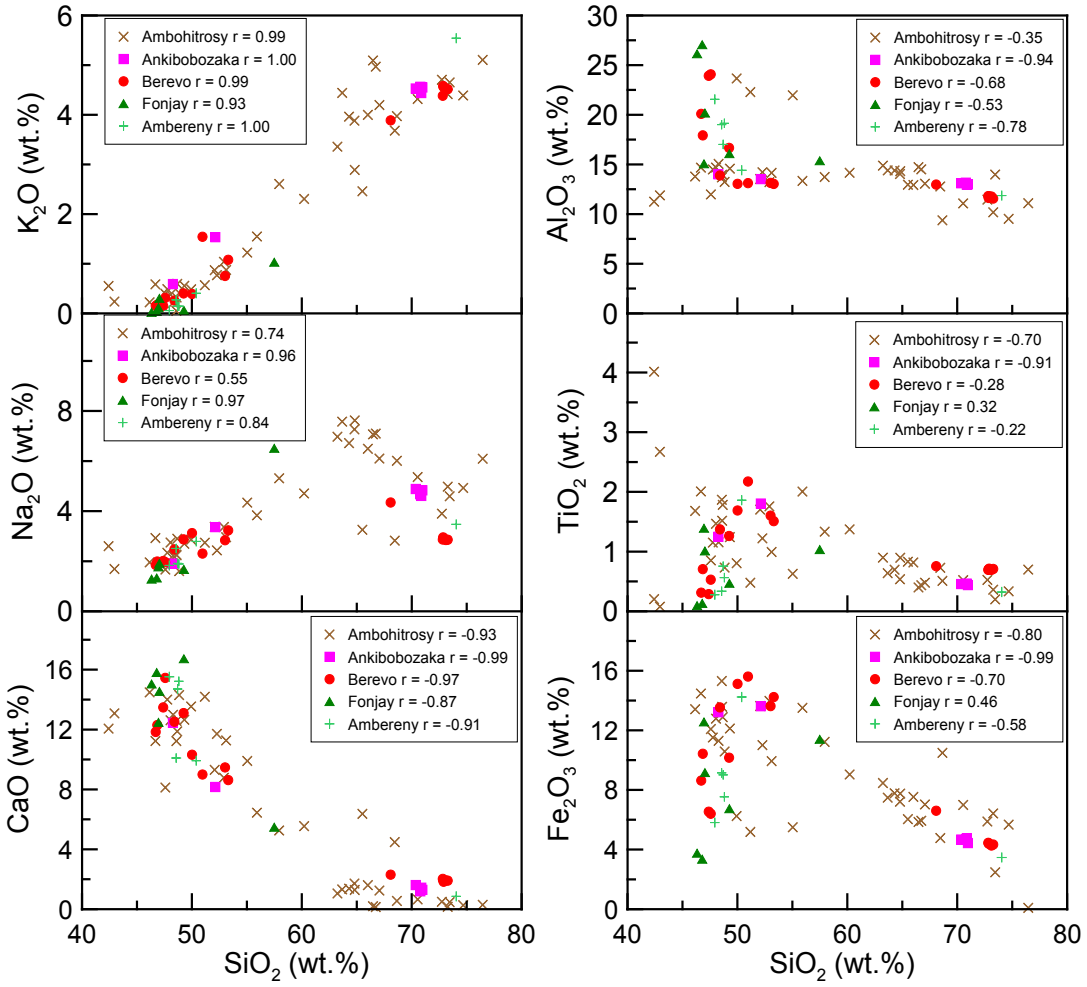

Figure 5.8: Plots of major and minor elements versus SiO_2 (wt. %) for the Ankibobozaka, Berevo, Fonjay, Ambereny and Ambohitrosy Complexes.

5.2.3 Major Elements vs. MgO

Figure 5.9 shows diagrams of MgO versus major elements for the Ankibobozaka, Berevo, Fonjay, Ambereny and Ambohitrosy Complexes. All of the complexes show a strong negative correlation for MgO against SiO_2 with r values of -0.99 for the Ankibobozaka Complex, -0.89 for the Berevo Complex, -0.76 for the Fonjay Complex, -0.90 for the Ambereny Complex and -0.82 for the Ambohitrosy Complex. Similarly, the plot of MgO against K_2O shows strong negative correlations for all the complexes with r values of -1.00 for the Ankibobozaka Complex, -0.79 for the Berevo Complex, -0.86 for the Fonjay Complex, -0.89 for the Ambereny Complex and -0.82 for the Ambohitrosy Complex. MgO plotted against Na_2O shows strong negative correlations for the Ankibobozaka Complex (r = -0.99), the Fonjay Complex (r = -0.82), the Ambereny Complex (r = -0.71) and the Ambohitrosy Complex (r = -0.80) where as the Berevo Complex shows a weak negative correlation (r = -0.36). MgO plotted against CaO shows a strong positive correlation for all the

complexes with r values of 1.00 for the Ankibobozaka Complex, 0.87 for the Berevo Complex, 0.74 for the Fonjay Complex, 0.74 for the Ambereny Complex and 0.77 for the Ambohitrosy Complex.

There is a strong positive correlation between Al_2O_3 and MgO (Figure 5.9) for the Ankibobozaka Complex (r = 0.97) and the Ambereny Complex (r = 0.77), the Berevo Complex shows a weak positive correlation (r = 0.58) and both the Fonjay and the Ambohitrosy Complex show no correlation (r = -0.02 and r =0.01 respectively). MgO plotted against Fe_2O_3 shows strong positive correlation for the Ankibobozaka Complex (r = 0.96) and Ambohitrosy Complex (r = 0.64) where as the Berevo and Ambereny Complexes show a weak positive correlation (r = 0.51 and r = 0.44 respectively). The Fonjay Complex shows no correlation for Fe_2O_3 versus MgO(r = -0.14) and shows no correlation with MgO plotted against TiO_2 (r = -0.07). The Ambereny Complex also shows no correlation with MgO plotted against TiO_2 (r = -0.03). MgO vs. TiO_2 also shows a strong positive correlation for the Ankibobozaka Complex (r = 0.85) and a weak positive correlation for the Berevo Complex (r = 0.21) and Ambohitrosy Complex (r = 0.47).

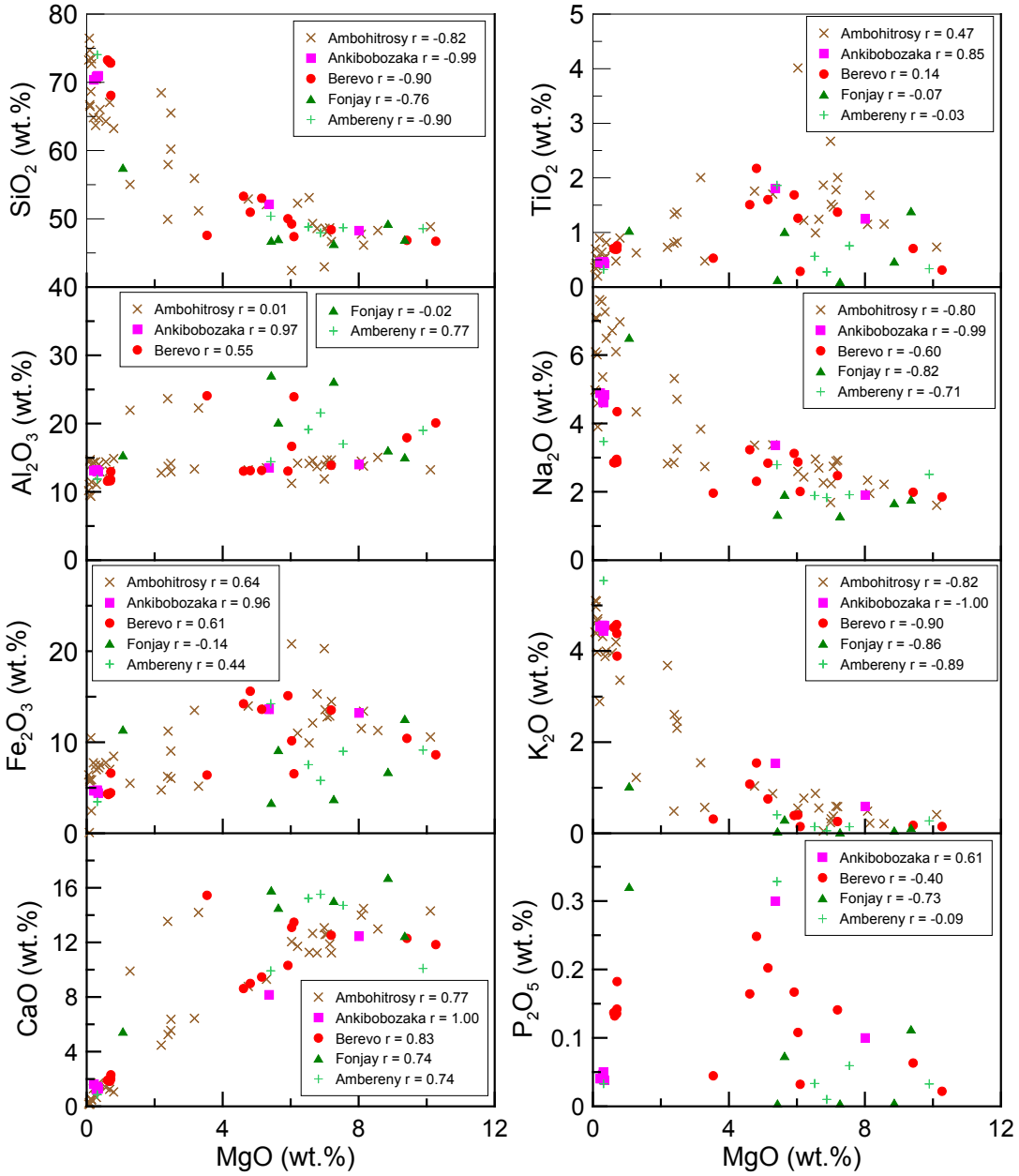

Figure 5.9: Plots of major and minor elements versus MgO (wt. %) for the Ankibobozaka, Berevo, Fonjay, Ambereny and Ambohitrosy Complexes.

5.2.4 Trace Elements vs. SiO_2

Figure 5.10 shows plots of SiO_2 versus trace elements for the Ankibobozaka Complex, the Berevo Complex, the Fonjay Complex and the Ambereny Complex. The Ambohitrosy Complex has been disregarded due to insufficient trace element data. All four complexes have a strong positive correlation for SiO_2 plotted against Rb with r values equal to 0.99 for the Ankibobozaka Complex, 0.99 for the Berevo Complex, 0.91 for the Fonjay Complex and 1.00 for the Ambereny Complex. SiO_2 plotted against Ni shows strong negative correlations

for the Ankibobozaka (r = -0.91), Berevo (r = -0.66), Fonjay (r = -0.76) and Ambereny Complexes (r = -0.66). SiO_2 plotted against Sr shows a strong negative correlation for the Berevo Complex (r = -0.91), Ankibobozaka Complex (r = -0.61) and the Fonjay Complex (r = -0.64) where as the Ambereny Complex shows a weak negative correlation (r = -0.55).

There is a strong positive correlation between Y and SiO_2 (Figure 5.10) for all four complexes with r values of 0.98 for the Ankibobozaka Complex, 0.82 for the Berevo Complex, 0.91 for the Fonjay Complex and 0.96 for the Ambereny Complex. SiO_2 plotted against Zr shows similar correlations with r values of 0.99 for the Ankibobozaka Complex, 0.95 for the Berevo Complex and 0.88 for the Fonjay and Ambereny Complexes. SiO_2 plotted against Nb follows the previous two cases with r values of 0.99 for the Ankibobozaka Complex, 0.98 for the Berevo Complex, 0.87 for the Fonjay Complex and 0.95 for the Ambereny Complex.

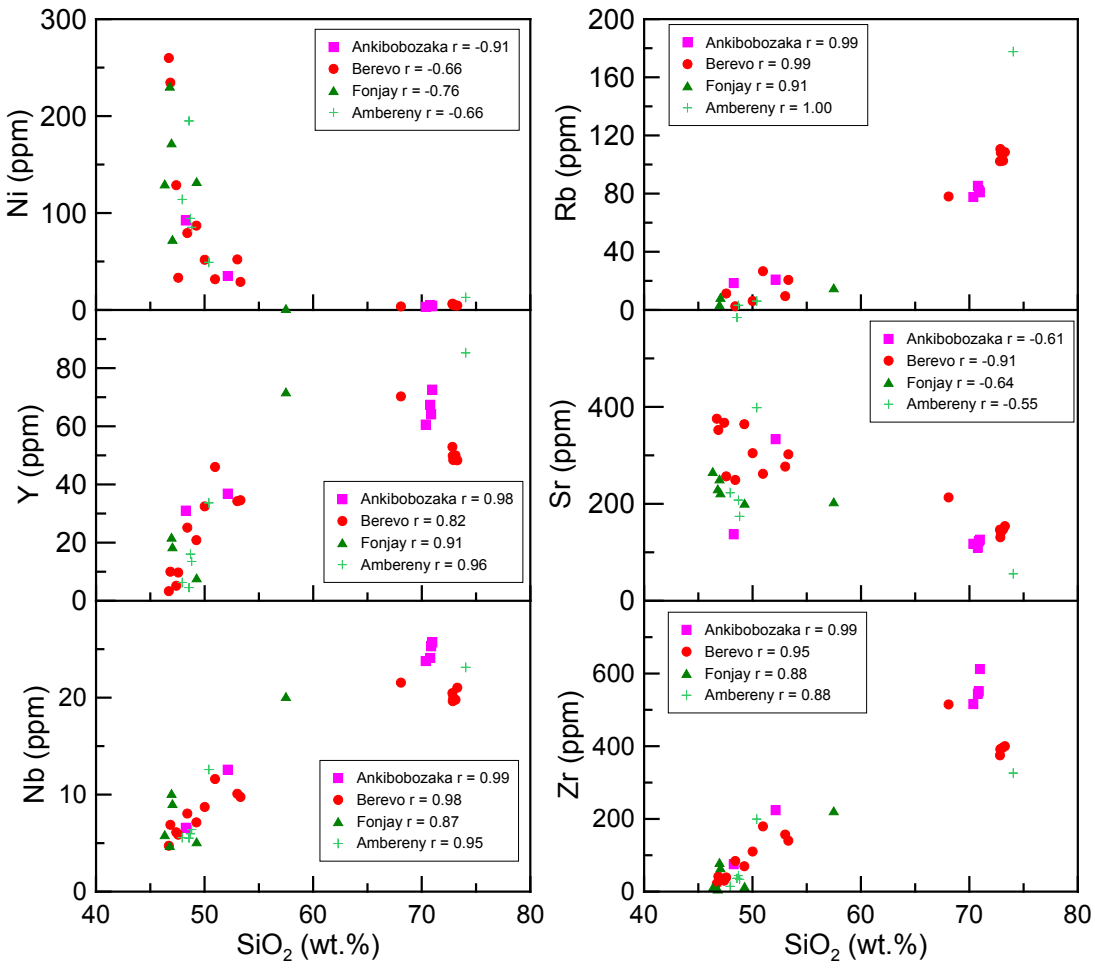

Figure 5.10: Plots of trace elements against SiO_2 for the Ankibobozaka, Berevo, Fonjay and Ambereny Complexes.

5.2.5 Trace Elements vs. Zr

Figure 5.11 shows plots of Zr (ppm) versus trace elements for the Ankibobozaka Complex, Berevo Complex, Fonjay Complex and Ambereny Complex. There is a strong positive correlation between Y and Zr for all four complexes with r values equal to 0.99 for the Ankibobozaka Complex, 0.93 for the Berevo Complex, 0.99 for the Fonjay Complex and 0.96 for the Ambereny Complex. Zr plotted against Th shows similar correlations with r values equal to 0.99 for the Ankibobozaka Complex, 0.93 for the Berevo Complex, 1.00 for the Fonjay Complex and 0.89 for the Ambereny Complex. The correlation between Zr and Sr is strong and negative for the Berevo Complex (r = -0.87) where as the correlations for the Ankibobozaka, Fonjay and Ambereny Complexes are weak and negative (r = -0.51, r = -0.41 and r = -0.36 respectively).

There is a strong positive correlation between Nb and Zr (Figure 5.11) for all of the complexes with r values equal to 1.00 for the Ankibobozaka Complex, 0.99 for the Berevo Complex, 1.00 for the Fonjay Complex and 0.98 for the Ambereny Complex. The correlations between Zr plotted against Rb are strong and positive for all four complexes (Ankibobozaka r = 0.97, Berevo r = 0.91, Fonjay r =0.87, Ambereny r = 0.84). All four complexes taken together show a strong positive correlation between Zr and Ba, with r greater than 0.97 in all complexes.

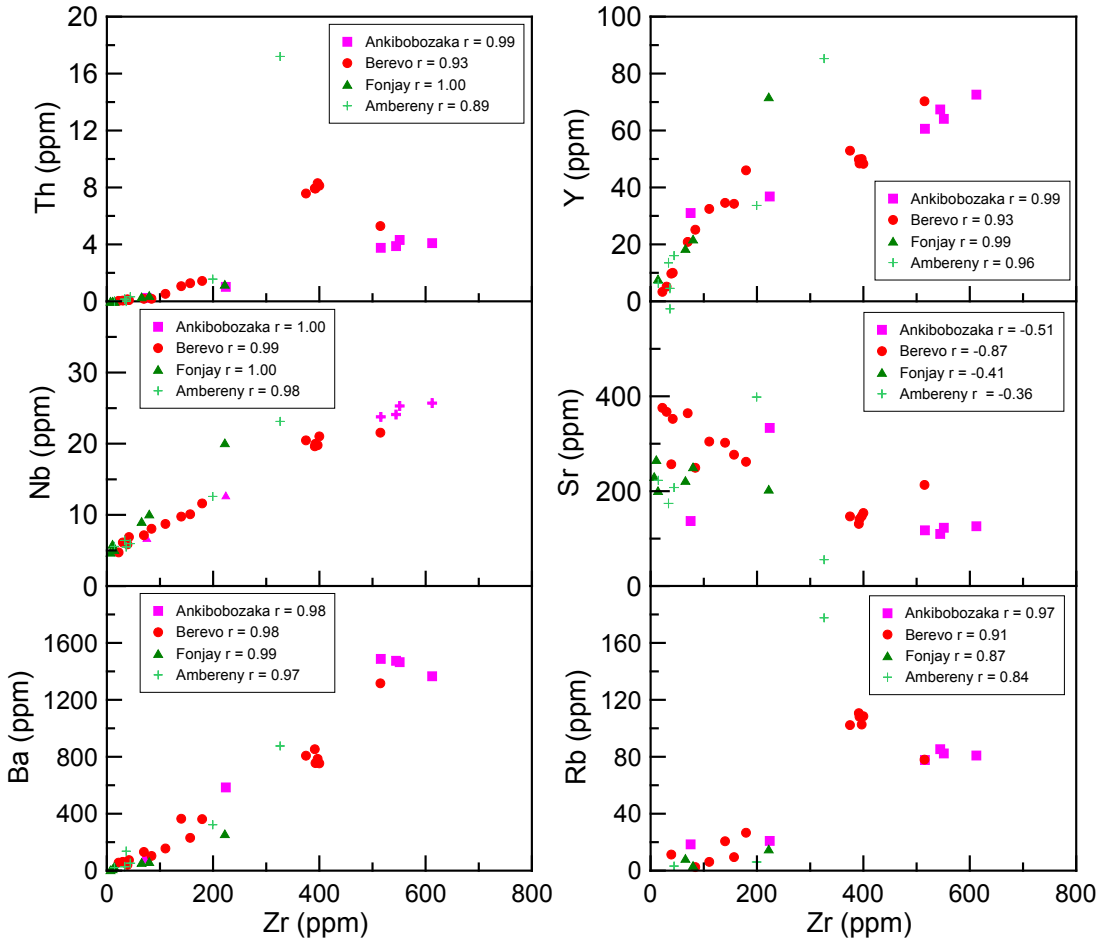

Figure 5.11: Plots of trace elements against Zr (ppm) for the Ankibobozaka, Berevo, Fonjay and Ambereny Complexes.

5.2.6 Rare Earth Element Patterns

Chondrite-normalised REE patterns are shown in Figure 5.12 and have been calculated according to Nakamura (1974). The Ankibobozaka Complex, Berevo Complex and Ambereny complex have similar REE patterns in that the felsic samples of each complex generally have a higher concentration of LREE compared to HREE. The more mafic samples have a straight/flat pattern but in some cases a decrease in concentration of LREE giving a slight slope is observed. The Eu anomalies for the three complexes are similar in that the felsic samples have low Eu anomalies and the mafic samples have high Eu anomalies. The average Eu/Eu* is 0.79 for the Ankibobozaka Complex, 1.03 for the Berevo Complex and 1.27 for the Ambereny Complex. The Fonjay Complex, consisting of gabbros only, generally has a low concentration of REE and has a high Eu anomaly. The Fonjay Complex also has two samples (MI06011 and MI06013) which have the lowest concentration of REE in comparison with the other complexes. The samples MI06011 and MI06013 also have the highest Eu anomalies with Eu/Eu* = 4.38 and 3.44 respectively. The Ambohitrosy Complex

has a REE pattern which is straight, although a few of the felsic samples have higher concentrations of LREE and HREE compared to the rest of the complex. The REE pattern of the Ambohitrosy Complex has very few cases of REE patterns crossing one another. The Ambohitrosy Complex also has low Eu anomalies for felsic samples and high Eu anomalies for mafic samples and has an average Eu/Eu* of 0.80.

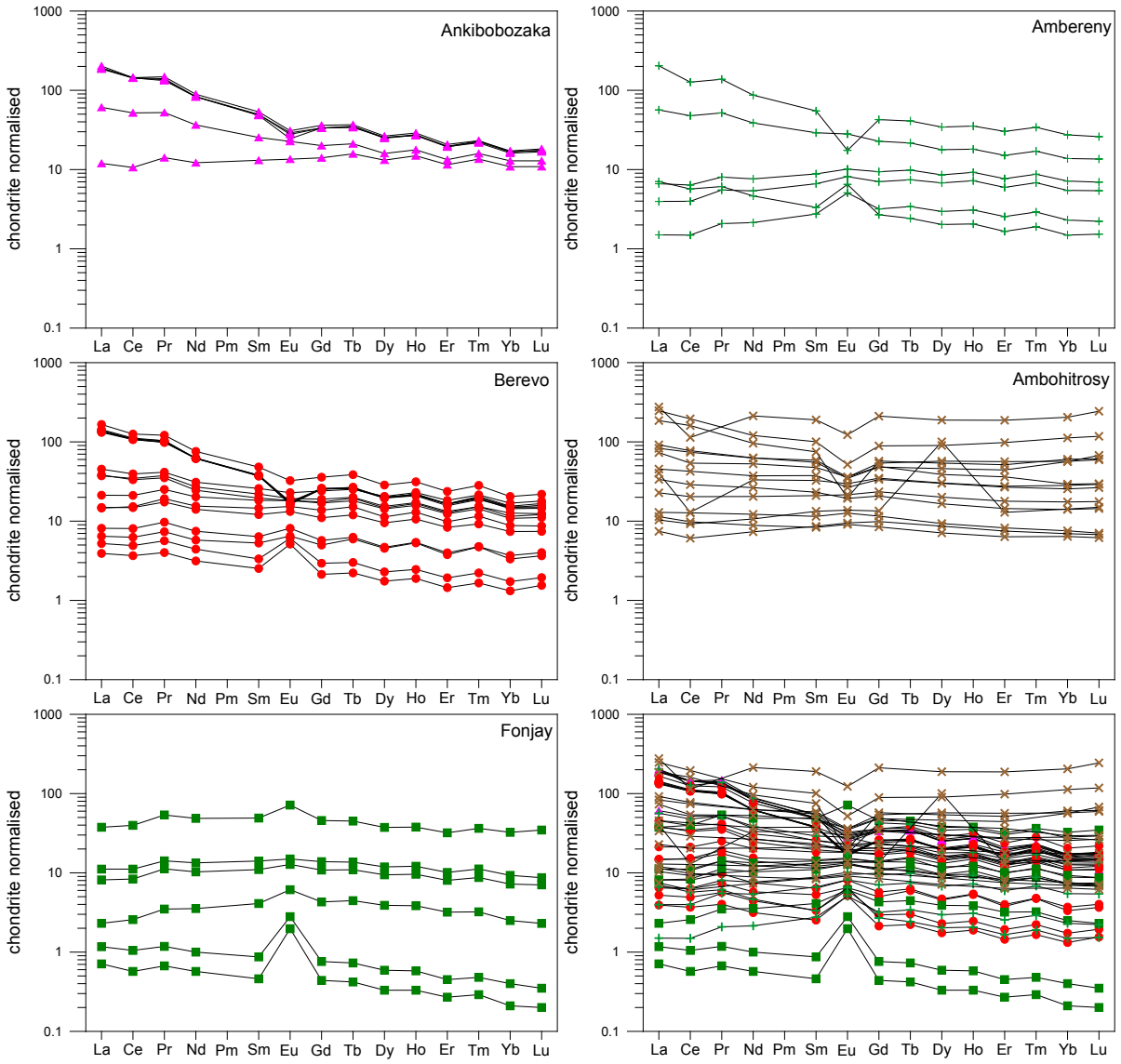

Figure 5.12: REE patterns for the Ankibobozaka, Berevo, Fonjay, Ambereny and Ambohitrosy Complexes.

5.3 Dykes of the Maningoza Suite

The dykes of the Maningoza Suite are composed of four groups based on where they where sampled. Five samples were sampled from the Berevo Complex, three samples from the Ambolodia Formation, two samples from the Sambao Formation and three from the surrounding basement. All groups are shown together in variation and REE plots.

5.3.1 Classification

Classification of the dykes is described by the use of the TAS diagram. As shown in Figure 5.13 two samples of the Berevo dykes classify as trachytes, one as a rhyolite, one as an andesite and one as a basaltic trachyandesite. The Ambolodia dykes have one sample that classifies as a rhyolite and two that classify as basalt. The two samples of the Sambao dykes are both classified as basalts. The basement dykes have one sample classified as a basalt, one sample as a basaltic andesite and one as a rhyolite.

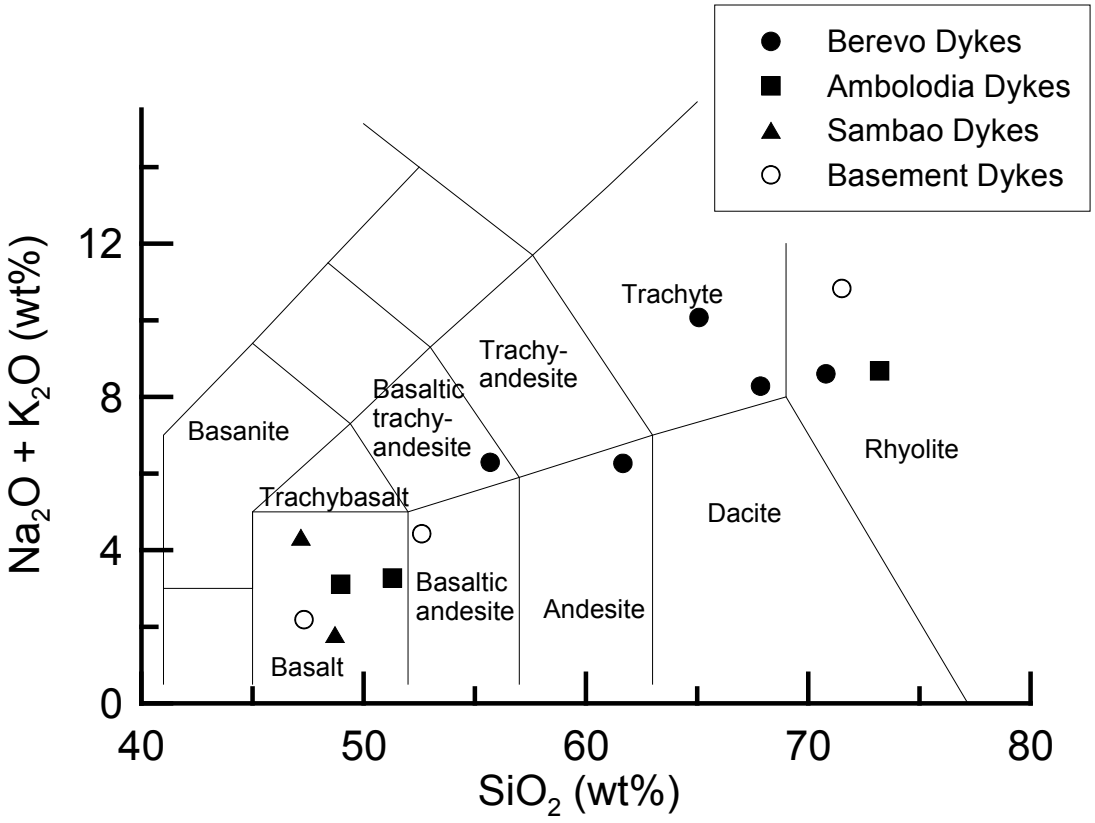

Figure 5.13: Plots of the Maningoza Complexes on the TAS Diagram.

5.3.2 Major Elements vs. SiO_2

Figure 5.14 shows diagrams of major elements plotted against SiO_2 for the dykes of the Maningoza Suite. Strong negative correlations are observed between SiO_2 and CaO (r = -0.94), as well as Fe_2O_3 (r = - 0.93). The plot of SiO_2 against Al_2O_3 is overall a negative correlation (r = -0.50) but with a gentle slope. A strong positive correlation is observed between SiO_2 and K_2O (r = 0.97) and a weak positive correlation is observed between SiO_2 and Na_2O (r = 0.46). The plot of SiO_2 against TiO_2 has positive slope from 45-55 SiO_2 wt. % at which point it changes to a negative slope.

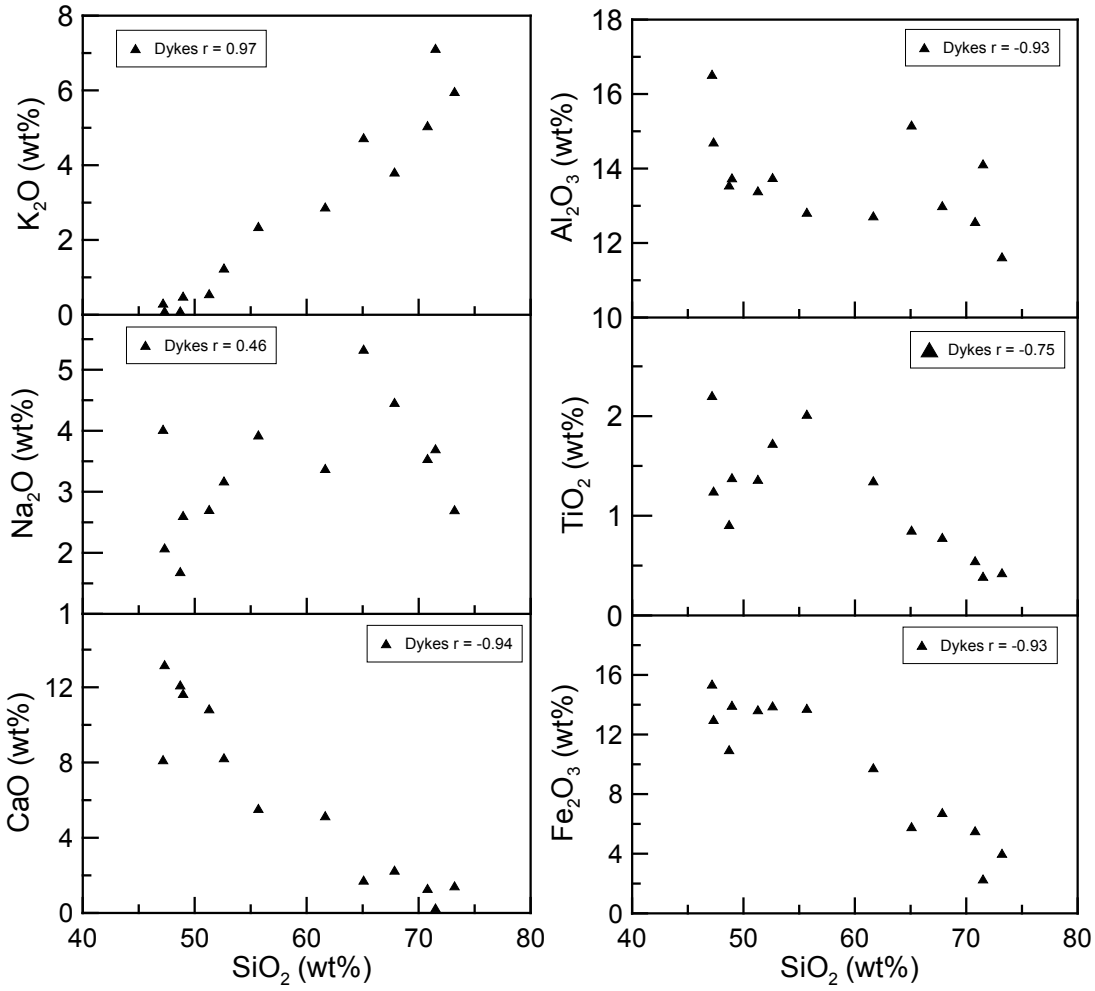

Figure 5.14: Plots of major elements versus SiO_2 (wt. %) for the dykes of the Maningoza Suite.

5.3.3 Major Elements vs. MgO

The dykes of the Maningoza Suite show a strong negative correlation (Figure 5.15) between MgO and SiO_2 (r = -0.89), as well as K_2O (r = -0.88). A strong positive correlation is observed between MgO and CaO (r = 0.94) and no correlation is observed between MgO and P_2O_5. The plots of MgO against Fe_2O_3 and TiO_2 have changes in slopes that begin as positive (0-4 MgO wt. %) but then flatten out and change to a negative slope. A weak positive correlation is observed between MgO and Al_2O_3 (r = -0.32) and a strong negative correlation is observed between MgO and Na_2O (r = -0.72).

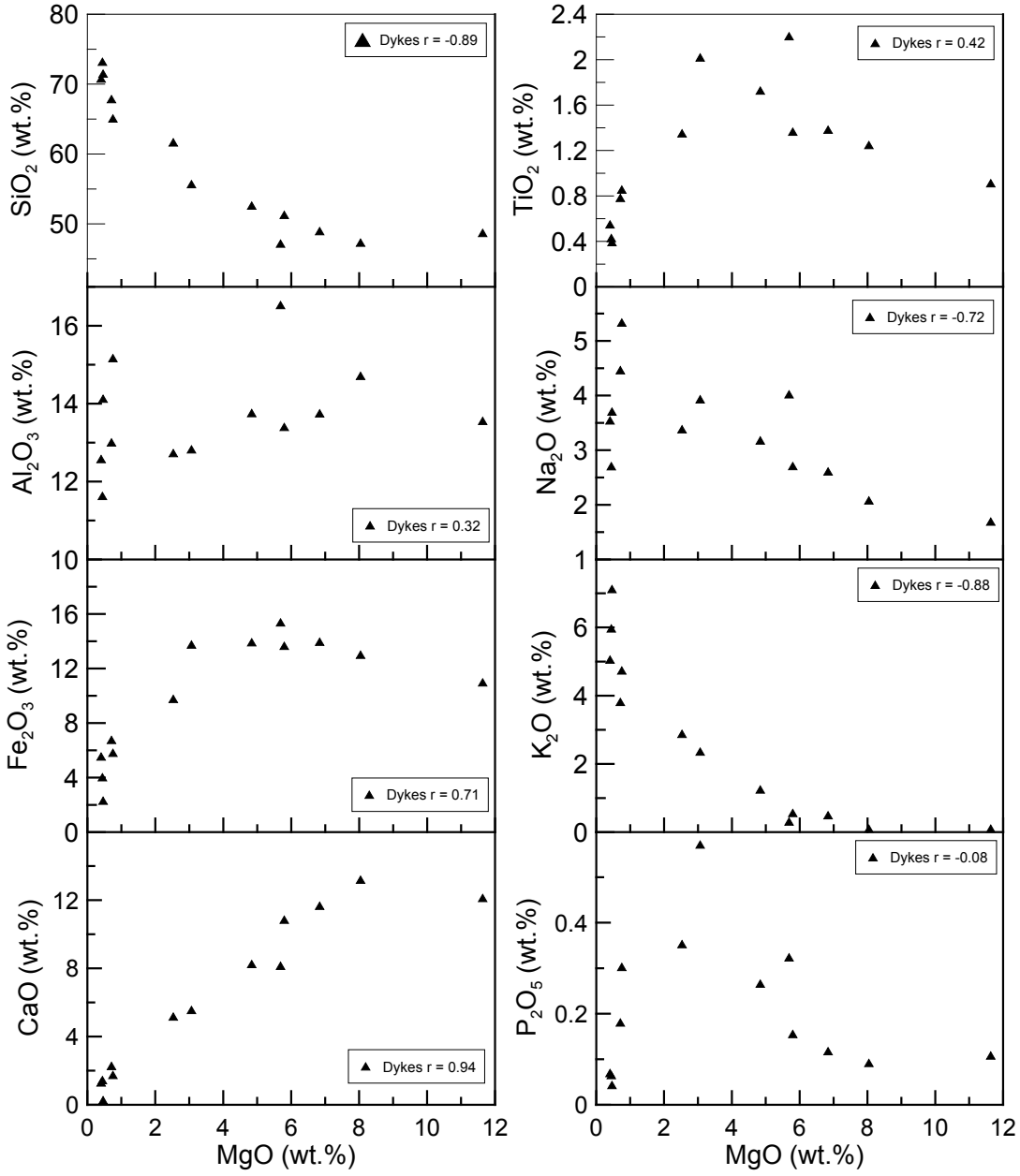

Figure 5.15: Plots of major elements versus MgO (wt. %) for the dykes of the Maningoza Suite.

5.3.4 Trace Elements vs. SiO_2

Figure 5.16 shows diagrams of trace elements plotted against SiO_2 for the dykes of the Maningoza Suite. Strong positive correlations are observed between SiO_2 and trace elements Zr (r = 0.83), Rb (r = 0.96), and Y (r = 0.83). The plot of SiO_2 and Nb also has a positive correlation of r = 0.68. A negative slope is observed between SiO_2 and Ni (r = -0.61) but at about 55 silica wt. % the slope flattens out. The plot of SiO_2 and Sr (r = -0.50) is a positive slope till at 55% silica wt. % it gradually changes to a negative slope.

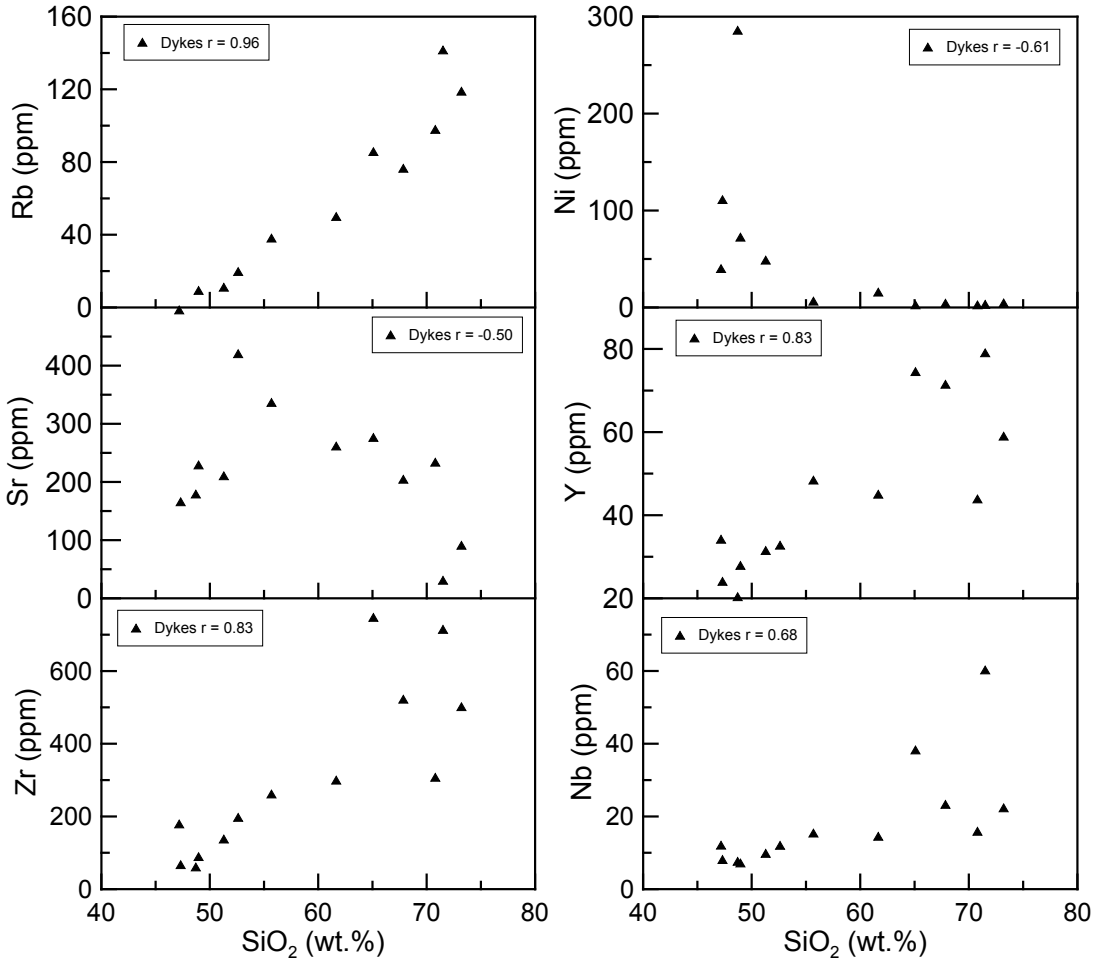

Figure 5.16: Plots of trace elements against SiO_2 for the dykes of the Maningoza Suite.

5.3.5 Trace Elements vs. Zr

The dykes of the Maningoza Suite shows a strong negative correlation (Figure 5.17) between Zr and trace elements Y (r = 0.98), Th (r = 0.93), Nb (r = 0.90), and Rb (r = 0.83). The correlation between Zr and Ba is positive with an r value of 0.69 and there is no correlation between and Sr and Zr.

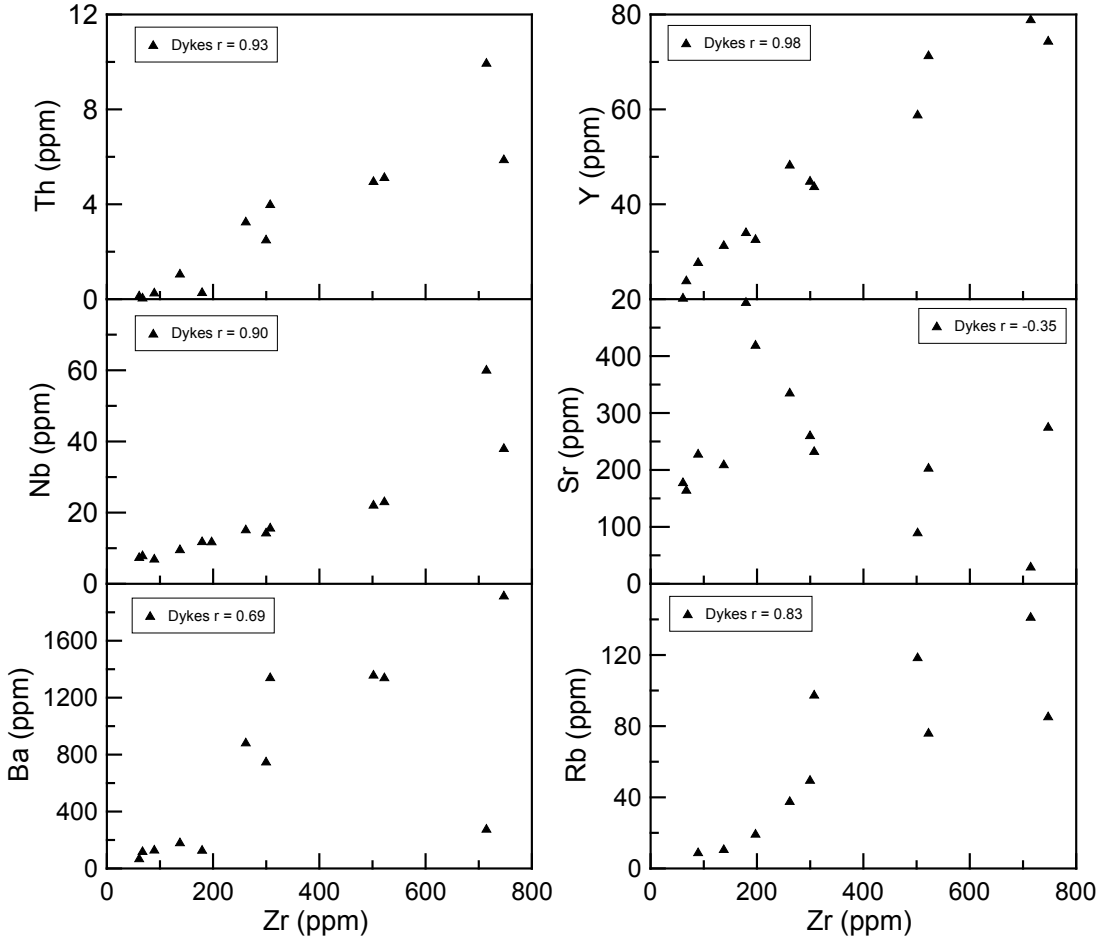

Figure 5.17: Plots of trace elements versus Zr (ppm) for the dykes of the Maningoza Suite.

5.3.6 Rare Earth Element Patterns

Chondrite-normalised REE patterns are shown in Figure 5.18 and have been calculated using the normalising factors given by Nakamura (1974). The dykes of the Maningoza Suite have a low concentration of HREE for the mafic and felsic samples. The felsic samples have a higher concentration of LREE than the mafic samples and the felsic samples show a slightly positive slope from HREE to LREE. Basement dyke sample MI06034 (rhyolite) has the highest concentration of REE and basement dyke sample PF06138 (dolerite) has the

lowest concentration of LREE. The Eu/Eu* average is 0.87 with the lowest Eu anomalies (0.42) belonging to the most felsic samples and the highest Eu anomalies (1.10) belonging to the most mafic samples.

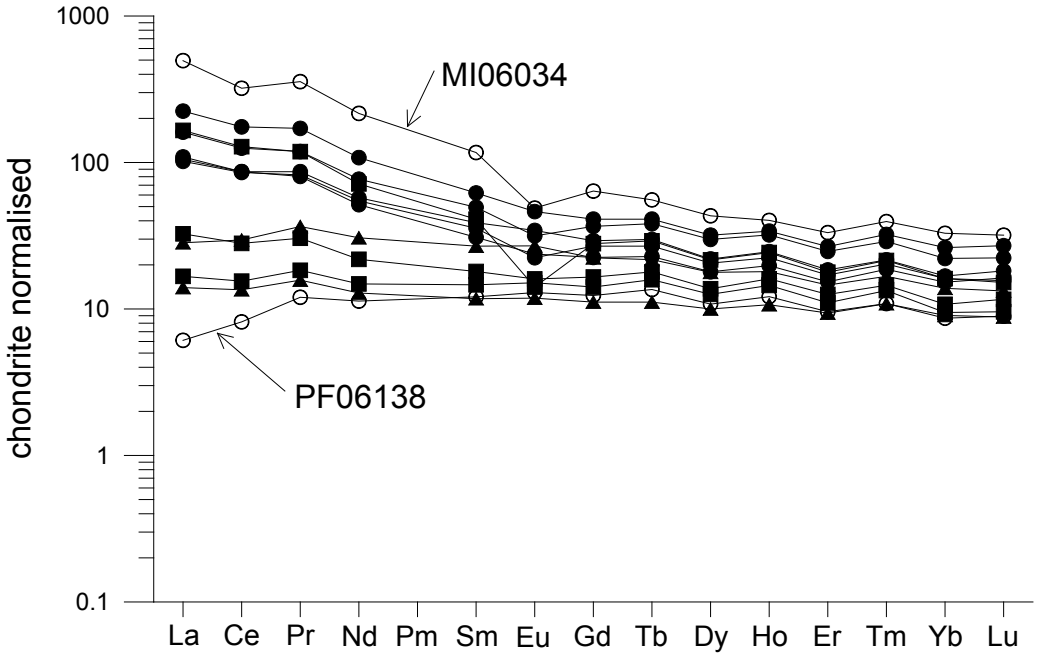

Figure 5.18: REE patterns for the dykes of the Maningoza Suite.

5.4 Comparison within the Maningoza Suite

The Maningoza Suite has a large number of samples which plot with in the basalt and rhyolite fields on the TAS diagram as shown in Figure 5.19. The Fonjay Complex does not have a sample representative of rhyolite. The volcanic formations and the dykes show a full range of rock types from mafic to intermediate to felsic. The Ambohitrosy also shows a full range in rock types but the trend line is higher than the trend observed for the volcanic formations and dykes. This suggests that the Ambohitrosy Complex as a whole appears to be more alkaline than the rest of the complexes. The Ambohitrosy Complex also has samples which fall into the picrobasalt and basanite type fields.

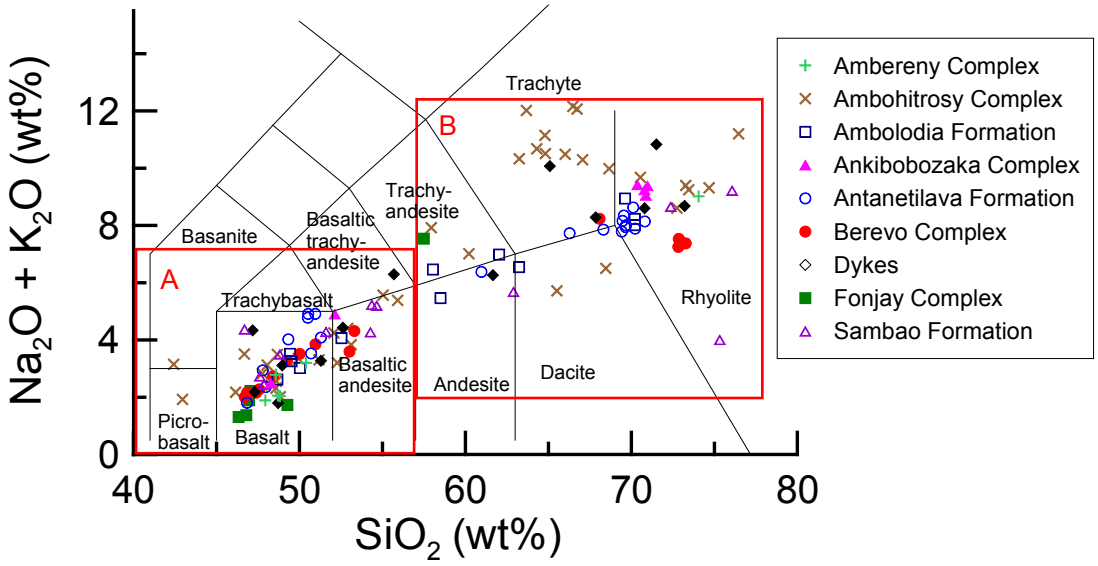

Figure 5.19: TAS diagram showing plots of all samples of the Maningoza Suite. Areas A and B are expanded in Figure 5.20.

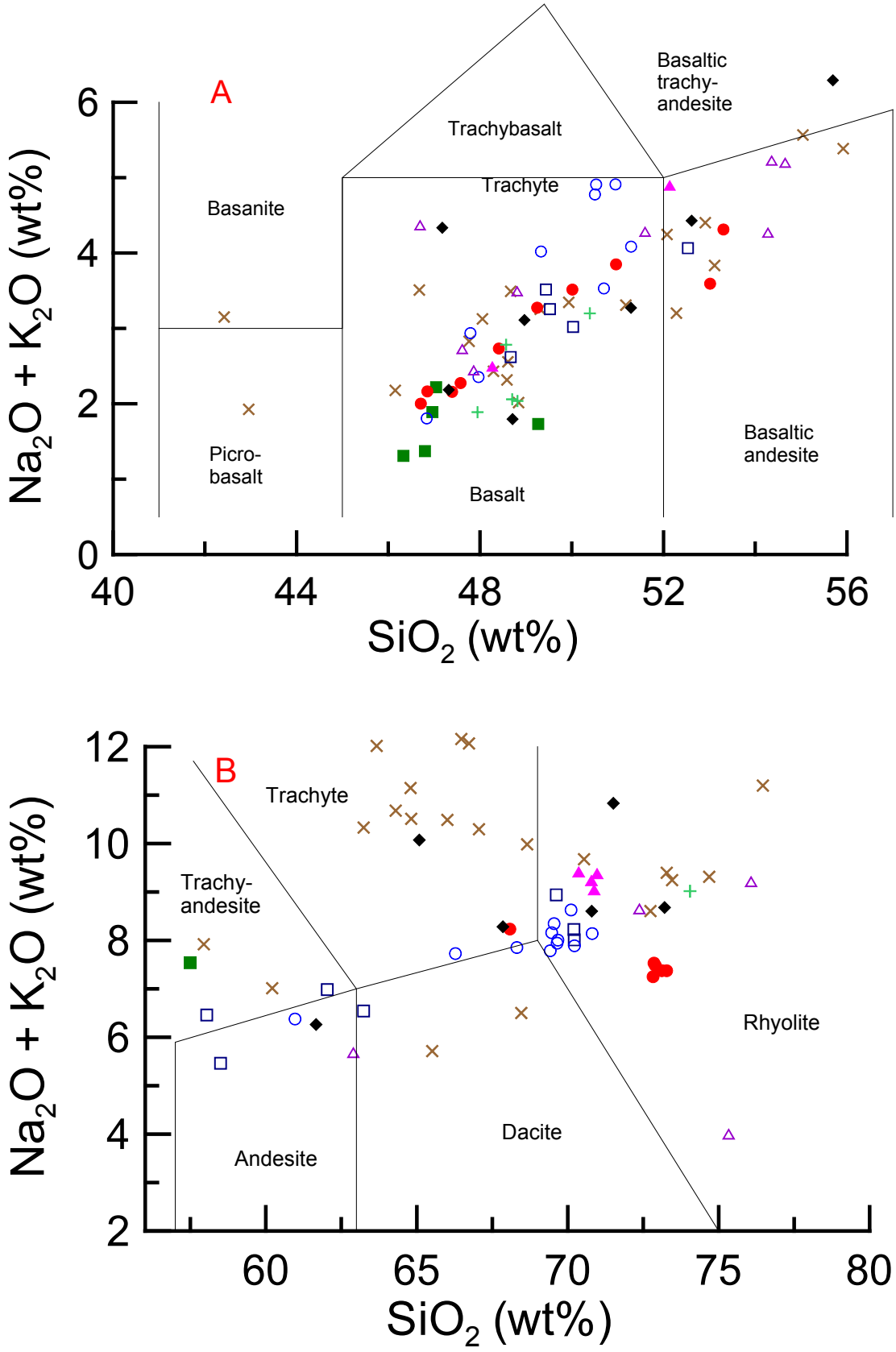

Figure 5.20: Areas A and B showing expanded portions of the TAS diagram in Figure 5.19. The legend represented in Figure 5.19 applies to Areas A and B.

Figure 5.21 shows major elements versus SiO_2 and MgO for the Maningoza Suite. The complexes and formations of the Maningoza Suite show similar trends for major element variations especially for major elements such SiO_2, MgO, K_2O and TiO_2. The deviations are observed with Al_2O_3 and CaO are most likely associated with plagioclase accumulation giving rise to higher than expected Al_2O_3 and CaO wt. %. These deviations are mostly noted within the samples of low silica wt. %.

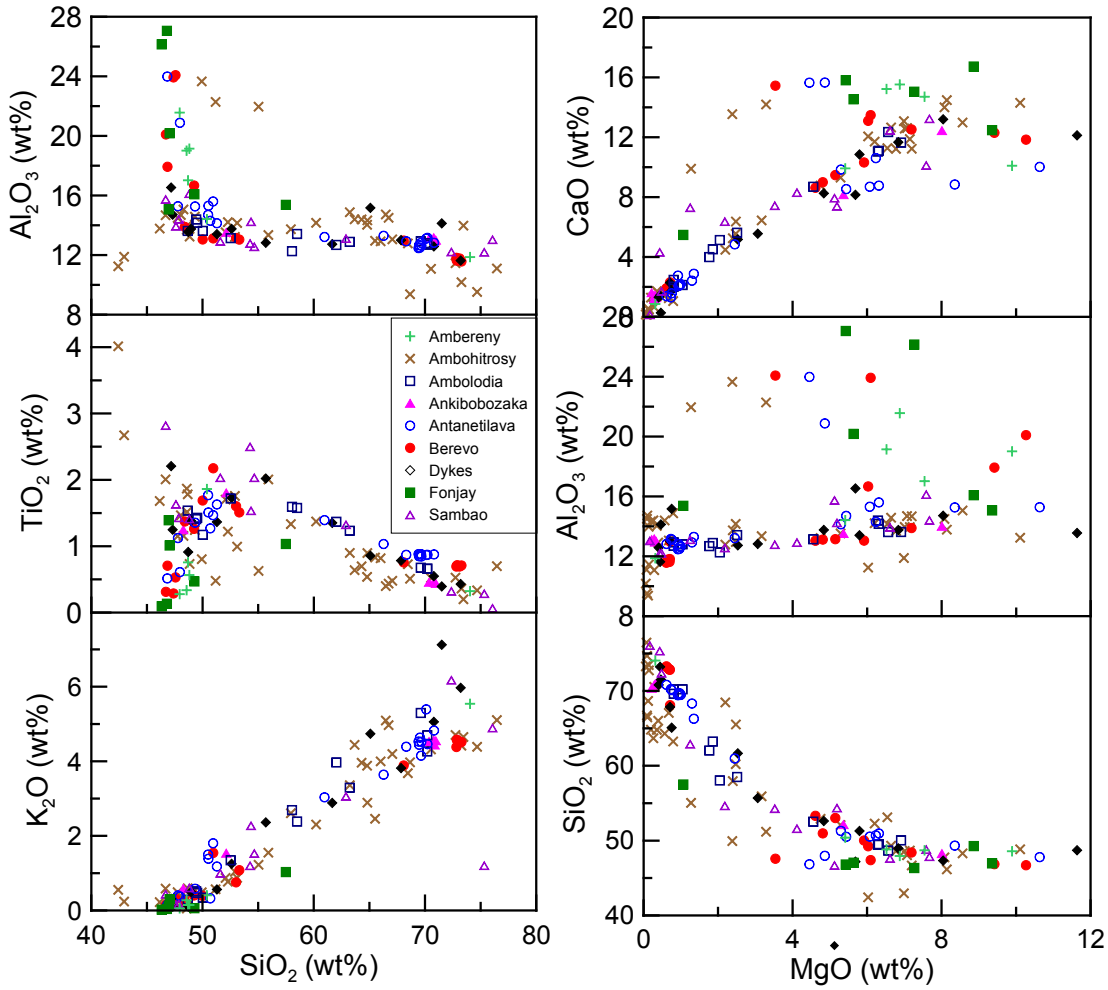

Figure 5.21: Major elements versus SiO_2 and MgO for the Maningoza Suite.

Figure 5.22 shows trace elements versus SiO_2 and Zr for the Maningoza Suite and strong positive correlations are observed between SiO_2 and Zr as well as SiO_2 and Rb. These strong positive correlations suggest fractional crystallisation as an evolution of the Maningoza Suite as these incompatible trace elements increase as silica increases. The variation diagram of SiO_2 and Sr shows a negative slope as is expected between Sr and silica if feldspar is fractionated. High concentrations of Sr are also observed with some of the mafic samples and there is less correlation. This is due to Sr being a compatible element with feldspar and some mafic samples of the Maningoza Suite being feldspar cumulates.

Other incompatible trace elements plotted against Zr show a positive slope with only a few samples deviating off the trends. Most notably are two felsic dykes samples (PF06009 and MI06034) and three felsic Sambao Formation samples (BY6F098B, BY6F148 and BY6F106).

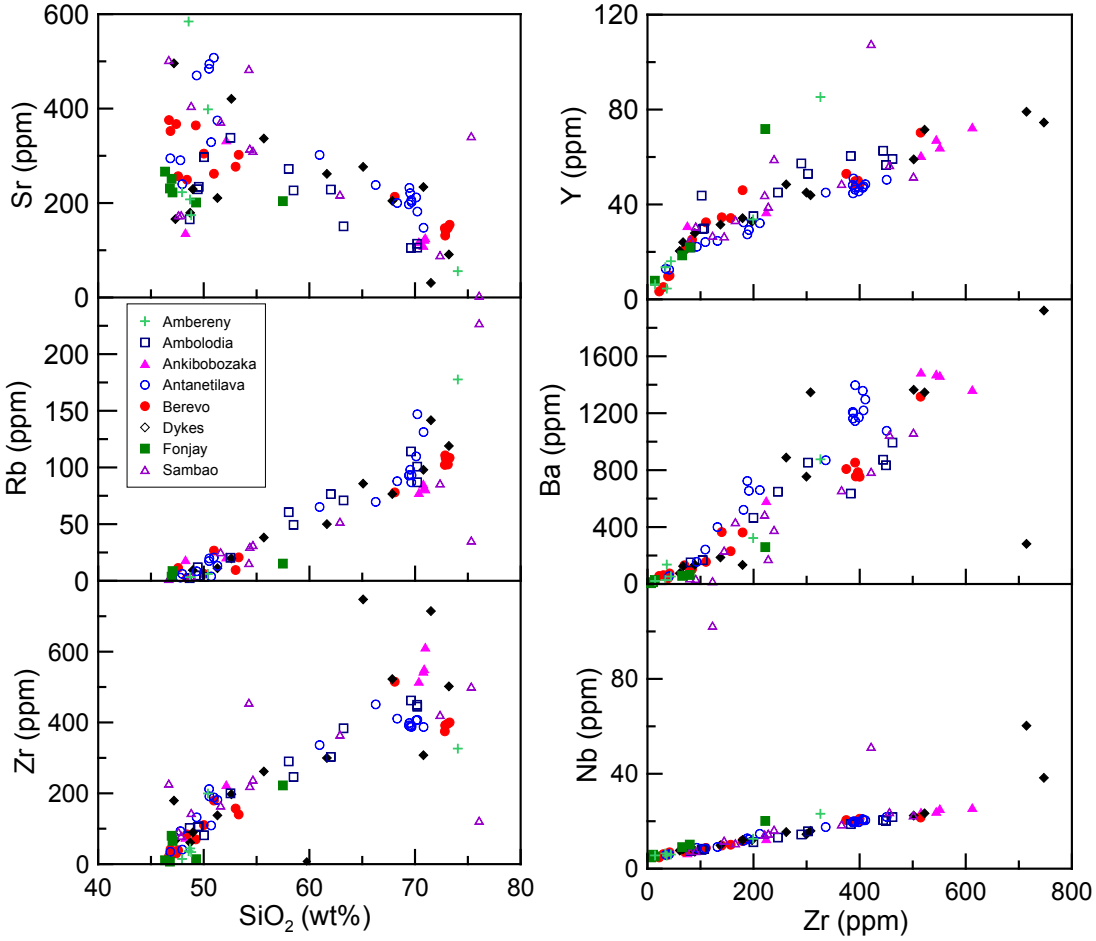

Figure 5.22: Trace elements versus SiO_2 and Zr for the Maningoza Suite

Figure 5.23 shows REE patterns for the Maningoza Suite. Samples from the Fonjay Complex show the lowest concentration of REE compared to the rest of the Maningoza Suite and the Ambohitrosy Complex has the highest concentration of HREE. The dykes and sample BY6F098B (Sambao Formation) have the highest concentration of LREE compared to the rest of the Maningoza Suite. The Ambereny, Berevo and Ambohitrosy Complexes have samples with low concentrations of REE. Samples BY6F148 (Sambao Formation) and PF06129 (Antanetilava Formation) also have low concentrations of REE. The Ankibobozaka Complex, Ambolodia Formation, Antanetilava Formation and Sambao Formation have similar REE patterns to each other with a range of high and low concentrations of LREE and low concentrations of HREE. The range in concentration of LREE is distinguished by the mafic and felsic rock types of the complexes, with the mafic types having low concentrations of

LREE and the felsic types having high concentrations of LREE. This is also observed for Eu anomalies as mafic rock types tend to have high Eu anomalies and felsic rock types tend to have low Eu anomalies. An exception to this is the Sambao sample BY6F148 which has low REE concentrations like most mafic samples but has an unusual low Eu anomaly. Many of the samples from the complexes and formations overlap between 1 and 200 on the REE plots and show similar patterns described for the Ankibobozaka Complex, Ambolodia Formation, Antanetilava Formation and Sambao Formation with the exceptions described previously.

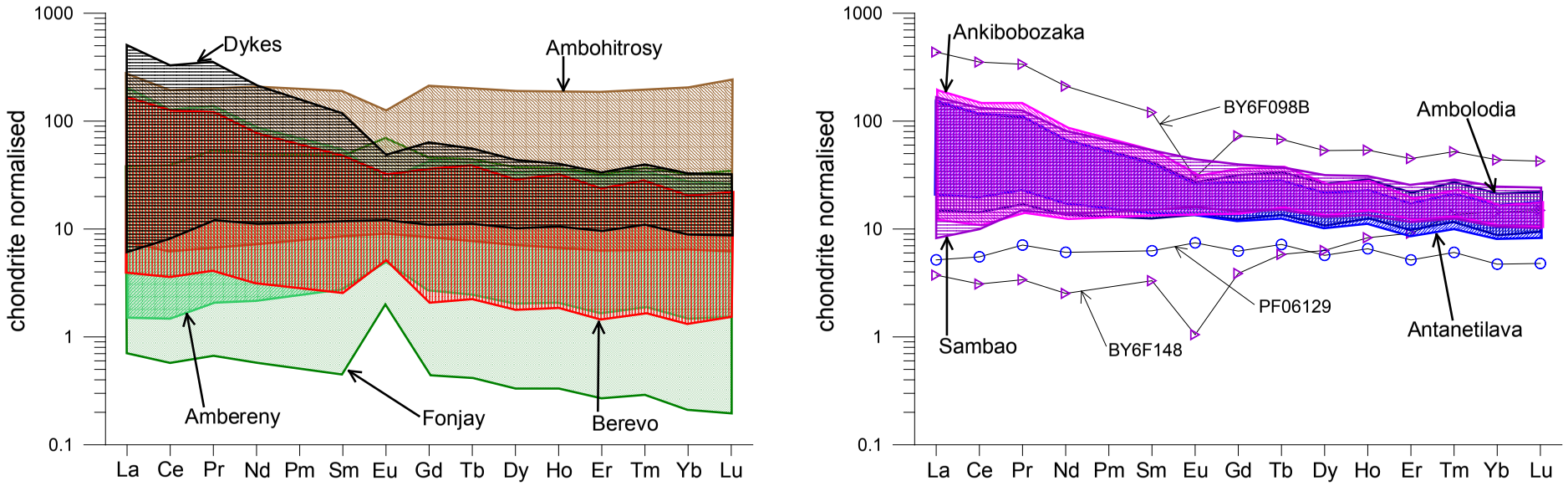

Figure 5.23: REE patterns for the Maningoza Suite.

6 ISOTOPES

6.1 Oxygen Isotopes

Whole-rock $\delta^{18}O$ values were obtained for 40 samples where at least one mafic and one felsic sample was chosen from each of the Complexes (Ankibobozaka, Berevo, Fonjay and Ambereny) and Formations (Ambolodia, Antanetilava and Sambao) and two samples from the dyke swarm were included. Mineral $\delta^{18}O$ values where obtained for the Berevo Complex where clinopyroxene and plagioclase was analysed. The samples that showed the least petrographic evidence of alteration were chosen for whole-rock and mineral analysis.

The Ankibobozaka Complex has whole-rock $\delta^{18}O$ values that range from 3.9 to 7.9‰, with an average of 6.32 ± 1.50‰ (1σ, n = 5) as shown in Figure 6.1 and Table 6.1. The Antanetilava Formation has similar whole-rock $\delta^{18}O$ values to the Ankibobozaka Complex with a range of 3.8 to 8.8‰, and an average of 6.13 ± 1.42‰ (1σ, n = 11). The Berevo Complex and the Ambolodia Complex both have very large ranges with the Berevo Complex ranging from 3.5 to 11.3‰, and an average of 5.87 ± 2.49‰ (1σ, n = 9) and the Ambolodia Complex ranging from 4.8 to 12.4‰, with an average of 7.41 ± 3.03‰ (1σ, n = 5). The Ambolodia Complex has consistent higher whole-rock $\delta^{18}O$ values than the Berevo Complex.

The Sambao Formation has, overall, high whole-rock $\delta^{18}O$ values that range from 6.1 to 11.4‰, with an average of 9.56 ± 3.01‰ (1σ, n = 3). The Fonjay Complex has low whole-rock $\delta^{18}O$ values overall that range from 2.3 to 6.7‰, with an average of 4.03 ± 2.34‰ (1σ, n = 3). The Ambereny Complex has a more restricted range with a minimum of 4.7‰ and a maximum 6.9‰, and an average of 5.97 ± 1.14‰ (1σ, n = 3). The basement dykes have the most restricted range of whole-rock $\delta^{18}O$ values from 6.3 to 7.8‰, with an average of 7.02 ± 1.09‰ (1σ, n = 2). This is due to the small number of samples (2) analysed.

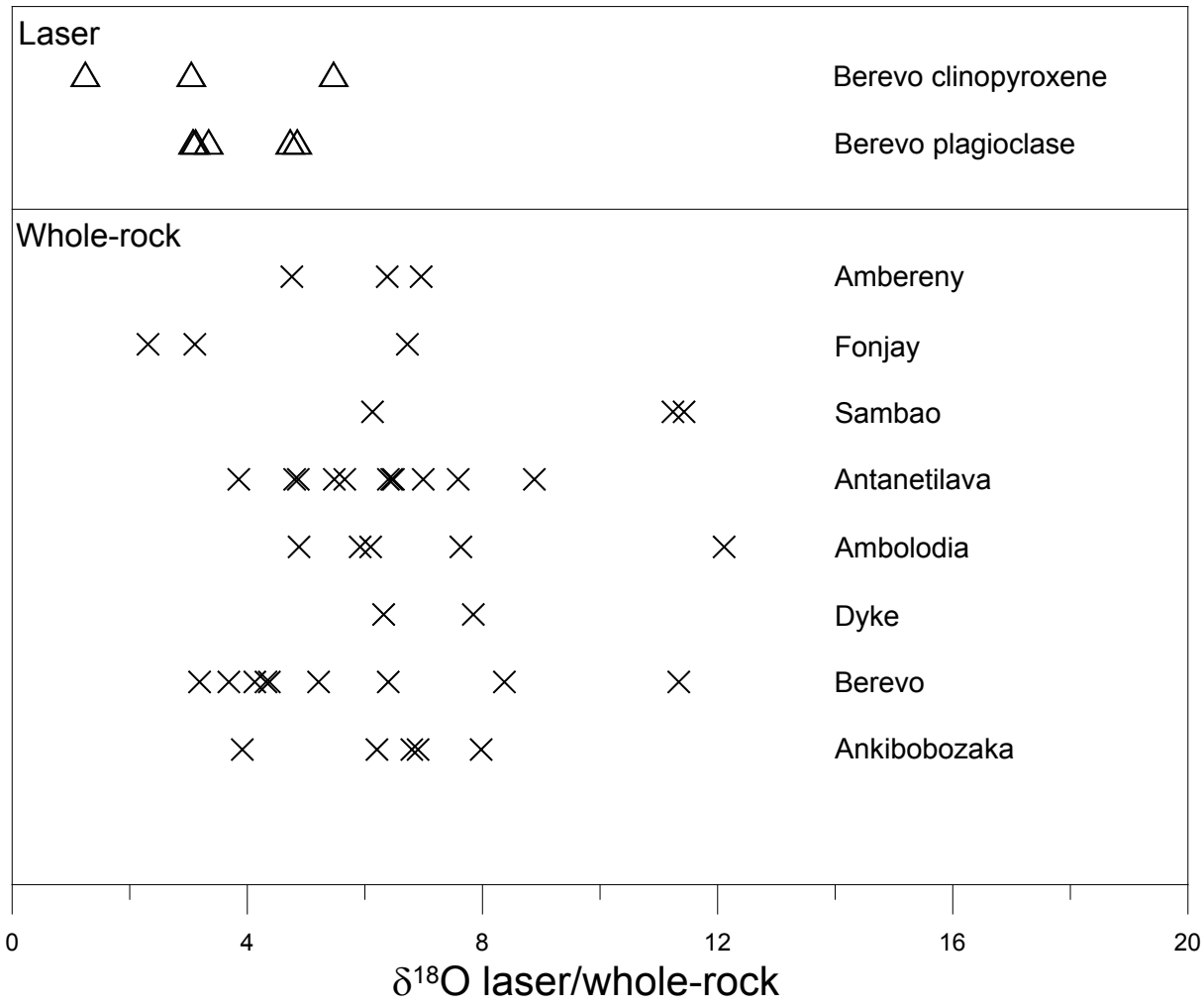

Figure 6.1: Whole-rock and mineral oxygen isotope compositions for the Maningoza Suite.

Sample	$\delta^{18}O$	Sample		$\delta^{18}O$
Whole Rock Analysis		**Mineral Analysis**		
Ankibobozaka		Clinopyroxene		Plagioclase
PF06001	6.2			
PF06002	8.0			
PF06004	3.9			
PF06005	6.8			
PF06006	6.9			
Berevo				
PF06009	8.4			
PF06012	3.2			
PF06013	4.4	PF06013	3.0	3.1
		PF06013	1.2	3.3
PF06017	4.1			
PF06018	6.4			
PF06020	4.3	PF06020	5.5	3.1
PF06026	3.7			
PF06027	5.2	PF06027		4.7
		PF06027		4.9
PF06028	11.3			
Basement Dyke				
PF06071	7.8			
PF06138	6.3			
Ambolodia				
PF06119	7.6			
PF06120	12.1			
PF06121	5.9			
PF06123	6.1			
PF06128	4.9			
Antanetilava				
PF06129	3.9			
PF06130	4.8			
PF06131	6.4			
PF06132	4.9			
PF06134	8.9			
PF06143	6.5			
PF06144	7.0			
PF06145	5.5			
PF06148	6.5			
PF06152	7.6			
PF06153	5.7			
Sambao				
BY6F091	6.1			
BY6F98B	11.4			
BY6F103	11.2			
Fonjay				
M106010	2.3			
MI06010 rp	3.1			
M106011	6.7			
Ambereny				
MI06014	6.4			
MI06016	7.0			
MI06019	4.8			

Table 6.1: Oxygen isotope results from whole-rocks and minerals for the Maningoza Suite.

The Ankibobozaka Complex shows a strong positive correlation of increasing whole-rock $\delta^{18}O$ values with increasing SiO_2 (r = 0.84), Zr (r = 0.92) and Nb (r = 0.91) as shown in Figure 6.2 and Figure 6.3. The Antanetilava Formation and Sambao Formation are similar to the Ankibobozaka Complex in that they also show strong correlations of increasing whole-rock $\delta^{18}O$ values with increasing SiO_2 (r = 0.82, r = 0.89), Zr (r = 0.87, r = 0.99) and Nb (r = 0.86, r = 0.72). Figure 6.2 shows strong correlations of decreasing whole-rock $\delta^{18}O$ values with increasing MgO for the Ankibobozaka Complex (r = -0.90), Antanetilava Formation (r = -0.61) and Sambao Formation (r = -0.99). Figure 6.3 shows no apparent correlation for whole-rock $\delta^{18}O$ values against Sr for the Ankibobozaka Complex, Antanetilava Formation or Sambao Formation.

The Ambereny Complex shows strong correlations of increasing whole-rock $\delta^{18}O$ values with increasing SiO_2 (r = 0.68), Zr (r = 0.66) and Nb (r = 0.71). On the other hand the Ambereny Complex shows an unusually strong correlation of decreasing whole-rock $\delta^{18}O$ values with increasing Sr (r = -0.99) and MgO (r = -0.89). The Fonjay Complex and the basement dykes have too few data points for any reasonable correlation to be made.

The Berevo Complex shows weak correlations of increasing whole-rock $\delta^{18}O$ values with increasing SiO_2 (r = 0.42), Zr (r = 0.46) and Nb (r = 0.45). Figure 6.2 shows a weak correlation of decreasing whole-rock $\delta^{18}O$ values with increasing MgO (r = -0.51). There is almost no correlation between whole-rock $\delta^{18}O$ values and Sr for the Berevo Complex. The Ambolodia Complex shows no apparent correlation of whole-rock $\delta^{18}O$ values with any of the elements in Figure 6.2 and Figure 6.3.

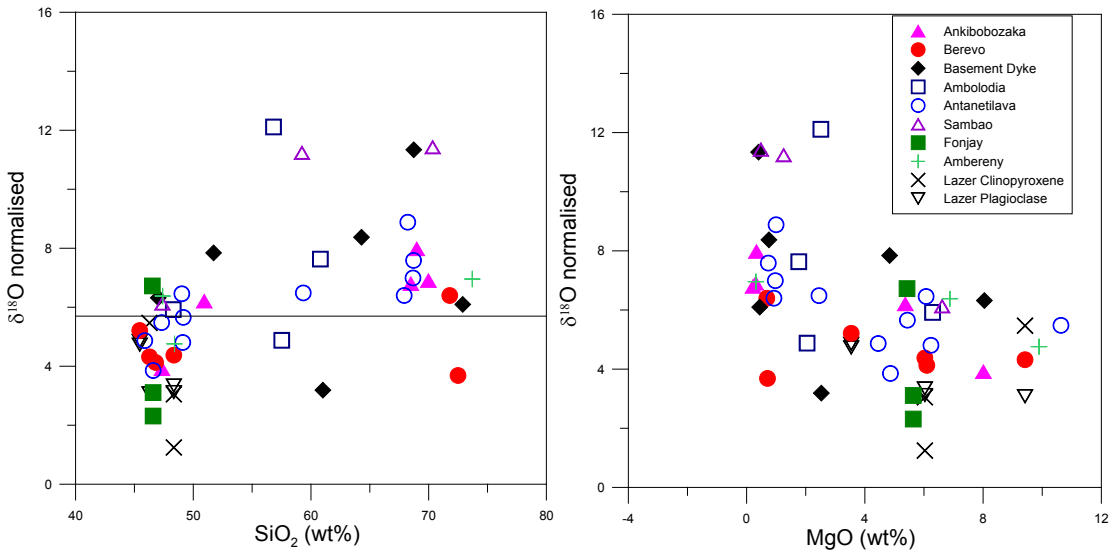

Figure 6.2: Graphs showing $\delta^{18}O$ of whole-rocks and minerals versus major element SiO_2 and MgO.

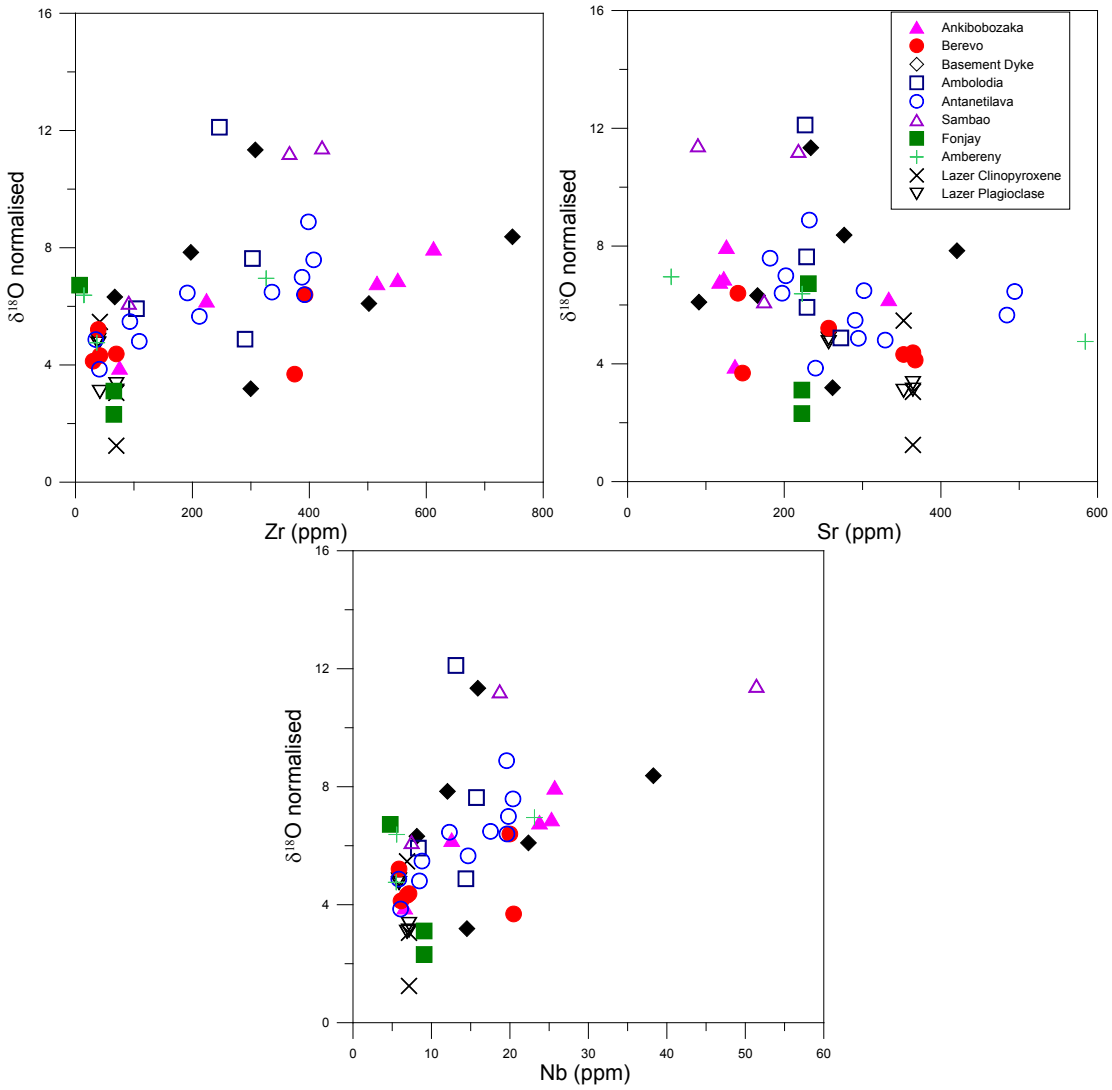

Figure 6.3: Graphs showing $\delta^{18}O$ of whole-rocks and minerals versus trace elements Zr, Sr and Rb.

Figure 6.4 shows that for the Fonjay Complex, Ambolodia Formation, Sambao Formation and the dykes there is a strong positive correlation between whole-rock $\delta^{18}O$ and loss on ignition (LOI) wt. % ($r > 0.75$ for all four groups). The Berevo Complex also shows a positive correlation ($r = 0.60$) if sample PF06027 (LOI wt. % = 2.9) is excluded. This suggests that the increase in whole-rock $\delta^{18}O$ value is related to alteration for these five groups. The Ankibobozaka Complex and Antanetilava Formation show a weak negative correlation ($r < 0.35$). The Ambereny Complex has a strong negative correlation and although there is only three data points it appears more like the Ankibobozaka Complex and Antanetilava Formation.

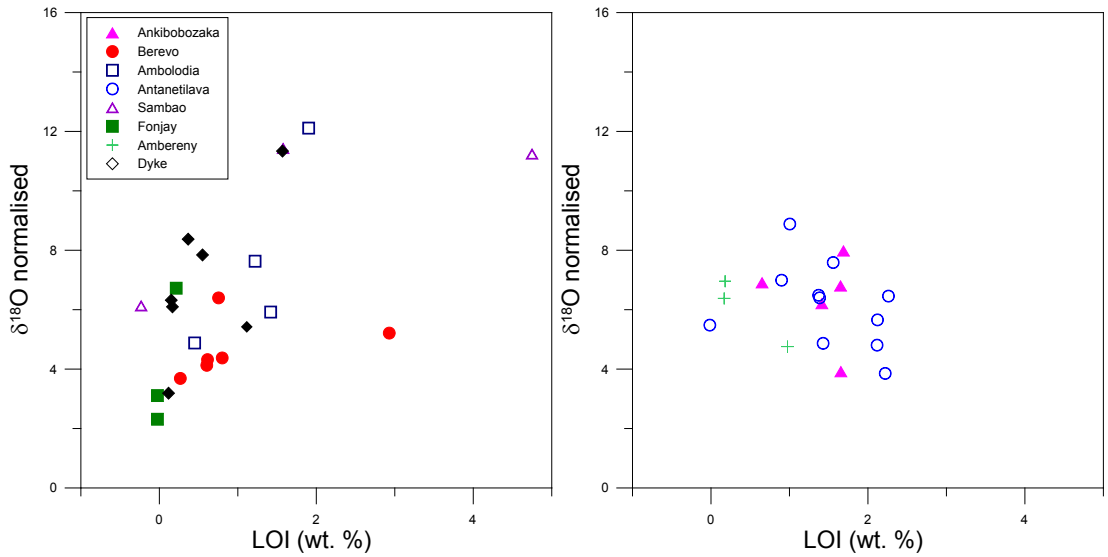

Figure 6.4: Plot of LOI versus $\delta^{18}O$ of whole-rocks for the Maningoza Suite. LOI = loss on ignition.

The plagioclase and clinopyroxene minerals from the Berevo Complex have lower $\delta^{18}O$ values than the whole-rock $\delta^{18}O$ values as shown in Table 6.1. The difference between mineral $\delta^{18}O$ values and whole-rock $\delta^{18}O$ values ranges from 0.3‰ to 3.2‰ for the three gabbroic samples. An exception to this is the clinopyroxene of sample PF06020 which has a 1.2‰ higher $\delta^{18}O$ value than the whole-rock value. Figure 6.5 shows that the whole-rock $\delta^{18}O$ is not in equilibrium with the $\delta^{18}O$ of coexisting plagioclase and clinopyroxene in the Berevo samples. The $\delta^{18}O$ of plagioclase and coexisting clinopyroxene are in equilibrium with each other for sample PF06013 but not for sample PF06020. It is possible that the groundmass of the samples are altered and homogenised where as the larger phenocrysts have had varied amounts alteration. This suggests that the internal oxygen isotope equilibrium of phenocryst phases is high and that the groundmass has largely homogenised with an external fluid (Criss and Taylor 1986).

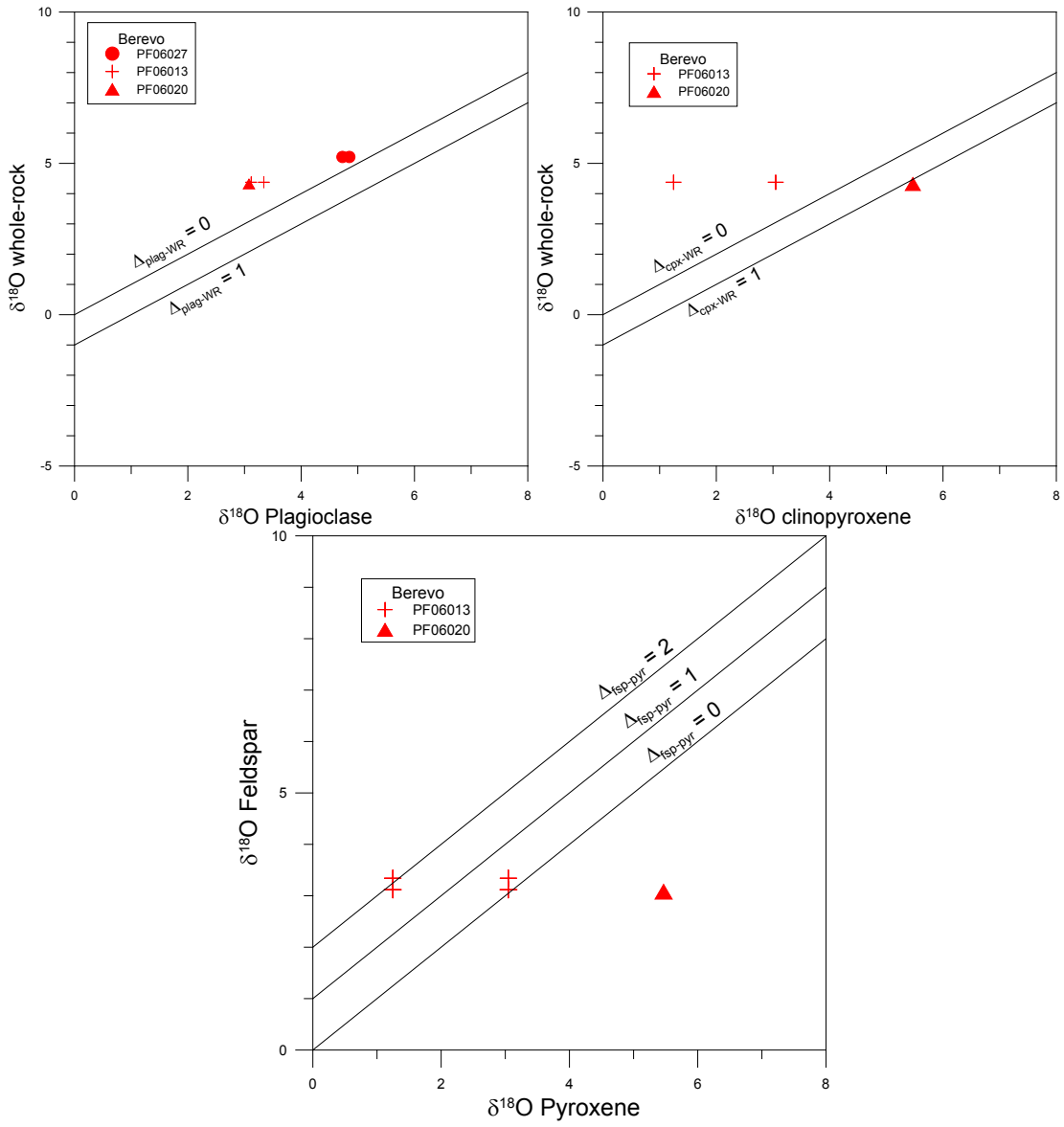

Figure 6.5: Plots of clinopyroxene and plagioclase $\delta^{18}O$ versus whole-rock $\delta^{18}O$ as well as feldspar $\delta^{18}O$ versus clinopyroxene $\delta^{18}O$.

6.2 Hydrogen

The whole-rock δD and H_2O^+ values for 24 samples of the Maningoza Suite are shown in Table 6.2 and at least one mafic and one felsic sample was selected, if possible, from each complex. The δD values for the Ankibobozaka Complex range from -79‰ to -127‰ and has an average of -104‰ shown in Figure 6.6. The Berevo Complex has values between -71‰ and -121‰ with an average of -97‰. The Fonjay Complex δD values range from -89‰ to -99‰ with an average of -96‰. The δD values of the Ambereny Complex are between -73‰ and -102‰ with an average of -85‰. The δD values for the Ambolodia Formation range from -64‰ to -98‰ with an average of -75‰. The Antanetilava Formation has a range of δD

values from -62‰ to -80‰ with an average of -70‰. The Sambao Formation has δD values between -74‰ and -86‰ with an average -80‰. The Basement dykes have a range of δD values between -89‰ and -109‰ with an average of -99‰.

The Ankibobozaka Complex has H_2O^+ values that range between 0.13% and 1.28%. This is similar to those of the Ambereny Complex, which has values that range between 0.21% and 1.23%. The Fonjay Complex has low H_2O^+ percentages (below 0.20%). The Berevo Complex has H_2O^+ values that range from 0.11% to 0.69%, which is similar to the Sambao Formation which has values that range from 0.18% to 0.59%. The Ambolodia Formation and the Antanetilava Formation are both similar with the highest concentrations of H_2O^+ up to 2.15% and 1.78%, respectively. The Basement dykes have H_2O^+ values that range between 0.42% and 0.52%.

Complex name	Sample name	δD	wt.% H_2O	$\delta^{18}O$
Standard	CG bi	-62	3.8	
	CG bi	-64	3.3	
Ankibobozaka	PF06001	-79	1.3	6.2
	PF06002	-127	0.13	8.0
	PF06004	-88	1.2	3.9
	PF06005	-124	0.21	6.8
Berevo	PF06012	-121	0.11	3.2
	PF06017	-71	0.69	4.1
	PF06026	-108	0.14	3.7
	PF06028	-90	0.57	11.3
Dykes	PF06071	-109	0.42	7.8
	PF06138	-89	0.52	6.3
Ambolodia	PF06119	-72	1.2	7.6
	PF06120	-66	2.1	12.1
	PF06123	-98	0.14	6.1
	PF06128	-64	0.93	4.9
Antanetilava	PF06129	-62	1.8	3.9
	PF06134	-68	0.67	8.9
	PF06145	-80	0.46	5.5
Sambao	BY6F091	-86	0.18	6.1
	BY6F098B	-74	0.59	11.4
Fonjay	M106010	-99	0.12	2.3
	M106010	-99	0.12	3.1
	M106011	-89	0.20	6.7
Ambereny	M106014	-81	0.23	6.4
	M106016	-102	0.21	7.0
	M106019	-73	1.2	4.8

Table 6.2: Hydrogen isotope and H_2O^+ values for the Maningoza Suite. Also included are the relevant oxygen isotope values and standard values.

Figure 6.6 also shows the range for magmatic waters and all of the complexes, except for the Fonjay Complex and the basement dykes, have one or more samples within that range. The Antanetilava Formation has all of its samples lying within the range of magmatic waters and the Ambolodia Formation only has one of its samples outside of this range. The Ambereny, Berevo and Ankibobozaka Complexes all have one sample within the range of magmatic water (δD values between -40‰ and -80‰).

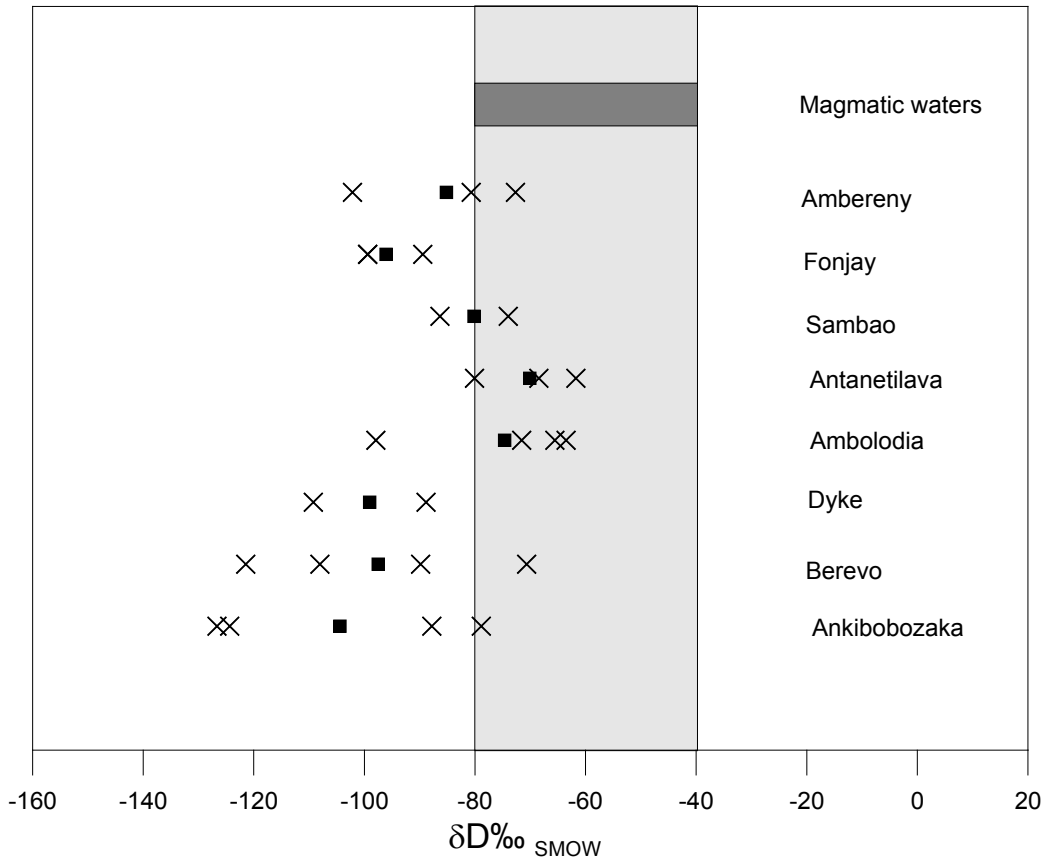

Figure 6.6: Whole-rock δD values obtained for the Maningoza Suite. Crosses represent obtained values and the solid squares represent the average values for each complex. The δD range of magmatic waters is shown in grey.

Figure 6.7 shows low δD and H_2O^+ values, which are characteristic of water vapour exsolution and loss during magmatic evolution. The water exsolution may have occurred during the crystallisation of magma prior to eruption, this in turn causes a progressive lowering of δD and H_2O^+ in the residual melt (Taylor et al. 1983). The depletion of δD occurs as the heavier isotope D favours the H_2O in the melt rather than in the solid/crystallised state. Therefore the loss of water vapour would decrease the δD value in the remaining melt and/or in any late stage hydrous phases such as amphibole.

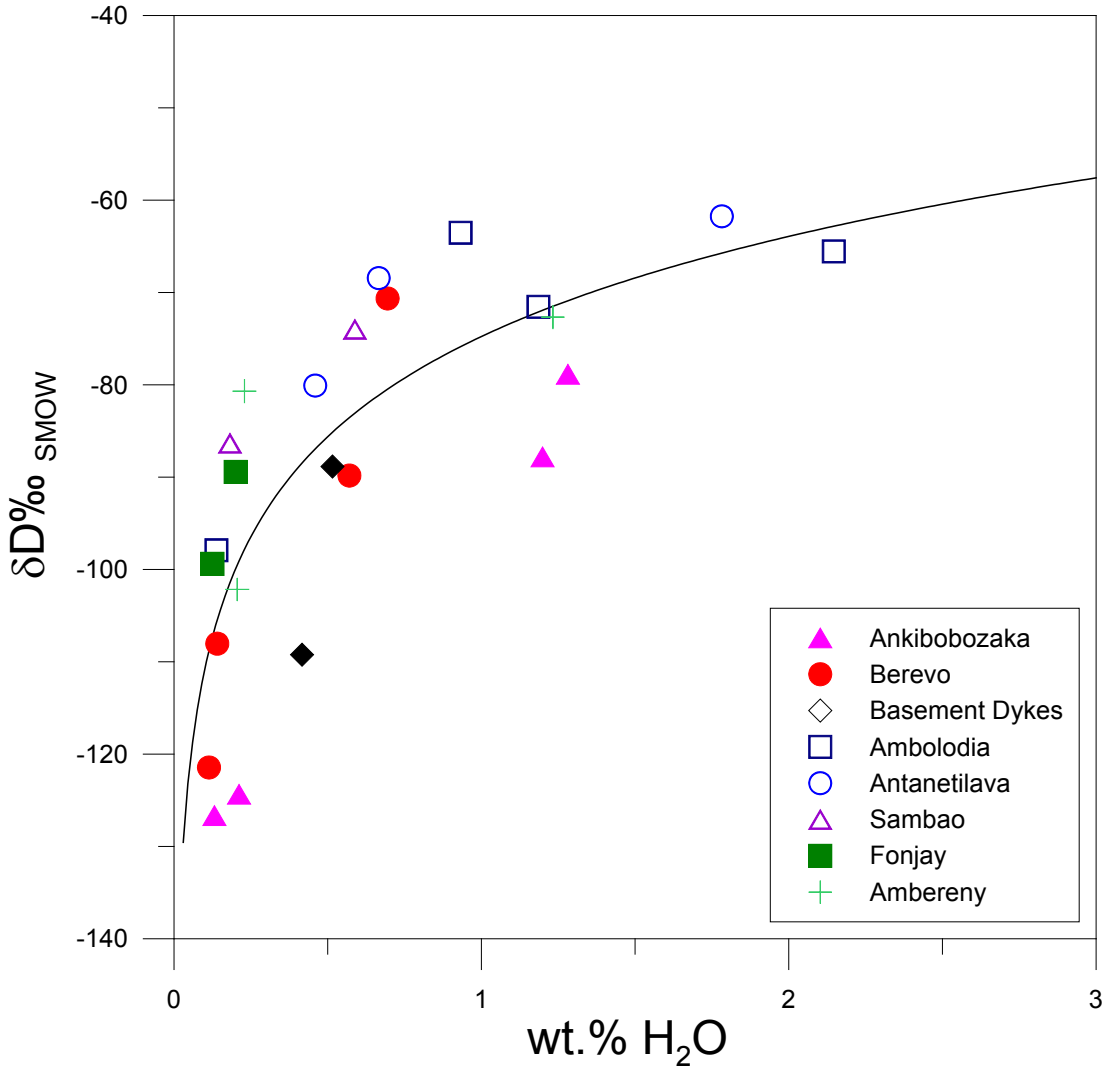

Figure 6.7: Plot of δD against H_2O^+. The lowest δD values are affected by analytical interference due to their corresponding low H_2O^+ concentrations. The low H_2O^+ concentration allows the blank to interfere in the measurement and lower the δD value. The data presented fits well with Rayleigh-type water vapour exsolution or degassing. As the loss of H_2O occurs there is a steady depletion of δD as shown by the curve.

Figure 6.8 shows plots of δD and H_2O^+ values versus loss on ignition (LOI) and good positive correlations are observed. The plot of H_2O^+ and LOI shows a positive linear trend that shows that most of the weight percentage lost during XRF analysis is related to water. The plot of δD and LOI show the same Rayleigh-type water exsolution as shown in Figure 6.7 again pointing out the similarities between H_2O^+ and LOI. Two samples of the Ankibobozaka Complex (PF06002 and PF06005) do not follow the trend and have much lower H_2O^+ values compared to their LOI values. In thin-section these samples contain calcite and so the higher amounts of LOI are likely due to CO_2 release.

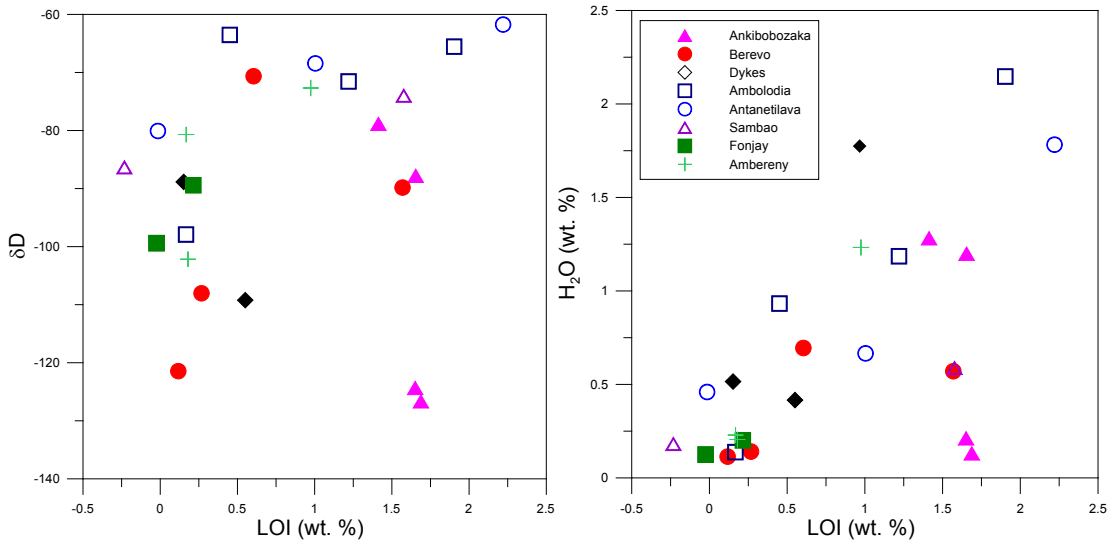

Figure 6.8: Plots of LOI (loss on ignition) against δD and against H_2O^+ for the Maningoza Suite.

Figure 6.9 shows a plot of δD against $\delta^{18}O$ and shows decreasing δD values with no change in $\delta^{18}O$. This further demonstrates the loss of H_2O vapour as water vapour loss prior to eruption has only a small effect on the $\delta^{18}O$ of the rock. Two samples, one from the Antanetilava Formation and one from the Ambolodia Formation, plot within the field of magmatic water suggesting they did not have contact with external hydrothermal fluids.

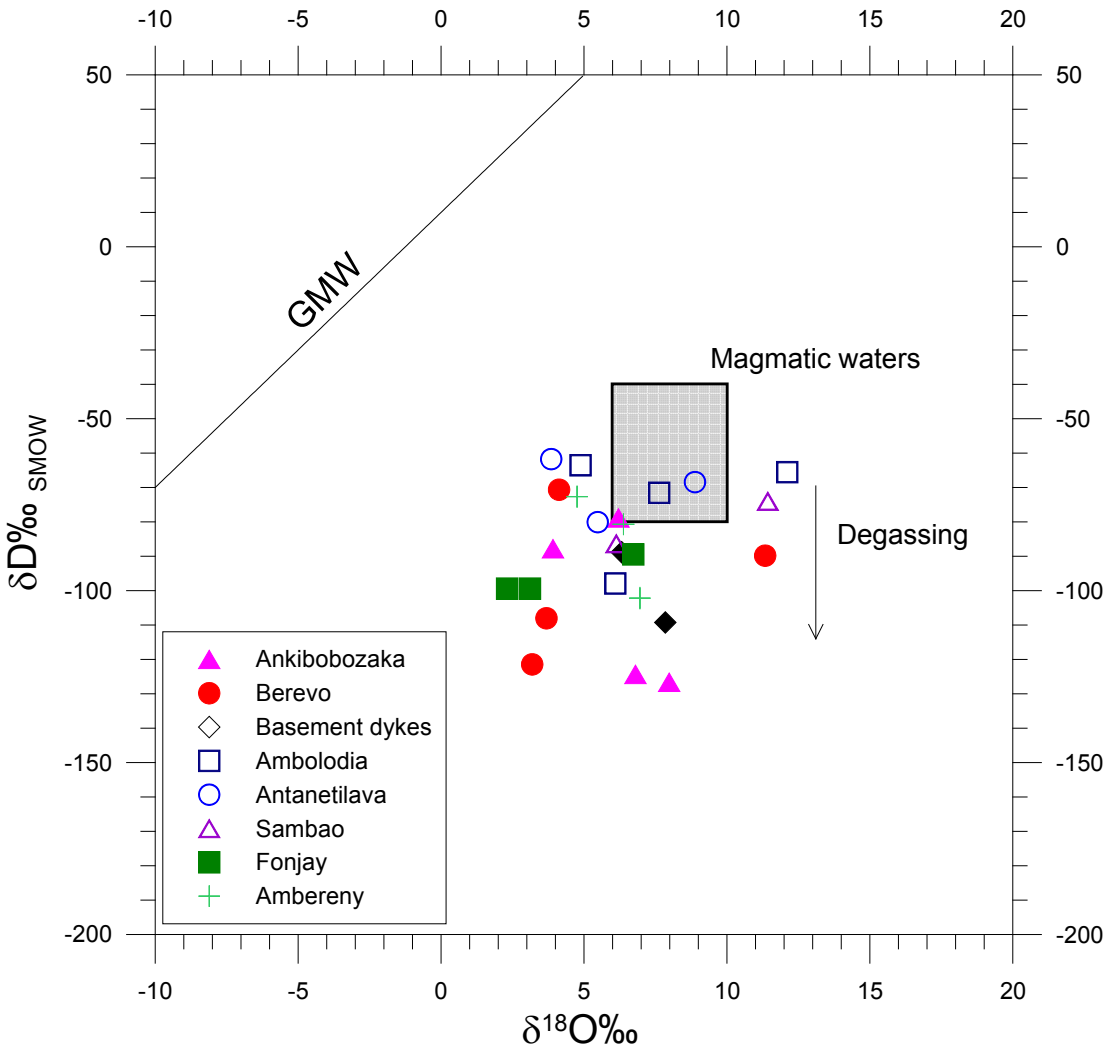

Figure 6.9: Plot of whole-rock δD against whole-rock $\delta^{18}O$ for the Maningoza Suite. Also included is the global meteoric water line (GMW) (Craig 1961). Magmatic water field: δD between -40‰ and -80‰; $\delta^{18}O$ between 6‰ and 10‰ shown in grey (Taylor 1986).

6.3 Ar-Ar Geochronology

The age analyses of samples PF06135 and PF06153 are shown in Figure 6.10 and Figure 6.11 respectively. Sample PF06135 has an Ar-Ar age of 91.33 ± 0.9 Ma and sample PF06153 has an Ar-Ar age of 95.48 ± 0.92 Ma. The average age of the two samples is 93.41 Ma. This average age is consistent with the Maningoza Suite being of the Cretaceous period as suggested by the Council for Geoscience (Macey et al. 2007).

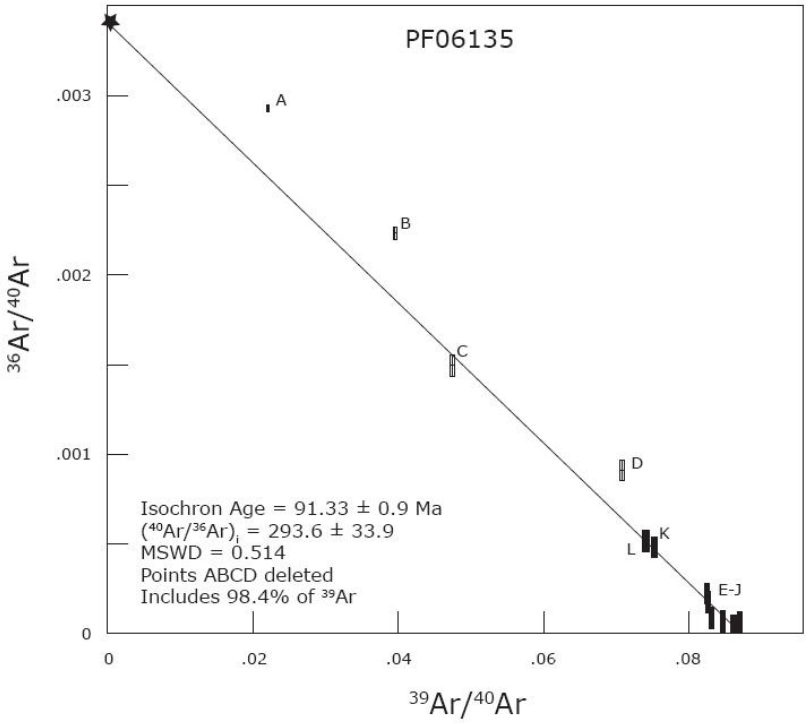

Figure 6.10: Plot of $^{36}Ar/^{40}Ar$ versus $^{39}Ar/^{40}Ar$ for the sample PF06135.

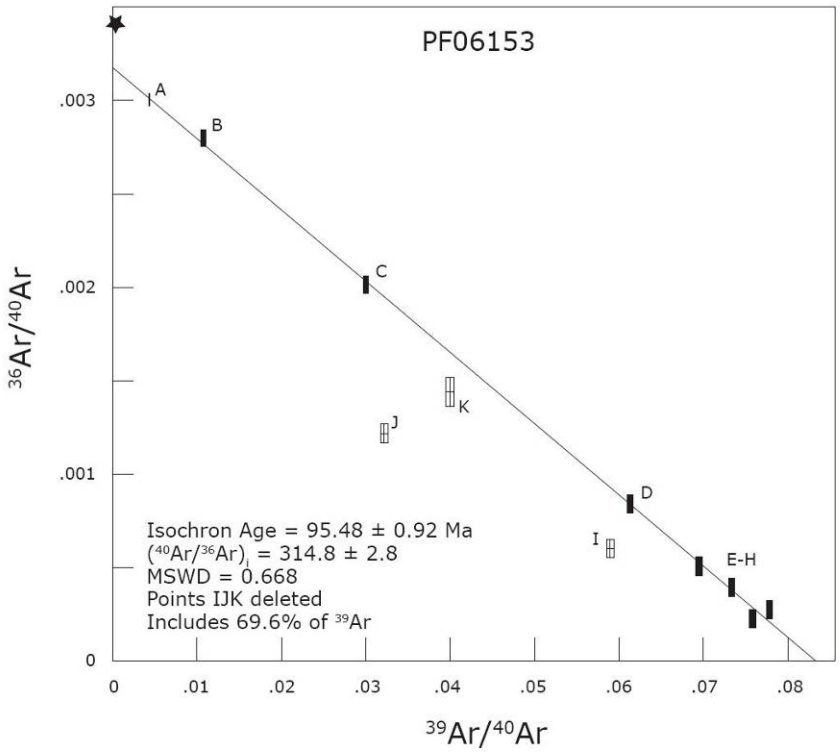

Figure 6.11: Plot of $^{36}Ar/^{40}Ar$ versus $^{39}Ar/^{40}Ar$ for the sample PF06153.

6.4 Radiogenic Isotopes

At least two samples from each complex were analysed with one sample representing the mafic end and the other sample representing the felsic end of the spectrum. The isotopes analysed were $^{87}Sr/^{86}Sr$ and $^{143}Nd/^{144}Nd$ with only 15 samples (including the standard) analysed for each due to the cost of the analysis procedure. The resultant data for strontium and neodymium is shown in Table 6.3 with initial/observed values and epsilon values from age correction calculations.

The age corrected value was calculated to 93.4 Ma which is the average Ar-Ar value for the Maningoza Suite age mentioned in section 6.3. The age corrected values for each is as follows: $^{87}Sr/^{86}Sr$ = 0.70461 and $^{143}Nd/^{144}Nd$ = 0.512514. The percentage standard error of the initial value for Sr and Nd isotopes is shown in Table 6.3 and is calculated by using the analytical errors on Rb, Sr and measured isotope ratios. The analytical errors are included in the calculation of the initial isotope ratio to obtain the highest and lowest possible initial value. The percentage standard error is half the difference between the highest and lowest possible initial values. The values of ε_{Sr} and ε_{Nd} are calculated using the equations below:

$$\varepsilon_{Sr} = \left(\frac{\left({}^{87}Sr/{}^{86}Sr \right)_o}{\left({}^{87}Sr/{}^{86}Sr \right)_i} - 1 \right) * 10000 \qquad \varepsilon_{Nd} = \left(\frac{\left({}^{143}Nd/{}^{144}Nd \right)_o}{\left({}^{143}Nd/{}^{144}Nd \right)_i} - 1 \right) * 10000$$

(*o* = initial and *i* = bulk earth value at the same age)

The equation used for calculating the $^{87}Rb/^{86}Sr$ ratio from Sr and Rb concentrations as well as the equation for calculating the $^{147}Sm/^{144}Nd$ from Nd and Sm concentrations are as follows:

$$\frac{{}^{87}Rb}{{}^{86}Sr} = \left(\frac{Rb}{Sr} \right) \times \left(2.692948 + 0.280304 \times \frac{{}^{87}Sr}{{}^{86}Sr_0} \right)$$

$$\frac{{}^{147}Sm}{{}^{144}Nd} = \left(\frac{Sm}{Nd} \right) \times \left(0.531497 + 0.142521 \times \frac{{}^{143}Nd}{{}^{144}Nd_0} \right)$$

The equations for calculating the age corrected values for $^{87}Sr/^{86}Sr$ and $^{143}Nd/^{144}Nd$ are as follows (where λ = decay constant and t = age):

$$\left(\frac{{}^{87}Sr}{{}^{86}Sr} \right)_0 = \left(\frac{{}^{87}Sr}{{}^{86}Sr} \right) - \left(\frac{{}^{87}Rb}{{}^{86}Sr} \right) \times \left(e^{\lambda t} - 1 \right) \qquad \left(\frac{{}^{143}Nd}{{}^{144}Nd} \right)_0 = \left(\frac{{}^{143}Nd}{{}^{144}Nd} \right) - \left(\frac{{}^{147}Sm}{{}^{144}Nd} \right) \times \left(e^{\lambda t} - 1 \right)$$

Sample	Rb	Sr	$^{87}Rb/^{86}Sr$	$^{87}Sr/^{86}Sr$	Sr0	%SE	ε_{Sr}
PF06001	20.25	300.00	0.195085	0.705867	0.705841	20	17.5
PF06005	72.18	132.66	1.573280	0.708980	0.708771	24	59.1
PF06017	1.07	326.30	0.009500	0.703816	0.703815	24	-11.2
PF06026	93.60	150.91	1.794433	0.714267	0.714029	22	133.8
PF06119	79.51	219.53	1.047234	0.708601	0.708462	19	54.7
PF06123	116.78	99.05	3.409503	0.710019	0.709566	31	70.4
PF06134	95.45	240.12	1.149602	0.710534	0.710381	18	82.0
PF06145	5.92	265.68	0.064353	0.704308	0.704299	21	-4.3
PF06138	1.26	164.13	0.022255	0.703051	0.703048	19	-22.1
MI06011	0.21	212.96	0.002866	0.703020	0.703019	27	-22.5
MI06014	0.77	211.56	0.010522	0.704276	0.704275	28	-4.7
MI06016	152.32	52.41	8.411643	0.718943	0.717828	50	187.7
BY6F091	1.85	154.94	0.034577	0.702975	0.702970	18	-23.2
BY6F098b	77.81	86.37	2.605040	0.709447	0.709101	26	63.8

Sample	Sm	Nd	$^{147}Sm/^{144}Nd$	$^{143}Nd/^{144}Nd$	Nd0	%SE	ε_{Nd}
PF06001	5.16	23.01	0.135622	0.512284	0.512201	76	-6.1
PF06005	10.01	51.96	0.116429	0.512067	0.511996	39	-10.1
PF06017	0.68	2.79	0.146831	0.512711	0.512621	1810	2.1
PF06026	7.71	39.46	0.118081	0.512060	0.511988	47	-10.3
PF06119	7.29	33.43	0.131762	0.512168	0.512088	52	-8.3
PF06123	8.33	45.03	0.111824	0.511997	0.511929	44	-11.4
PF06134	7.57	39.84	0.114919	0.512069	0.511999	46	-10.1
PF06145	2.92	11.12	0.158801	0.512598	0.512501	159	-0.3
PF06138	2.46	7.13	0.208275	0.513155	0.513028	292	10.0
MI06011	0.09	0.36	0.156714	0.512934	0.512838	25	6.3
MI06014	0.56	1.35	0.250690	0.512869	0.512716	263	3.9
MI06016	11.16	54.75	0.123190	0.512160	0.512085	39	-8.4
BY6F091	3.59	9.97	0.217870	0.513152	0.513019	91	9.9
BY6F098b	24.48	132.83	0.111426	0.512384	0.512316	21	-3.9

Table 6.3: Table of strontium and neodymium data showing the measured/initial values and epsilon values for the Maningoza Suite. Sr0 represents initial $^{87}Sr/^{86}Sr$, Nd0 represents initial $^{143}Nd/^{144}Nd$ and %SE is the percentage standard error on the initial values of Sr and Nd. Initial values are calculated to 93.4 Ma.

Figure 6.12 shows the $^{87}Sr/^{86}Sr$ versus $^{87}Rb/^{86}Sr$ data which would normally be an isochron diagram, however this is not the purpose here since the diagram is generated from data from different complexes. The different complexes did not necessarily form at the same time as each other. Using the data together in the diagram is only to see if there is correlation and hence if there is any age significance. An accurate isochron for each complex could not be completed for most complexes because there is only one or two data point(s) which is not enough to create an accurate isochron. This is the same for $^{143}Nd/^{144}Nd$ versus $^{147}Sm/^{144}Nd$ in Figure 6.13. It is interesting to note that the line of best fit on the Sr isochron diagram gives an age of 128 Ma which is close to the accepted age and the correlation of the 14 data points is strong (r = 0.87). The correlation of the data points for the line of best fit on the Nd

isochron diagram is also strong (r = 0.85) yet the age that is calculated is 1228 Ma which is much older than the accepted age.

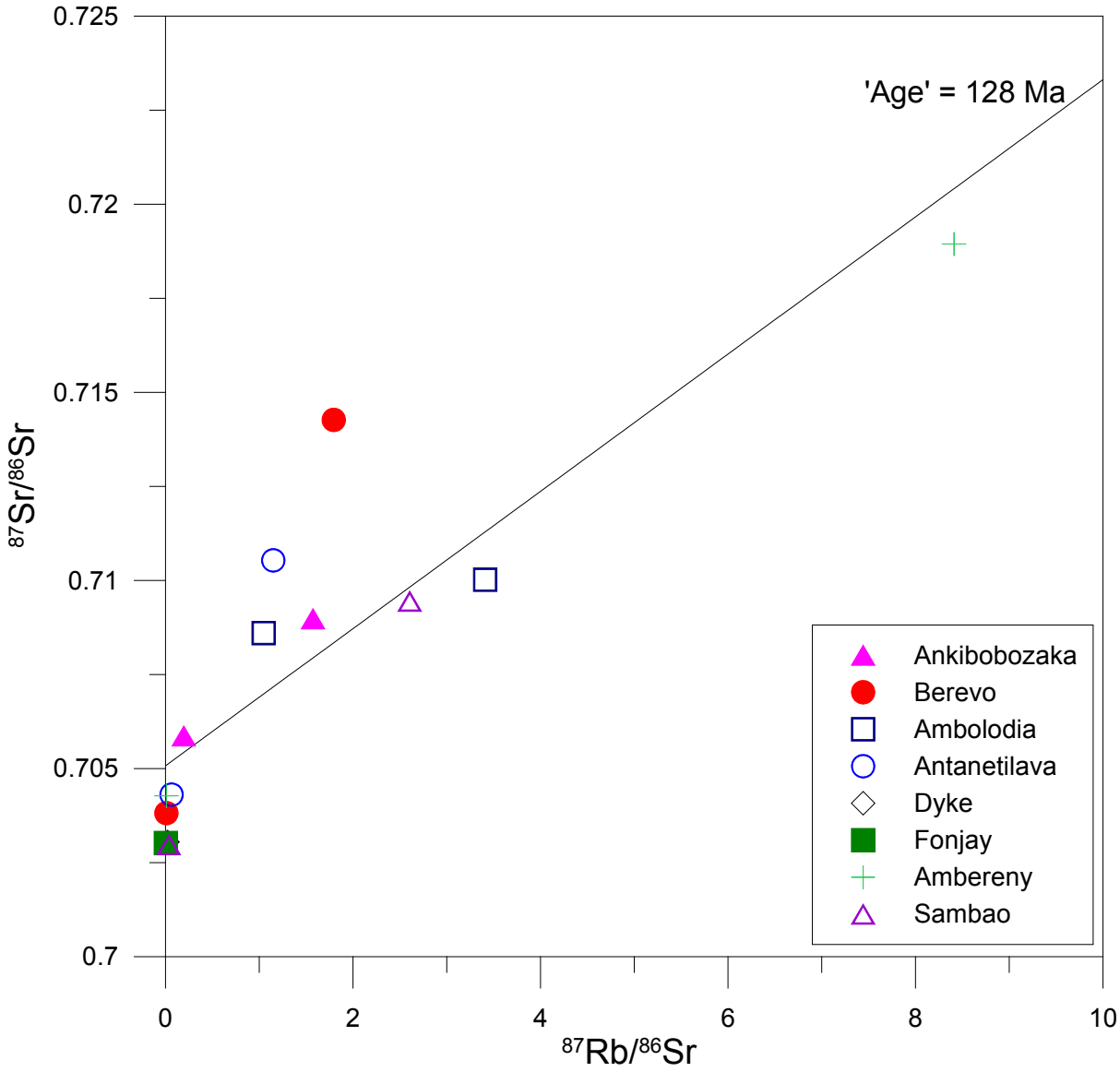

Figure 6.12: Plot of $^{87}Rb/^{86}Sr$ versus $^{87}Sr/^{86}Sr$ showing a line of best fit. The age is calculated using the slope of the line of best fit and the equation below: $slope(m) = (e^{\lambda t} - 1)$ where t = time in years and λ = Sr decay constant.

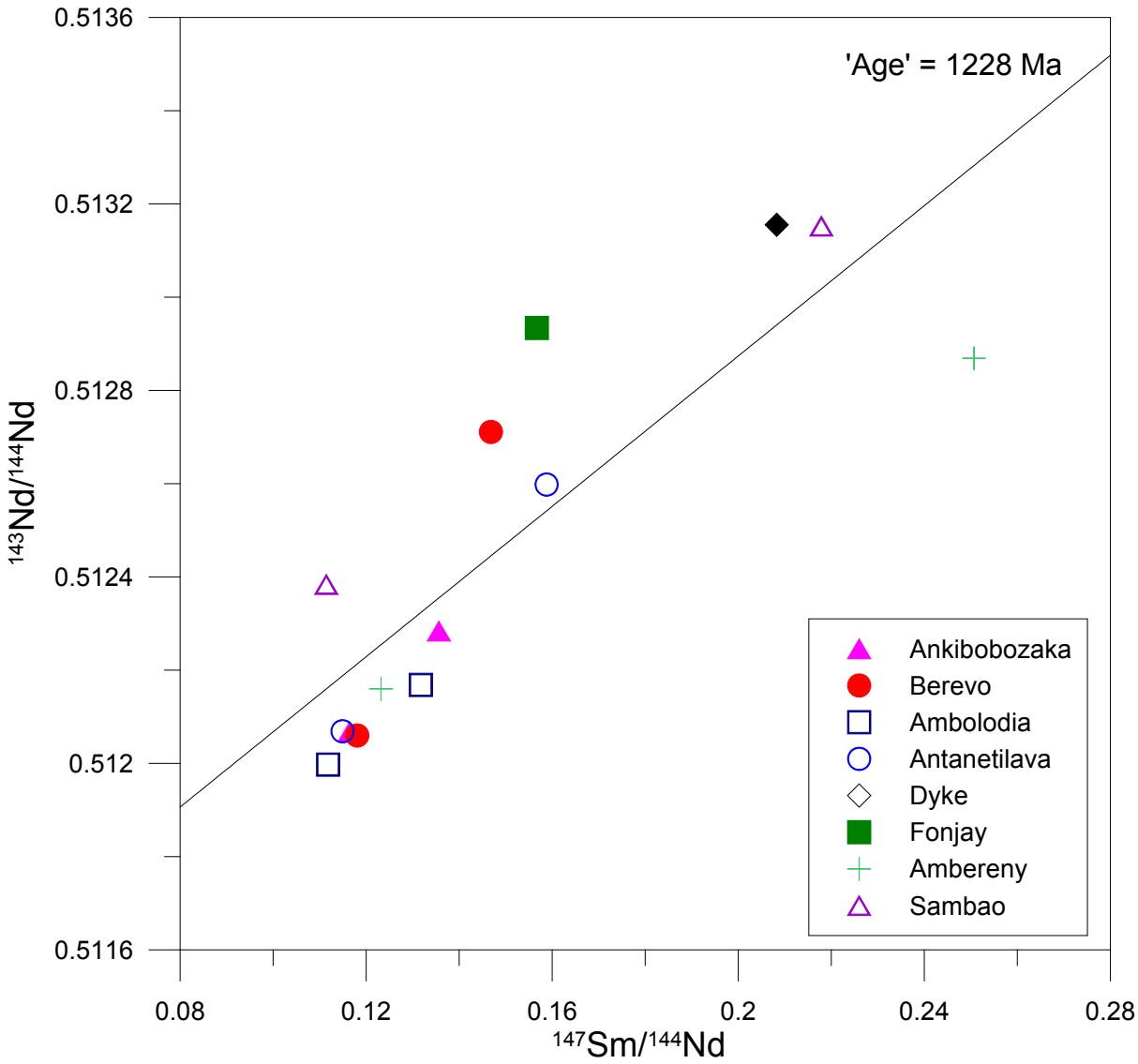

Figure 6.13: Plot of $^{147}Sm/^{144}Nd$ versus $^{143}Nd/^{144}Nd$ showing a line of best fit. The age is calculated using the slope of the line of best fit and the equation below: $slope(m) = (e^{\lambda t} - 1)$ where t = time in years and λ = Nd decay constant.

6.4.1 Variation of Strontium Isotopes with other parameters

The initial Sr isotope ratio ranges from 0.70297 to 0.71783 and has an average of 0.70753 ± 0.00451 (1σ, n = 14). Comparing the initial Sr isotope ratio against major and trace elements for each sample shows a good correlation with SiO_2, MgO, CaO and Zr (Figure 6.14). The r value is higher than 0.72 in all four cases. The Sr isotope ratio increases as SiO_2 and Zr increases and the Sr isotope ratio decreases as MgO and CaO increases. The Sr isotope ratio in the felsic samples is higher than that of their mafic counterparts and in most cases the Sr isotope ratio is proportional to how evolved the sample is.

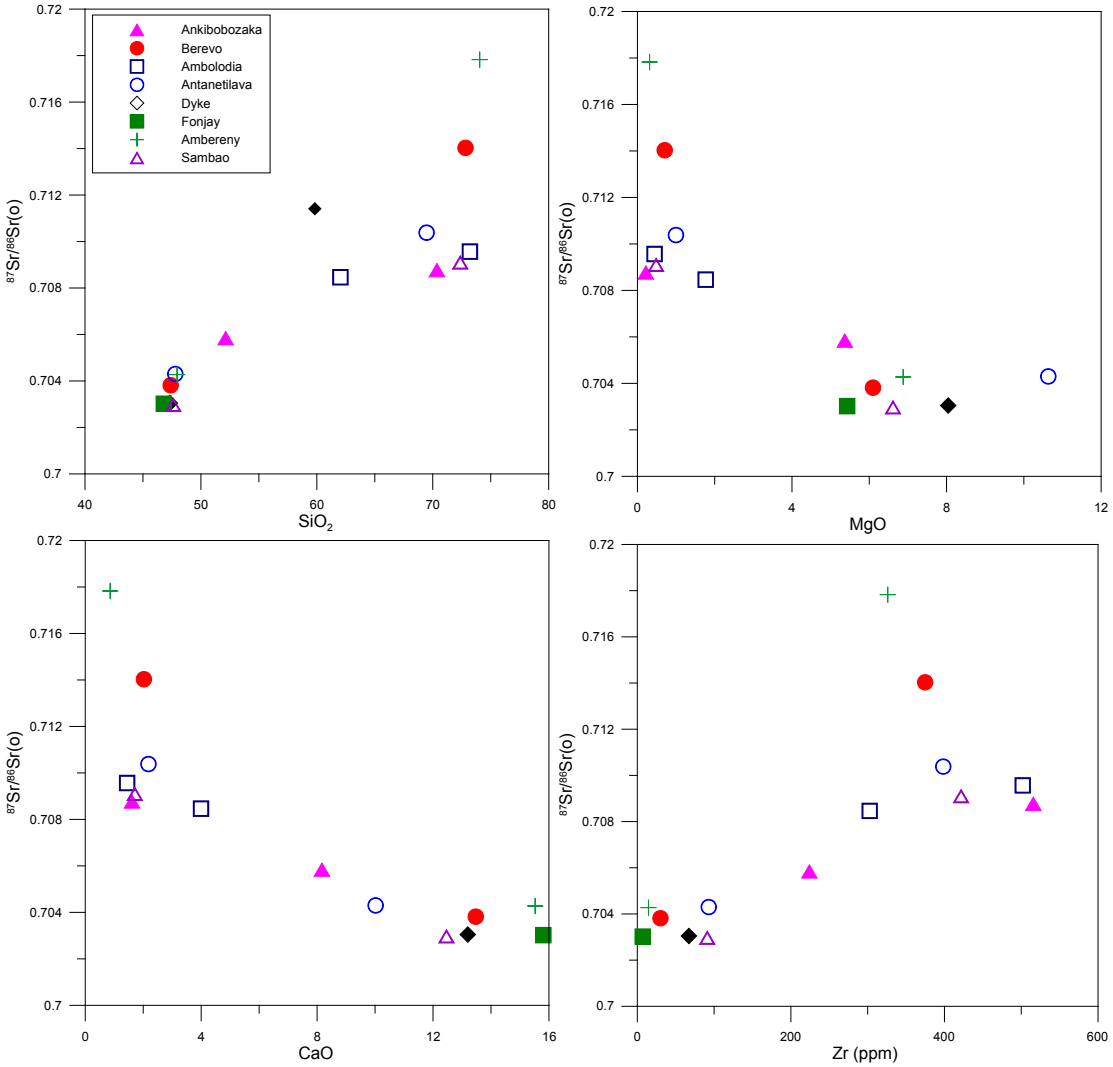

Figure 6.14: Graphs showing initial $^{87}Sr/^{86}Sr$ versus major and trace elements.

6.4.2 Variation of Neodymium Isotopes with other parameters

The initial Nd isotope ratio ranges from 0.511929 to 0.513028 with an average of 0.512380 ± 0.000400 (1σ, n = 14). The plot of initial Nd isotope ratio against major and trace elements (Figure 6.15) shows that there is a strong correlation for SiO_2, MgO, CaO and Zr ($r > 0.78$ in all four cases) as is the case with the Sr isotopes. The Nd isotope ratio decreases with increasing SiO_2 and Zr content and the Nd isotope ratio increases with increasing MgO and CaO content. So in this case the Nd isotope ratio is inversely proportional to how evolved the sample is.

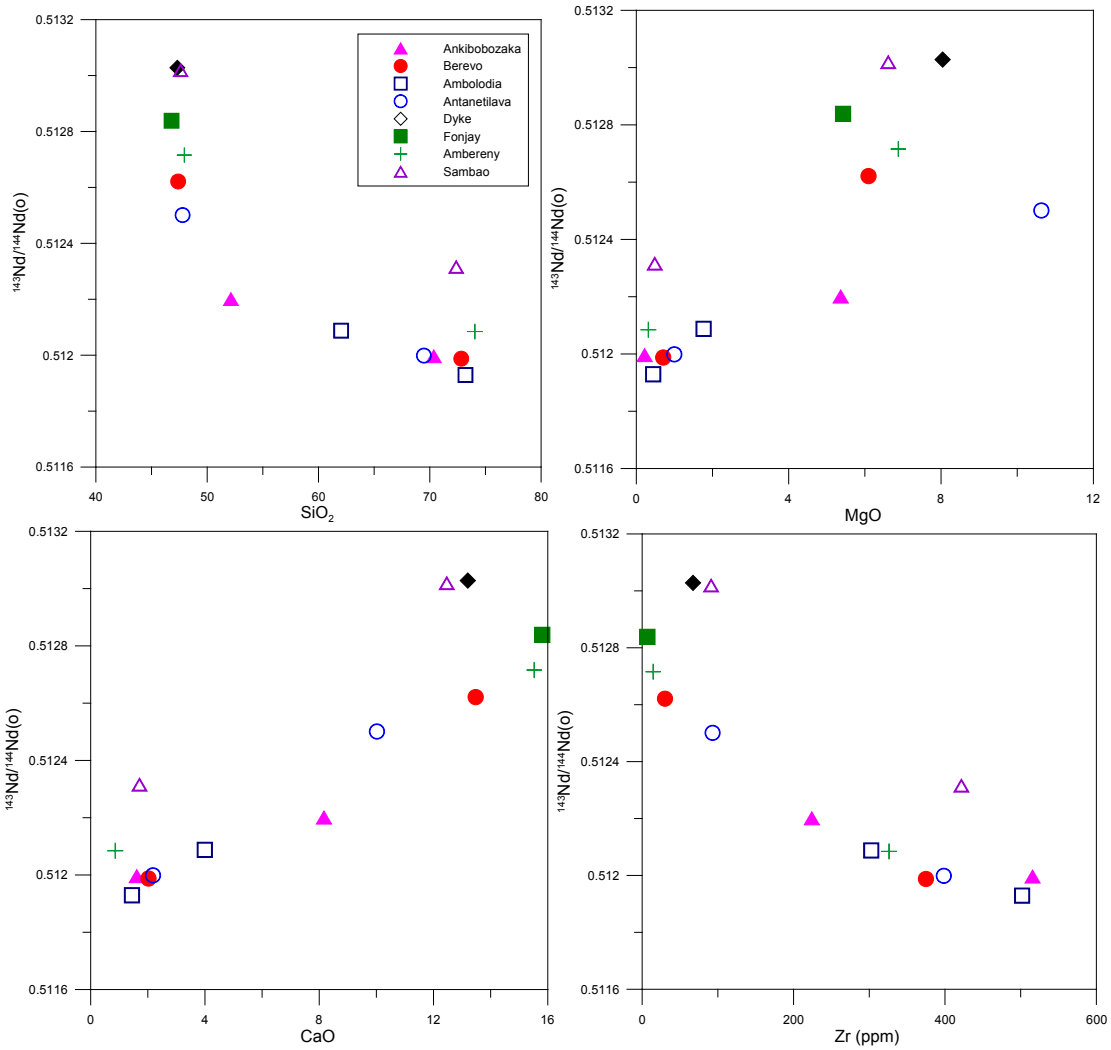

Figure 6.15: Graphs showing initial $^{143}Nd/^{144}Nd$ versus major and trace elements.

6.4.3 Comparison of Sr and Nd Isotopes

The mafic Sambao (BY6F091) and basement dyke (PF06138) samples have ε_{Sr} and ε_{Nd} values similar to MORB (mid oceanic ridge basalts) as shown in Figure 6.16. The mafic samples from Fonjay (MI06011), Ambereny (MI06014), Berevo (PF06017) and Antanetilava (PF06145) have ε_{Sr} and ε_{Nd} values of OIB (oceanic island basalts). The felsic samples from Sambao (BY6F098b), Antanetilava (PF06134), Berevo (PF06026) and Ambereny (MI06016) show signs of crustal contamination where as the mafic and felsic samples from Ankibobozaka and Ambolodia both show signs of crustal contamination. The felsic samples of the Maningoza Suite show signs of crustal contamination where as the mafic samples are generally similar to MORB and OIB. Exceptions to this are the Ankibobozaka Complex and Ambolodia Formation where their mafic and felsic samples show signs of crustal contamination.

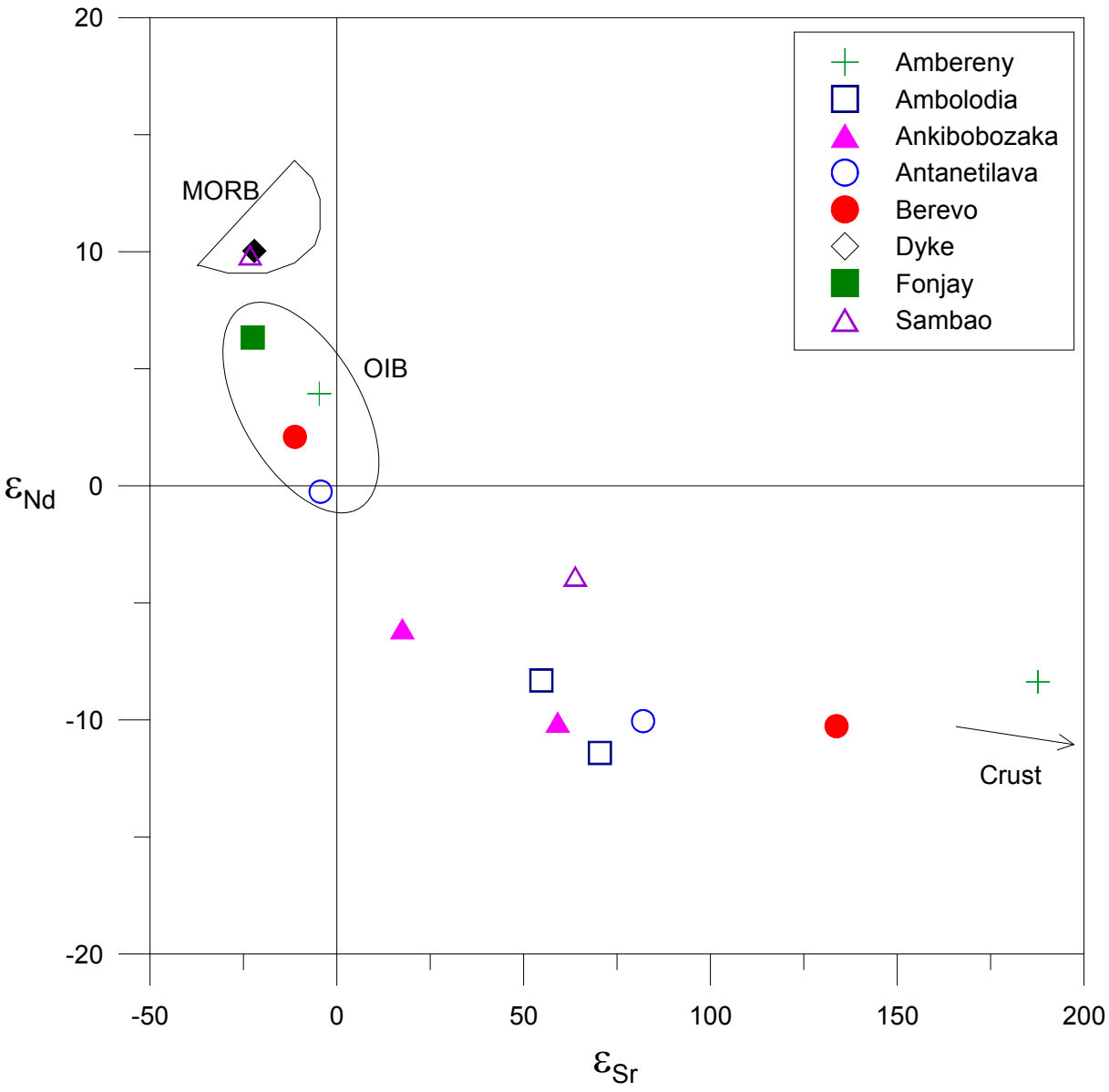

Figure 6.16: Graph of ε_{Sr} vs. ε_{Nd} showing all the samples analysed for the Maningoza Suite. The graph also shows fields for mid oceanic ridge basalts (MORB) and oceanic island basalts (OIB). The arrow reflects the direction of increasing crustal component.

6.5 Comparison of Stable and Radiogenic Isotopes

Whole-rock $\delta^{18}O$ values plotted against both ε_{Sr} and ε_{Nd} (calculated to 93.4 Ma) show little or no correlation as shown in Figure 6.17. The r value for whole-rock $\delta^{18}O$ versus ε_{Sr} is 0.14 (n = 14) and the r value for whole-rock $\delta^{18}O$ versus ε_{Nd} is -0.15 (n = 14). When the δD values are plotted against both ε_{Sr} and ε_{Nd} (Figure 6.17) strong correlations are observed, with the exception of four samples. This correlation suggests that δD is related to assimilation and from the trend that the contaminant has a higher δD value than the Maningoza Suite magma.

The four samples that lie off the trend line have low δD values and also low H_2O^+ values. The samples with low H_2O^+ values might represent incomplete extraction of water during the heating process and therefore inconsistent data. Also worth noting is that if these four samples are removed from the plots of whole-rock $\delta^{18}O$ versus ε_{Sr} and ε_{Nd} then the correlation is better (change from r value of 0.14 to 0.77 for Sr and change from r value of -0.15 to -0.47 for Nd). Figure 6.17 also shows a correlation between H_2O^+ values and the radiogenic isotopes with a positive correlation between water and strontium and a negative correlation between water and neodymium. It appears as if the water is behaving as an incompatible element, increasing in more evolved rocks and suggests that the water is probably magmatic in origin.

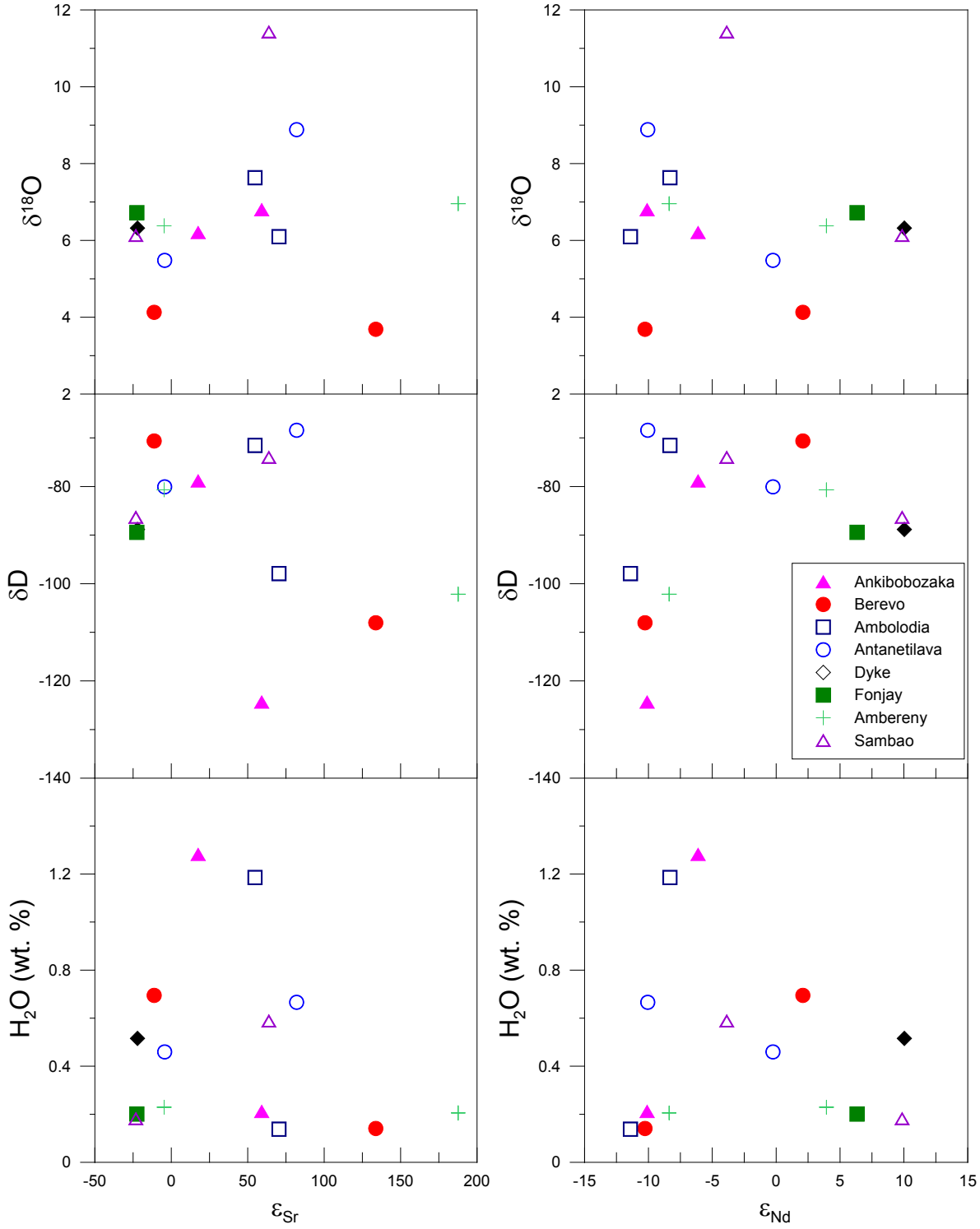

Figure 6.17: Plots of ε_{Sr} and ε_{Nd} versus whole-rock $\delta^{18}O$, δD and H_2O^+ (wt. %). The values for ε_{Sr} and ε_{Nd} have been calculated to 93.4 Ma.

6.6 Summary

Whole-rock $\delta^{18}O$ values lower than 5.7‰ are observed for the Antanetilava Formation, Ambolodia Formation, Ankibobozaka Complex, Berevo Complex, Fonjay Complex and Ambereny Complex. The Sambao Formation has whole-rock $\delta^{18}O$ values higher than 11‰ for two of its three samples. The Berevo Complex and Ambolodia Formation both have one sample with $\delta^{18}O$ values higher than 11‰. All of the complexes have $\delta^{18}O$ values which fall between 5.7‰ and 9‰. In all cases the $\delta^{18}O$ values of minerals are lower than the $\delta^{18}O$ values of the whole-rock of the same sample (except clinopyroxene of sample PF06020). Hydrogen isotopes show Rayleigh-type fractionation with low δD values associated with low H_2O^+ values suggestive of degassing. The Ankibobozaka Complex has two samples with low δD values (-127‰ and -124‰) and the Berevo Complex has one sample with low δD values (-121‰). The highest δD values are observed for the Antanetilava Formation (-62‰) and Ambolodia Formation (-64‰). All the complexes of the Maningoza Suite analysed for hydrogen isotopes appear associated with magmatic waters and show signs of degassing. Ar-Ar geochronology of two samples of the Maningoza Suite returned ages of 91.33 Ma and 95.48 Ma with an average 93.4 Ma. Radiogenic isotopes show strong correlations with major and trace elements suggesting evolution of the Maningoza Suite involves fractional crystallisation and assimilation. This is further investigated in the Chapter 7. The dyke swarm and Sambao Formation have samples which appear to be the most primitive amongst the Maningoza Suite. The Berevo and Ambereny Complexes have samples which are the most contaminated by a crustal component. Mafic samples of the Antanetilava Formation, Berevo Complex, Fonjay Complex and Ambereny Complex have similar ε_{Sr} and ε_{Nd} values to OIB. The Ankibobozaka Complex and Ambolodia Formation as well as the felsic samples of the Antanetilava and Sambao Formations show signs of crustal contamination. A comparison of stable and radiogenic isotopes shows some strong correlations and suggests that hydrogen isotopes are related to assimilation of a crustal component. Four samples deviate from the trends and their values probably represent incomplete water extraction during the heating process.

7 MODELLING AND DISCUSSION

The variations in the TAS diagrams presented in Chapter 5 indicate differentiation from basalt to rhyolite. This chapter attempts to put constraints on the mechanism of evolution of the magma by the use of major and trace elements and radiogenic isotopes. The major and trace elements are used to test for fractional crystallisation and the radiogenic isotopes are used to test for magma mixing. The Maningoza Suite is then compared to other Cretaceous igneous complexes from Madagascar to observe similarities and differences in mineral chemistry, major and trace elements and radiogenic isotopes. Radiogenic isotopes will also be used to compare the Maningoza Suite to other igneous complexes that may have evolved in the same way, for example the Deccan Trap lavas. Fractional crystallisation is explored first in this chapter, then magma mixing and finally comparisons are made with other igneous complexes associated with Gondwana break-up.

7.1 Fractional Crystallisation

Modelling of fractional crystallisation was attempted with the use of major and trace elements. Semi-quantitative major element modelling of fractional crystallisation was performed using graphical methods, and quantitative modelling was attempted using least squares mixing via the DOS program 'MIXER'. MIXER is based on the least squares approach of Bryan et al. (1969). Trace element modelling of fractional crystallisation was done using the Rayleigh Fractionation Law.

7.1.1 Major Element Modelling Via Variation Diagrams

Variation diagrams for major elements were first used as a semi-quantitative attempt to establish: the feasibility of fractional crystallisation as a model; the assemblages being crystallised; the amount of fractional crystallisation for each complex. The likely minerals involved in fractional crystallisation based on the phenocryst assemblages are plagioclase, augite, olivine and Ti-magnetite, and these are plotted on the variation diagrams. The compositions of these minerals were chosen from the data set in the mineral chemistry chapter (Chapter 4) as shown in Table 7.1. The program MIXER was used to refine the dataset for a representative composition of the minerals and is described in the next section.

The decrease observed in major elements such as Fe_2O_3, CaO and Al_2O_3 as silica increases suggest evolution by fractional crystallisation. For example if magnetite is being crystallised out of the liquid and then removed the remaining melt would have a significant drop in Fe_2O_3.

The same is similar for minerals like anorthite which would decrease the amount of Al_2O_3 and CaO in the residual magma. This would lead to a decrease in these major elements as silica increases.

In an attempt to constrain the amount of fractional crystallisation occurring from the mafic end-member to felsic end-member, major elements such as Al_2O_3 and Fe_2O_3 were plotted against SiO_2 and MgO. Also plotted within these variation diagrams are minerals that reflect the crystallising assemblage. The method used is limited to the use of only three minerals per complex as the method relies on the use of triangular diagrams during the calculation. A fourth mineral can be shown on the diagrams as well to show that the mineral is not involved in the fractional crystallisation process.

Mineral	SiO_2	TiO_2	Al_2O_3	FeO	MnO	MgO	CaO	Na_2O	K_2O	Total
Plagioclase	53.69	0.07	28.28	1.37	0.06	0.07	10.96	4.79	0.42	99.72
Augite	48.83	1.18	3.33	14.07	0.36	13.28	18.91	0.46	0.05	100.47
Ti-Magnetite	2.39	11.58	2.06	76.53	0.77	0.02	2.38	0.00	0.00	95.73
Olivine	37.45	0.05	0.01	25.75	0.56	36.12	0.05	0.00	0.00	100.00

Table 7.1: Major element weight percentages for the minerals plagioclase, augite, Ti-magnetite and olivine. The data was taken from the mineral chemistry dataset (Tables A1 to A4 in the Appendix) and then refined using the program MIXER for the best representative compositions.

All the complexes were modelled using plagioclase, augite and Ti-magnetite based on trends observed on the variation diagrams. Figure 7.1, Figure 7.2 and Figure 7.3 show selected variation diagrams that were used in calculating the amount of fractional crystallisation for each complex. The variation diagrams shown are SiO_2 plotted against CaO and Al_2O_3. Also included on the diagrams are the minerals plagioclase, augite and magnetite-used in the calculation for each complex-as well as olivine. The line indicates fractional crystallisation from the mafic sample to the felsic sample.

Figure 7.1 also shows that for SiO_2 plotted against CaO some of the samples for the Ambolodia, Antanetilava and Sambao Formation appear have undergone fractionation of augite before fractionating an assemblage of plagioclase, augite and magnetite. The Antanetilava Formation also appears to show fractionation of plagioclase before fractionating the main assemblage as shown in the plot of SiO_2 against Al_2O_3.

Figure 7.2 shows a similar behaviour of augite fractionation for the Ankibobozaka, Ambohitrosy and Fonjay Complexes in the plot of SiO_2 against CaO. The Fonjay and Ambohitrosy Complexes also appear to show plagioclase fractionation before fractionating

out an assemblage of plagioclase, augite and magnetite as shown in the plot of SiO_2 against Al_2O_3.

Figure 7.3 also shows signs of plagioclase fractionation before fractionating out an assemblage of plagioclase, augite and magnetite for the Berevo and Ambereny Complexes as shown in the plot of SiO_2 against Al_2O_3.

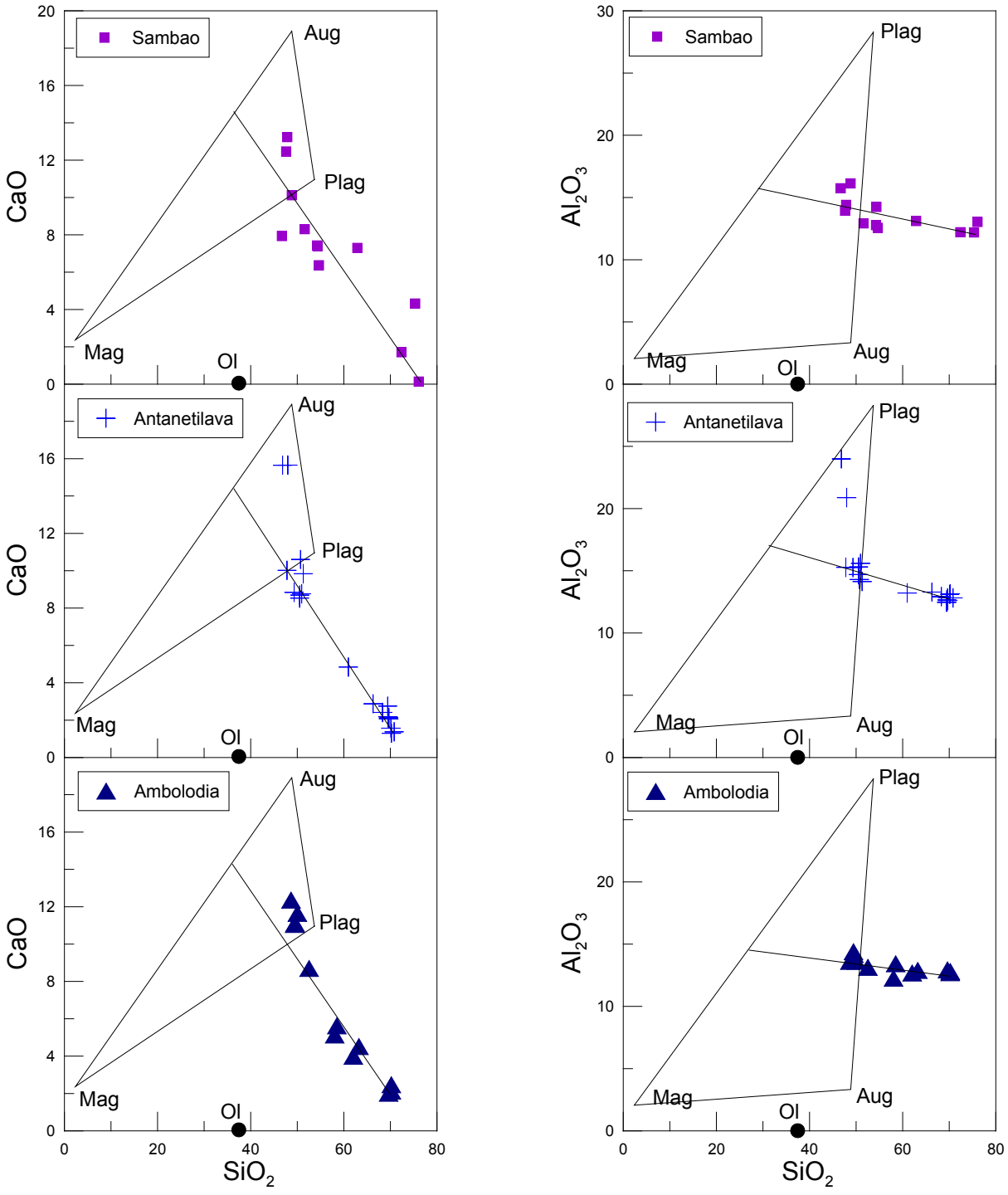

Figure 7.1: Selected variation diagrams SiO_2 against MgO and Al_2O_3 for the Ambolodia, Antanetilava and Sambao Formations. Included in the diagram are the minerals used in the calculation where Plag = plagioclase, Aug = augite, Mag = magnetite and Ol = olivine.

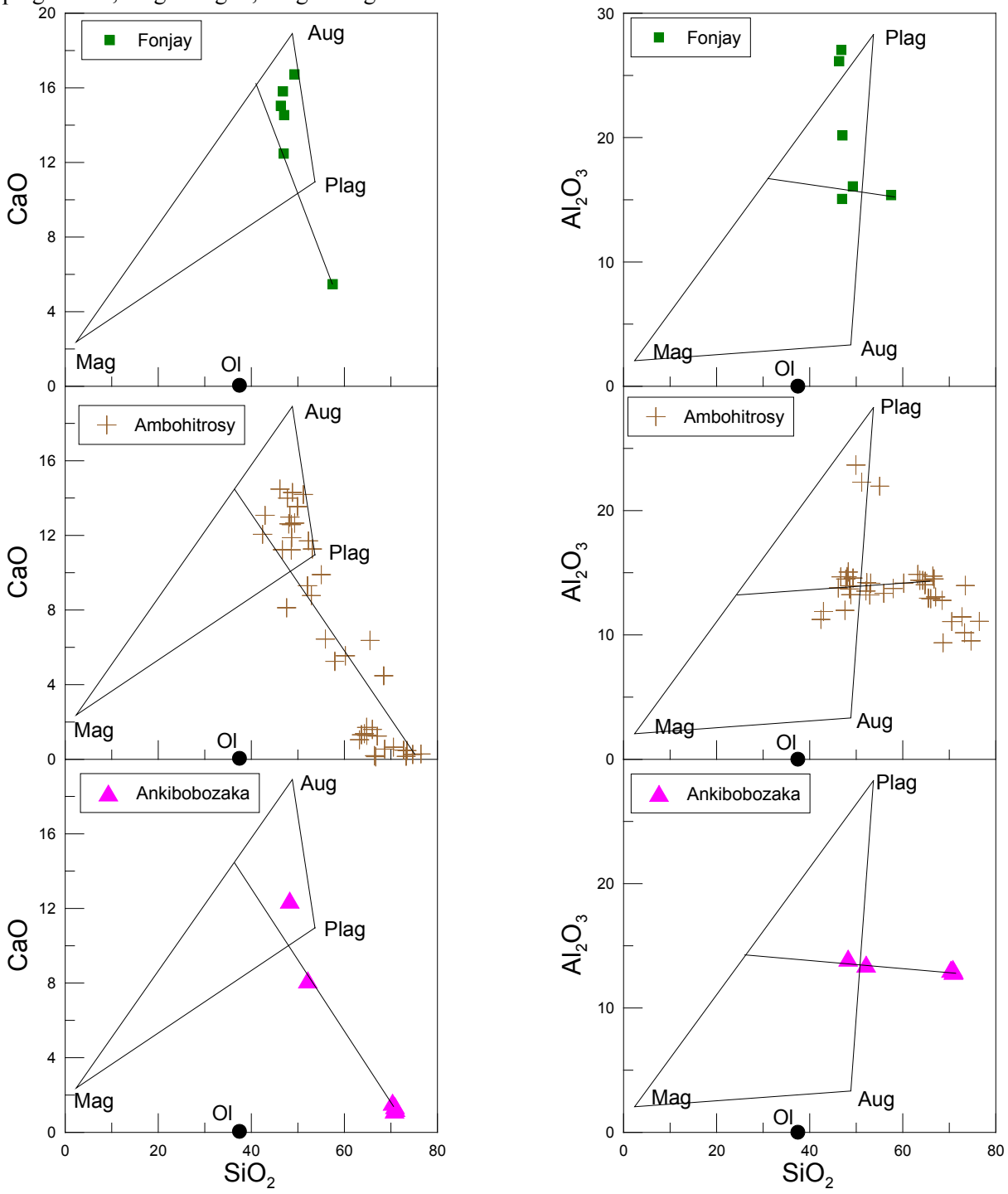

Figure 7.2: Selected variation diagrams SiO_2 against MgO and Al_2O_3 for the Ankibobozaka, Ambohitrosy and Fonjay Complexes. Included in the diagram are the minerals used in the calculation where Plag = plagioclase, Aug = augite, Mag = magnetite and Ol = olivine.

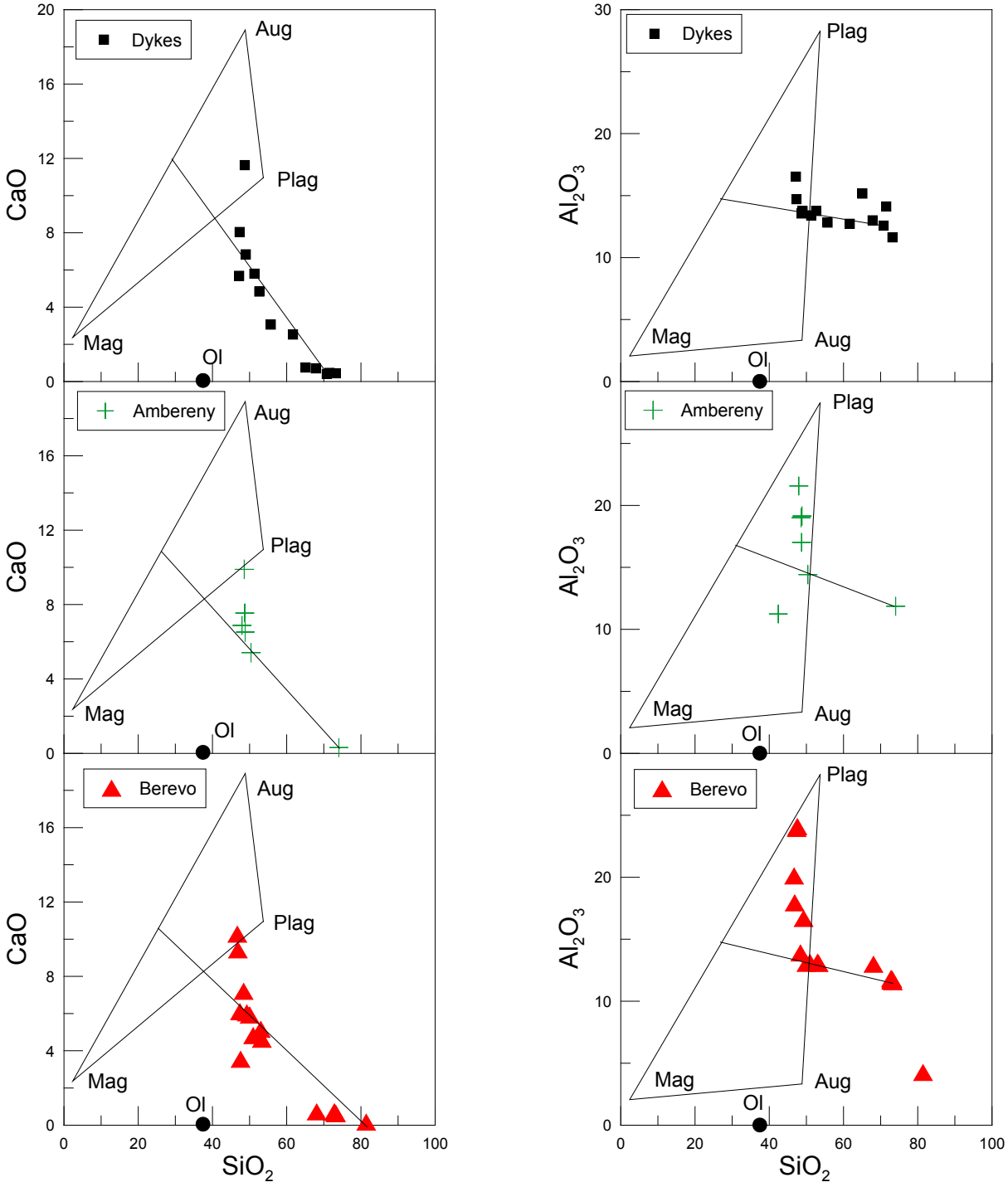

Figure 7.3: Selected variation diagrams SiO_2 against MgO and Al_2O_3 for the Berevo and Ambereny Complexes as well as the dyke swarm. Included in the diagram are the minerals used in the calculation where Plag = plagioclase, Aug = augite, Mag = magnetite and Ol = olivine.

Table 7.2 gives an estimate of how much fractional crystallisation each complex has undergone according to the calculations done using the variation diagram technique described previously. The amount of fractional crystallisation is expressed as a percentage and was calculated from the lowest SiO_2 to the highest SiO_2. An attempt was made to exclude cumulates from the calculation. The lowest amount of fractionation estimated is

found in the Sambao Formation (68%) and the Ambolodia Formation (69%). The Ankibobozaka and Berevo Complexes both have 76% fractional crystallisation and the Antanetilava Formation has 80% fractional crystallisation. The dyke swarm and the Ambolodia Formation are estimated to have undergone 81% and 82% fractional crystallisation respectively. The highest amounts of fractionation are estimated for the Fonjay Complex (84%) and the Ambereny Complex (86%).

Table 7.2 also shows that the highest percentage of plagioclase fractionation is estimated for the Fonjay (60%) and Ambohitrosy Complexes (50%). The Antanetilava Formation and Ambereny Complex are both estimated to fractionate out 45% plagioclase. The Ankibobozaka Complex, Berevo Complex, Sambao Formation and the Ambolodia Formation are all estimated to fractionate 40% plagioclase. The lowest amounts of plagioclase being fractionated out are estimated to be in the dyke swarm (35%). The estimated amount of augite being fractionated ranges between 40% and 50% for all complexes except for the Fonjay Complex which is estimated to have fractionated 35% augite. Magnetite is estimated to have fractionated between 10% and 20% for all complexes except for the Fonjay Complex which fractionates 5% magnetite.

Complex	Plagioclase	Augite	Magnetite	Fractionation %
Ankibobozaka	40	50	10	76
Berevo	40	45	15	76
Ambolodia	40	45	15	69
Antanetilava	45	45	10	80
Sambao	40	40	20	68
Dykes	35	50	15	81
Fonjay	60	35	5	84
Ambereny	45	42	13	86
Ambohitrosy	50	40	10	82

Table 7.2: The amount of fractionation calculated from the lowest SiO_2 wt. % to highest SiO_2 wt. % and the amount of plagioclase, augite, magnetite and olivine being fractionated for each complex.

7.1.2 Major Element Modelling using the Least Squares Method

The program MIXER has been used in conjunction with the variation diagrams method in the above section to refine mineral compositions and to check the accuracy of the variation diagrams method. The MIXER program models crystal fractionation by using the least squares method. Table 7.3 shows the outputs for fractional crystallisation from PF06150 (parent) to PF06147 (daughter) for the Antanetilava Formation and from PF06136 (parent) to PF06116 (daughter) for the Ambolodia Formation. The modelling in MIXER was done by

calculating the addition of crystals back into the liquid (i.e. addition required from the daughter sample to reach the parent sample). The samples were chosen because they are fine-grained volcanic samples and are most likely to represent liquids.

As shown in Table 7.3 the amount of crystal fractionation is 76.5% for the Antanetilava Formation and 65.1% for the Ambolodia Formation. The minerals being fractionated out are plagioclase, clinopyroxene, Ti-magnetite and olivine. Mineral proportions have been recalculated to 100% giving 46% plagioclase, 38% clinopyroxene, 11% Ti-magnetite and 5% olivine for the Antanetilava Formation. For the Ambolodia Formation the mineral proportions are 41% plagioclase, 37% clinopyroxene, 17% Ti-magnetite and 4% olivine.

A comparison between the least squares method and the variation diagrams method shows a good correlation with the Antanetilava Formation estimated to have 80% fractional crystallisation with the variation diagrams method and 76.5% for the least squares method. The Ambolodia Formation has a fractional crystallisation estimate of 69% for the variation diagram method and 65.1% for the least squares method. In terms of the minerals assemblage the estimates of plagioclase and Ti-magnetite are similar with a maximum difference of 2% between the two methods. The main difference between the two methods is the estimates of clinopyroxene and olivine where the variation diagrams method does not include olivine and therefore compensates with higher percentages of clinopyroxene.

	PF06150 obs	PF06150 calc	Diff.	Mix	wt.%
SiO_2	51.29	51.29	0.00	PF06147	23.5
TiO_2	1.63	1.57	-0.06	Plagioclase	35.5
Al_2O_3	14.14	14.19	0.05	Ti-Magnetite	8.6
FeO	13.24	13.25	0.01	Clinopyroxene	28.7
MnO	0.19	0.23	0.04	Olivine	3.7
MgO	5.30	5.30	0.00		
CaO	9.84	9.85	0.01	Total	100.0
Na_2O	2.91	2.62	-0.29		
K_2O	1.18	1.30	0.12		
Sum of Squares			0.11		

	PF06136 obs	PF06136 calc	Diff.	Mix	wt.%
SiO_2	52.53	52.50	-0.03	PF06116	35.2
TiO_2	1.72	1.84	0.12	Plagioclase	27.0
Al_2O_3	13.14	13.16	0.02	Ti-Magnetite	11.2
FeO	14.82	14.80	-0.02	Clinopyroxene	24.5
MnO	0.21	0.25	0.04	Olivine	2.9
MgO	4.56	4.60	0.04		
CaO	8.69	8.73	0.04	Total	100.8
Na_2O	2.72	2.80	0.08		
K_2O	1.35	1.63	0.28		
Sum of Squares			0.10		

Sample	PF06150	PF06147	PF06136	PF06116
SiO_2	51.29	70.81	52.53	70.21
TiO_2	1.63	0.88	1.72	0.66
Al_2O_3	14.14	12.82	13.14	12.7
FeO	13.24	5.05	14.82	4.65
MnO	0.19	0.06	0.21	0.11
MgO	5.30	0.62	4.56	0.81
CaO	9.84	1.38	8.69	2.47
Na_2O	2.91	3.32	2.72	3.96
K_2O	1.18	4.83	1.35	4.26

Table 7.3: Modelling of crystal fractionation from PF06150 to PF06147 for the Antanetilava Formation, and from PF06116 to PF06136 for the Ambolodia Formation. Compositions of all four samples are also given. Samples PF06150 and PF06136 represent the parent rocks and the samples PF06147 and PF06116 represent the daughter rocks.

7.1.3 Trace Element Modelling

The amount of fractional crystallisation has been further investigated by the use of trace elements. The trace element concentrations for felsic end-member rocks can be estimated using partition coefficients and the amount of fractionation calculated using major elements. The calculated value is then compared to the actual trace element concentrations in felsic

end-members in the same complex for accuracy and variations. The Rayleigh Fractionation Law was used as the model for trace elements and partition coefficients used are shown in Table 7.4. The Rayleigh Fractionation Law is described below:

$$\frac{Cl}{Co} = F^{(\overline{D}-1)} \text{ and } \overline{D} = \sum_{i=1}^{n} D_i W_i$$

Where Cl = concentration of element in liquid

Co = concentration of element in initial liquid

F = weight fraction of liquid remaining

$\overline{D}$ = bulk partition coefficient

D = mineral/melt partition coefficient

W = weight fraction of mineral in extract

Element	Plagioclase	Clinopyroxene	Magnetite	Olivine
U	0.093	0.04	0.	0.002
Ba	0.31	0.026	0.	0.01
Nb	0.06	0.005	0.4	0.01
Zr	0.1	0.1	0.1	0.012
Y	0.1	0.9	0.2	0.01
Sr	4.4	0.06	0.	0.014
Rb	0.041	0.031	0.	0.01
La	0.38	0.056	2.	0.007
Ce	0.27	0.09	2.	0.006
Eu	2.1	0.51	1.	0.007
Yb	0.09	0.62	1.5	0.014
V	0.	1.35	26.	0.06
Ni	0.	34.	153.	0.7
Cr	0.	1.5	29.	22.

Table 7.4: Partition coefficients used in the trace elements calculations for the minerals plagioclase, clinopyroxene, magnetite and olivine taken from Rollinson 1993.

Table 7.5 and Table 7.6 show that the calculated values for Zr are much higher than the actual values for all complexes. In general the difference is between 100 and 200ppm. This is possibly due the high percentages of crystal fractionation as shown in section 7.1.1, which are used in the calculation. The calculated concentration of Zr increases exponentially as the percentage of fractional crystallisation increases. Nb shows a similar characteristic of higher calculated concentrations than the actual concentrations except for the Ambolodia and Sambao Formation. Both formations have the lowest estimates of fractional crystallisation

(68% for Sambao and 69% for Ambolodia) and it is likely that an accessory mineral containing Nb is being fractionated in the other complexes. The trace element Y is consistent with all complexes except for the Berevo Complex, the Antanetilava Formation and the dyke swarm. Sr is consistent with all complexes except for the Antanetilava Formation, Sambao Formation and Fonjay Complex. Rb is consistent with all complexes except for the Antanetilava Formation, Fonjay Complex and Ambereny Complex.

The calculated concentrations for Ba are always higher than the actual concentrations except for the Fonjay Complex and the dyke swarm. The discrepancy is likely due to the fact Ba substitutes for potassium in micas and K-feldspar which are not included in the modelling (Green 1980). The Fonjay Complex has calculated concentrations close to that of the actual concentrations which is explained by there being little or no fractionation of K-feldspar and micas in the complex. The dyke swarm has higher concentration of Ba than calculated suggesting the sample has a higher amount of K-feldspar than expected. The trace element U is consistent with all the complexes of the Maningoza Suite. The compatible elements V, Ni and Cr are inconsistent with all of the complexes of the Maningoza Suite. The partition coefficients for V, Ni and Cr are important to obtain good calculated concentrations and it is possible that because the modelling excludes olivine the bulk D values could give rise to the inconsistencies observed in Tables 7.5 and 7.6.

Trace element	Ambolodia PF60-136	bulk D	PF60-126		Antanetilava PF60-150	bulk D	PF60-147	
			Actual	Calculated			Actual	Calculated
U	0.39	0.06	0.76	1.2	0.20	0.06	1.5	0.88
Ba	465.	0.14	834.	1261.	521.	0.15	1209.	2000.
Nb	11.	0.09	20.	32.	12.	0.07	19.	51.
Zr	200.	0.1	450.	565.	181.	0.10	387.	754.
Y	35.	0.48	57.	64.	32.	0.47	48.	75.
Sr	338.	1.79	114.	136.	375.	2.01	148.	76.
Rb	20.	0.03	87.	62.	13.	0.03	131.	61.
La	19.	0.48	48.	34.	19.	0.40	42.	49.
Ce	43.	0.45	99.	82.	43.	0.36	84.	117.
Eu	1.7	1.22	1.6	1.3	1.6	1.27	1.6	1.0
Yb	2.7	0.54	3.8	4.7	2.5	0.47	3.2	5.8
V	436.	4.51	25.	7.6	386.	3.21	46.	12.
Ni	25.	38.3	3.4	0.00	146.	30.6	8.9	0.00
Cr	24.	5.03	6.4	0.23	52.	3.58	5.9	0.87

Trace element	Sambao BY6F-098	bulk D	BY6F-098B		Ankibobozaka PF60-001	bulk D	PF06002	
			Actual	Calculated			Actual	Calculated
U	0.36	0.05	1.4	1.1	0.19	0.06	0.34	0.73
Ba	381.	0.13	789.	1021.	585.	0.14	1366.	1968.
Nb	16.	0.11	51.	46.	13.	0.07	26.	47.
Zr	239.	0.10	422.	666.	224.	0.10	612.	795.
Y	59.	0.44	108.	112.	37.	0.51	73.	73.
Sr	311.	1.78	90.	127.	333.	1.79	126.	110.
Rb	32.	0.03	86.	96.	21.	0.03	81.	82.
La	20.	0.57	144.	33.	20.	0.38	62.	48.
Ce	47.	0.54	305.	80.	45.	0.35	124.	111.
Eu	3.3	1.24	2.3	2.5	1.7	1.20	1.9	1.3
Yb	5.1	0.58	9.6	8.2	2.8	0.50	3.5	5.8
V	7.4	5.74	7.9	0.03	400.	3.28	3.1	16.
Ni		44.2		0.00	46.	32.3	11.	0.00
Cr	1.4	6.4	4.5	0.00	35.	3.65	4.2	0.84

Table 7.5: Selected trace element calculations for the Ambolodia, Antanetilava and Sambao Formations as well as the Ankibobozaka Complex. Calculated and actual values for the felsic end-member are included as well as the bulk partition coefficient D.

Trace element	Berevo PF60-032	bulk D	PF60-016		Fonjay M106-010	bulk D	M106-008	
			Actual	Calculated			Actual	Calculated
U	0.21	0.06	1.3	0.80	0.09	0.07	0.26	0.47
Ba	365.	0.14	754.	1252.	57.	0.20	259.	251.
Nb	9.8	0.09	21.	36.	9.1	0.06	20.	51.
Zr	140.	0.10	400.	506.	66.	0.10	222.	341.
Y	35.	0.48	48.	73.	19.	0.39	72.	57.
Sr	302.	1.79	154.	98.	222.	2.66	204.	11.
Rb	21.	0.03	108.	82.	8.6	0.04	15.	50.
La	13.	0.48	46.	27.	2.7	0.35	12.	8.9
Ce	29.	0.45	94.	63.	7.2	0.29	34.	26.
Eu	1.4	1.22	1.3	1.0	0.98	1.49	5.5	0.40
Yb	2.8	0.54	3.2	5.4	1.6	0.35	1.2	5.3
V	418.	4.51	31.	2.8	119.	1.77	0.58	29.
Ni	18.	38.3	14.	0.00		19.6		0.00
Cr	29.	5.03	4.5	0.09	73.	1.98	1.4	12.

Trace element	Ambereny M106-021	bulk D	M106-016		Dykes PF60-138	bulk D	PF60-123	
			Actual	Calculated			Actual	Calculated
U	0.30	0.06	3.3	1.8	0.03	0.05	0.81	0.14
Ba	323.	0.15	876.	1664.	125.	0.12	1347.	538.
Nb	13.	0.08	23.	74.	12.	0.08	16.	55.
Zr	199.	0.10	326.	1134.	197.	0.10	308.	880.
Y	34.	0.45	85.	98.	33.	0.52	44.	73.
Sr	398.	2.01	56.	57.	421.	1.57	234.	163.
Rb	6.1	0.03	178.	39.	20.	0.03	98.	99.
La	19.	0.45	67.	53.	2.0	0.46	36.	4.9
Ce	41.	0.42	110.	127.	7.1	0.44	75.	18.
Eu	2.2	1.29	1.3	1.2	1.0	1.14	1.8	0.79
Yb	3.0	0.50	6.0	8.0	1.9	0.57	3.4	3.9
V	188.	3.95	4.0	0.63	373.	4.58	2.8	0.98
Ni		34.2		0.00	290.	40.0	6.1	0.00
Cr	49.	4.40	13.	0.07	111.	5.10	2.6	0.12

Table 7.6: Selected trace element calculations for the Berevo, Fonjay and Ambereny Complexes as well as the dyke swarm. Calculated and actual values for the felsic end-member are included as well as the bulk partition coefficient D.

Figure 7.4 shows REE plots comparing the actual and calculated concentrations of the elements La, Ce, Eu and Yb taken from Tables 7.5 and 7.6. The comparisons show that the actual and calculated concentrations of all four elements are consistent in the Ambolodia Formation, Antanetilava Formation, Ankibobozaka Complex, Ambereny Complex and Berevo Complex. The concentrations of the elements Eu and Yb are consistent for the Sambao Formation but the calculated concentrations for La and Ce are much lower than the actual concentrations. The dyke swarm is similar to the Sambao Formation with calculated concentrations for La and Ce being much lower than the actual concentrations. The calculated concentrations for Eu are also lower than the actual concentrations and only the element Yb is consistent in the dyke swarm. The elements La and Ce are consistent in the Fonjay Complex but the calculated concentrations for Eu are much lower than the actual

concentrations and the calculated concentrations for Yb are much higher than the actual concentrations.

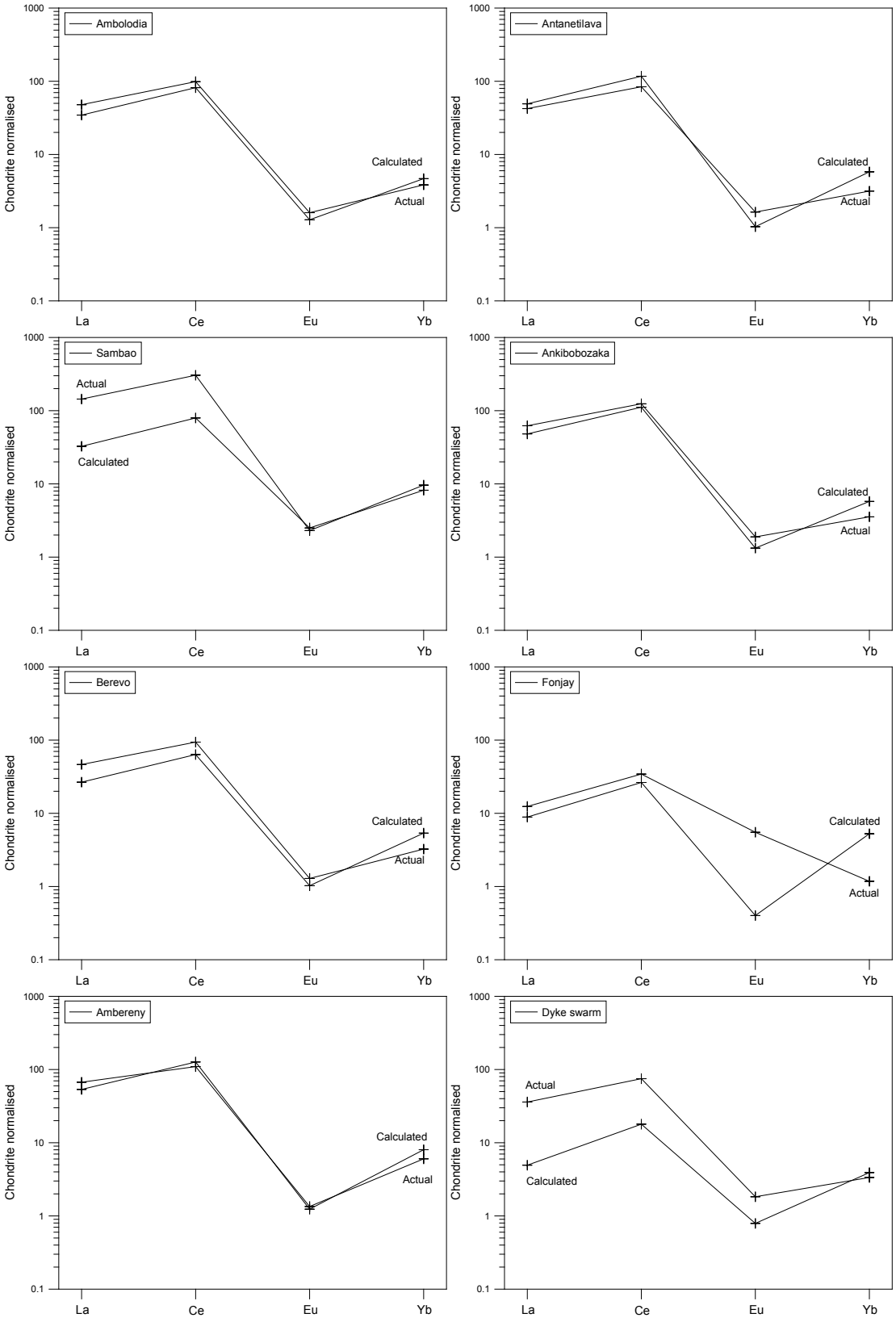

Figure 7.4: REE plots comparing the actual values and calculated concentrations of La, Ce, Eu and Yb for the different complexes of the Maningoza Suite.

7.2 Magma mixing

Modelling of mixing relationships between end-members has been attempted using the Sr and Nd isotope data as the ratios are not affected by differentiation or if the sample is a cumulate. This provides a method to model the Maningoza Suite for possible contamination by using a primitive end-member from the Maningoza Suite and lower crust end-members. There is a lack of available radiogenic and stable isotope data on the surrounding basement rocks of the Maningoza Suite (Bekodoka and Ambohipaky inliers) and in an attempt to model possible contamination other lower crust/basement rock that is likely to be similar to the inliers are investigated. General mixing equations obtained from Langmuir et al. (1978) were used to determine how much mixing of each isotope ratio was needed to achieve the same values as felsic end members of the Maningoza Suite.

The general mixing equations $Ax + Bxy + Cy + D = 0$ and $x = -\frac{(Cy + D)}{(A + By)}$ were used, where

x = variable along abscissa

y = variable along ordinate

A, B, C, D = coefficients of general variables x and y.

In this case the x variable is the initial $^{87}Sr/^{86}Sr$ ratio and the y variable is the initial $^{143}Nd/^{144}Nd$.

Sample BY6F091 was chosen as the Maningoza Suite's most primitive sample with the highest initial Nd ratio and lowest initial Sr ratio (Table 7.7). Table 7.7 also shows Sr and Nd data for possible contaminants that are Archaean in age and related to Madagascar. Sr and Nd data was taken from Melluso et al. (2001) on the Mailaka area for a Precambrian leucogranite which could have similar radiogenic isotopes to the Bekodoka and Ambohipaky inliers. The Mailaka area is also located in central west Madagascar. The Maevatanana gneisses represent the Archaean basement rocks of north-central Madagascar with Sr and Nd data taken from Tucker et al. (1999). Sr and Nd data for Precambrian rocks of the Indian Dharwar craton and Tanzania craton are also included in the mixing models as the Neoarchaean rocks of the Antananarivo Block (Bekodoka and Ambohipaky inliers) have been postulated as being associated with either of these cratons (Tucker et al. 1999, Kroner et al 2000, Collins et al 2000, and Collins and Windley 2002). Sr and Nd data for the Dharwar tronalitic-trondhjemitic-granodioritic (TTG) basement was taken from Jayananda et al. (2000) and data for the Tanzanian craton was taken from Möller et al. (1998).

Contaminant	Sr	Sr 93 Ma	Nd	Nd 93 Ma
BY6F091	155	0.702970	10.0	0.513019
Mailaka leucogranite	265	0.721111	16.4	0.511153
Maevatanana gneiss	216	0.721377	29.3	0.511305
Dharwar TTG	322	0.724494	37.3	0.510716
Tanzania gneiss	574	0.718527	21.5	0.511020

Table 7.7: Sr and Nd concentrations as well as initial Sr ratios and initial Nd ratios for selected contaminants. Initial Sr and Nd ratios for all contaminants are calculated to 93 Ma.

Figure 7.5 shows the plot of initial neodymium ratio against initial strontium ratio with mixing curves between the Maningoza Suite (Table 6.3) and the different contaminants mentioned above. Sample BY6F091 was used as one end-member and the contaminants were used as the other end-member in the equations. All the data of the Maningoza Suite are included on the plot to observe if the data fits any of the mixing curves. The primitive samples of the Maningoza Suite have a similar trend to the mixing curve between BY6F091 and the Maevatanana gneiss as well the curve between BY6F091 and the Dharwar TTG. It appears that approximately 35% mixing could occur between sample BY6F091 and a contaminant similar to the Maevatanana gneiss although two samples of the Maningoza Suite deviate from the curve. Similarly about 20% mixing could occur between sample BY6F091 and a contaminant similar to the Dharwar TTG. It is possible that the two samples that deviate from the mixing curves have either come into contact with a different contaminant at a later stage or that a contaminant other than the ones selected here is the main end-member with partial melting playing a major role.

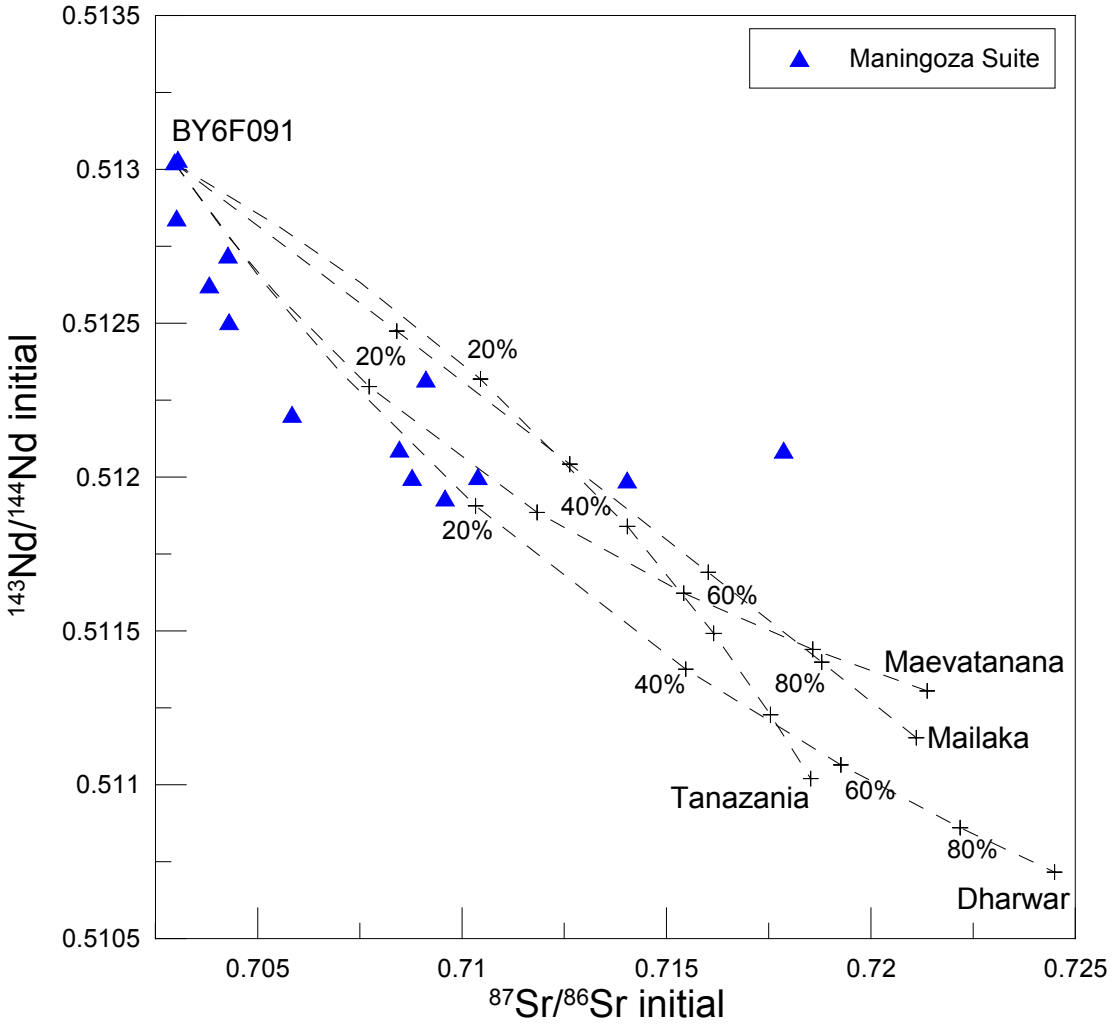

Figure 7.5: Plot of initial $^{143}Nd/^{144}Nd$ against $^{87}Sr/^{86}Sr$ showing the mixing curves between the Maningoza Suite (sample BY6F091 as an end-member) and the selected contaminants in Table 7.7 as the other end-members. The percentages indicate the amount of simple mixing between the Maningoza Suite and selected end-members.

Figure7.6 shows mixing curves between sample BY6F091 and the selected possible contaminants and also includes mixing curves with partial melts of the contaminants. This is done to illustrate the effect of partial melting on the source contaminant. The percentages represent the amount of mixing and the dotted lines represent different amounts of partial melting of the source contaminant. Figure 7.6 also shows that for the curves between the Maningoza Suite and the Mailaka leucogranite, the Dharwar TTG and the Maevatanana gneisses have significant changes in Nd first followed by a significant change in Sr. This suggests that the contaminants have high Nd and low Sr concentrations and the source (sample BY6F091) has low Nd and high Sr concentrations. The Tanzania gneisses have much higher concentrations of Sr and lower concentrations of Nd but as partial melting occurs the Sr concentration is decreased and the Nd concentration is increased.

Mixing between the Maningoza Suite and partial melts of the Mailaka leucogranite estimates up to 20% mixing with a 60% partial melt and roughly 35% mixing with a 45% partial melt. Roughly 20% mixing with a 45% partial melt of the Maevatanana gneisses is estimated as well as 35% mixing with a 25% partial melt is estimated. Mixing with the Dharwar TTG is estimated to roughly 10% mixing with a 30% partial melt and 20% mixing with a 15% partial melt. Roughly 10% mixing with a 60% partial melt of the Tanzania gneisses as well as 25% mixing with 45% and 30% partial melts is estimated. Three data points of the Maningoza Suite do not plot on the partial melt mixing curves of the Maevatanana gneisses and four data points do not plot on the partial melt mixing curves of the Dharwar TTG. For the Tanzania gneisses and Mailaka leucogranite only two data points of the Maningoza Suite do not plot on the partial melt mixing curves.

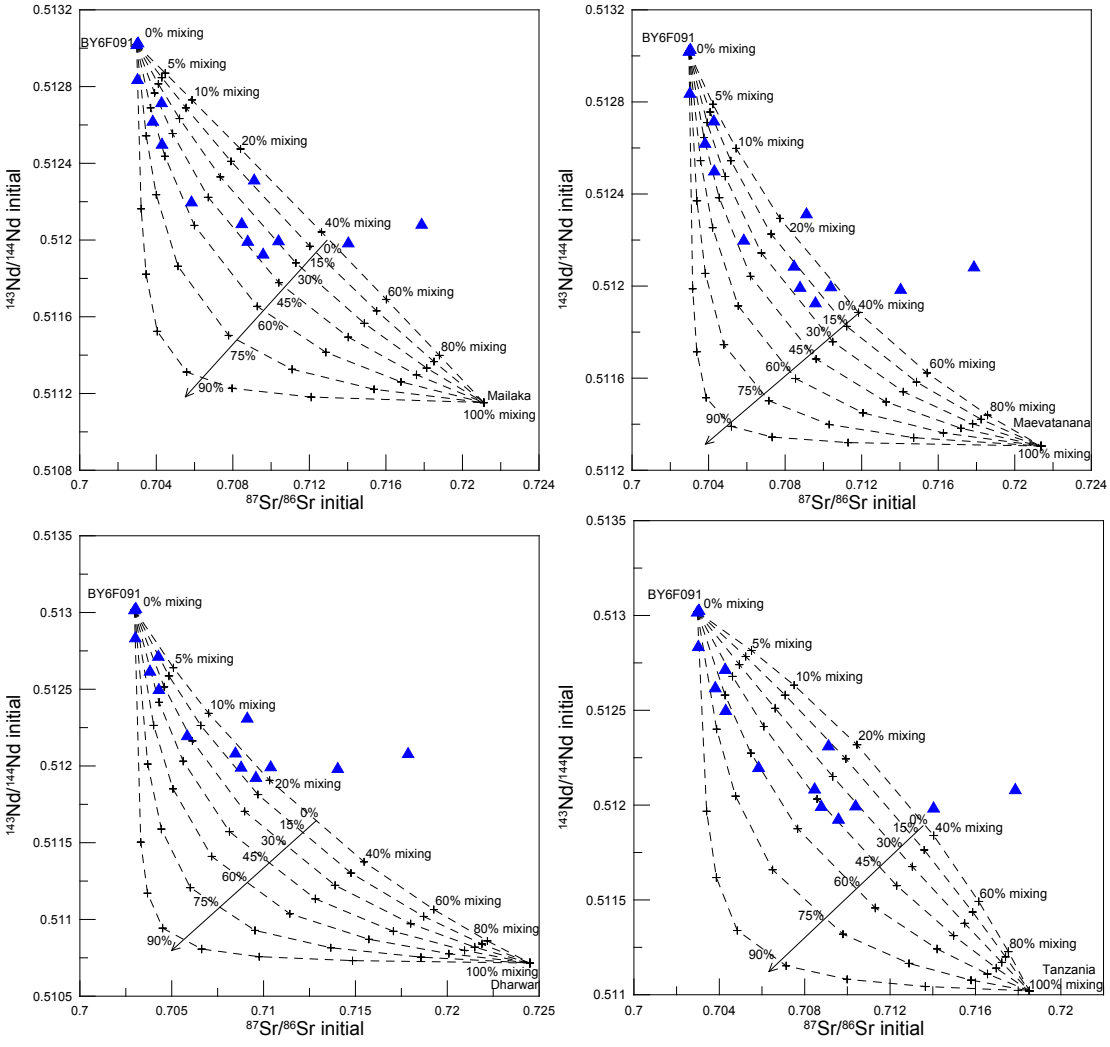

Figure 7.6: Plots of initial $^{143}Nd/^{144}Nd$ against $^{87}Sr/^{86}Sr$ showing the simple mixing between sample BY6F091 of the Maningoza Suite and the partial melts of the possible contaminants. The percentages represent the amount of mixing with the contaminant. The arrow represents the direction of increasing partial melting of the contaminant and the dotted lines each represent a different percentage of partial melting starting at 0% and ending at 90% with increments of 15%.

In summary each complex of the Maningoza Suite was treated separately in the fractional crystallisation modelling as different methods of differentiation for the complexes can occur. The amount of fractional crystallisation estimated using the variation diagrams method ranges from 68% to 86% for the Maningoza Suite with assemblages of 35% - 60% plagioclase, 35% - 50% augite and 5% - 20% magnetite. The two examples of fractional crystallisation using the least squares method are consistent with the variation diagrams method except that the least squares method has lower percentages of augite to accommodate for inclusion of olivine in the modelling. Trace element modelling tended to agree for elements such as U, Zr, Sr, Y and Rb for at least 5 different complexes. Nd and Ba were less consistent as explained by an accessory mineral compatible with Nb being fractionated and the modelling not including K-feldspar (Ba compatible). Compatible elements V, Ni and Cr were inconsistent in all cases possibly due to olivine not being included in the modelling. The modelling of the four REE agreed for the Ambolodia Formation, Antanetilava Formation, Ankibobozaka Complex, Ambereny Complex and Berevo Complex. Two of the four REE were inconsistent for the Fonjay Complex, Sambao Formation and the dyke swarm. The magma mixing of the Maningoza Suite is modelled with all samples grouped together as the isotopes data is less affected by variations in magmatic differentiation and the mantle end-member and crustal end-member are the same. Without partial melting included in the mixing equations a 35% mix between the mantle end-member and the Maevatanana gneisses and a 20% mix between the mantle end-member and the Dharwar TTG is estimated. If partial melting is included in to the mixing equations then all four contaminants can be considered with a range of 10% - 35% mixing occurring depending on source contaminant. The partial melting of the contaminants ranges from 15% (Dharwar TTG) to 60% (Mailaka leucogranite and Tanzania gneisses). In general it is estimated that the mixing with higher partial melts of the contaminant is less than the mixing with lower partial melts.

7.3 Comparisons with Madagascan and Other Similar Complexes

The Maningoza Suite data has been further investigated by comparing it to the data of other complexes that are similar in type and/or age. The Maningoza Suite data sets are first compared to complexes from Madagascar that are similar in age and secondly to complexes that are likely similar in type.

7.3.1 Comparisons with other Madagascan Complexes

The Maningoza Suite is compared to the following Cretaceous igneous complexes: Mailaka (Melluso et al. 2001), Antampombato-Ambatovy (Melluso et al. 2005), Androy (Mahoney et al. 2008) and the Morondava Complex (Bardintzeff et al. 2001). The Maningoza Suite is compared to these complexes because they are of a similar age and are suggested to be related to Gondwana rift magmatism. The locations of the complexes are shown in Figure 7.7. The mineral chemistry from the Mailaka, Antampombato-Ambatovy and Morondava complexes is compared to the Maningoza Suite as shown in Figures 7.8, 7.9 and 7.10. Selected major elements and trace elements from the all the complexes mentioned, except the Morondava Complex, are compared to the Maningoza Suite and as shown in Figures 7.11 and 7.12. The radiogenic isotopes Sr and Nd have also been compared between the Maningoza Suite, Antampombato-Ambatovy, Androy, and Mailaka Complexes as shown in Figure 7.13.

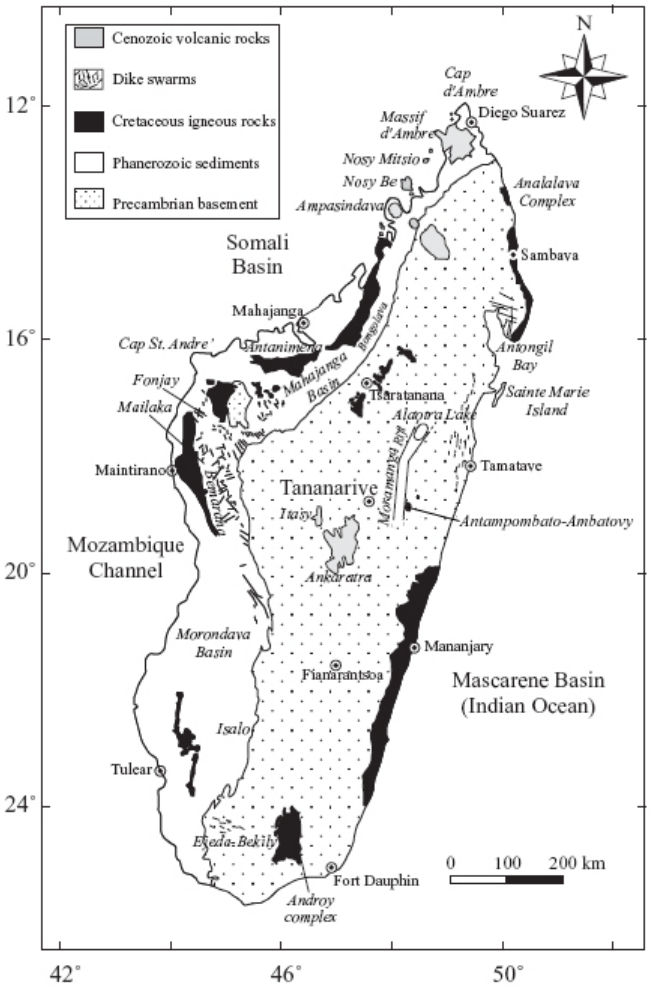

Figure 7.7: Map of Madagascar showing the locations of Cretaceous igneous rocks. Modified after Melluso et al. 2005.

The Maningoza Suite feldspars range from $An_{95}Ab_3Or_2$ to $An_0Ab_{99}Or_1$ and from $An_0Ab_{99}Or_1$ to $An_0Ab_2Or_{98}$ (Figure 7.8). The Antampombato-Ambatovy Complex feldspars have a similar range of anorthite to albite with $An_{88}Ab_{11}Or_0$ to $An_5Ab_{91}Or_4$ but not as much orthoclase ($An_5Ab_{71}Or_{24}$). The Mailaka Complex plagioclases have a range of anorthite to albite that is not as wide as the Maningoza Suite with $An_{72}Ab_{28}Or_0$ to $An_9Ab_{86}Or_5$. The Morondava Complex has anorthite rich plagioclases ($An_{82}Ab_{18}Or_0$) similar to the Maningoza Suite but the Morondava plagioclases' highest albite percentage is 57% ($An_{42}Ab_{57}Or_1$).

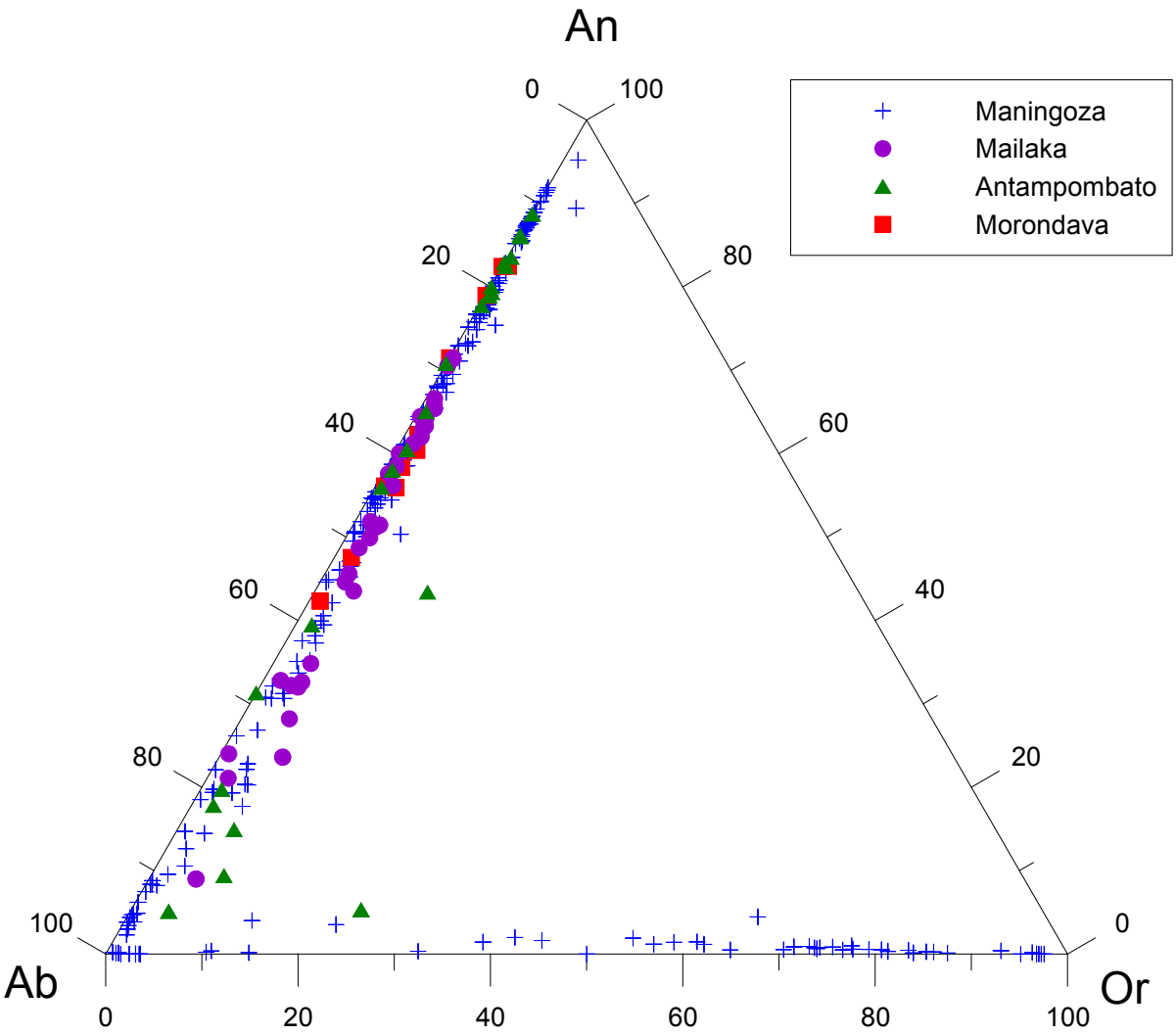

Figure 7.8: Ternary diagram for feldspars with the Maningoza Suite, Mailaka Complex, Antampombato-Ambatovy Complex and Morondava Complex plotted. An = anorthite, Ab = albite and Or = orthoclase.

The Maningoza Suite pyroxenes are all augitic in composition and are Mg-rich. The composition of the pyroxenes from the Maningoza Suite typically ranges from $En_{49}Fs_{19}Wo_{33}$ to $En_{41}Fs_{14}Wo_{45}$. Figure 7.9 shows that the Morondava Complex pyroxenes are also augitic in composition ($En_{41}Fs_{14}Wo_{45}$ to $En_{37}Fs_{26}Wo_{37}$) with the exception of one sample being

pigeonite-type in composition ($En_{57}Fs_{33}Wo_{10}$). The Antampombato-Ambatovy Complex has a much wider variety of pyroxene compositions than the Maningoza Suite and the Morondava Complex. The pyroxenes are classified as diopside ($En_{41}Fs_{9}Wo_{50}$), augite ($En_{44}Fs_{14}Wo_{42}$) and ferrosilite ($En_{25}Fs_{72}Wo_{3}$). The Mailaka Complex has an even wider variety of pyroxene compositions and they are classified as diopside ($En_{28}Fs_{26}Wo_{46}$), hedenbergite ($En_{7}Fs_{47}Wo_{46}$), augite ($En_{41}Fs_{33}Wo_{26}$), enstatite ($En_{76}Fs_{20}Wo_{4}$) and ferrosilite ($En_{25}Fs_{74}Wo_{1}$).

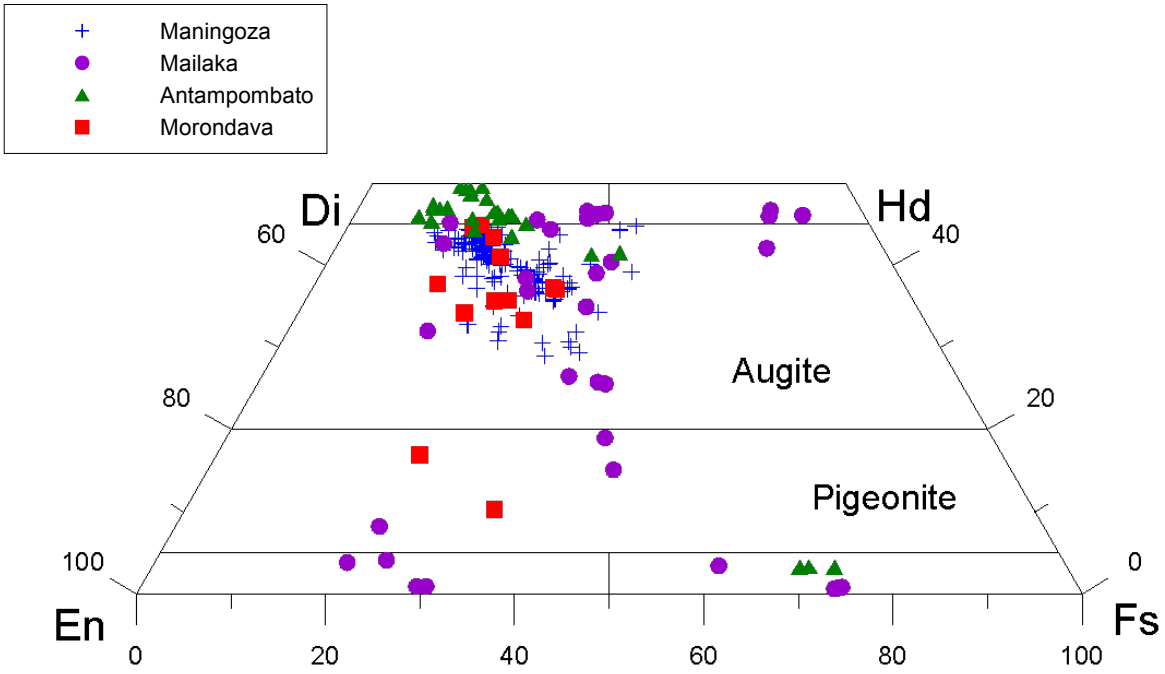

Figure 7.9: The Maningoza Suite, Mailaka Complex, Antampombato-Ambatovy Complex and Morondava Complex plotted on the pyroxene quadrilateral. Di = diopside, Hd = hedenbergite, En = enstatite and Fs = ferrosilite

The olivines of the Maningoza Suite range from a composition of Fo_{74} to Fo_{45} as shown in Figure 7.10. The Antampombato-Ambatovy Complex olivines all have forsterite compositions that are higher than that of the Maningoza Suite. The olivines range from Fo_{87} to Fo_{75} in composition. The Morondava Complex has olivines which range from Fo_{88} to Fo_{29}, a higher forsterite composition than the Antampombato-Ambatovy Complex and a lower forsterite composition that the Maningoza Suite olivines. The Mailaka Complex olivines have the widest range of forsterite compositions, ranging from Fo_{83} to little as Fo_{6}.

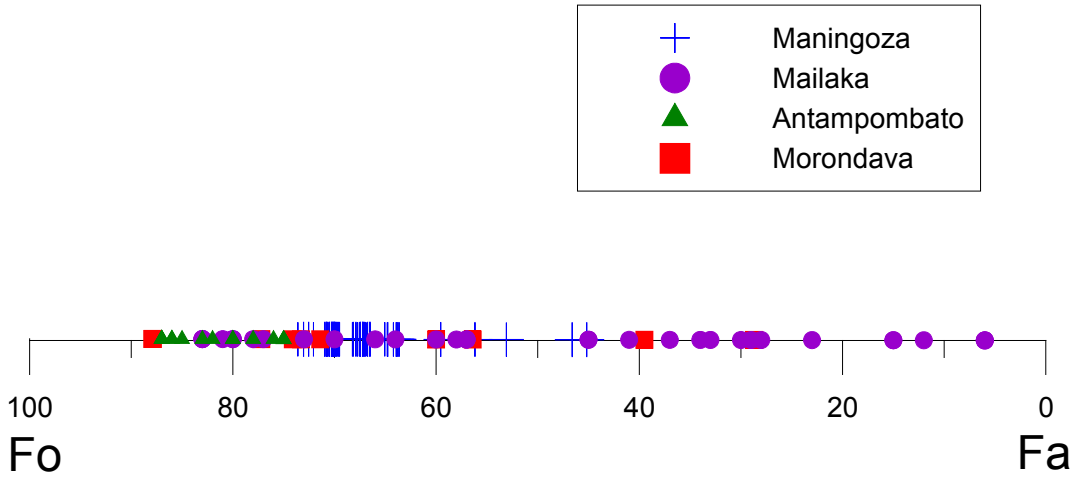

Figure 7.10: Olivine compositions for the Maningoza Suite, Mailaka Complex, Antampombato-Ambatovy Complex and Morondava Complex plotted on a Fo/Fa line. Fo = forsterite and Fa = fayalite.

Major and Trace Elements

The Maningoza Suite shows a negative correlation between MgO and SiO_2 as shown in Figure 7.11. The Mailaka Complex and the Androy Complex show very similar trends of decreasing MgO and the Maningoza Suite samples overlap the data of these two complexes. The Antampombato-Ambatovy Complex also shows a similar trend to that found in the Maningoza Suite but has more mafic samples (higher MgO and lower SiO_2 wt. % concentration) than the Maningoza Suite. For TiO_2 plotted against SiO_2 the Maningoza Suite first shows a positive trend then a negative trend after roughly 54% SiO_2. The Antampombato-Ambatovy and Mailaka Complexes follow the same trend where as the Androy Complex, although following the same trend, has much higher concentrations of TiO_2. The plot of Al_2O_3 against SiO_2 shows the Maningoza Suite has a steep decrease of Al_2O_3 as SiO_2 increases which levels out to a gentler slope at roughly 50% SiO_2. The Mailaka and the Androy Complexes have the same slopes as the gentle slope of the Maningoza Suite. The Antampombato-Ambatovy Complex also follows the gentle slope of the Maningoza Suite but has a positive trend for its samples that are less than 50% SiO_2. The plot of CaO versus SiO_2 shows similar trends of decreasing CaO as SiO_2 increases for the Maningoza Suite, Mailaka Complex and Androy Complex. The Antampombato-Ambatovy Complex first shows an increase of CaO and then a decrease of CaO as SiO_2 increases. The trend of decreasing CaO as SiO_2 increase for the Antampombato-Ambatovy Complex is similar to that of the Maningoza Suite.

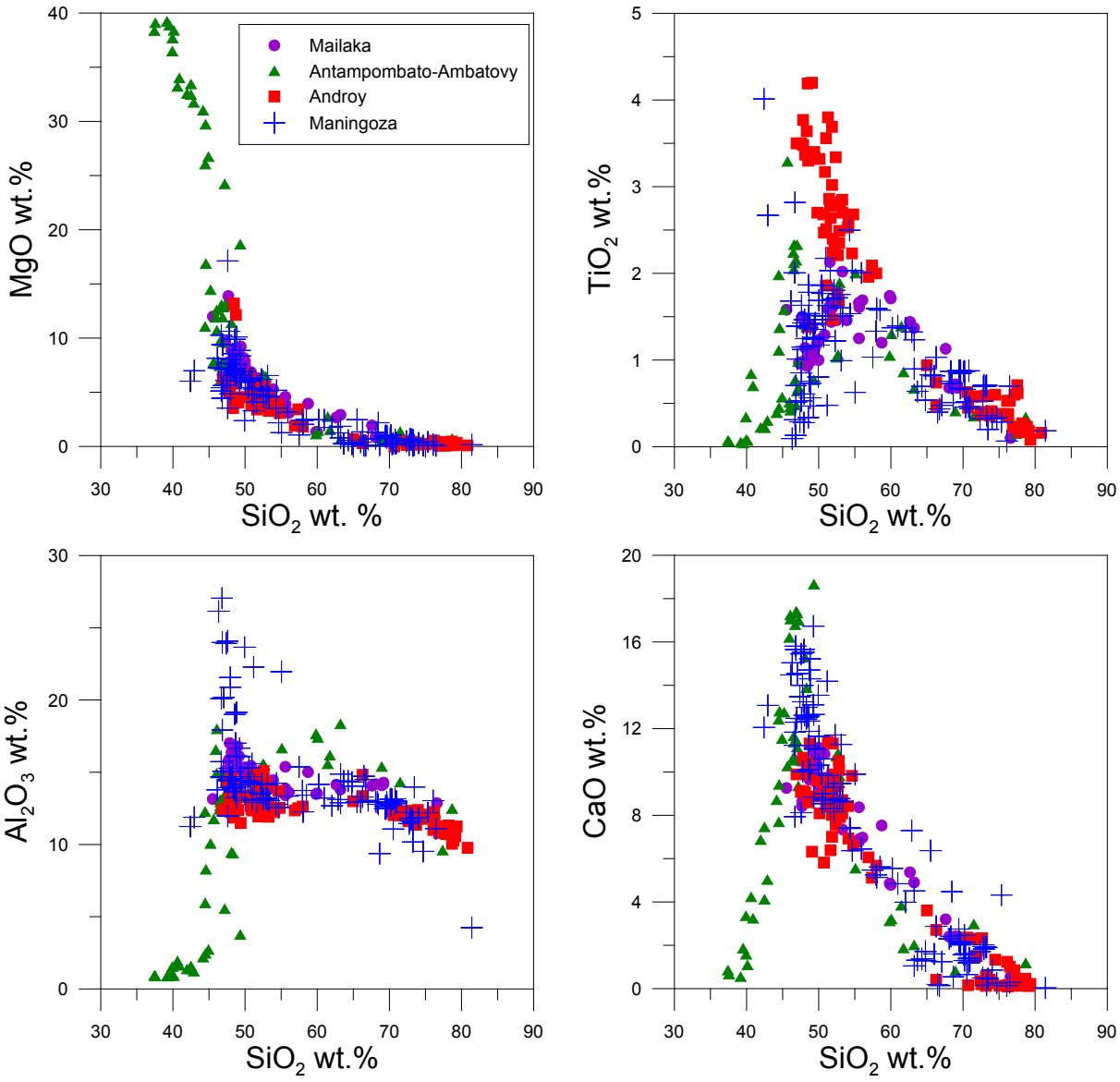

Figure 7.11: Plots of major elements against SiO_2 wt. % for the Maningoza Suite, Androy Complex, Antampombato-Ambatovy Complex and Mailaka Complex.

Figure 7.12 shows positive trends for Zr and Nb plotted against SiO_2 for the Maningoza Suite. The Mailaka Complex follows the same trends and plots closely with the Maningoza Suite. The Androy Complex and Antampombato-Ambatovy Complex show similar trends but the data is more widespread. The Maningoza Suite shows increasing Rb as Zr increases as well as increasing Nb as Zr increases and the Mailaka Complex again plots closely with the Maningoza Suite. The Antampombato-Ambatovy Complex shows a similar trend with the Maningoza Suite but its data set is more widespread where as the Androy Complex shows similar trends but has much higher concentrations of Zr, Rb and Nb. The trace elements Zr, Rb and Nb of the Androy Complex form two separate groups.

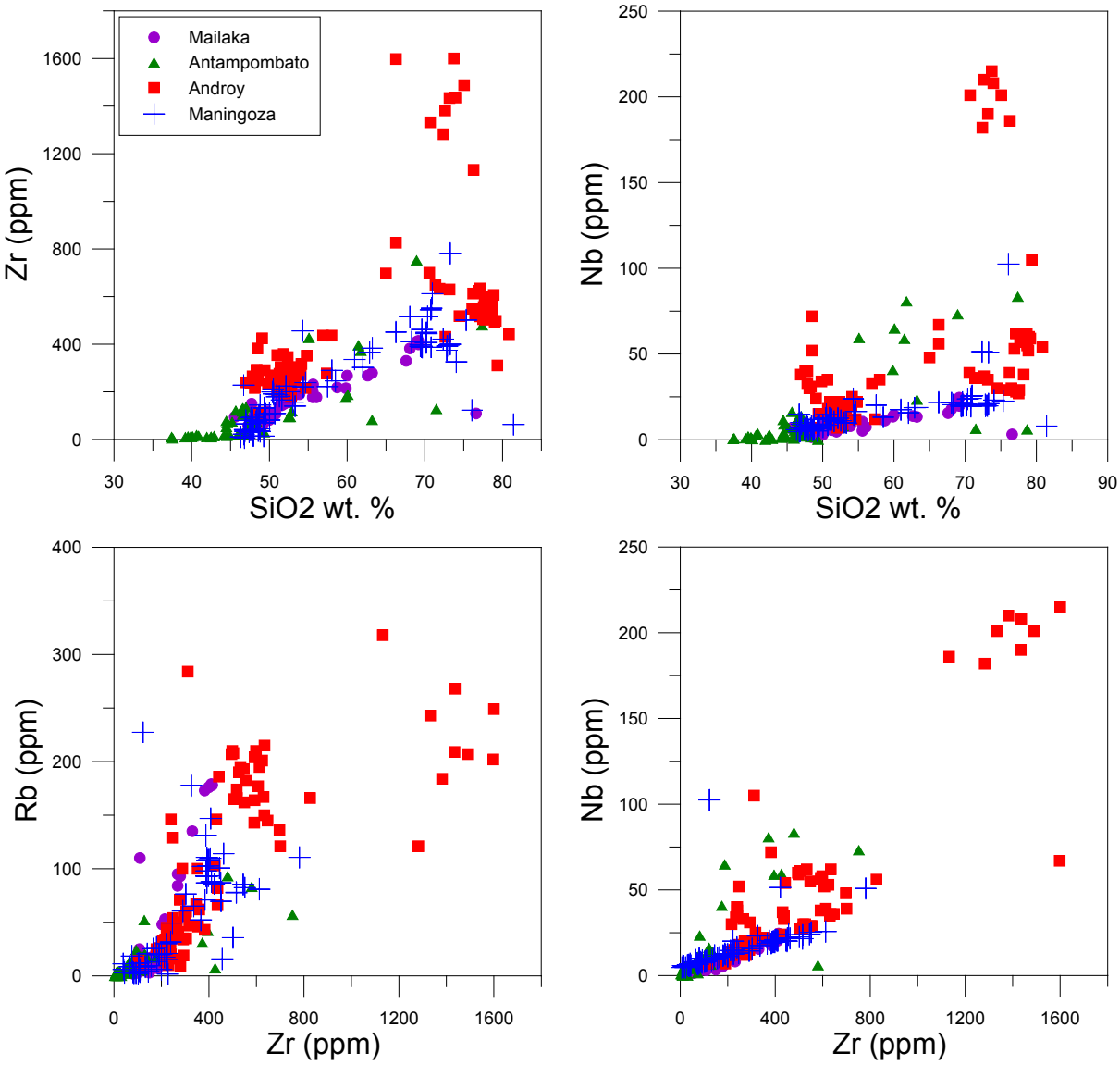

Figure 7.12: Plots of trace elements against SiO_2 wt. % and against Zr (ppm) for the Maningoza Suite, Androy Complex, Antampombato-Ambatovy Complex and Mailaka Complex.

Radiogenic Isotopes

A study of the radiogenic isotope data shows that the Maningoza Suite has similar ε_{Sr} and ε_{Nd} values when compared to the Antampombato-Ambatovy Complex. Two samples from the Maningoza Suite plots within the field of the Antampombato-Ambatovy Complex with positive ε_{Nd} values and negative ε_{Sr} values (Figure 7.13). The same two samples also plot within the field of the Mailaka Complex. A further 6 samples of the Maningoza Suite plot within the Mailaka Complex, with one sample having negative ε_{Sr} and positive ε_{Nd} values, another sample having negative ε_{Sr} and ε_{Nd} values and the last four having positive ε_{Sr} and negative ε_{Nd} values. This means 8 out of the 14 samples of the Maningoza Suite plot within the field of the Mailaka Complex. Three samples from the Maningoza Suite plot within the field of the Androy Complex with one of the samples also plotting with in the Mailaka Complex's field.

These three samples have positive ε_{Sr} and negative ε_{Nd} values. This leaves four samples from the Maningoza Suite and these do not plot in any of the other complex's fields. Two of these last four samples have negative ε_{Sr} and positive ε_{Nd} values and the other two have positive ε_{Sr} and negative ε_{Nd} values.

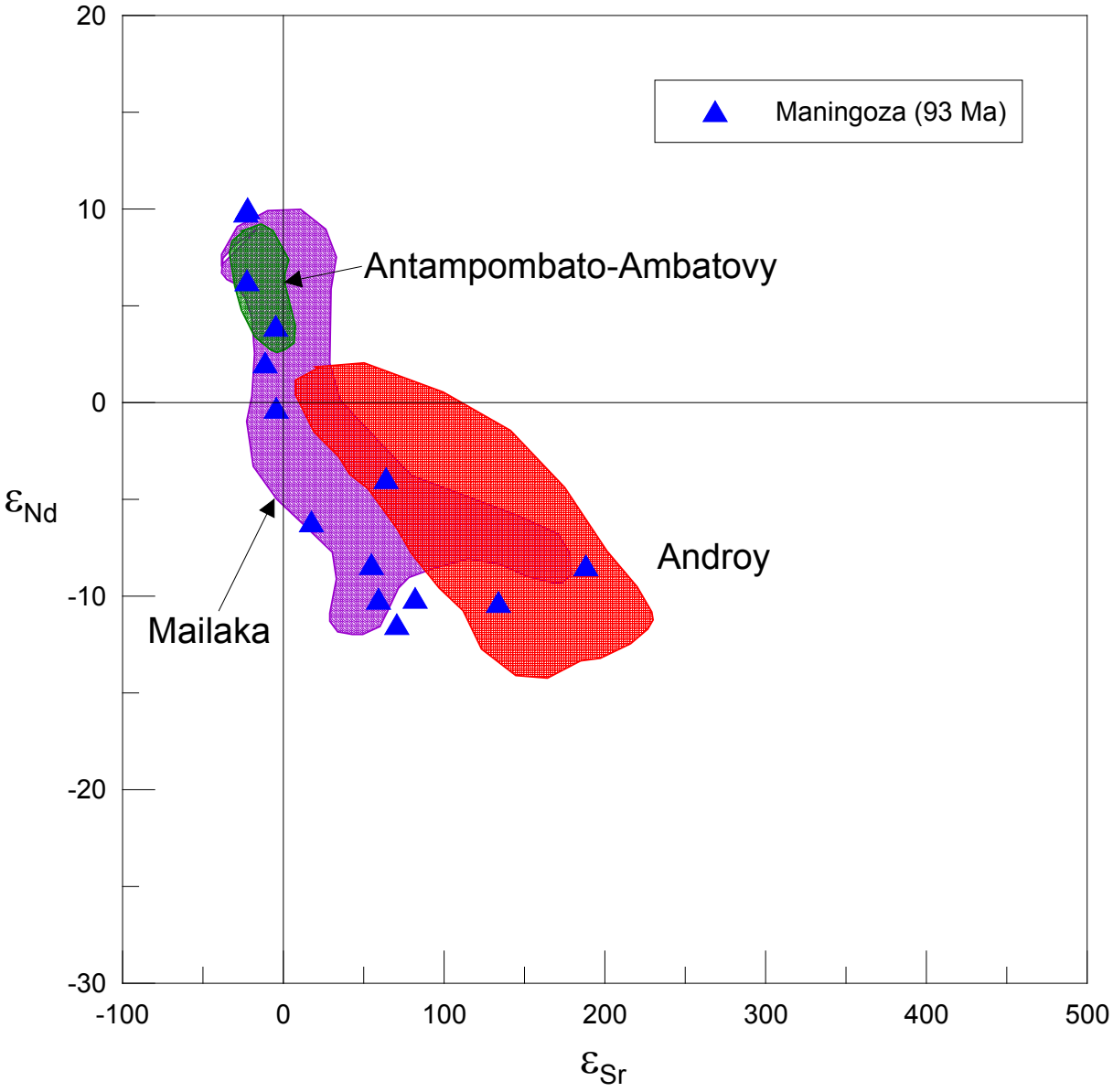

Figure 7.13: Plot of ε_{Sr} against ε_{Nd} for the Maningoza Suite, Antampombato-Ambatovy Complex, Mailaka Complex and Androy Complex.

7.3.2 Comparison with the Karoo Large Igneous Province and Deccan Traps

The Maningoza Suite was compared with rhyolites of the Jurassic Lebombo volcanic rifted margin of southern Africa and the Cretaceous/Tertiary Deccan Traps of India which are also associated with the gradual break-up of Gondwana (Dostal et al. 1992). These three igneous complexes might have a similar primitive end-member even though the ages are different as

the mantle source may not have changed much over 120 Ma. Comparing the suites to each other provides further constraints on the volcanism during the period of the break-up of Gondwana. Data for the Deccan Traps are taken from Lightfoot et al. (1987) and Lightfoot and Hawkesworth (1988), and the data for the Lebombo rhyolites are taken from Miller and Harris (2007).

Karoo Large Igneous Province

The data from the Maningoza Suite were compared to the data from rhyolites of the Lebombo rifted volcanic margin located in the Karoo large igneous province of south east Africa. Figure 7.14 shows the radiogenic isotope ratios of the felsic samples of Maningoza Suite and the Lebombo rhyolites for Sr and Nd. The felsic samples of the Maningoza Suite have higher ε_{Sr} and lower ε_{Nd} values than the Lebombo rhyolites and only two samples of the Maningoza Suite plot near the Southern Lebombo field. This suggests that the Lebombo rhyolites and the felsic samples of the Maningoza Suite are different and that different contaminants were involved.

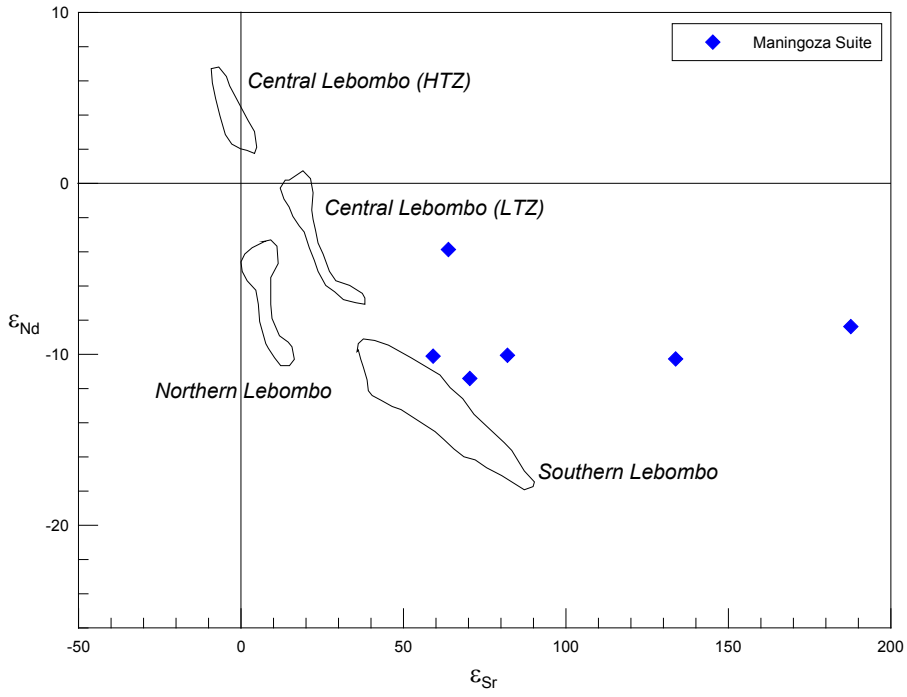

Figure 7.14: Plot of ε_{Sr} against ε_{Nd} for the felsic samples of the Maningoza Suite and the rhyolites of the Lebombo rifted volcanic margin. Epsilon values have been calculated to 93Ma for the Maningoza Suite and 179Ma for the Lebombo rhyolites. The Lebombo rhyolite fields are taken from Miller and Harris 2007.

Deccan Trap Lavas

The Deccan Trap lavas of the Western Ghats in India were compared to the Maningoza Suite with the use of Sr and Nd isotopes. Figure 7.15 shows ε_{Sr} and ε_{Nd} values for six formations of the Deccan Trap lavas as well data from the Maningoza Suite. The Maningoza Suite has much lower ε_{Sr} values and higher ε_{Nd} values than the Deccan Trap lavas. This difference could be due to a different mantle source. Overall the Maningoza Suite trend follows closely with the Mahabaleshwar, Desur, Poladpur and Bushe Formations of the Deccan Traps. The highest ε_{Sr} and lowest ε_{Nd} values of the Maningoza Suite plot close to the Bushe Formation of the Deccan Traps. This is likely due to the Maningoza Suite assimilating a similar contaminant to that of the Deccan Traps.

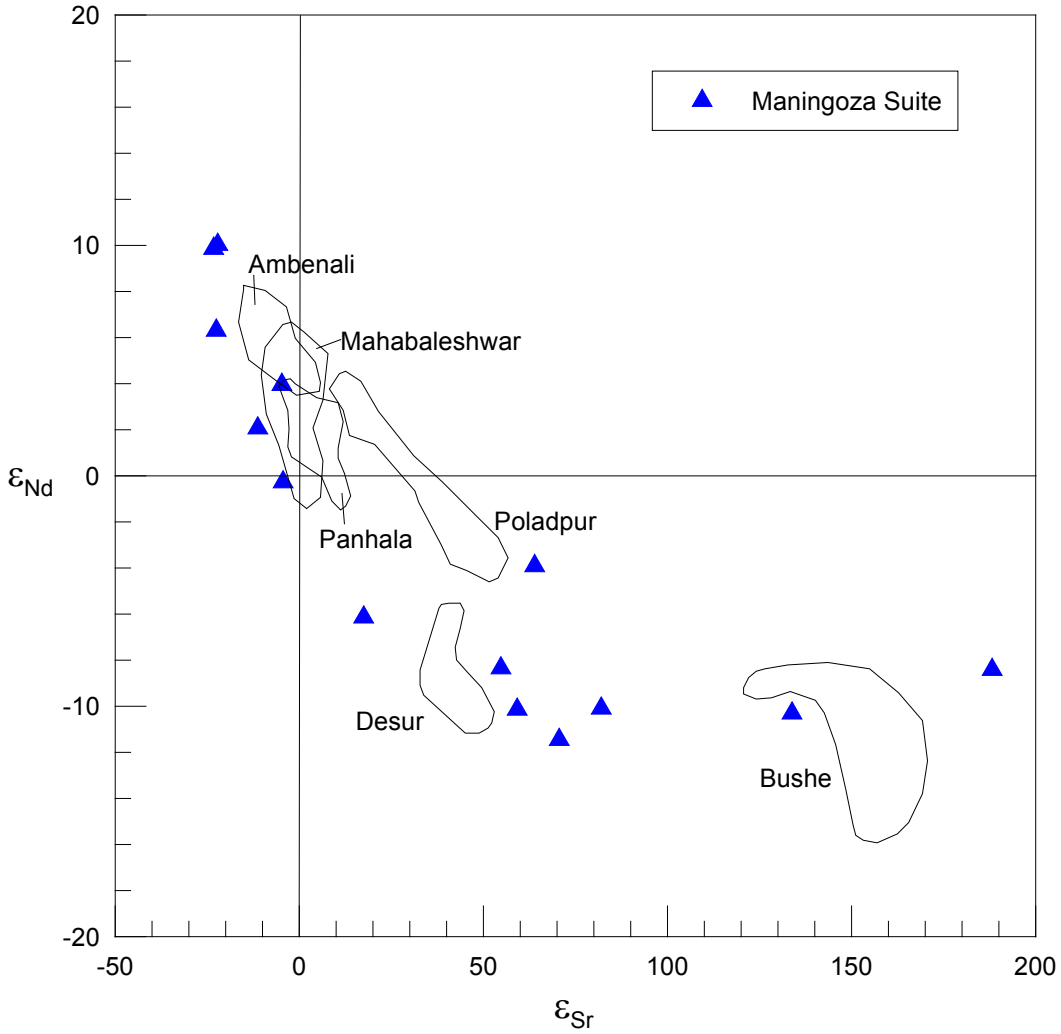

Figure 7.15: Plot of ε_{Sr} against ε_{Nd} for the Maningoza Suite and six formations of the Deccan Trap lavas. Epsilon values have been calculated to 90Ma for the Maningoza Suite and 60Ma for the Deccan Trap lavas. The Deccan Trap lava fields are taken from Lightfoot and Hawkesworth 1988, and Lightfoot et al. 1990.

7.4 Summary

The geochemical modelling of the Maningoza Suite gives estimates of 68% to 86% fractional crystallisation with assemblages of 35% - 60% plagioclase, 35% - 50% augite and 5% - 20% magnetite. The graphical method and least squares method are consistent with each other except that the least squares method allows olivine to be included into the calculation along with plagioclase, augite and Fe-Ti oxide. As a result the two methods only differ in that the least squares method estimates lower proportions of augite to accommodate for olivine. Fractional crystallisation modelling works for the variations observed in major and trace elements, however, the radiogenic isotopes Sr and Nd suggest assimilation is also occurring. Simple magma mixing modelling was done to estimate the amount of mixing required between a primitive source and crustal contaminant to accommodate the Maningoza Suite data. Without partial melting included in the mixing equations a 35% mix between the mantle end-member and the Maevatanana gneisses and a 20% mix between the mantle end-member and the Dharwar TTG is estimated. If partial melting is included in the mixing equations then all four contaminants can be considered with a range of 10% - 35% mixing occurring depending on source contaminant. The partial melting of the contaminants ranges from 15% (Dharwar TTG) to 60% (Mailaka leucogranite and Tanzania gneisses).

The Maningoza Suite has similar feldspar compositions to the Androy, Antampombato-Ambatovy and Mailaka Complexes except that the Maningoza Suite has more compositions ranging towards orthoclase. The Maningoza Suite has the smallest range in clinopyroxenes with all compositions being augitic and most similar to the Androy Complex. The Antampombato-Ambatovy and Mailaka Complexes have more widespread compositions of clinopyroxenes than the Maningoza Suite. The Mailaka and Androy Complexes also have more widespread olivine compositions than the Maningoza Suite. The Antampombato-Ambatovy Complex has small ranges in olivine composition like that of the Maningoza Suite but they have higher forsterite compositions. The Antampombato-Ambatovy Complex also shows different correlations in the major element variation diagrams where as the Androy and Mailaka Complexes show the same correlations to the Maningoza Suite. The trace element variation diagrams show that the Androy Complex has two distinct groups in its dataset where as the Mailaka and Antampombato-Ambatovy Complexes compare well to the Maningoza Suite. The Mailaka and Antampombato-Ambatovy Complexes appear to have a similar source to that of the Mailaka Complex when ε_{Nd} and ε_{Sr} are plotted against each other. The Maningoza Suite shows similar contamination to the Androy and Mailaka Complexes where as the Antampombato-Ambatovy Complex shows no contamination. Overall the Maningoza Suite is similar to the Mailaka Complex. Comparison of the felsic

samples of the Maningoza Suite to the Lebombo rhyolites shows that they are very different from each other and that they had different contaminants to each other. Comparison of the Maningoza Suite and the Deccan Trap lavas shows that it is possible that a similar primitive source and that a similar contaminant were involved in the generation of these magmas.

8 CONCLUSIONS

- The Maningoza Suite consists of the Ambereny, Ambohitrosy, Ankibobozaka, Berevo, Fonjay and Maningoza Complexes. The Maningoza Complex further consists of the Ambolodia, Antanetilava and Sambao Formations. The Ambereny, Ankibobozaka and Fonjay Complexes consist of fine- to medium-grained rocks and the Ambohitrosy Complex consists of fine- and coarse-grained rocks. The dykes of the Maningoza Suite consist of fine- to medium-grained rocks and the Berevo Complex consists of fine- to coarse-grained rocks. The Antanetilava Formation consists of fine- to medium-grained rocks and the Ambolodia and Sambao Formations only consist of fine-grained rocks.

- Mineral chemistry of the Maningoza Suite shows a large range in feldspar compositions. These range from almost pure anorthite ($An_{95}Ab_5Or_0$) through albite to orthoclase ($An_0Ab_2Or_{98}$) for most of the complexes. The Fonjay Complex has only calcium-rich feldspars ($An_{88}Ab_{12}Or_0$ – $An_{59}Ab_{39}Or_2$) reflective of its mafic samples and the Sambao Formation has feldspars which are mainly sodium-rich tending towards the anorthite end-member ($An_{51}Ab_{47}Or_2$ – $An_4Ab_{96}Or_0$). Clinopyroxenes of the Maningoza Suite all have an augitic composition plotting below the field of diopside with little variation on the pyroxene quadrilateral. Olivine compositions for the Ambereny, Ambohitrosy and Berevo Complexes are magnesium-rich with a range in composition of Fo_{74} to Fo_{64}. The olivine composition of the dyke swarm is slightly more iron-rich with a composition of Fo_{60} to Fo_{45}. Oxide compositions range from $Hm_{100}Ilm_0$ (Berevo Complex) to $Hm_{17}Ilm_{83}$ (Fonjay Complex).

- TAS diagram classifications for the volcanic formations Ambolodia, Antanetilava and Sambao show samples within the basalt field. The three formations show a trend of evolution from basalt towards rhyolite with the Sambao and Antanetilava Formations having samples in the rhyolite field and the Ambolodia Formation having samples only as evolved as a dacite. TAS diagram classifications for the hypabyssal complexes Ambereny, Ankibobozaka, Berevo and Fonjay show most samples within the basalt and rhyolite field with only 5 samples out of 34 not within those two fields. The Ambohitrosy Complex has a much wider range than the other four complexes with samples plotting within the basanite, picrobasalt and basalt fields to the trachyte, dacite and rhyolite fields. The Ambohitrosy Complex also shows samples that are intermediate in silica composition similar to that of volcanic formations where as the

Ankibobozaka, Berevo and Ambereny Complexes have no intermediate samples. The Fonjay Complex has one intermediate sample within the trachyandesite field.

- The trends observed in variation diagrams of major elements plotted against SiO_2 suggest fractional crystallisation. All the complexes show that there is a constant negative correlation between CaO and SiO_2 which suggests fractionation of a mineral such as plagioclase and/or clinopyroxene. Titanium and iron show positive correlations with SiO_2 at first and then negative correlations with SiO_2. An explanation for this change in correlation could be the start of Fe-Ti oxide fractionation. Variation diagrams of trace elements plotted against SiO_2 also suggest fractional crystallisation.

- The volcanic rocks of the Ambolodia, Antanetilava and Sambao Formations show similar REE patterns to each other where the mafic samples have low concentrations of REE and the felsic samples have low concentrations of HREE and high concentrations of LREE. Typically the felsic samples also show an increasing negative Eu anomaly indicating fractionation of feldspars. Sample BY6F148 of the Sambao Formation is an exception as it is a felsic sample (SiO_2 = 76% wt.) that has lower concentrations of LREE than HREE and has a large negative Eu anomaly. The complexes show a similar pattern to the volcanic formations where the mafic samples have low concentrations of REE and the felsic samples have low concentrations of HREE and high concentrations of LREE. The Berevo, Ankibobozaka, Ambereny and Ambohitrosy Complexes show negative Eu anomalies in the felsic samples similar to that of the volcanic formations distinctive of fractionation of feldspars. The Berevo, Fonjay and Ambereny Complex also show positive Eu anomalies in their mafic samples which also have the lowest concentration of HREE and LREE. This implies that these samples are feldspar cumulates.

- The Ar - Ar geochronology of the Maningoza Suite gives an average age of 93.4 Ma and is consistent with the Maningoza Suite being emplaced during the Cretaceous. This confirms that the Maningoza Suite is associated with the break-up of Gondwana.

- Whole-rock $\delta^{18}O$ values compared with mineral $\delta^{18}O$ values suggest that the minerals and surrounding rock are not in equilibrium. In the Berevo Complex the mineral $\delta^{18}O$ values are lower than the whole-rock values. It is possible that the whole-rock $\delta^{18}O$ values of the ground-mass has been altered and homogenised to slightly higher values than the mineral $\delta^{18}O$ values.

- Low whole-rock $\delta^{18}O$ values suggest either low $\delta^{18}O$ magma emplacement or hydrothermal alteration after emplacement. Low whole-rock $\delta^{18}O$ values are observed from the Antanetilava Formation, Ambolodia Formation, Ankibobozaka Complex, Berevo Complex, Fonjay Complex and Ambereny Complex.

- The hydrogen isotopes can be explained by Rayleigh-type fractionation suggesting degassing in the samples with low δD values has occurred. The combined oxygen and hydrogen isotopes composition suggests that the fluid involved in these rocks is magmatic in origin.

- Radiogenic isotopes show good correlations with major and trace elements and this is typical of fractional crystallisation associated with assimilation. The plot of ε_{Nd} versus ε_{Sr} shows that one sample of Sambao Formation and one sample of the dyke swarm are the most primitive samples of the Maningoza Suite. The samples of the Maningoza Suite show a trend towards a crustal component. The Berevo Complex and the Ambereny Complex show the most evidence that a crustal component is involved.

- Stable isotopes compared to radiogenic isotopes suggests that the stable isotopes are somewhat associated with assimilation of a crustal component but more data is required for a better understanding.

- The estimated amount of fractional crystallisation in the Maningoza Suite ranges from 68% to 86% with mineral assemblages of 35% - 60% plagioclase, 35% - 50% augite and 5% - 20% Ti-Fe oxide. While one method was used to model the fractional crystallisation of all the complexes of the Maningoza Suite a second method was used on two complexes to confirm the results. Both methods agreed on the estimated amount of fractional crystallisation for each complex as well as the amount of plagioclase and Ti-Fe oxide. Differences between the two methods only occurred for the minerals olivine and augite.

- Trace elements were applied in calculations using the Rayleigh Fractionation Law to further investigate the estimates of fractional crystallisation in the Maningoza Suite. Trace element modelling agreed for elements such as U, Zr, Sr, Y and Rb for at least 5 different complexes. Trace elements V, Ni, Cr, Nd and Ba were inconsistent explained by a necessary mineral not included into the calculation. The calculation of

the four REE agreed for 5 of the complexes with at least two elements being consistent in the other 3 complexes.

- The simple magma mixing of the Maningoza Suite was estimated using a primitive end-member from the Maningoza Suite and a potential crustal component similar to the Archaean basement surrounding the Maningoza Suite. This was done due to a lack of radiogenic data on the Archaean basement around the Maningoza Suite and a representative of the lower crust was required. Four components were chosen and the Maningoza Suite data fitted only two of these simple magma mixing curves. A 35% mix between the mantle end-member and the Maevatanana gneisses and a 20% mix between the mantle end-member and the Dharwar TTG was estimated. If partial melting was considered and included into the equations then it was possible for the Maningoza Suite data to fit on all four of the components' partial melt mixing curves.

- Even though the partial melt mixing curves allowed for better fits of the Maningoza Suite data at least two samples did not fit on any of the mixing curves. Its likely that a different contaminant than the ones represented here is involved and due to the curvature of the Maningoza Suite data its likely that this unknown contaminant has undergone partial melting. Data on the surrounding basement rocks (e.g. Bekodoka and Ambohipaky inliers) is required to get a better understanding of the situation.

- The Maningoza Suite shows many similarities when compared to other Cretaceous igneous complexes located around Madagascar. In terms of mineral chemistry the range in feldspars are similar with the Maningoza Suite having more orthoclase compositions. Both the Maningoza Suite and Morondava Complex have clinopyroxenes that have augitic compositions. The Mailaka and Antampombato-Ambatovy Complexes have more diverse clinopyroxene compositions that also include augite. The Mailaka and Morondava Complexes have a much wider range of olivine composition than the Maningoza Suite and the Antampombato-Ambatovy Complex has much higher Fo content than the Maningoza Suite olivines.

- The major element data for Androy and Mailaka Complexes compares well with the Maningoza Suite data with similar correlations. The Antampombato-Ambatovy Complex has data which compares to the Maningoza Suite but at very low silica wt. percentages the Antampombato-Ambatovy Complex shows different correlations in certain variation diagrams. The trace element data of the Mailaka and

Antampombato-Ambatovy Complexes compare well to that of the Maningoza Suite but the trace element of the Androy Complex shows two separate groups.

- Radiogenic data suggests that the Maningoza Suite is most similar to the Mailaka Complex in Madagascar as both have data that ranges from primitive to contaminated and the Maningoza Suite has most of its samples plotting within the Mailaka data field. As the Mailaka Complex is the closest complex to the Maningoza Suite (roughly 100 to 200km's distance) it is entirely possible that the primitive and contaminant sources are related.

- The Maningoza Suite was also compared to Deccan Trap lavas and to rhyolites of Lebombo rifted volcanic margin using radiogenic isotopes data. This was done as the three complexes could have a similar primitive end-member as the mantle source might have not changed over 120 Ma. The Deccan Trap lavas and the Maningoza Suite show similar trends and the data of the Maningoza Suite plots closely with data from the Deccan Traps. When compared with the Lebombo rhyolites the Maningoza Suite shows contamination with a source higher in ε_{Sr} and ε_{Nd}. The Maningoza Suite compares well with the Deccan Trap lavas and the primitive source and contaminant could be the same as some authors suggest links between the Madagascan and Indian basements.

ACKNOWLEDGEMENTS

I would like to express my sincere thanks to all of the people who supported and encouraged me throughout my dissertation.

A special thanks to my supervisor Prof. Chris Harris for his expert guidance, helpful advice and scientific insight from the beginning till the end of this dissertation. His help and attention was invaluable.

Thanks to Dr Paul Macey of the Council for Geoscience for supplying the samples, on which this dissertation is based, his insights into the field area and expert advice.

Thanks also go to Ernest Stout for guidance with the preparation of samples and David Wilson for supplying expertly prepared petrographic thin-sections. Thanks must go to Fayrooza Rawoot for her help with sample preparation for ICP-MS analysis and her expertise in the stable isotopes laboratory. Andreas Späth is greatly thanked for running the ICP-MS samples and Assoc. Prof. David Reid for running the XRF samples. Prof. Anton le Roex is thanked for his help and guidance with the microprobe analysis. Thanks go to Shireen Govender for providing invaluable assistance in preparing the samples for radiogenic isotopes analysis and Petrus le Roux for his expertise in collecting the radiogenic data.

Much needed funding for this project comes from the Council for Geoscience, National Research Foundation and a UCT research grant.

I am incredibly grateful to my parents whose encouragement, love and support allowed me to get to where I am today. All of my friends are greatly appreciated for their kindness and caring through this period of my life.

This dissertation is dedicated to Kate. Ultimately her love, understanding and encouragement got me through till the end of this dissertation.

REFERENCES

Adams, S., Titus, R., Pietersen, K. Tredoux, G. & Harris, C. 2001. Hydrochemical characteristics of aquifers near Sutherland in the Western Karoo, South Africa. *Journal of Hydrology.* 241(1-2):91-103.

Ashwal, L.D. & Tucker, R.D. 1999. Geology of Madagascar: A brief outline. *Gondwana Research.* 2(3):335-339.

Ashwal, L.D., Demaiffe, D. & Torsvik, T.H. 2002. Petrogenesis of Neoproterozoic granitoids and related rocks from the Seychelles: The case for an Andean-type arc origin. *Journal of Petrology.* 43(1):45-83.

Ashwal, L.D., Hamilton, M.A., Morel, V.P.I. & Rambeloson, R.A. 1998. Geology, petrology and isotope geochemistry of massif-type anorthosites from southwest Madagascar. *Contributions to Mineralogy and Petrology.* 133(4):389-401.

Aulbach, S., Rudnick, R.L. & McDonough, W.F. 2008. Li-Sr-Nd isotope signatures of the plume and cratonic lithospheric mantle beneath the margin of the rifted Tanzanian craton (Labait). *Contributions to Mineralogy and Petrology.* 155(1):79-92.

Baker, J.A., Thirlwall, M.F. & Menzies, M.A. 1996. Sr-Nd-Pb isotopic and trace element evidence for crustal contamination of plume-derived flood basalts: Oligocene flood volcanism in western Yemen. *Geochimica et Cosmochimica Acta.* 60(14):2559-2581.

Bardintzeff, J.M., Bonin, B. & Rasamimanana, G. 2001. The Cretaceous Morondava volcanic province (west Madagascar): Mineralogical, petrological and geochemical aspects. *Journal of African Earth Sciences.* 32(2):299-316.

Baron, R.P. & Mouneyres, L. 1904. Rapport sur une tournée géologique effectuée en 1903 dans l'ouest et le nord-ouest de Madagascar. *Bulletin Économique de Madagascar.* :1–20.

Barrabe, L. 1929. Contribution à l'étude stratigraphique et pétrographique de la partie médiane du pays Sakalava. *Mé. Soc. Géol. Fr.* 12:3-4.

Bauer, J. 1958. Besalampy F.41, Ambohipaky G.41,1/100 000. *Service Géologique de Madagascar.*

Bauer, J. 1959. Tsimandira E – 42, Marovoaikely F – 42, 1/100 000. *Service Géologique de Madagascar.*

Bauer, J. 1960. Besalampy F.41, Ambohipaky G.41, 1/100 000. *Service Géologique de Madagascar.*

Bauer, J. 1961. Cap Saint-André F.40, Ankasakasa G.40, 1/100 000. *Service Géologique de Madagascar.*

Bauer, J., Biro, P.H., Heilammer, R. & De Vendegies, A. 1958. Tambohorano D.E – 43, F – 43, 1/100 000. *Service Géologique de Madagascar.*

Bauer, J., Biro, P.H., Heilammer, R. & De Vendegies, A. 1959. Antranogoaika F – 44, Morafenobe G – 44, 1/100 000. *Service Géologique de Madagascar.*

Besairie, H. 1969. Carte géologique à 1/500 000, de Madagascar, 8 feuilles: 1: Diego Suarez; 2: Antalaha; 3: Majunga; 4: Tamatave; 5: Tananarive; 6: Morondava; 7: Fianarantsoa; 8: Ampanihy. *Antananarivo: Bureau Géologique, Madagascar.*

Besairie, H. 1971. Carte géologique au 1:2,000,000 et notice explicative. *Doc. Bureau Géologique, Madagascar.* 184.

Besairie, H. 1971. Description géologique du massif ancien de Madagascar. Document du Bureau Géologique Madagascar. no. 177. no. 177a: centre nord et centre nordest; 177b: région côtière orientale; 177c: région centrale — système de graphite; 177d: région centrale — système du Vohibory; 177e: le sud; 177f: le nord. *Antananarivo: Bureau Géologique de Madagascar.* :956.

Bhaskar Rao, Y.J., Sivaraman, T.V., Pantulu, G.V.C. Gopalan, K. & Naqvi, S.M. 1992. Rb-Sr ages of late Archean metavolcanics and granites, Dharwar craton, South India and evidence for Early Proterozoic thermotectonic event(s). *Precambrian Research.* 59(1-2):145-170.

Borthwick, J. & Harmon, R.S. 1982. A note regarding ClF_3 as an alternative to BrF_5 for oxygen isotope analysis. *Geochimica et Cosmochimica Acta.* 46(9):1665-1668.

Boulanger, J. & Riedel, A. 1959. Prospection Régionale de la région Cap Saint-André, Morafenobe. *Archives BUMIFOM, Tananarive.*

Brewer, T.S., Collins, A.S., Kröner, A., Windley, B.F. & Razakamanana, T. 2001. Multiphase granitoid magmatism in central Madagascar: evidence for subduction of the Mozambique Ocean. *Journal of Conference Abstracts. EUG.* 362.

Carmichael, I., Turner, F. & Verhoogen, J. 1974. Igneous Petrology. *New York: Mc Graw-Hill*. 739.

Chand, S. & Subrahmanyam, C. 2003. Rifting between India and Madagascar – mechanism and isostasy. *Earth and Planetary Science Letters.* 210(1-2):317-332.

Collins, A.S., Fitzsimons, I.C.W., Hulscher, B. & Razakamanana, T. 2003. Structure of the eastern margin of the East African Orogen in central Madagascar. *Precambrian Research.* 123(2-4):111-133.

Collins, A.S., Fitzsimons, I.C.W., Kinny, P.D., Brewer, T.S., Windley, B.F., Kröner, A. & Razakamanana, T. The Archaean rocks of central Madagascar: Their place in Gondwana. *Fourth International Archaean Symposium.* :294–296.

Collins, A.S., Razakamanana, T. & Windley, B.F. 2000. Neoproterozoic extensional detachment in central Madagascar: Implications for the collapse of the East African Orogen. *Geological Magazine.* 137(1):39.

Collins, A.S. & Windley, B.F. 2002. The tectonic evolution of central and northern Madagascar and its place in the final assembly of Gondwana. *The Journal of Geology.* 110:325-339.

Collins, A.S. 2006. Madagascar and the amalgamation of Central Gondwana. *Gondwana Research.* 9(1-2):3-16.

Compton, J.S. 2007. Holocene evolution of the Anichab Pan on the south-west coast of Namibia. *Sedimentology.* 54(1):55-70.

Cooper, A.F. 1976. Concentrically zoned ultramafic pods from the Haast Schist Zone, South Island, New Zealand. *New Zealand Journal of Geology and Geophysics.* 19:603–623.

Coplen, T.B. 1988. Normalization of oxygen and hydrogen isotope data. *Chemical Geology: Isotope Geoscience Section.* 72(4):293-297.

Cox, R., Fernandez, A. & Schreurs, G. 2004. Discussion on tectonic evolution of the Proterozoic Itremo Group metasediments in Central Madagascar Special Publication 206, 2003, 381-399. *Journal of Geological Society.* 161(3):539-541.

Craig, H. 1961. Isotopic variations in meteoric waters. *Science.* 133:1702.

Criss, R.E. & Taylor, H.P. 1986. Meteoric-hydrothermal systems. *Reviews in Mineralogy and Geochemistry.* 16(1):373.

de Wit, M.J. 2003. Madagascar: Heads it's a continent, tails it's an island. *Annual Review of Earth and Planetary Sciences.* 31:213-248.

Donoghue, E., Troll, V.R., Harris, C., O'Halloran, A., Walter, T.R. & Pérez Torrado, F.J. 2008. Low-temperature hydrothermal alteration of intra-caldera tuffs, Miocene Tejeda caldera, Gran Canaria, Canary Islands. *Journal of Volcanology and Geothermal Research.* 176(4):551-564.

Dostal, J., Dupuy, C., Nicollet, C. & Cantagrel, J.M. 1992. Geochemistry and petrogenesis of Upper Cretaceous basaltic rocks from southern Malagasy. *Chemical Geology.* 97(3-4):199-218.

Droop, G.T.R. 1987. A general equation for estimating Fe^{3+} concentrations in ferromagnesian silicates and oxides from microprobe analyses, using stoichiometric criteria. *Mineralogical Magazine.* 51:431.

Dumas, L. 1923. Rapport au sujet des travaux de la mission d'étude des terrains bitumineux à Madagascar. *Arch. Serv. Min. Mad.*

Duncan, A.R., Erlank, A.J. & Betton, P.J. 1984. Appendix 1: Analytical techniques and data base descriptions. *Special Publication, Geological Society of South Africa.* 13:389-395.

Duncan, R.A. 1981. Hotspots in the Southern Oceans - an absolute frame of reference for motion of the Gondwana continents. *Tectonophysics.* 74(1-2):29-42.

Fagereng, Å., Harris, C., La Grange, M. & Stevens, G. 2008. Stable isotope study of the Archaean rocks of the Vredefort impact structure, central Kaapvaal Craton, South Africa. *Contributions to Mineralogy and Petrology.* 155(1):63-78.

Floran, R.J. & Papike, J.J. 1978. Mineralogy and petrology of the Gunflint Iron Formation, Minnesota-Ontario: Correlation of compositional and assemblage variations at low to moderate grade. *Journal of Petrology.* 19(2):215.

Geiger, M., Clark, D.N. & Mette, W. 2004. Reappraisal of the timing of the breakup of Gondwana based on sedimentological and seismic evidence from the Morondava Basin, Madagascar. *Journal of African Earth Sciences.* 38(4):363-381.

Ghosh, J.G., de Wit, M.J. & Zartman, R.E. 2004. Age and tectonic evolution of Neoproterozoic ductile shear zones in the Southern Granulite Terrain of India, with implications for Gondwana studies. *Tectonics.* 23(3).

Goncalves, P., Nicollet, C. & Montel, J. 2004. Petrology and in situ U-Th-Pb monazite geochronology of ultrahigh-temperature metamorphism from the Andriamena mafic unit, north-central Madagascar. Significance of a petrographical PT path in a polymetamorphic context. *Journal of Petrology.* 45(10):1923-1957.

Green, T.H. 1980. Island arc and continent-building magmatism - A review of petrogenic models based on experimental petrology and geochemistry. *Tectonophysics.* 63(1-4):367-385.

Gregoire, M., Bell, D.R. & Le Roex, A.P. 2003. Garnet Lherzolites from the Kaapvaal Craton (South Africa): Trace element evidence for a metasomatic history. *Journal of Petrology.* 44(4):629-657.

Halliday, A.N., Lee, D., Tommasini, S. Davies, G.R., Paslick, C.R., Godfrey, F.J. & James, D.E. 1995. Incompatible trace elements in OIB and MORB and source enrichment in the sub-oceanic mantle. *Earth and Planetary Science Letters.* 133(3-4):379-395.

Handke, M.J., Tucker, R.D. & Ashwal, L.D. 1999. Neoproterozoic continental arc magmatism in west-central Madagascar. *Geology.* 27(4):351-354.

Hanson, G.N. & Langmuir, C.H. 1978. Modelling of major elements in mantle-melt systems using trace element approaches. *Geochimica et Cosmochimica Acta.* 42(6):725-741.

Harris, C. & Ashwal, L. 2002. The origin of low $d^{18}O$ granites and related rocks from the Seychelles. *Contributions to Mineralogy and Petrology.* 143(3):366-376.

Harris, C. & Erlank, A.J. 1992. The production of large-volume, low-$\delta^{18}O$ rhyolites during the rifting of Africa and Antarctica: The Lebombo Monocline, southern Africa. *Geochimica et Cosmochimica Acta.* 56(9):3561-3570.

Harris, C., Smith, H.S. & le Roex, A.P. 2000. Oxygen isotope composition of phenocrysts from Tristan da Cunha and Gough Island lavas: Variation with fractional crystallization and evidence for assimilation. *Contributions to Mineralogy and Petrology.* 138(2):164-175.

Harris, C., Oom, B.M. & Diamond, R.E. 1999. A preliminary investigation of the oxygen and hydrogen isotope hydrology of the greater Cape Town area and an assessment of the potential for using stable isotopes as tracers. *Water SA.* 25(1):15.

Harris, N.B.W., Bartlett, J.M. & Santosh, M. 1996. Neodymium isotope constraints on the tectonic evolution of East Gondwana. *Journal of Southeast Asian Earth Sciences.* 14(3-4):119-125.

Hartnady, C.J.H. & Le Roex, A.P. 1985. Southern Ocean hotspot tracks and the Cenozoic absolute motion of the African, Antarctic, and South American plates. *Earth and Planetary Science Letters.* 75(2-3):245-257.

Haugerud, R.A. & Kunk, M.J. 1988. ArAr*, a computer program for reduction of ^{40}Ar-^{39}Ar data. *United States Geological Survey, Open-File Report.* 88(261):68.

Hauzenberger, C.A., Sommer, H., Fritz, H., Bauernhofer, A., Kröner, A., Hoinkes, G., Wallbrecher, E. & Thoni, M. 2007. SHRIMP U-Pb zircon and Sm-Nd garnet ages from the granulite-facies basement of SE Kenya: evidence for Neoproterozoic polycyclic assembly of the Mozambique Belt. *Journal of the Geological Society.* 164(1):189-201.

Heilammer, R. 1959. Bemolanga H.44, Marotsialeha I.44, 1/100 000. *Service Géologique de Madagascar.*

Heilammer, R. & Bauer, J. 1959. Ankavitra G.43 andrafi alava H.43, 1/100 000. *Service Géologique de Madagascar.*

Hietanen, A. 1971. Distribution of elements in biotite-hornblende pairs and in an orthopyroxene-clinopyroxene pair from zoned plutons, northern Sierra Nevada, California. *Contributions to Mineralogy and Petrology.* 30(2):161-176.

Hindermeyer, J. & Hourcq, V. 1960. Bevary H.41 andranomavo I.41, 1/100 000. *Service Géologique de Madagascar.*

Hindermeyer, J. & Hourcq, V. 1960. Maroboaly H.40, Soalala I.40, 1/100 000. *Service Géologique de Madagascar.*

Hottin, G. 1976. Précambrien de Madagascar. *Bulletin du Bureau de Recherche Géologique et Minière (BRGM).* 4:151-199.

Hottin, G. 1976. Présentation et essai d'interprétation du Précambrien de Madagascar. *Bulletin du bureau de recherches géologiques et minières: géologie générale,, Paris, 1976, 2.* :117-153.

Hourcq, V. 1949. Notices explicatives Besalampy–Sonlal. *Serv. Géol., Tananarive.*

Hulscher, B., Collins, A.S., Dahl, K.L., Fitzsimons, I.C.W., Johnson, S.P., Jonsson, M.K., Passmore, A.R. & Powell, C.M. 2001. Evidence for 800 Ma and possibly older deformation and Plutonism in Madagascar. *Geological Society of Australia Abstracts.*Geological Society of Australia; 1999. 64:91-92.

International Symposium on the Precambrian Geology and Mineral Resources of Madagascar and International Field Workshop on Proterozoic Geology of Madagascar UNESCO-IUGS-IGCP-348/368. 1999. *Gondwana Research.* 2(3):501-502.

Ito, E., White, W.M. & Gopel, C. 1987. The O, Sr, Nd and Pb isotope geochemistry of MORB. *Chem Geol.* 62:157-176.

Jayananda, M., Moyen, J.F., Martin, H., Peucat, J.J., Auvray, B. & Mahabaleswar, B. 2000. Late Archaean (2550-2520 Ma) juvenile magmatism in the Eastern Dharwar craton, southern India: Constraints from geochronology, Nd-Sr isotopes and whole rock geochemistry. *Precambrian Research.* 99(3-4):225-254.

Khan, R.M.K., Das Sharma, S., Patil, D.J. & Naqvi, S.M. 1996. Trace, rare-earth element, and oxygen isotopic systematics for the genesis of banded iron-formations: Evidence from Kushtagi schist belt, Archaean Dharwar Craton, India. *Geochimica et Cosmochimica Acta.* 60(17):3285-3294.

Koenig, R. & Tortochaux, F. 1949. Etude géologique des feuilles Bekodoka, Bebao, Tambohorono. *Trav. Bur. Géol. Madag.* 4.

Kracek, F.C. & Neuvonen, K.J. 1952. Thermochemistry of plagioclase and alkali feldspars. *American Journal of Science, Bowen.* 1952:293–318.

Kröner, A., Hegner, E., Collins, A., Windley, B.F., Brewer, T.S., Razakamanana, T. & Pidgeon, R.T. 2000. Age and magmatic history of the Antananarivo block, Central Madagascar, as derived from zircon geochronology and Nd isotopic systematics. *American Journal of Science.* 300(April):251-288.

Kröner, A., Muhongo, S., Hegner, E. & Wingate, M.T.D. 2003. Single-zircon geochronology and Nd isotopic systematics of Proterozoic high-grade rocks from the Mozambique belt of southern Tanzania (Masasi area): Implications for Gondwana assembly. *Journal of Geological Society.* 160(5):745-757.

Kröner, A., Windley, B.F., Jaecke, P., Collins, A.S., Brewer, T.S., Nemchin, A. & Razakamanana, T. 1999. New zircon ages for Precambrian granites, gneisses and granulites from Central and Southern Madagascar: Significance for correlations in east Gondwana. *Gondwana Research.* 2(3):351-352.

Kunk, M.J. & McAleer, R. 2008. $^{40}Ar/^{39}Ar$ data for white mica, biotite, and K-feldspar samples from low-grade metamorphic rocks in the Westminster Terrane and adjacent rocks, Maryland. *United States Geological Survey, Reston, Virginia.*

Kusky, T.M., Toraman, E. & Raharimahefa, T. 2007. The Great Rift Valley of Madagascar: An extension of the Africa–Somali diffusive plate boundary? *Gondwana Research.* 11(4):577-579.

Langmuir, C.H., Vocke, R.D.J., Hansona, G.N. & Hart, S.R. 1978. A general mixing equation with applications to Icelandic basalts. *Earth and Planetary Science Letters.* 37(3).

Lardeaux, J.M., Martelat, J.E., Nicollet, C., Pili, E., Rakotondrazafy, R. & Cardon, H. 1999. Metamorphism and tectonics in Southern Madagascar: An overview. *Gondwana Research.* 2(3):355-362.

Lawrence, J.R. & Taylor, H.P. 1971. Deuterium and oxygen-18 correlation: Clay minerals and hydroxides in Quaternary soils compared to meteoric waters. *Geochimica et Cosmochimica Acta.* 35(10):993-1003.

le Bas, M.J., le Maitre, R.W., Streckeisen, A. & Zanettin, B. 1986. IUGS subcommission on the systematics of igneous rocks, a chemical classification of volcanic rocks based on the total alkali-silica diagram. *Journal of Petrology.* 27(3):745-750.

le Roex, A.P. 1985. Geochemistry, mineralogy and magmatic evolution of the basaltic and trachytic lavas from Gough Island, South Atlantic. *Journal of Petrology.* 26(1):149.

Le Roex, A.P., Erlank, A.J. & Needham, H.D. 1981. Geochemical and mineralogical evidence for the occurrence of at least three distinct magma types in the 'Famous' region. *Contributions to Mineralogy and Petrology.* 77(1):24-37.

le Roex, A., Späth, A. & Zartman, R. 2001. Lithospheric thickness beneath the southern Kenya Rift: Implications from basalt geochemistry. *Contributions to Mineralogy and Petrology.* 142(1):89-106.

le Roux, P.J., le Roex, A.P., Schilling, J., Shimizu, N., Perkins, W.W. & Pearce, N.J.G. 2002. Mantle heterogeneity beneath the southern Mid-Atlantic Ridge: Trace element evidence for contamination of ambient asthenospheric mantle. *Earth and Planetary Science Letters.* 203(1):479-498.

Lightfoot, P.C., Hawkesworth, C.J., Devey, C.W., Rogers, N.W. & van Calsteren, P.W.C. 1990. Source and differentiation of Deccan Trap lavas: Implications of geochemical and mineral chemical variations. *Journal of Petrology.* 31(5):1165.

Lightfoot, P.C., Hawkesworth, C.J. & Sethna, S.F. 1987. Petrogenesis of rhyolites and trachytes from the Deccan Trap: Sr, Nd and Pb isotope and trace element evidence. *Contributions to Mineralogy and Petrology.* 95(1):44-54.

Lightfoot, P.C. & Hawkesworth, C.J. 1988. Origin of Deccan Trap lavas: Evidence from combined trace element and Sr-, Nd-and Pb-isotope studies. *Earth and Planetary Science Letters.* 91(1-2):89-104.

Macey, P.H., Armstrong, R.A., Botha, P.M.W., Haddon, I.G., Wilson, M., Bisnath, A., Yibas, B. & Ingram, B. 2007. Project de gouvernance des ressources minerales services d'assistance tichnique pour le leve geologique des Zone E et F. *CGS Status Report and the Resubmission of the Zone F Geological Report, Council for Geoscience.* :1-69.

Mahoney, J., Nicollet, C. & Dupuy, C. 1991. Madagascar basalts: tracking oceanic and continental sources. *Earth and Planetary Science Letters.* 104(2-4):350-363.

Mahoney, J.J., Frei, R., Tejada, M.L.G., Mo, X.X., Leat, P.T. & Nagler, T.F. 1998. Tracing the Indian Ocean mantle domain through time: Isotopic results from Old West Indian, East Tethyan, and South Pacific seafloor. *Journal of Petrology.* 39(7):1285.

Mahoney, J.J., Saunders, A.D., Storey, M. & Tandriamanantenasoa, A. 2008. Geochemistry of the Volcan de l' Androy Basalt-Rhyolite Complex, Madagascar Cretaceous Igneous Province. *Journal of Petrology.* 49(6):1069-1096.

Manya, S. & Maboko, M.A.H. 2008. Geochemistry and geochronology of Neoarchaean volcanic rocks of the Iramba-Sekenke greenstone belt, central Tanzania. *Precambrian Research.* 163(3-4):265-278.

McMillan, A., Harris, N.B.W., Holness, M., Ashwal, L., Kelley, S. & Rambeloson, R. 2003. A granite–gabbro complex from Madagascar: constraints on melting of the lower crust. *Contributions to Mineralogy and Petrology.* 145(5):585-599.

Meert, J.G., Hall, C., Nédélec, A. & Razanatseheno, M.O. 2001. Cooling of a late-syn orogenic pluton: Evidence from laser K-feldspar modelling of the Carion granite, Madagascar. *Gondwana Research.* 4(3):541-550.

Meert, J.G. & Tamrat, E. 2006. Paleomagnetic evidence for a stationary Marion hotspot: Additional paleomagnetic data from Madagascar. *Gondwana Research.* 10(3-4):340-348.

Melluso, L., Morra, V., Brotzu, P. & Mahoney, J.J. 2001. The Cretaceous igneous province of Madagascar: Geochemistry and petrogenesis of lavas and dykes from the central-western sector. *Journal of Petrology.* 42(7):1249-1278.

Melluso, L., Morra, V., Brotzu, P., Tommasini, S., Renna, M.R., Duncan, R.A., Francoisi, L., D'amelio, F. 2005. Geochronology and petrogenesis of the Cretaceous Antampombato-Ambatovy complex and associated dyke swarm, Madagascar. *Journal of Petrology.* 46(10):1963-1996.

Melluso, L., Morra, V., Brotzu, P., Franciosi, L., Lieberknecht, A.M.P. & Bennio, L. 2003. Geochemical provinciality in the Cretaceous basaltic magmatism of northern Madagascar: Mantle source implications. *Journal of the Geological Society.* 160(3):477-488.

Melluso, L., Morra, V., Brotzu, P., Razafiniparany, A., Ratrimo, V. & Razafimahatratra, D. 1997. Geochemistry and Sr-isotopic composition of the late cretaceous flood basalt sequence of northern Madagascar: Petrogenetic and geodynamic implications. *Journal of African Earth Sciences.* 24(3):371-390.

Melluso, L., Cucciniello, C., Petrone, C.M., Lustrino, M., Morra, V., Massimo, T. & Vasconcelos, L. 2008. Petrology of Karoo volcanic rocks in the southern Lebombo monocline, Mozambique. *Journal of African Earth Sciences.* 52(4-5):139-151.

Melluso, L. Sheth, H.C., Mahoney, J.J., Morra, V., Petrone, C.M. & Storey, M. 2009. Correlations between silicic volcanic rocks of the St Mary's Islands (southwestern India) and eastern Madagascar: Implications for Late Cretaceous India-Madagascar reconstructions. *Journal of the Geological Society.* 166(2):283-294.

Mette, W. 2004. Middle to Upper Jurassic sedimentary sequences and marine biota of the early Indian Ocean (Southwest Madagascar): some biostratigraphic, palaeoecologic and palaeobiogeographic conclusions. *Journal of African Earth Sciences.* 38(4):331-342.

Mikova, J. & Denkova, P. 2007. Modified chromatographic separation scheme for Sr and Nd isotope analysis in geological silicate samples. *Journal of Geosciences*. 52:221-226.

Miller, J.A. & Harris, C. 2007. Petrogenesis of the Swaziland and northern Natal Rhyolites of the Lebombo Rifted volcanic margin, South East Africa. *Journal of Petrology.* 48(1):185-218.

Milner, S.C. & le Roex, A.P. 1996. Isotope characteristics of the Okenyenya igneous complex, northwestern Namibia: Constraints on the composition of the early Tristan plume and the origin of the EM 1 mantle component. *Earth and Planetary Science Letters.* 141(1-4):277-291.

Möller, A., Mezger, K. & Schenk, V. 1998. Crustal age domains and the evolution of the continental crust in the Mozambique belt of Tanzania: Combined Sm–Nd, Rb–Sr,and Pb–Pb isotopic evidence. *Journal of Petrology.* 39(4):749-783.

Nakamura, N. 1974. Determination of REE, Ba, Fe, Mg, Na and K in carbonaceous and ordinary chondrites. *Geochimica et Cosmochimica Acta.* 38(5):757-775.

Newhouse, W.H. & Glass, J.P. 1936. Some physical properties of certain iron oxides. *Economic Geology.* 31(7):699.

Papini, M. & Benvenuti, M. 1998. Lithostratigraphy, sedimentology and facies architecture of the Late Cretaceous succession in the central Mahajanga Basin, Madagascar. *Journal of African Earth Sciences.* 26(2):229-247.

Paquette, J.L., Goncalves, P., Devouard, B. & Nicollet, C. 2004. Micro-drilling ID-TIMS U-Pb dating of single monazites: A new method to unravel complex poly-metamorphic evolutions. Application to the UHT granulites of Andriamena (North-Central Madagascar). *Contributions to Mineralogy and Petrology.* 147(1):110-122.

Paquette, J.L., Nédélec, A., Moine, B. & Rakontondrazafy, M. 1994. U-Pb, single zircon Pb-evaporation, and Sm-Nd isotopic study of a granulite domain in SE Madagascar. *The Journal of geology.* 102:523-538.

Pearson, D.G., Carlson, R.W., Shirey, S.B., Boyd, F.R. & Nixon, P.H. 1995. Stabilisation of Archaean lithospheric mantle: A Re-Os isotope study of peridotite xenoliths from the Kaapvaal craton. *Earth and Planetary Science Letters.* 134(3-4):341-357.

Peucat, J.J., Mahabaleswar, B. & Jayananda, M. 1993. Age of younger tonalitic magmatism and granulitic metamorphism in the South Indian transition zone (Krishnagiri area); comparison with older Peninsular gneisses from the Gorur–Hassan area. *Journal of Metamorphic Geology.* 11(6):879-888.

Piqué, A. 1999. L'évolution géologique de Madagascar et la dislocation du Gondwana: Une introduction (The geological evolution of Madagascar: An introduction). *Journal of African Earth Sciences.* 28(4):919-930.

Piqué, A., Laville, E., Bignot, G., Rabarimanana, M. & Thouin, C. 1999. L'ouverture et le développement du bassin de Morondava (Madagascar) du Carbonifère supérieur au Jurassique moyen. Données stratigraphiques, sédimentaires, paléontologiques et structurales (The initiation and development of the Morondava Basin Madagascar from the Late Carboniferous to the Middle Jurassic: Sedimentary, palæontological and structural data). *Journal of African Earth Sciences.* 28(4):931-948.

Piqué, A., Laville, E., Chotin, P., Chorowicz, J., Rakontondraompiana, S. & Thouin, C. 1999. L'extension à Madagascar du Néogène à l'Actuel: Arguments structuraux et géophysiques (Neogene and present extension in Madagascar: Structural and geophysical data). *Journal of African Earth Sciences.* 28(4):975-983.

Pitfield, P., Bauer, W., Schofield, D., Kusky, T. & Randriamananjara, T. 2006. Reappraisal of the geology and structural evolution of the Precambrian basement in north and east-central Madagascar. *Geophysical Research Abstracts.* 8:02019.

Raharimahefa, T. & Kusky, T.M. 2006. Structural and remote sensing studies of the southern Betsimisaraka Suture, Madagascar. *Gondwana Research.* 10(1-2):186-197.

Rakotosolofo, N.A., Torsvik, T.H., Ashwal, L.D., Eide, E.A. & de Wit, M.J. 1999. The Karoo Supergroup revisited and Madagascar-Africa fits. *Journal of African Earth Sciences.* 29(1):135-151.

Rambeloson, R.A., Yoshida, M., Ramasiarinoro, V., Le Duc, L. & Ralison, B. 2003. The Central Granites-Gneiss-Migmatite Belt (CGGMB) of Madagascar: The Eastern Neoproterozoic Suture of the East African Orogen. *Gondwana Research.* 6(4):641-651.

Ranaivoarivelo, A. 1997. Etude pétrographique et géochimique du gisement de quartzites à magnétite de Soalala, Nord-Ouest de Madagascar. *Thèse de Diplôme Universitaire de Recherche, Université Paul Sabatier de Toulouse.*

Rasoamahenina, J.A., Raharinosy, M. & Rabeandrianarisoa, S. 1967. Ambohipaky G.41, Bevary H.41, Mangoboky G.42, Bekodoka H.42, 1/100 000. *Service Géologique de Madagascar.*

Rasoamahenina, J.A., Raharinosy, M. & Rabeandrianarisoa, S. 1967. Mangoboka G.42, Bekodoka H.42 Andolamosa G.43 Andrafialava H.43, 1/100 000. *Service Géologique de Madagascar.*

Rasoamahenina, J.A., Raharinosy, M. & Rabeandrianarisoa, S. 1968. Ankasakasa G.40, Maroboaly H.40, Ambohipaky G.41, Bevary H.41, 1/100 000. *Service Géologique de Madagascar.*

Rasolofomanana, A.S. 1998. Les complexes annulaires de la province magmatique du Cap Saint-André: Géologie, pétrologie et géodynamique. *Thèse, Université Blaise Pascal.*

Razafimanantsoa, A.P. 1969. Ampoza I43, 1:100 000 scale geological map. *Service Géologique de Madagascar.*

Rollinson, H.R. 1993. Using geochemical data: Evaluation, presentation, interpretation. *New York, John Wiley and Sons.* 352.

Savin, S.M. & Epstein, S. 1970. The oxygen and hydrogen isotope geochemistry of clay minerals. *Geochimica et Cosmochimica Acta.* 34(1):25-42.

Savin, S.M. & Epstein, S. 1970. The oxygen isotopic compositions of coarse grained sedimentary rocks and minerals. *Geochimica et Cosmochimica Acta.* 34(3):323-329.

Savin, S.M. & Epstein, S. 1970. The oyxgen and hydrogen isotope geochemistry of ocean sediments and shales. *Geochimica et Cosmochimica Acta.* 34(1):43-63.

Schandelmeier, H., Bremer, F. & Holl, H. 2004. Kinematic evolution of the Morondava rift basin of SW Madagascar - from wrench tectonics to normal extension. *Journal of African Earth Sciences.* 38(4):321-330.

Sharp, Z.D. 1990. A laser-based microanalytical method for the in situ determination of oxygen isotope ratios of silicates and oxides. *Geochimica et Cosmochimica Acta.* 54(5):1353-1357.

Smith, W.H.F. & Sandwell, D.T. 1997. Global sea floor topography from satellite altimetry and ship depth soundings. *Science.* 277(5334):1956.

Smyth, J.R. & Hatton, C.J. 1977. A coesite-sanidine grospydite from the Roberts Victor kimberlite. *Earth and Planetary Science Letters.* 34(2):284-290.

Spencer, E. 1930. A contribution to the study of moonstone from Ceylon and other areas and of the stability-relations of the alkali-felspars. *Mineralogical Magazine.* 22(130):291-367.

Staudacher, T., Jessberger, E.K., Dorflinger, D. & Kiko, J. 1978. A refined ultrahigh-vacuum furnace for rare gas analysis. *Journal of Physics E: Scientific Instruments.* 11:781.

Steiger, R.H. & Jäger, E. 1977. Subcommission on geochronology: Convention on the use of decay constants in geochronology and cosmochronology. *Earth and Planetary Science Letters.* 36:359-362.

Stern, R.J. 2002. Crustal evolution in the East African Orogen: A neodymium isotopic perspective. *Journal of African Earth Sciences.* 34(3-4):109-117.

Storey, M., Mahoney, J.J. & Saunders, A.D. 1997. Cretaceous basalts in Madagascar and the transition between plume and continental lithosphere mantle sources. *Geophysical monograph.* 100:95-122.

Storey, M., Mahoney, J.J., Saunders, A.D. & Duncan, R.A. 1995. Timing of hot spot-related volcanism and the breakup of Madagascar and India. *Science.* 267:852-855.

Subramaniam, A.P. 1956. Mineralogy and petrology of the Sittampundi complex, Salem district, Madras State, India. *Geological Society of America Bulletin.* 67(3):317.

Taylor, B.E., Eichelberger, J.C. & Westrich, H.R. 1983. Hydrogen isotopic evidence of rhyolitic magma degassing during shallow intrusion and eruption. *Nature.* 306:541-545.

Taylor, B.E. 1986. Magmatic volatiles; isotopic variation of C, H, and S. *Reviews in Mineralogy and Geochemistry.* 16(1):185.

Torsvik, T.H., Tucker, R.D., Ashwal, L.D., Eide, E.A., Rakotosolofo, N.A. & de Wit, M.J. 1998. Late Cretaceous magmatism in Madagascar: Palaeomagnetic evidence for a stationary Marion hotspot. *Earth and Planetary Science Letters.* 164(1-2):221-232.

Tortochaux, F. 1950. Etude complémentaire de la Sakoa et de la Sakamena du Sud-Ouest. *Thèse Paris (manuscript).*

Tucker, R.D., Ashwal, L.D., Hamilton, M.A., Torsvik, T.H. & Carter, L.M. 1999. Neoproterozoic silicic magmatism of northern Madagascar, Seychelles, and NW India: Clues to Rodinia's assembly and dispersal. *Geol. Soc. Am. Abstr. Program.* A317.

Tucker, R.D., Ashwal, L.D., Handke, M.J., Hamilton, M.A., Le Grange, M. & Rambeloson, R.A. 1999. U - Pb geochronology and isotope geochemistry of the Archean and Proterozoic rocks of north - central Madagascar. *The Journal of geology.* 107:135-153.

Tucker, R.D., Kusky, T.M., Buchwaldt, R. & Handke, M.J. 2007. Neoproterozoic nappes and superposed folding of the Itremo Group, west-central Madagascar. *Gondwana Research.* 12(4):356-379.

Vennemann, T.W. & Smith, H.S. 1990. The rate and temperature of reaction of ClF_3 with silicate minerals, and their relevance to oxygen isotope analysis. *Chemical Geology: Isotope Geoscience section.* 86(1):83-88.

Vincent, E.A. & Phillips, R. 1954. Iron-titanium oxide minerals in layered gabbros of the Skaergaard intrusion, East Greenland: Part I. Chemistry and ore-microscopy. *Geochimica et Cosmochimica Acta.* 6:1-4.

Yoshida, M., Muhongo, S., Rambeloson, R. & Janardhan, A.S. 1999. Madagascar within Gondwanaland: Introduction. *Gondwana Research.* 2(3):333-333.

APPENDIX

Additional Mineral Chemistry Data for the Maningoza Suite

The feldspar, clinopyroxene, olivine and opaque mineral analyses presented in Tables 4.1, 4.2, 4.3 and 4.4 of Chapter 4 represent subsets of the entire database aquired for these minerals in the Maningoza Suite. The complete set of feldspar data is listed in Tables A1.1 to A1.6 and the complete set of clinopyroxene data is listed in Table A2.1 to A2.4. The complete set of olivine data is presented in Table A3.1 and the complete set of opaque mineral data is presented in Table A4.1.

Formation	Antanetilava																					
Sample	PF06130	PF06130	PF06130	PF06130	PF06130	PF06130	PF06130	PF06130	PF06130	PF06130	PF06130	PF06130	PF06130	PF06130	PF06130	PF06130	PF06130	PF06130	PF06130	PF06130	PF06130	PF06132
SiO_2	47.00	46.95	46.42	47.15	47.00	47.11	46.97	47.09	47.08	46.10	54.60	45.85	46.03	49.52	48.19	54.60	57.01	50.56	54.34	47.28	46.25	47.56
Al_2O_3	36.69	36.42	36.04	35.92	36.12	36.03	34.69	35.54	35.60	34.45	27.61	34.20	32.60	31.75	27.73	28.11	27.15	31.08	27.43	32.12	34.97	34.92
Fe_2O_3	0.40	0.43	0.41	0.47	0.43	0.47	0.38	0.43	0.43	0.43	0.61	0.49	0.44	0.67	0.51	0.95	0.79	0.79	0.95	0.43	0.47	0.52
CaO	17.95	17.82	18.00	17.73	17.76	17.70	16.10	17.46	17.33	17.25	10.29	17.53	15.87	14.78	10.11	10.89	9.61	14.34	10.76	14.63	17.69	17.44
Na_2O	1.28	1.21	1.22	1.38	1.33	1.34	2.19	1.41	1.46	1.52	4.99	1.29	1.83	3.15	4.17	5.52	6.44	3.47	5.73	2.77	1.37	1.46
K_2O	0.03	0.01	0.02	0.04	0.03	0.03	0.04	0.03	0.01	0.04	0.94	0.02	0.03	0.05	0.10	0.11	0.13	0.04	0.10	0.24	0.01	0.02
Total	103.60	103.03	102.31	102.92	102.90	102.90	100.51	102.22	102.14	100.00	99.31	99.64	96.97	100.23	91.11	100.42	101.37	100.53	99.49	97.82	100.99	102.17
Si^{4+}	2.088	2.096	2.090	2.108	2.102	2.107	2.145	2.118	2.118	2.122	2.490	2.120	2.177	2.262	2.391	2.466	2.539	2.300	2.479	2.216	2.110	2.140
Al^{3+}	1.922	1.917	1.913	1.894	1.905	1.899	1.867	1.885	1.889	1.870	1.485	1.864	1.818	1.710	1.622	1.497	1.426	1.667	1.475	1.775	1.881	1.852
Fe^{3+}	0.015	0.016	0.015	0.018	0.016	0.018	0.014	0.016	0.016	0.016	0.023	0.019	0.017	0.025	0.021	0.036	0.029	0.030	0.036	0.017	0.018	0.020
Ca^{2+}	0.855	0.852	0.868	0.850	0.851	0.848	0.788	0.841	0.836	0.851	0.503	0.869	0.804	0.724	0.538	0.527	0.459	0.699	0.526	0.735	0.865	0.841
Na^{+}	0.110	0.105	0.107	0.120	0.115	0.116	0.194	0.123	0.127	0.136	0.441	0.115	0.168	0.279	0.401	0.483	0.556	0.306	0.507	0.252	0.121	0.127
K^{+}	0.002	0.001	0.001	0.002	0.002	0.002	0.002	0.002	0.001	0.002	0.055	0.001	0.002	0.003	0.006	0.006	0.008	0.002	0.006	0.015	0.001	0.001
Sum	5.005	4.998	5.007	5.005	5.004	5.002	5.019	5.001	5.001	5.011	5.015	5.005	4.998	5.023	5.000	5.028	5.028	5.021	5.039	5.029	5.009	4.997
An	88.5	89.0	88.9	87.5	87.9	87.8	80.1	87.1	86.7	86.1	50.3	88.2	82.6	72.0	56.9	51.8	44.9	69.4	50.6	73.4	87.6	86.7
Ab	11.4	11.0	10.9	12.3	11.9	12.0	19.7	12.7	13.2	13.7	44.2	11.7	17.2	27.8	42.5	47.6	54.4	30.4	48.8	25.1	12.3	13.1
Or	0.2	0.1	0.1	0.2	0.2	0.2	0.2	0.2	0.1	0.2	5.5	0.1	0.2	0.3	0.7	0.6	0.7	0.2	0.6	1.5	0.1	0.1

Formation	Antanetilava																					
Sample	PF06132	PF06132	PF06132	PF06132	PF06132	PF06132	PF06132	PF06132	PF06132	PF06129	PF06129	PF06129	PF06129	PF06129	PF06129	PF06129	PF06129	PF06129	PF06129	PF06148	PF06148	PF06148
SiO_2	55.44	47.52	47.31	47.26	47.27	47.85	45.77	47.41	46.89	47.07	47.41	47.34	47.34	47.16	47.19	51.10	53.02	50.25	54.86	62.66	53.69	57.61
Al_2O_3	29.34	34.80	34.58	34.75	34.58	33.77	34.56	34.64	35.18	35.25	35.00	35.56	35.14	35.36	34.98	32.52	31.39	32.75	29.66	20.44	28.28	24.79
Fe_2O_3	0.98	0.55	0.53	0.46	0.47	0.51	1.48	0.51	0.46	0.54	0.52	0.45	0.48	0.47	0.45	0.69	1.02	0.62	0.75	2.35	1.37	0.79
CaO	11.66	17.52	17.32	17.44	17.45	16.71	16.63	17.51	17.85	17.52	17.60	17.78	17.65	17.59	17.80	15.09	13.44	15.36	11.79	2.76	10.96	8.02
Na_2O	5.23	1.45	1.57	1.52	1.38	1.89	1.25	1.46	1.17	1.37	1.41	1.35	1.41	1.33	1.29	3.07	4.06	2.79	5.20	8.70	4.79	5.83
K_2O	0.11	0.03	0.02	0.02	0.02	0.03	0.02	0.02	0.02	0.01	0.01	0.02	0.00	0.01	0.02	0.03	0.05	0.02	0.06	0.49	0.42	0.40
Total	102.98	102.11	101.57	101.70	101.42	101.04	100.74	101.78	101.78	101.99	102.16	102.73	102.24	102.09	101.97	102.85	103.27	102.08	102.54	98.90	99.72	97.57
Si^{4+}	2.443	2.141	2.143	2.137	2.143	2.175	2.099	2.143	2.120	2.123	2.135	2.120	2.130	2.124	2.130	2.272	2.341	2.252	2.427	2.827	2.448	2.643
Al^{3+}	1.524	1.848	1.846	1.853	1.848	1.810	1.868	1.846	1.875	1.875	1.858	1.878	1.864	1.877	1.861	1.705	1.634	1.730	1.547	1.087	1.520	1.341
Fe^{3+}	0.036	0.021	0.020	0.017	0.018	0.019	0.057	0.019	0.018	0.020	0.020	0.017	0.018	0.018	0.017	0.026	0.038	0.023	0.028	0.089	0.052	0.030
Ca^{2+}	0.551	0.846	0.840	0.845	0.848	0.814	0.817	0.848	0.865	0.847	0.849	0.853	0.851	0.849	0.861	0.719	0.636	0.737	0.559	0.133	0.535	0.394
Na^{+}	0.447	0.127	0.138	0.133	0.121	0.167	0.111	0.128	0.102	0.120	0.123	0.117	0.123	0.117	0.113	0.265	0.348	0.242	0.446	0.761	0.423	0.519
K^{+}	0.006	0.002	0.001	0.001	0.001	0.002	0.001	0.001	0.001	0.001	0.001	0.001	0.000	0.001	0.001	0.002	0.003	0.001	0.003	0.028	0.025	0.023
Sum	5.019	4.998	5.003	5.002	4.994	5.003	5.022	4.999	4.994	4.999	4.998	5.000	4.999	4.996	4.996	5.008	5.016	5.004	5.022	5.024	5.014	4.956
An	54.9	86.8	85.8	86.3	87.4	82.9	87.9	86.8	89.3	87.5	87.3	87.8	87.4	87.9	88.4	72.9	64.5	75.2	55.4	14.5	54.4	42.1
Ab	44.5	13.0	14.1	13.6	12.5	17.0	12.0	13.1	10.6	12.4	12.7	12.1	12.6	12.1	11.5	26.9	35.2	24.7	44.2	82.5	43.1	55.4
Or	0.6	0.2	0.1	0.1	0.1	0.2	0.1	0.1	0.1	0.1	0.1	0.1	0.0	0.1	0.1	0.2	0.3	0.1	0.3	3.0	2.5	2.5

Table A1.1: Feldspar compositions for the Maningoza Suite.

Formation	Antanetilava															Sambao						
Sample	PF06148	PF06148	PF06148	PF06148	PF06148	PF06148	PF06148	PF06153	PF06153	PF06153	PF06153	PF06153	PF06153	PF06153	PF06153	BY6F103	BY6F103	BY6F103	BY6F103	BY6F103	BY6F103	BY6F103
SiO_2	63.01	55.00	58.36	63.19	55.86	55.82	58.60	58.33	62.00	64.71	54.25	62.59	64.50	54.12	56.17	57.10	56.11	60.30	67.68	67.49	58.43	56.59
Al_2O_3	21.63	27.11	20.48	23.07	24.93	27.03	24.58	20.81	22.55	18.33	28.41	23.25	18.57	28.26	26.37	26.44	26.34	24.11	20.14	20.20	25.64	26.22
Fe_2O_3	1.19	1.44	3.54	0.42	3.72	0.86	0.86	9.17	2.00	0.26	1.31	0.26	0.30	1.25	1.59	0.84	1.39	0.94	0.04	0.19	1.03	1.37
CaO	3.74	9.93	5.15	4.02	6.67	7.48	6.97	1.84	3.43	0.00	11.16	4.45	0.03	10.52	9.04	8.94	9.49	6.10	0.77	0.90	7.85	9.02
Na_2O	9.03	5.25	7.98	8.87	5.88	6.69	6.87	8.34	8.24	0.33	4.73	8.63	0.40	4.54	4.42	5.68	5.68	7.42	10.77	10.84	6.33	5.86
K_2O	0.10	0.35	0.09	0.24	0.48	0.28	0.39	0.43	0.87	16.53	0.33	0.06	16.41	0.22	0.38	0.46	0.38	0.32	0.05	0.06	0.49	0.40
Total	99.27	99.41	99.91	99.90	99.60	98.45	98.51	102.62	99.90	100.22	100.43	99.27	100.30	99.21	98.46	99.58	99.64	99.35	99.50	99.68	99.91	99.67
Si^{4+}	2.817	2.506	2.658	2.798	2.552	2.549	2.662	2.637	2.772	2.993	2.453	2.786	2.982	2.467	2.565	2.578	2.547	2.708	2.969	2.960	2.624	2.564
Al^{3+}	1.140	1.456	1.100	1.204	1.343	1.455	1.317	1.109	1.189	0.999	1.515	1.220	1.012	1.519	1.420	1.407	1.410	1.276	1.042	1.045	1.358	1.400
Fe^{3+}	0.045	0.055	0.135	0.016	0.142	0.033	0.033	0.347	0.075	0.010	0.050	0.010	0.012	0.048	0.061	0.032	0.053	0.035	0.002	0.007	0.039	0.052
Ca^{2+}	0.179	0.485	0.251	0.191	0.327	0.366	0.339	0.089	0.164	0.000	0.541	0.212	0.002	0.514	0.442	0.433	0.462	0.294	0.036	0.042	0.378	0.438
Na^{+}	0.783	0.464	0.705	0.761	0.521	0.592	0.605	0.731	0.714	0.030	0.415	0.745	0.036	0.401	0.391	0.497	0.500	0.646	0.916	0.922	0.551	0.515
K^{+}	0.006	0.020	0.005	0.013	0.028	0.016	0.023	0.025	0.050	0.975	0.019	0.004	0.968	0.013	0.022	0.027	0.022	0.018	0.003	0.003	0.028	0.023
Sum	5.001	5.005	5.060	4.987	5.049	5.026	4.991	5.186	5.015	5.010	5.003	4.978	5.014	4.979	4.928	4.978	5.006	4.985	4.970	4.980	4.985	5.003
An	18.5	50.0	26.2	19.8	37.3	37.6	35.1	10.5	17.7	0.0	55.5	22.1	0.2	55.4	51.7	45.2	46.9	30.6	3.8	4.4	39.5	44.9
Ab	80.9	47.9	73.3	78.9	59.5	60.8	62.6	86.5	76.9	3.0	42.6	77.5	3.6	43.3	45.7	52.0	50.8	67.4	95.9	95.3	57.6	52.8
Or	0.6	2.1	0.5	1.4	3.2	1.7	2.3	3.0	5.4	97.0	2.0	0.4	96.2	1.3	2.6	2.8	2.2	1.9	0.3	0.3	3.0	2.4

Complex	Sambao Formation			Ankibobozaka													Berevo					
Sample	BY6F103	BY6F103	BY6F103	PF06004	PF06004	PF06004	PF06004	PF06004	PF06002	PF06002	PF06002	PF06002	PF06002	PF06002	PF06002	PF06002	PF06017	PF06017	PF06017	PF06017	PF06017	PF06017
SiO_2	56.44	55.23	55.49	51.50	50.60	51.31	52.16	50.71	67.21	68.45	67.18	65.72	65.91	67.96	67.42	71.42	48.95	47.71	48.55	48.06	50.67	48.31
Al_2O_3	26.45	27.12	26.88	30.17	31.30	30.80	30.47	31.26	21.42	21.15	21.03	21.08	20.28	20.42	20.50	18.12	32.03	32.97	32.29	32.43	30.54	32.08
Fe_2O_3	1.30	1.46	2.36	1.08	0.86	0.91	1.02	0.95	0.37	0.13	0.25	0.12	0.12	0.09	0.33	0.19	0.70	0.69	0.67	0.67	0.56	0.64
CaO	9.02	10.18	9.40	12.37	13.58	12.86	12.47	13.20	0.63	0.49	0.70	0.85	0.05	0.04	0.08	0.07	15.55	16.52	15.93	15.86	14.00	15.75
Na_2O	5.82	5.10	4.68	4.29	3.47	3.93	4.34	3.95	11.19	11.33	8.11	9.65	11.66	11.94	10.33	7.35	2.35	1.93	2.17	2.06	3.01	2.18
K_2O	0.42	0.34	0.37	0.09	0.07	0.08	0.08	0.08	0.14	0.18	3.68	2.34	0.11	0.22	1.91	5.36	0.14	0.09	0.12	0.12	0.21	0.13
Total	99.65	99.68	99.71	99.66	100.13	100.11	100.68	100.41	100.96	101.76	100.97	99.76	98.16	100.71	100.61	102.56	99.84	99.98	99.85	99.26	99.09	99.18
Si^{4+}	2.557	2.510	2.521	2.355	2.305	2.335	2.359	2.306	2.919	2.943	2.941	2.912	2.941	2.956	2.951	3.076	2.247	2.194	2.230	2.220	2.330	2.233
Al^{3+}	1.413	1.453	1.440	1.626	1.681	1.652	1.625	1.676	1.097	1.072	1.085	1.101	1.067	1.047	1.058	0.920	1.733	1.787	1.749	1.766	1.656	1.748
Fe^{3+}	0.049	0.055	0.090	0.041	0.033	0.035	0.039	0.036	0.013	0.005	0.009	0.004	0.004	0.003	0.012	0.007	0.027	0.027	0.026	0.026	0.022	0.025
Ca^{2+}	0.438	0.496	0.458	0.606	0.663	0.627	0.604	0.643	0.029	0.022	0.033	0.040	0.002	0.002	0.004	0.003	0.765	0.814	0.784	0.785	0.690	0.780
Na^{+}	0.511	0.449	0.412	0.380	0.307	0.347	0.381	0.348	0.942	0.945	0.688	0.829	1.009	1.007	0.877	0.614	0.209	0.172	0.193	0.185	0.268	0.195
K^{+}	0.024	0.020	0.022	0.005	0.004	0.005	0.005	0.005	0.008	0.010	0.206	0.132	0.006	0.012	0.107	0.295	0.008	0.005	0.007	0.007	0.012	0.008
Sum	5.001	4.995	4.973	5.024	5.008	5.013	5.020	5.029	5.008	4.998	4.964	5.019	5.033	5.029	5.011	4.917	4.994	5.001	4.993	4.992	4.980	4.992
An	45.0	51.4	51.3	61.1	68.1	64.1	61.1	64.6	3.0	2.3	3.5	4.0	0.2	0.2	0.4	0.3	77.9	82.1	79.6	80.4	71.1	79.3
Ab	52.5	46.6	46.2	38.4	31.5	35.4	38.5	35.0	96.2	96.7	74.3	82.8	99.2	98.6	88.8	67.4	21.3	17.4	19.6	18.9	27.7	19.9
Or	2.5	2.0	2.4	0.5	0.4	0.5	0.5	0.5	0.8	1.0	22.2	13.2	0.6	1.2	10.8	32.3	0.8	0.5	0.7	0.7	1.2	0.8

Table A1.2: Feldspar compositions for the Maningoza Suite

Complex	Berevo																					
Sample	PF06017	PF06017	PF06017	PF06018	PF06018	PF06018	PF06018	PF06018	PF06018	PF06018	PF06018	PF06018	PF06018	PF06018	PF06018	PF06018	PF06020	PF06020	PF06020	PF06020	PF06020	PF06020
SiO_2	48.17	49.03	50.91	66.31	64.99	63.72	66.35	65.17	65.41	64.98	64.56	64.13	65.31	66.31	67.80	66.64	48.47	49.79	48.37	49.00	52.12	50.35
Al_2O_3	32.22	31.85	30.63	19.04	18.36	20.07	18.79	18.24	18.45	18.23	18.33	18.11	18.36	18.77	20.17	20.91	33.04	32.28	32.93	32.19	30.13	31.45
Fe_2O_3	0.64	0.72	0.54	0.19	0.08	0.14	0.23	0.11	0.13	0.45	0.17	0.14	0.16	0.11	0.06	0.16	0.57	0.45	0.66	0.66	0.58	0.62
CaO	15.39	15.25	13.76	0.29	0.03	0.05	0.32	0.02	0.17	0.18	0.05	0.12	0.13	0.10	1.22	1.69	16.09	15.24	16.24	15.69	13.13	14.64
Na_2O	2.36	2.55	3.19	6.69	1.78	1.59	5.98	1.37	2.70	2.92	1.53	2.46	2.91	2.63	10.17	10.19	2.12	2.50	2.08	2.38	3.66	2.87
K_2O	0.21	0.13	0.22	6.52	14.22	14.15	7.52	14.66	12.85	12.22	14.49	13.13	12.65	13.21	0.04	0.08	0.06	0.11	0.09	0.11	0.26	0.20
Total	99.22	99.59	99.32	99.08	99.49	99.83	99.29	99.63	99.75	99.06	99.19	98.15	99.64	101.16	99.47	99.75	100.39	100.40	100.47	100.13	99.99	100.20
Si^{4+}	2.227	2.255	2.334	2.990	2.999	2.934	2.996	3.006	2.997	2.996	2.994	2.994	2.997	2.997	2.972	2.926	2.213	2.264	2.210	2.243	2.370	2.295
Al^{3+}	1.756	1.727	1.655	1.012	0.999	1.089	1.000	0.992	0.997	0.991	1.002	0.997	0.993	1.000	1.042	1.082	1.778	1.731	1.774	1.737	1.615	1.690
Fe^{3+}	0.025	0.028	0.021	0.007	0.003	0.005	0.009	0.004	0.005	0.017	0.007	0.005	0.006	0.004	0.002	0.006	0.022	0.017	0.025	0.025	0.022	0.024
Ca^{2+}	0.762	0.751	0.676	0.014	0.001	0.003	0.016	0.001	0.008	0.009	0.002	0.006	0.006	0.005	0.057	0.080	0.787	0.743	0.795	0.769	0.640	0.715
Na^{+}	0.212	0.227	0.284	0.585	0.159	0.142	0.524	0.123	0.240	0.261	0.138	0.223	0.259	0.230	0.864	0.868	0.188	0.220	0.184	0.211	0.323	0.254
K^{+}	0.013	0.007	0.013	0.375	0.837	0.831	0.433	0.863	0.751	0.719	0.857	0.782	0.741	0.762	0.002	0.004	0.003	0.006	0.005	0.007	0.015	0.012
Sum	5.006	4.998	4.985	4.984	4.999	5.008	4.982	4.990	5.000	4.998	5.002	5.009	5.006	4.999	4.940	4.968	4.993	4.983	4.997	4.996	4.989	4.992
An	77.3	76.2	69.5	1.4	0.1	0.3	1.6	0.1	0.8	0.9	0.2	0.6	0.6	0.5	6.2	8.4	80.5	76.6	80.7	77.9	65.5	72.9
Ab	21.4	23.1	29.2	60.1	16.0	14.5	53.8	12.4	24.0	26.4	13.8	22.0	25.7	23.1	93.5	91.2	19.2	22.7	18.7	21.4	33.0	25.9
Or	1.3	0.7	1.3	38.5	83.9	85.2	44.5	87.5	75.2	72.7	86.0	77.4	73.6	76.4	0.3	0.5	0.3	0.7	0.5	0.7	1.5	1.2

Complex	Berevo											Dykes										
Sample	PF06020	PF06020	PF06020	PF06027	PF06027	PF06027	PF06027	PF06027	PF06027	PF06027	PF06027	PF06028	PF06028	PF06028	PF06028	PF06071	PF06071	PF06071	PF06071	PF06071	PF06071	PF06071
SiO_2	52.41	51.73	50.59	45.56	44.73	45.75	45.33	45.01	45.85	45.74	46.40	66.14	66.84	67.02	67.87	54.76	58.61	54.64	55.60	55.24	58.43	55.19
Al_2O_3	29.93	30.71	31.68	34.35	34.16	34.95	35.10	35.33	34.43	34.16	34.12	18.22	20.25	20.01	19.60	28.90	26.98	28.80	28.24	28.12	26.81	29.31
Fe_2O_3	0.64	0.61	0.62	0.50	1.09	0.51	0.41	0.44	0.56	0.44	0.55	0.57	0.21	0.22	0.50	1.20	0.90	1.26	0.82	0.87	0.69	0.81
CaO	12.91	13.71	14.69	18.15	17.40	18.44	18.61	18.62	18.03	18.43	17.68	0.07	0.96	0.69	0.73	11.47	8.70	11.43	10.62	10.85	8.76	11.40
Na_2O	3.70	3.36	2.88	1.07	1.19	0.93	0.96	0.90	1.08	1.00	1.34	0.70	10.55	10.79	9.98	5.15	6.94	5.24	5.59	5.49	6.81	5.33
K_2O	0.23	0.22	0.14	0.02	0.02	0.01	0.02	0.01	0.01	0.02	0.02	14.77	0.09	0.11	0.17	0.24	0.44	0.23	0.28	0.26	0.43	0.23
Total	99.92	100.47	100.71	99.83	99.32	100.73	100.56	100.40	100.15	99.90	100.28	100.56	99.00	98.93	98.89	101.94	102.78	101.92	101.38	101.10	102.07	102.41
Si^{4+}	2.382	2.345	2.293	2.107	2.084	2.097	2.083	2.072	2.112	2.113	2.132	3.019	2.953	2.963	2.993	2.442	2.572	2.439	2.483	2.477	2.578	2.444
Al^{3+}	1.604	1.641	1.693	1.873	1.877	1.888	1.901	1.917	1.870	1.861	1.848	0.981	1.055	1.043	1.019	1.519	1.396	1.516	1.487	1.486	1.394	1.530
Fe^{3+}	0.024	0.023	0.023	0.019	0.043	0.019	0.016	0.017	0.021	0.017	0.021	0.022	0.008	0.008	0.019	0.045	0.033	0.047	0.030	0.033	0.025	0.030
Ca^{2+}	0.629	0.666	0.713	0.899	0.869	0.906	0.916	0.918	0.890	0.912	0.870	0.004	0.045	0.033	0.035	0.548	0.409	0.547	0.508	0.521	0.414	0.541
Na^{+}	0.326	0.295	0.253	0.096	0.108	0.082	0.086	0.080	0.096	0.090	0.120	0.062	0.904	0.925	0.853	0.445	0.590	0.454	0.484	0.477	0.583	0.458
K^{+}	0.013	0.012	0.008	0.001	0.001	0.001	0.001	0.001	0.001	0.001	0.001	0.860	0.005	0.006	0.009	0.014	0.025	0.013	0.016	0.015	0.024	0.013
Sum	4.983	4.987	4.988	5.004	5.032	5.000	5.009	5.010	5.001	5.002	5.003	4.951	4.973	4.981	4.929	5.026	5.034	5.034	5.021	5.024	5.027	5.025
An	65.0	68.4	73.2	90.3	88.9	91.6	91.3	91.9	90.2	90.9	87.8	0.4	4.7	3.4	3.9	54.4	39.9	53.9	50.4	51.4	40.6	53.5
Ab	33.7	30.3	26.0	9.6	11.0	8.3	8.6	8.0	9.7	9.0	12.1	6.7	94.7	95.9	95.1	44.2	57.7	44.8	48.0	47.1	57.1	45.2
Or	1.4	1.3	0.8	0.1	0.1	0.1	0.1	0.1	0.1	0.1	0.1	92.9	0.5	0.7	1.0	1.4	2.4	1.3	1.6	1.5	2.3	1.3

Table A1.3: Feldspar compositions for the Maningoza Suite

Complex	Dykes								Fonjay								Ambereny					
Sample	PF06071	PF06071	PF06138	PF06138	PF06138	PF06138	PF06138	PF06138	MI06010	MI06010	MI06010	MI06010	MI06010	MI06010	MI06010	MI06010	MI06014	MI06014	MI06014	MI06014	MI06014	MI06014
SiO_2	56.71	54.60	47.59	55.92	49.58	55.39	55.20	50.48	47.39	49.51	47.90	51.72	47.75	46.90	54.52	54.29	48.21	49.70	51.15	50.57	48.80	50.84
Al_2O_3	27.96	26.87	34.55	28.61	32.88	29.05	25.94	32.24	34.69	33.52	34.58	31.75	35.51	35.19	30.83	30.74	33.68	33.49	31.38	32.31	33.63	32.89
Fe_2O_3	1.10	3.94	0.52	0.81	0.67	0.81	4.21	0.89	0.43	0.39	0.40	0.48	0.36	0.42	0.42	0.43	0.55	0.44	0.48	0.42	0.44	0.39
CaO	9.94	10.03	17.30	10.79	15.66	11.38	8.50	14.85	17.23	15.74	16.95	13.88	17.40	17.70	12.32	12.32	16.54	15.65	14.06	14.63	16.29	14.91
Na_2O	5.96	5.28	1.66	5.79	2.61	5.28	5.77	3.17	1.55	2.44	1.79	3.52	1.59	1.35	4.58	4.60	2.10	2.71	3.75	3.21	2.30	3.25
K_2O	0.32	0.27	0.00	0.10	0.03	0.08	0.10	0.05	0.09	0.15	0.09	0.30	0.09	0.06	0.36	0.34	0.05	0.08	0.09	0.08	0.04	0.09
Total	102.28	102.02	101.81	102.23	101.68	102.19	101.52	101.84	101.47	101.85	101.78	101.75	102.73	101.64	103.17	102.84	101.26	102.20	101.02	101.34	101.63	102.49
Si^{4+}	2.509	2.460	2.149	2.476	2.234	2.455	2.492	2.269	2.147	2.224	2.161	2.317	2.135	2.123	2.397	2.395	2.187	2.226	2.310	2.278	2.202	2.266
Al^{3+}	1.458	1.427	1.840	1.494	1.746	1.518	1.381	1.709	1.853	1.775	1.839	1.677	1.872	1.878	1.598	1.599	1.801	1.768	1.671	1.716	1.789	1.728
Fe^{3+}	0.041	0.148	0.020	0.030	0.025	0.030	0.159	0.033	0.016	0.015	0.015	0.018	0.013	0.016	0.016	0.016	0.021	0.016	0.018	0.016	0.017	0.014
Ca^{2+}	0.471	0.484	0.837	0.512	0.756	0.541	0.411	0.715	0.836	0.758	0.819	0.666	0.834	0.859	0.580	0.582	0.804	0.751	0.681	0.706	0.788	0.712
Na^{+}	0.511	0.461	0.145	0.497	0.228	0.454	0.505	0.276	0.136	0.213	0.157	0.306	0.138	0.119	0.390	0.394	0.185	0.235	0.328	0.280	0.201	0.281
K^{+}	0.018	0.015	0.000	0.006	0.001	0.005	0.006	0.003	0.005	0.009	0.005	0.017	0.005	0.004	0.020	0.019	0.003	0.004	0.005	0.005	0.002	0.005
Sum	5.024	5.061	5.003	5.026	5.006	5.013	5.071	5.014	4.997	4.998	5.000	5.005	5.000	4.999	5.008	5.011	5.006	5.008	5.019	5.005	5.004	5.012
An	47.1	50.4	85.2	50.5	76.7	54.1	44.6	71.9	85.5	77.4	83.5	67.4	85.4	87.5	58.6	58.5	81.1	75.8	67.1	71.2	79.5	71.4
Ab	51.1	48.0	14.8	49.0	23.1	45.4	54.8	27.8	13.9	21.7	16.0	30.9	14.1	12.1	39.4	39.6	18.6	23.8	32.4	28.3	20.3	28.1
Or	1.8	1.6	0.0	0.6	0.2	0.5	0.6	0.3	0.6	0.9	0.5	1.7	0.5	0.4	2.1	1.9	0.3	0.4	0.5	0.5	0.2	0.5

Complex	Ambereny																					
Sample	MI06014	MI06014	MI06015	MI06015	MI06015	MI06015	MI06015	MI06015	MI06015	MI06015	MI06015	MI06015	MI06015	MI06015	MI06015	MI06015	MI06015	MI06015	MI06015	MI06016	MI06016	MI06016
SiO_2	51.51	51.22	65.08	64.81	65.11	65.09	65.21	66.27	65.88	66.00	65.20	65.98	63.31	60.81	60.09	61.92	61.82	63.71	63.42	65.55	65.21	66.70
Al_2O_3	32.51	32.90	18.46	18.46	18.57	18.67	18.49	19.49	18.74	18.42	18.66	18.80	22.80	24.73	24.14	22.91	23.55	22.59	22.26	19.06	18.53	20.83
Fe_2O_3	0.49	0.49	0.17	0.28	0.39	0.17	0.29	0.49	0.21	0.29	0.22	0.18	0.37	0.38	0.47	0.23	0.37	0.32	0.33	0.14	0.00	0.10
CaO	14.25	14.70	0.15	0.15	0.10	0.37	0.19	0.41	0.30	0.28	0.10	0.23	4.42	6.27	6.23	4.54	5.38	4.06	3.82	0.09	0.00	1.51
Na_2O	3.66	3.31	2.79	2.74	3.21	4.79	2.38	6.41	4.24	4.37	2.11	4.14	8.20	7.48	7.27	8.12	7.84	8.31	8.44	3.75	0.36	10.28
K_2O	0.10	0.08	11.98	12.13	11.71	8.87	12.70	7.17	10.36	9.64	13.51	10.42	0.60	0.56	0.47	0.57	0.40	0.72	0.58	10.59	16.32	0.07
Total	102.66	102.83	98.70	98.61	99.11	98.04	99.38	100.35	99.79	99.04	99.86	99.83	99.74	100.29	98.73	98.33	99.44	99.72	98.92	99.24	100.50	99.53
Si^{4+}	2.289	2.274	3.001	2.995	2.992	2.991	2.996	2.966	2.992	3.008	2.991	2.993	2.808	2.702	2.710	2.788	2.758	2.824	2.831	2.989	2.998	2.932
Al^{3+}	1.703	1.722	1.003	1.006	1.006	1.011	1.002	1.028	1.003	0.990	1.009	1.005	1.192	1.295	1.284	1.216	1.239	1.180	1.172	1.024	1.004	1.080
Fe^{3+}	0.018	0.018	0.007	0.011	0.015	0.006	0.011	0.019	0.008	0.011	0.008	0.007	0.014	0.014	0.018	0.009	0.014	0.012	0.012	0.005	0.000	0.004
Ca^{2+}	0.679	0.699	0.007	0.007	0.005	0.018	0.009	0.020	0.014	0.014	0.005	0.011	0.210	0.299	0.301	0.219	0.257	0.193	0.183	0.005	0.000	0.071
Na^{+}	0.315	0.285	0.249	0.246	0.286	0.427	0.212	0.556	0.373	0.386	0.188	0.364	0.705	0.644	0.636	0.709	0.678	0.714	0.731	0.332	0.032	0.876
K^{+}	0.005	0.005	0.705	0.715	0.687	0.520	0.744	0.409	0.600	0.561	0.791	0.603	0.034	0.032	0.027	0.033	0.023	0.041	0.033	0.616	0.957	0.004
Sum	5.016	5.009	4.975	4.982	4.991	4.976	4.981	5.002	4.993	4.970	4.993	4.987	4.965	4.988	4.978	4.975	4.972	4.964	4.964	4.973	4.993	4.968
An	67.9	70.7	0.8	0.8	0.5	1.9	1.0	2.0	1.5	1.4	0.5	1.2	22.1	30.6	31.2	22.8	26.8	20.3	19.3	0.5	0.0	7.5
Ab	31.6	28.8	25.9	25.4	29.3	44.2	22.0	56.5	37.8	40.2	19.1	37.2	74.3	66.1	65.9	73.8	70.8	75.3	77.2	34.8	3.2	92.1
Or	0.5	0.5	73.3	73.9	70.2	53.9	77.1	41.6	60.8	58.4	80.4	61.6	3.6	3.2	2.8	3.4	2.4	4.3	3.5	64.7	96.8	0.4

Table A1.4: Feldspar compositions for the Maningoza Suite

Complex	Ambereny																		Ambohitrosy		
Sample	MI06016	MI06016	MI06016	MI06016	MI06016	MI06016	MI06016	MI06016	MI06016	MI06016	MI06016	MI06019	MI06019	MI06019	MI06019	MI06019	MI06019	MI06019	AB-15	AB-15	AB-15
SiO_2	65.17	66.69	65.93	63.92	63.56	64.72	64.55	68.19	64.29	65.14	66.98	53.71	53.37	54.37	52.15	53.52	53.19	54.32	53.58	52.24	48.44	48.01
Al_2O_3	20.49	19.04	18.70	22.64	22.55	18.55	18.89	21.67	18.68	18.41	21.10	30.00	30.30	29.81	31.17	30.41	29.84	30.18	30.79	29.67	31.90	31.98
Fe_2O_3	0.14	0.14	0.09	0.06	0.31	0.19	0.04	0.23	0.13	0.11	0.12	0.55	1.64	0.57	0.57	0.61	0.67	0.57	0.50	0.52	0.60	0.65
CaO	1.63	0.24	0.17	3.82	4.07	0.06	0.09	0.92	0.00	0.11	1.83	12.23	12.04	11.71	13.46	12.47	12.03	12.11	12.78	12.63	14.91	15.99
Na_2O	9.82	4.84	3.12	8.63	8.33	2.12	1.79	10.30	0.53	2.19	10.42	4.65	4.24	4.81	3.88	4.45	4.48	4.75	4.43	4.70	2.64	2.30
K_2O	0.10	9.78	12.04	0.24	0.78	14.12	13.88	0.07	15.85	12.92	0.08	0.22	0.20	0.25	0.18	0.19	0.19	0.21	0.20	0.18	0.19	0.09
Total	97.41	100.82	100.10	99.32	99.66	99.79	99.26	101.44	99.71	98.93	100.56	101.52	102.61	101.68	101.58	101.80	100.82	102.27	102.47	100.11	96.24	99.14
Si^{4+}	2.928	2.990	2.998	2.832	2.821	2.983	2.981	2.933	2.980	3.005	2.920	2.402	2.372	2.423	2.338	2.388	2.395	2.409	2.376	2.377	2.243	2.224
Al^{3+}	1.085	1.006	1.002	1.183	1.180	1.008	1.028	1.099	1.021	1.001	1.084	1.582	1.587	1.566	1.648	1.599	1.584	1.578	1.610	1.591	1.742	1.747
Fe^{3+}	0.005	0.005	0.003	0.002	0.011	0.007	0.002	0.008	0.005	0.004	0.005	0.021	0.061	0.021	0.022	0.023	0.025	0.021	0.019	0.020	0.023	0.025
Ca^{2+}	0.078	0.012	0.008	0.181	0.194	0.003	0.004	0.042	0.000	0.005	0.085	0.586	0.573	0.559	0.647	0.596	0.580	0.576	0.607	0.616	0.740	0.794
Na^{+}	0.855	0.421	0.275	0.741	0.717	0.189	0.160	0.859	0.048	0.196	0.881	0.403	0.365	0.416	0.337	0.385	0.391	0.409	0.381	0.415	0.237	0.207
K^{+}	0.006	0.559	0.698	0.013	0.044	0.830	0.818	0.004	0.937	0.760	0.004	0.012	0.012	0.014	0.010	0.011	0.011	0.012	0.011	0.010	0.011	0.005
Sum	4.960	4.996	4.988	4.954	4.969	5.023	4.994	4.949	5.002	4.973	4.980	5.013	5.021	5.007	5.009	5.008	5.011	5.011	5.012	5.035	5.006	5.008
An	8.3	1.2	0.9	19.4	20.3	0.3	0.4	4.7	0.0	0.5	8.8	58.5	60.3	56.6	65.1	60.1	59.1	57.8	60.8	59.2	74.9	78.9
Ab	91.0	42.4	28.0	79.2	75.1	18.5	16.3	94.9	4.9	20.4	90.7	40.3	38.4	42.0	33.9	38.8	39.8	41.0	38.1	39.8	24.0	20.5
Or	0.6	56.4	71.1	1.4	4.6	81.2	83.2	0.4	95.1	79.1	0.5	1.2	1.2	1.4	1.0	1.1	1.1	1.2	1.1	1.0	1.1	0.5

Complex	Ambohitrosy																					
Sample	AB-15	AB-15	AB-15	AB-15	AB-15	AB-15	AB-15	AB-07	AB-07	AB-07	AB-07	AB-07	AB-07	AB-07	AB-07	AB26a	AB26a	AB26a	AB26a	AB26a	AB26a	AB26b
SiO_2	48.49	47.51	52.65	48.99	48.34	48.34	48.99	53.27	52.37	52.47	51.96	52.54	53.65	52.88	50.93	51.40	50.97	50.20	51.65	51.51	54.32	55.72
Al_2O_3	31.72	31.93	28.90	31.94	31.48	31.45	31.63	28.98	28.45	28.98	29.25	29.76	29.29	28.96	27.96	29.50	29.50	30.10	29.57	30.09	28.39	27.56
Fe_2O_3	0.48	0.51	0.52	0.59	0.09	1.06	0.32	0.05	0.46	0.34	0.31	0.36	0.36	0.36	0.37	0.56	0.56	0.54	0.68	0.65	0.47	0.62
CaO	15.53	16.76	12.53	15.18	15.70	15.28	15.68	4.82	11.81	11.84	12.61	11.99	12.36	12.05	11.07	13.20	14.01	14.15	13.07	13.22	11.08	9.81
Na_2O	2.64	1.98	4.20	2.40	2.54	2.44	2.50	0.19	4.85	4.47	4.51	4.62	4.72	0.23	4.07	3.87	3.49	3.43	4.09	3.98	5.04	6.20
K_2O	0.17	0.12	0.21	0.13	0.07	0.48	0.13	0.19	0.16	0.24	0.14	0.18	0.23	0.16	0.21	0.09	0.16	0.12	0.16	0.15	0.05	0.23
Total	99.13	98.96	99.17	99.49	98.29	99.89	99.33	99.23	98.33	98.42	98.84	99.51	100.72	94.85	95.98	98.79	98.82	98.72	99.45	99.82	99.64	100.37
Si^{4+}	2.243	2.209	2.411	2.252	2.250	2.230	2.257	2.358	2.418	2.416	2.389	2.394	2.418	2.477	2.403	2.368	2.353	2.323	2.367	2.352	2.465	2.508
Al^{3+}	1.730	1.750	1.560	1.731	1.728	1.710	1.718	1.512	1.549	1.573	1.586	1.599	1.556	1.599	1.556	1.602	1.606	1.642	1.598	1.620	1.519	1.463
Fe^{3+}	0.019	0.020	0.020	0.023	0.004	0.041	0.012	0.002	0.018	0.013	0.012	0.014	0.014	0.014	0.015	0.022	0.022	0.021	0.026	0.025	0.018	0.023
Ca^{2+}	0.770	0.835	0.615	0.748	0.783	0.755	0.774	0.229	0.584	0.584	0.621	0.586	0.597	0.605	0.560	0.652	0.693	0.701	0.642	0.647	0.539	0.473
Na^{+}	0.237	0.178	0.373	0.214	0.229	0.218	0.223	0.016	0.434	0.399	0.402	0.408	0.412	0.021	0.372	0.346	0.312	0.308	0.363	0.352	0.443	0.541
K^{+}	0.010	0.007	0.012	0.008	0.004	0.028	0.008	0.011	0.009	0.014	0.008	0.010	0.013	0.010	0.013	0.005	0.009	0.007	0.009	0.009	0.003	0.013
Sum	5.013	5.005	4.998	4.989	5.002	5.037	4.998	4.898	5.023	5.003	5.023	5.015	5.016	4.735	5.010	5.003	5.001	5.010	5.017	5.017	4.994	5.034
An	75.7	81.8	61.5	77.1	77.0	75.4	77.0	89.4	56.8	58.6	60.2	58.3	58.4	95.2	59.2	65.0	68.3	69.0	63.3	64.2	54.7	46.0
Ab	23.3	17.5	37.3	22.1	22.6	21.8	22.2	6.4	42.2	40.0	39.0	40.7	40.3	3.3	39.4	34.5	30.8	30.3	35.8	35.0	45.0	52.7
Or	1.0	0.7	1.2	0.8	0.4	2.8	0.8	4.2	0.9	1.4	0.8	1.0	1.3	1.5	1.3	0.5	0.9	0.7	0.9	0.9	0.3	1.3

Table A1.5: Feldspar compositions for the Maningoza Suite

Complex	Ambohitrosy																					
Sample	AB26b	AB26b	AB26b	AB26b	AB26b	AB26b	AB26b	AB26b	AB26b	AB26b	AB26b	AB26b	AB26	AB26	AB26	AB26	95-05	95-05	95-05	95-05	AB-10	AB-10
SiO_2	55.25	52.96	53.32	53.30	52.68	54.25	52.47	52.40	55.21	52.89	53.24	52.77	54.11	52.41	53.00	53.22	54.38	52.24	59.66	55.19	66.65	59.98
Al_2O_3	28.39	29.14	29.36	28.56	29.56	28.08	29.24	29.51	27.75	28.98	29.59	29.16	28.80	29.35	29.18	29.16	27.19	27.95	23.74	26.41	21.52	24.65
Fe_2O_3	0.53	0.65	0.52	0.62	0.47	0.70	0.70	0.69	0.45	0.56	0.66	0.79	0.42	0.78	0.70	0.62	1.01	1.11	0.76	0.82	0.15	0.21
CaO	10.98	12.30	12.08				12.77		10.17	12.22	12.74	12.86	11.47	12.56	12.36	11.87	11.14	13.42	6.45	9.58	2.02	6.69
Na_2O	5.29	4.59	4.50	4.57	4.51	5.25	4.27	4.38	5.62	4.70	4.51	4.54	5.22	4.49	4.48	4.81	4.96	3.81	6.99	5.84	10.37	7.22
K_2O	0.12	0.13	0.12	0.26	0.22	0.20	0.20	0.24	0.17	0.07	0.13	0.18	0.09	0.13	0.22	0.17	0.21	0.14	0.68	0.38	0.30	0.69
Total	100.77	99.97	99.99	87.52	87.57	88.69	99.93	87.36	99.54	99.59	101.06	100.49	100.16	99.95	100.20	100.05	99.08	98.92	98.46	98.36	101.06	99.53
Si^{4+}	2.477	2.408	2.417	2.624	2.590	2.642	2.391	2.585	2.501	2.412	2.396	2.394	2.446	2.388	2.405	2.415	2.488	2.411	2.707	2.533	2.899	2.689
Al^{3+}	1.501	1.562	1.569	1.658	1.713	1.612	1.571	1.716	1.482	1.558	1.570	1.560	1.535	1.576	1.561	1.560	1.467	1.520	1.270	1.429	1.103	1.303
Fe^{3+}	0.020	0.025	0.020	0.026	0.019	0.029	0.027	0.028	0.017	0.021	0.025	0.030	0.016	0.030	0.027	0.024	0.039	0.043	0.029	0.031	0.005	0.008
Ca^{2+}	0.527	0.599	0.587	0.000	0.000	0.000	0.624	0.000	0.494	0.597	0.614	0.625	0.556	0.613	0.601	0.577	0.546	0.664	0.314	0.471	0.094	0.321
Na^{+}	0.460	0.405	0.395	0.436	0.430	0.496	0.377	0.419	0.494	0.416	0.394	0.399	0.458	0.397	0.394	0.423	0.440	0.341	0.615	0.520	0.874	0.628
K^{+}	0.007	0.008	0.007	0.016	0.014	0.012	0.012	0.015	0.010	0.004	0.007	0.010	0.005	0.008	0.013	0.010	0.012	0.008	0.039	0.022	0.017	0.039
Sum	5.001	5.014	4.998	4.770	4.773	4.802	5.014	4.771	5.007	5.017	5.017	5.028	5.017	5.024	5.016	5.017	5.003	5.000	4.982	5.020	4.995	4.992
An	53.05	59.25	59.31	0.00	0.00	0.00	61.59	0.00	49.51	58.73	60.50	60.40	54.56	60.27	59.63	57.13	54.70	65.52	32.40	46.50	9.55	32.51
Ab	46.26	40.01	39.98	96.39	96.89	97.55	37.27	96.52	49.51	40.87	38.76	38.59	44.93	38.99	39.11	41.89	44.07	33.66	63.54	51.30	88.76	63.50
Or	0.69	0.75	0.70	3.61	3.11	2.45	1.15	3.48	0.99	0.40	0.74	1.01	0.51	0.74	1.26	0.97	1.23	0.81	4.07	2.20	1.69	3.99

Complex	Ambohitrosy																		
Sample	AB-10	AB-10	AB-10	AB-10	AB-10	AB-10	AB-10	AB-10	AB-10	AB-10	AB-10	95-14	95-14	95-14	95-14	95-14	95-14	AB09	AB09
SiO_2	64.96	68.94	65.50	58.45	60.23	60.36	66.81	65.31	58.35	58.80	59.44	65.84	69.93	68.11	64.04	67.92	63.61	68.73	70.13
Al_2O_3	19.49	20.99	21.97	26.10	25.25	24.79	21.09	22.54	26.58	25.35	25.02	18.08	19.21	18.87	17.55	18.62	17.54	19.74	19.20
Fe_2O_3	0.08	0.18	0.30	0.36	0.21	0.21	0.20	0.20	0.24	0.21	0.09	0.31	0.88	0.67	0.47	0.65		0.21	0.75
CaO	0.93	0.98	2.63	8.07	6.61	6.48	1.71	3.12	7.84	7.18	6.78		0.02	0.04				0.02	0.03
Na_2O	3.47	10.47	9.82	6.91	7.57	7.91	10.41	9.90	6.50	6.89	7.02	5.51	11.45	9.51	0.27	11.18	0.30	11.36	8.69
K_2O	11.54	0.14	0.36	0.48	0.22	0.22	0.21	0.16	0.38	0.62	0.54	8.38	0.18	1.67	16.44	0.27	16.24	0.23	2.30
Total	100.53	101.71	100.67	100.47	100.10	100.16	100.61	101.27	100.00	99.08	98.97	98.18	101.76	98.96	98.84	98.64	97.69	100.33	101.17
Si^{4+}	2.948	2.958	2.867	2.610	2.679	2.686	2.915	2.844	2.608	2.651	2.675	3.015	3.009	3.017	3.007	3.013	3.013	2.992	3.035
Al^{3+}	1.043	1.062	1.134	1.374	1.324	1.301	1.085	1.157	1.400	1.348	1.328	0.976	0.974	0.985	0.972	0.974	0.980	1.013	0.980
Fe^{3+}	0.003	0.006	0.011	0.013	0.008	0.008	0.007	0.007	0.009	0.008	0.003	0.012	0.032	0.025	0.018	0.024	0.000	0.008	0.027
Ca^{2+}	0.045	0.045	0.123	0.386	0.315	0.309	0.080	0.146	0.375	0.347	0.327	0.000	0.001	0.002	0.000	0.000	0.000	0.001	0.001
Na^{+}	0.305	0.871	0.833	0.598	0.653	0.683	0.881	0.836	0.563	0.602	0.613	0.489	0.955	0.817	0.025	0.962	0.028	0.959	0.729
K^{+}	0.668	0.008	0.020	0.027	0.012	0.012	0.012	0.009	0.022	0.036	0.031	0.490	0.010	0.094	0.985	0.015	0.981	0.013	0.127
Sum	5.015	4.951	4.992	5.013	4.991	5.007	4.987	5.000	4.982	4.994	4.981	4.985	4.984	4.944	5.010	4.988	5.002	4.987	4.903
An	4.4	4.9	12.6	38.2	32.1	30.8	8.2	14.7	39.1	35.2	33.7	0.0	0.1	0.2	0.0	0.0	0.0	0.1	0.2
Ab	30.0	94.3	85.3	59.1	66.6	68.0	90.6	84.4	58.7	61.2	63.1	50.0	98.9	89.5	2.4	98.4	2.7	98.6	85.0
Or	65.6	0.8	2.1	2.7	1.3	1.2	1.2	0.9	2.3	3.6	3.2	50.0	1.0	10.3	97.6	1.6	97.3	1.3	14.8

Table A1.6: Feldspar compositions for the Maningoza Suite

Formation	Antanetilava																						
Sample	PF06130	PF06130	PF06130	PF06130	PF06130	PF06130	PF06130	PF06130	PF06130	PF06130	PF06130	PF06130	PF06130	PF06130	PF06130	PF06130	PF06130	PF06130	PF06130	PF06130	PF06130	PF06130	PF06130
SiO_2	49.52	49.75	50.25	49.63	50.91	51.89	53.00	51.71	51.05	50.34	50.90	51.73	51.98	51.84	50.32	52.01	51.62	50.71	51.40	51.47	50.73	50.51	52.05
TiO_2	0.99	0.95	0.91	1.05	0.96	0.78	0.47	0.84	0.73	1.06	0.89	0.81	0.63	0.75	0.80	0.71	0.75	1.22	0.81	0.78	0.80	0.69	0.63
Al_2O_3	5.23	5.41	5.66	5.18	5.46	3.73	2.33	4.14	3.48	5.28	5.04	4.45	3.82	3.51	5.44	3.88	4.26	3.16	4.14	3.05	5.08	4.12	3.42
FeO	8.51	7.47	7.58	8.63	8.31	8.49	9.15	9.32	9.92	8.72	8.88	8.51	9.06	10.41	7.79	9.68	9.15	15.73	8.79	12.93	9.07	9.59	9.98
MnO	0.19	0.13	0.18	0.23	0.20	0.20	0.26	0.21	0.28	0.17	0.23	0.15	0.28	0.27	0.24	0.28	0.21	0.44	0.25	0.31	0.31	0.23	0.24
MgO	13.71	14.28	14.19	13.81	14.07	14.91	15.88	14.38	14.36	13.87	14.15	14.25	14.43	14.34	13.94	14.84	14.19	12.55	14.35	13.47	14.03	14.66	14.58
CaO	20.67	20.60	20.48	20.04	21.07	20.46	19.39	20.06	19.58	20.76	20.36	21.01	20.55	19.67	21.27	19.78	20.79	17.56	20.54	19.01	20.51	19.97	19.64
Na_2O	0.32	0.29	0.30	0.31	0.30	0.28	0.20	0.32	0.32	0.29	0.29	0.29	0.29	0.39	0.48	0.33	0.31	0.36	0.27	0.36	0.31	0.38	0.32
Total	99.46	99.25	100.08	99.20	101.50	100.86	100.88	101.32	99.87	100.66	101.13	101.35	101.17	101.31	100.56	101.68	101.43	101.74	100.77	101.38	101.09	100.29	100.98
Si^{4+}	1.858	1.860	1.864	1.864	1.864	1.907	1.947	1.901	1.907	1.862	1.875	1.895	1.910	1.911	1.861	1.904	1.895	1.899	1.897	1.914	1.871	1.880	1.919
Ti^{4+}	0.033	0.032	0.031	0.035	0.033	0.027	0.016	0.029	0.025	0.036	0.030	0.028	0.022	0.025	0.027	0.024	0.026	0.041	0.027	0.026	0.027	0.023	0.021
Al^{3+}	0.231	0.238	0.247	0.229	0.236	0.162	0.101	0.179	0.153	0.230	0.219	0.192	0.165	0.153	0.237	0.167	0.184	0.139	0.180	0.134	0.221	0.181	0.149
Fe^{2+}	0.267	0.234	0.235	0.271	0.254	0.261	0.281	0.287	0.310	0.270	0.274	0.261	0.278	0.321	0.241	0.296	0.281	0.493	0.271	0.402	0.280	0.299	0.308
Mn^{2+}	0.006	0.004	0.006	0.007	0.006	0.006	0.008	0.007	0.009	0.005	0.007	0.005	0.009	0.009	0.008	0.009	0.006	0.014	0.008	0.010	0.010	0.007	0.007
Mg^{2+}	0.766	0.796	0.784	0.773	0.768	0.817	0.869	0.788	0.800	0.764	0.777	0.778	0.790	0.788	0.768	0.809	0.776	0.700	0.789	0.746	0.771	0.813	0.801
Ca^{2+}	0.831	0.825	0.814	0.806	0.827	0.806	0.763	0.790	0.784	0.823	0.804	0.824	0.809	0.777	0.843	0.776	0.818	0.705	0.812	0.757	0.811	0.797	0.776
Na^{+}	0.023	0.021	0.021	0.023	0.021	0.020	0.014	0.023	0.023	0.021	0.021	0.020	0.021	0.028	0.034	0.024	0.022	0.026	0.019	0.026	0.022	0.027	0.023
Sum	4.016	4.010	4.003	4.008	4.009	4.005	4.000	4.004	4.011	4.011	4.007	4.002	4.004	4.011	4.021	4.010	4.009	4.017	4.005	4.015	4.013	4.028	4.005
En	41.0	42.8	42.6	41.6	41.4	43.2	45.2	42.1	42.0	41.0	41.7	41.6	41.9	41.6	41.3	42.8	41.3	36.6	42.0	39.0	41.2	42.5	42.3
Fs	14.6	12.8	13.1	15.0	14.1	14.1	15.0	15.7	16.8	14.8	15.1	14.2	15.2	17.4	13.4	16.1	15.3	26.5	14.8	21.5	15.5	16.0	16.7
Wo	44.4	44.4	44.3	43.4	44.6	42.6	39.7	42.2	41.2	44.2	43.2	44.1	42.9	41.0	45.3	41.0	43.5	36.9	43.2	39.5	43.3	41.6	41.0

Formation	Antanetilava																						
Sample	PF06130	PF06130	PF06130	PF06130	PF06132	PF06132	PF06132	PF06132	PF06132	PF06132	PF06132	PF06132	PF06132	PF06132	PF06132	PF06132	PF06132	PF06129	PF06129	PF06129	PF06129	PF06129	PF06129
SiO_2	41.64	51.16	50.39	50.36	50.15	51.80	51.21	51.98	50.47	50.84	51.69	51.41	51.87	51.09	51.88	52.40	51.51	52.64	51.04	52.31	52.31	53.29	52.45
TiO_2	0.29	0.83	0.88	0.95	1.08	0.75	0.91	0.74	1.03	0.98	0.85	0.82	0.66	0.86	0.75	0.55	0.90	0.60	0.85	0.71	0.66	0.46	0.63
Al_2O_3	9.87	2.27	5.09	5.09	3.33	2.30	4.94	3.64	3.31	3.21	3.16	4.53	3.35	4.71	3.10	1.75	2.21	3.26	4.82	3.55	3.59	1.96	3.35
FeO	25.33	15.67	8.86	9.01	13.95	16.23	8.71	10.12	15.14	14.27	12.94	8.46	10.07	8.93	11.63	14.32	16.12	9.97	9.24	10.56	10.25	9.39	9.82
MnO	0.56	0.45	0.22	0.16	0.33	0.44	0.23	0.27	0.36	0.35	0.36	0.22	0.27	0.28	0.25	0.38	0.43	0.25	0.20	0.30	0.30	0.25	0.27
MgO	10.34	13.12	13.81	14.05	12.26	12.05	14.19	14.40	11.95	13.42	13.54	14.27	14.79	14.33	13.93	14.93	12.18	14.87	14.23	15.04	14.79	16.40	14.99
CaO	8.97	17.10	20.80	20.30	19.07	17.73	20.42	19.87	18.15	17.80	19.00	20.90	19.60	21.01	19.77	16.51	18.22	20.10	20.75	19.66	20.20	19.15	20.24
Na_2O	0.19	0.29	0.31	0.27	0.41	0.40	0.29	0.32	0.36	0.40	0.31	0.27	0.30	0.26	0.34	0.28	0.34	0.32	0.26	0.33	0.27	0.21	0.28
Total	97.28	100.91	100.63	100.53	100.60	101.73	101.26	101.41	100.78	101.29	101.87	101.13	101.00	101.77	101.68	101.14	101.95	102.10	101.64	102.59	102.53	101.29	102.10
Si^{4+}	1.688	1.928	1.868	1.868	1.894	1.941	1.881	1.910	1.905	1.900	1.912	1.889	1.913	1.873	1.915	1.950	1.930	1.920	1.873	1.904	1.905	1.950	1.913
Ti^{4+}	0.009	0.028	0.030	0.032	0.036	0.025	0.031	0.025	0.034	0.033	0.029	0.028	0.023	0.029	0.025	0.018	0.030	0.021	0.029	0.024	0.023	0.016	0.022
Al^{3+}	0.472	0.101	0.222	0.223	0.148	0.102	0.214	0.158	0.147	0.141	0.138	0.196	0.146	0.204	0.135	0.077	0.098	0.140	0.209	0.152	0.154	0.085	0.144
Fe^{2+}	0.859	0.494	0.275	0.279	0.441	0.509	0.268	0.311	0.478	0.446	0.400	0.260	0.311	0.274	0.359	0.446	0.505	0.304	0.284	0.321	0.312	0.287	0.300
Mn^{2+}	0.019	0.014	0.007	0.005	0.011	0.014	0.007	0.009	0.011	0.011	0.011	0.007	0.008	0.009	0.008	0.012	0.014	0.008	0.006	0.009	0.009	0.008	0.008
Mg^{2+}	0.625	0.737	0.763	0.777	0.690	0.673	0.777	0.789	0.672	0.747	0.746	0.782	0.813	0.783	0.766	0.828	0.680	0.808	0.778	0.816	0.803	0.894	0.815
Ca^{2+}	0.390	0.690	0.826	0.807	0.772	0.712	0.804	0.782	0.734	0.713	0.753	0.823	0.775	0.825	0.782	0.658	0.731	0.786	0.816	0.767	0.788	0.751	0.791
Na^{+}	0.015	0.022	0.022	0.019	0.030	0.029	0.020	0.023	0.027	0.029	0.022	0.019	0.021	0.019	0.024	0.021	0.025	0.022	0.019	0.023	0.019	0.015	0.020
Sum	4.076	4.013	4.013	4.010	4.022	4.005	4.003	4.007	4.010	4.022	4.012	4.005	4.010	4.016	4.014	4.010	4.013	4.009	4.014	4.017	4.014	4.005	4.012
En	33.0	38.1	40.8	41.6	36.1	35.3	41.9	41.7	35.5	39.0	39.1	41.8	42.6	41.4	40.0	42.6	35.2	42.4	41.3	42.6	42.0	46.1	42.6
Fs	46.4	26.3	15.0	15.2	23.6	27.4	14.8	16.9	25.8	23.8	21.5	14.3	16.7	14.9	19.2	23.5	26.9	16.4	15.4	17.3	16.8	15.2	16.1
Wo	20.6	35.7	44.2	43.2	40.3	37.3	43.3	41.4	38.7	37.2	39.4	44.0	40.6	43.6	40.8	33.9	37.9	41.2	43.3	40.1	41.2	38.7	41.3

Table A2.1: Clinopyroxene compositions for the Maningoza Suite

Formation	Antanetilava																					
Sample	PF06129	PF06129	PF06148	PF06148	PF06148	PF06148	PF06148	PF06148	PF06148	PF06148	PF06148	PF06148	PF06153	PF06153	PF06153	PF06153	PF06153	PF06153	PF06153	PF06153	PF06153	PF06153
SiO_2	51.91	51.62	50.07	50.46	49.99	50.46	50.29	50.66	51.42	50.12	50.17	48.83	49.89	50.10	49.69	49.68	50.11	50.22	50.43	50.53	50.47	51.81
TiO_2	0.57	0.70	1.07	1.12	1.13	1.13	0.71	1.15	0.97	1.17	1.21	1.18	1.13	1.35	1.21	1.28	1.25	1.11	1.14	1.12	1.25	0.90
Al_2O_3	3.28	3.45	2.94	2.85	3.11	2.94	7.92	2.91	1.71	2.65	2.91	3.33	2.88	2.30	2.84	3.34	3.05	2.72	2.66	2.78	2.48	1.52
FeO	9.43	11.17	12.92	12.86	14.43	13.18	12.18	12.90	14.76	15.35	14.24	14.07	14.41	17.36	15.96	14.79	15.24	14.34	14.69	15.05	16.62	15.75
MnO	0.24	0.33	0.26	0.17	0.31	0.31	0.31	0.22	0.29	0.29	0.24	0.36	0.27	0.33	0.34	0.22	0.31	0.17	0.30	0.29	0.38	0.28
MgO	14.84	14.35	14.40	14.24	13.82	14.45	11.69	14.40	15.16	13.95	14.24	13.28	14.05	13.13	14.04	14.35	14.45	14.38	14.19	14.13	13.70	14.51
CaO	20.25	19.31	19.70	19.89	19.79	20.18	17.87	20.02	18.73	19.34	19.71	18.91	19.27	18.94	18.54	18.44	18.73	19.51	19.41	19.28	18.05	18.81
Na_2O	0.28	0.29	0.39	0.40	0.52	0.42	1.25	0.46	0.39	0.43	0.44	0.46	0.39	0.44	0.37	0.38	0.41	0.39	0.41	0.34	0.37	0.34
Total	100.83	101.26	101.87	102.16	103.27	103.21	102.43	102.88	103.43	103.32	103.26	100.48	102.46	103.95	103.10	102.66	103.71	102.96	103.32	103.59	103.34	103.92
Si^{4+}	1.915	1.907	1.867	1.875	1.853	1.861	1.840	1.870	1.893	1.860	1.856	1.855	1.861	1.863	1.852	1.848	1.850	1.863	1.866	1.865	1.874	1.905
Ti^{4+}	0.019	0.024	0.036	0.038	0.038	0.038	0.024	0.039	0.033	0.039	0.041	0.039	0.038	0.046	0.041	0.043	0.042	0.037	0.038	0.038	0.042	0.030
Al^{3+}	0.143	0.150	0.129	0.125	0.136	0.128	0.342	0.127	0.074	0.116	0.127	0.149	0.127	0.101	0.125	0.147	0.133	0.119	0.116	0.121	0.109	0.066
Fe^{2+}	0.291	0.345	0.403	0.400	0.447	0.407	0.373	0.398	0.455	0.476	0.441	0.447	0.450	0.540	0.497	0.460	0.471	0.445	0.455	0.465	0.516	0.484
Mn^{2+}	0.008	0.010	0.008	0.005	0.010	0.010	0.010	0.007	0.009	0.009	0.008	0.012	0.009	0.010	0.011	0.007	0.010	0.005	0.009	0.009	0.012	0.009
Mg^{2+}	0.816	0.790	0.800	0.789	0.763	0.794	0.638	0.792	0.832	0.771	0.785	0.752	0.781	0.727	0.780	0.796	0.795	0.795	0.783	0.777	0.758	0.795
Ca^{2+}	0.800	0.765	0.787	0.792	0.786	0.798	0.701	0.792	0.739	0.769	0.781	0.770	0.770	0.754	0.740	0.735	0.741	0.775	0.770	0.763	0.718	0.741
Na^{+}	0.020	0.021	0.028	0.029	0.038	0.030	0.088	0.033	0.028	0.031	0.031	0.034	0.028	0.032	0.027	0.027	0.029	0.028	0.029	0.024	0.027	0.024
Sum	4.011	4.013	4.059	4.052	4.074	4.066	4.020	4.058	4.063	4.073	4.070	4.060	4.064	4.073	4.072	4.064	4.071	4.067	4.066	4.062	4.057	4.055
En	42.6	41.4	40.0	39.7	38.1	39.6	37.1	39.8	40.9	38.1	39.0	38.0	38.9	35.8	38.4	39.8	39.4	39.3	38.8	38.6	37.8	39.2
Fs	15.6	18.6	20.6	20.4	22.8	20.7	22.2	20.4	22.8	24.0	22.2	23.2	22.8	27.1	25.1	23.4	23.8	22.3	23.0	23.5	26.3	24.3
Wo	41.8	40.0	39.4	39.9	39.2	39.7	40.7	39.8	36.3	38.0	38.8	38.9	38.3	37.1	36.5	36.8	36.7	38.4	38.2	37.9	35.8	36.5

Complex	Ankibobozaka						Dykes															
Sample	PF06004	PF06004	PF06004	PF06004	PF06004	PF06004	PF06138	PF06138	PF06138	PF06138	PF06138	PF06138	PF06071	PF06071	PF06071	PF06071	PF06071	PF06071	PF06071	PF06071	PF06071	PF06071
SiO_2	50.27	50.90	50.01	50.71	50.11	50.17	53.43	53.93	52.31	52.12	51.52	51.66	51.58	52.09	53.72	52.53	52.37	52.29	53.65	52.51	51.96	51.46	51.92
TiO_2	0.78	0.73	0.80	0.65	0.79	0.89	0.39	0.41	0.65	0.83	0.92	0.99	0.99	0.94	0.67	0.65	0.69	1.10	0.60	0.79	1.00	1.18	0.75
Al_2O_3	4.52	4.62	4.73	4.13	4.06	4.33	2.62	2.30	3.86	2.03	3.70	3.41	2.19	2.74	1.44	1.73	1.01	1.82	1.33	1.25	2.57	2.03	1.14
FeO	9.06	7.69	8.20	8.70	7.86	8.01	6.15	7.15	7.49	12.81	9.55	10.70	16.52	11.51	13.88	13.49	19.39	18.68	14.18	17.47	12.71	18.33	19.05
MnO	0.21	0.13	0.17	0.22	0.18	0.15	0.15	0.15	0.16	0.34	0.29	0.26	0.44	0.33	0.35	0.40	0.47	0.56	0.42	0.44	0.39	0.47	0.48
MgO	15.06	15.89	15.40	14.97	15.33	15.12	16.27	16.57	15.34	13.77	14.15	13.74	14.41	14.59	16.37	15.85	13.36	13.65	16.64	14.80	14.88	13.51	11.76
CaO	20.40	20.55	19.96	20.11	20.56	20.49	20.63	20.72	20.78	18.69	20.25	19.85	14.66	18.61	15.89	15.91	14.20	14.63	15.37	14.08	17.84	14.85	16.48
Na_2O	0.29	0.24	0.25	0.24	0.29	0.24	0.27	0.20	0.26	0.37	0.31	0.31	0.32	0.33	0.28	0.24	0.25	0.32	0.24	0.26	0.32	0.29	0.32
Total	100.71	101.03	99.92	99.84	99.35	99.62	100.43	101.54	101.00	100.97	100.71	100.96	101.14	101.22	102.65	100.85	101.76	103.05	102.48	101.65	101.69	102.16	101.91
Si^{4+}	1.861	1.867	1.862	1.887	1.874	1.871	1.955	1.952	1.911	1.942	1.905	1.913	1.932	1.925	1.958	1.950	1.969	1.938	1.960	1.959	1.918	1.926	1.961
Ti^{4+}	0.026	0.025	0.027	0.022	0.026	0.030	0.013	0.014	0.022	0.028	0.031	0.034	0.033	0.032	0.023	0.022	0.023	0.037	0.021	0.026	0.034	0.040	0.025
Al^{3+}	0.197	0.200	0.208	0.181	0.179	0.190	0.113	0.098	0.166	0.089	0.161	0.149	0.097	0.119	0.062	0.076	0.045	0.079	0.057	0.055	0.112	0.090	0.051
Fe^{2+}	0.281	0.236	0.255	0.271	0.246	0.250	0.188	0.216	0.229	0.399	0.295	0.331	0.517	0.356	0.423	0.419	0.610	0.579	0.433	0.545	0.392	0.574	0.602
Mn^{2+}	0.007	0.004	0.005	0.007	0.006	0.005	0.005	0.005	0.005	0.011	0.009	0.008	0.014	0.010	0.011	0.013	0.015	0.018	0.013	0.014	0.012	0.015	0.015
Mg^{2+}	0.831	0.869	0.854	0.830	0.854	0.840	0.887	0.894	0.835	0.765	0.780	0.758	0.804	0.804	0.889	0.877	0.749	0.754	0.906	0.823	0.819	0.753	0.662
Ca^{2+}	0.809	0.808	0.796	0.802	0.824	0.819	0.809	0.804	0.814	0.746	0.802	0.787	0.588	0.737	0.621	0.633	0.572	0.581	0.602	0.563	0.706	0.595	0.667
Na^{+}	0.021	0.017	0.018	0.018	0.021	0.017	0.019	0.014	0.019	0.026	0.022	0.022	0.024	0.024	0.020	0.017	0.019	0.023	0.017	0.018	0.023	0.021	0.024
Sum	4.034	4.026	4.025	4.017	4.030	4.022	3.990	3.998	4.001	4.007	4.006	4.003	4.010	4.007	4.007	4.007	4.002	4.010	4.008	4.005	4.016	4.013	4.007
En	43.1	45.3	44.7	43.5	44.3	43.9	47.0	46.6	44.4	39.8	41.3	40.2	41.8	42.1	45.7	45.2	38.5	39.0	46.4	42.3	42.4	38.9	34.0
Fs	14.9	12.5	13.6	14.5	13.0	13.3	10.2	11.5	12.4	21.3	16.1	18.0	27.6	19.2	22.3	22.2	32.1	30.9	22.8	28.7	21.0	30.4	31.7
Wo	42.0	42.1	41.7	42.0	42.7	42.8	42.8	41.9	43.2	38.8	42.5	41.8	30.6	38.7	31.9	32.6	29.4	30.1	30.8	28.9	36.6	30.7	34.3

Table A2.2: Clinopyroxene compositions for the Maningoza Suite

Complex	Berevo										Fonjay								Ambereny				
Sample	PF06020	PF06020	PF06020	PF06020	PF06027	PF06027	PF06027	PF06027	PF06027	PF06027	MI06010	MI06010	MI06010	MI06010	MI06010	MI06010	MI06010	MI06010	MI06014	MI06014	MI06014	MI06014	MI06014
SiO_2	52.53	51.98	51.51	51.32	50.90	51.33	51.09	51.50	50.17	50.70	50.93	51.35	50.85	50.91	50.94	50.63	50.94	50.68	52.46	51.93	52.65	51.84	51.57
TiO_2	0.48	0.47	0.71	0.69	0.76	0.67	0.57	0.57	0.90	0.60	1.03	1.07	0.91	0.86	0.98	1.10	1.02	0.97	0.69	0.81	0.69	0.80	0.98
Al_2O_3	2.80	3.10	3.59	3.32	2.93	2.71	3.45	2.13	2.69	3.87	5.08	4.17	4.87	5.32	5.10	5.29	5.03	4.01	3.24	3.38	2.60	3.30	3.29
FeO	6.19	5.83	6.68	7.34	11.24	11.24	7.92	11.46	13.87	10.00	8.39	8.88	9.54	8.40	8.58	8.10	8.73	9.86	9.34	9.35	8.22	9.10	8.83
MnO	0.15	0.15	0.11	0.16	0.29	0.26	0.24	0.26	0.37	0.25	0.25	0.25	0.32	0.20	0.22	0.20	0.25	0.36	0.25	0.23	0.23	0.32	0.29
MgO	16.36	16.35	15.66	15.63	14.65	14.42	15.86	15.36	13.45	15.41	14.49	14.19	14.09	14.21	14.52	14.45	14.23	14.11	15.01	14.59	14.93	14.62	14.57
CaO	21.48	21.54	21.46	21.06	19.68	19.85	20.78	19.07	18.56	18.53	20.95	20.58	20.41	20.86	20.91	20.84	20.53	19.40	20.31	20.49	21.15	20.41	20.55
Na_2O	0.27	0.25	0.31	0.28	0.34	0.31	0.25	0.30	0.34	0.36	0.29	0.35	0.40	0.34	0.35	0.31	0.36	0.40	0.30	0.41	0.30	0.36	0.38
Total	100.91	100.54	100.79	100.70	100.81	100.80	100.57	100.67	100.37	99.90	101.54	101.17	101.74	101.41	101.75	101.14	101.24	99.84	101.84	101.55	100.93	100.94	100.72
Si^{4+}	1.925	1.915	1.899	1.901	1.897	1.911	1.891	1.919	1.898	1.890	1.864	1.892	1.870	1.867	1.862	1.859	1.871	1.892	1.918	1.910	1.936	1.913	1.908
Ti^{4+}	0.016	0.016	0.024	0.023	0.026	0.022	0.019	0.019	0.030	0.020	0.035	0.036	0.031	0.029	0.034	0.037	0.035	0.032	0.024	0.027	0.023	0.027	0.033
Al^{3+}	0.121	0.135	0.156	0.145	0.129	0.119	0.151	0.094	0.120	0.170	0.219	0.181	0.211	0.230	0.220	0.229	0.218	0.177	0.140	0.147	0.113	0.144	0.144
Fe^{2+}	0.190	0.180	0.206	0.227	0.350	0.350	0.245	0.357	0.439	0.312	0.257	0.274	0.293	0.258	0.262	0.249	0.268	0.308	0.286	0.288	0.253	0.281	0.273
Mn^{2+}	0.005	0.005	0.003	0.005	0.009	0.008	0.007	0.008	0.012	0.008	0.008	0.008	0.010	0.006	0.007	0.006	0.008	0.012	0.008	0.007	0.007	0.010	0.009
Mg^{2+}	0.894	0.898	0.860	0.863	0.814	0.800	0.875	0.853	0.758	0.856	0.790	0.779	0.772	0.777	0.791	0.791	0.779	0.785	0.818	0.800	0.818	0.804	0.803
Ca^{2+}	0.844	0.850	0.848	0.836	0.786	0.792	0.824	0.761	0.752	0.740	0.822	0.812	0.804	0.820	0.819	0.820	0.808	0.776	0.796	0.807	0.833	0.807	0.815
Na^{+}	0.019	0.018	0.022	0.020	0.025	0.023	0.018	0.021	0.025	0.026	0.021	0.025	0.029	0.024	0.025	0.022	0.025	0.029	0.021	0.029	0.021	0.025	0.027
Sum	4.014	4.016	4.019	4.021	4.034	4.026	4.031	4.032	4.033	4.026	4.015	4.007	4.020	4.012	4.020	4.014	4.012	4.012	4.009	4.015	4.004	4.011	4.012
En	46.3	46.5	44.9	44.7	41.5	41.0	44.8	43.1	38.7	44.7	42.1	41.6	41.1	41.7	42.1	42.4	41.8	41.7	42.9	42.0	42.8	42.3	42.3
Fs	10.1	9.5	10.9	12.0	18.3	18.4	12.9	18.5	23.0	16.7	14.1	15.0	16.1	14.2	14.3	13.7	14.8	17.0	15.4	15.5	13.6	15.3	14.9
Wo	43.7	44.0	44.2	43.3	40.1	40.6	42.2	38.5	38.4	38.6	43.8	43.4	42.8	44.1	43.6	44.0	43.4	41.3	41.7	42.5	43.6	42.4	42.9

Complex	Ambereny				Ambohitrosy																		
Sample	MI06014	MI06014	MI06014	MI06019	AB15	AB15	AB15	AB15	AB15	AB15	AB15	AB07	AB07	AB07	AB07	AB07	AB07	AB07	AB07	AB07	AB07	AB07	AB07
SiO_2	51.91	51.85	52.49	53.86	51.55	50.73	50.47	50.02	51.16	51.55	51.16	50.50	50.63	50.49	50.18	50.22	50.67	51.27	50.79	50.95	50.26	51.04	51.39
TiO_2	0.93	0.98	0.74	0.42	0.76	0.70	0.94	0.89	0.73	0.12	0.82	1.08	0.96	1.06	0.90	1.00	0.97	0.86	1.06	0.98	1.03	1.06	0.96
Al_2O_3	2.96	3.32	3.12	1.74	2.47	2.82	3.23	2.97	2.71	2.29	2.30	2.98	2.93	3.17	2.92	2.88	3.17	2.71	3.01	2.77	3.29	2.90	2.82
FeO	8.80	9.50	8.99	8.36	9.48	11.47	11.28	10.72	9.46	13.92	9.17	8.41	8.17	8.54	8.68	8.35	8.36	8.57	9.51	8.45	8.65	8.51	8.21
MnO	0.18	0.22	0.28	0.25	0.27		0.29	0.34	0.28	0.17	0.30	0.26	0.22	0.19	0.19	0.32	0.11	0.35	0.20	0.20	0.24	0.27	0.29
MgO	14.90	15.22	14.85	15.66	14.97	14.82	14.83	13.89	13.66	11.53	13.12	14.33	14.46	13.78	13.94	14.36	14.34	14.66	14.22	14.47	13.92	14.24	14.43
CaO	20.67	19.76	20.72	21.12	20.40	18.56	18.17	20.68	21.46	21.01	21.88	21.34	21.65	21.53	20.72	21.27	21.52	21.50	21.31	21.45	20.98	21.78	21.68
Na_2O	0.38	0.29	0.35	0.33	0.26		0.53	0.32	0.35	0.91	0.29	0.30	0.41	0.43	0.34	0.40	0.38	0.36	0.31	0.37	0.36	0.36	0.39
Total	100.92	101.36	101.77	101.76	100.32	99.14	100.24	100.20	100.05	102.82	99.12	99.40	99.74	99.45	97.98	99.13	99.79	100.56	100.64	99.91	98.88	100.45	100.36
Si^{4+}	1.914	1.905	1.920	1.959	1.919	1.914	1.894	1.887	1.918	1.929	1.933	1.898	1.898	1.899	1.910	1.896	1.897	1.907	1.893	1.906	1.898	1.901	1.910
Ti^{4+}	0.032	0.033	0.025	0.014	0.026	0.023	0.031	0.029	0.024	0.004	0.027	0.036	0.032	0.035	0.030	0.033	0.032	0.029	0.036	0.033	0.034	0.036	0.032
Al^{3+}	0.129	0.144	0.135	0.075	0.108	0.125	0.143	0.132	0.120	0.101	0.102	0.132	0.129	0.141	0.131	0.128	0.140	0.119	0.132	0.122	0.146	0.127	0.124
Fe^{2+}	0.271	0.292	0.275	0.254	0.295	0.362	0.354	0.338	0.296	0.436	0.290	0.264	0.256	0.269	0.276	0.264	0.262	0.266	0.296	0.264	0.273	0.265	0.255
Mn^{2+}	0.006	0.007	0.009	0.008	0.009	0.000	0.009	0.011	0.009	0.005	0.010	0.008	0.007	0.006	0.006	0.010	0.003	0.011	0.006	0.006	0.008	0.009	0.009
Mg^{2+}	0.819	0.833	0.809	0.849	0.830	0.833	0.830	0.781	0.763	0.643	0.739	0.803	0.808	0.773	0.791	0.808	0.800	0.813	0.790	0.807	0.783	0.790	0.799
Ca^{2+}	0.817	0.778	0.812	0.823	0.814	0.750	0.731	0.836	0.862	0.843	0.886	0.859	0.870	0.868	0.845	0.861	0.863	0.857	0.851	0.860	0.849	0.869	0.863
Na^{+}	0.027	0.020	0.025	0.023	0.019	0.000	0.039	0.023	0.025	0.066	0.021	0.022	0.030	0.031	0.025	0.029	0.028	0.026	0.022	0.027	0.026	0.026	0.028
Sum	4.015	4.013	4.010	4.006	4.019	4.007	4.033	4.038	4.019	4.074	4.007	4.022	4.031	4.021	4.015	4.031	4.025	4.027	4.028	4.025	4.018	4.025	4.022
En	42.8	43.6	42.5	43.9	42.6	42.8	43.1	39.7	39.5	33.4	38.4	41.5	41.6	40.3	41.2	41.6	41.5	41.7	40.6	41.6	40.9	40.9	41.5
Fs	14.5	15.6	14.9	13.5	15.6	18.6	18.9	17.8	15.8	22.9	15.6	14.1	13.6	14.3	14.7	14.1	13.8	14.3	15.6	14.0	14.7	14.2	13.7
Wo	42.7	40.7	42.6	42.6	41.8	38.6	38.0	42.5	44.7	43.7	46.0	44.4	44.8	45.3	44.1	44.3	44.8	44.0	43.8	44.4	44.4	45.0	44.8

Table A2.3: Clinopyroxene compositions for the Maningoza Suite

Complex	Ambohitrosy																						
Sample	AB07	AB07	AB07	AB07	AB07	AB07	AB07	AB07	AB26A	AB26A	AB26A	AB26A	AB26A	AB26A	AB26A	AB26A	AB26A	AB26A	AB26A	AB26A	AB26A	AB26A	AB26A
SiO_2	50.81	50.17	50.01	50.42	51.09	51.23	49.60	51.20	50.38	50.12	50.47	49.96	50.46	49.41	50.97	42.53	50.64	50.78	50.31	51.40	51.58	51.34	50.71
TiO_2	1.10	1.01	1.02	1.03	0.89	0.99	0.93	1.05	1.00	0.78	0.95	0.84	0.99	1.08	0.88	0.99	0.95	0.86	0.89	0.90	0.87	0.91	0.91
Al_2O_3	3.02	2.86	3.17	3.00	2.78	2.83	3.05	2.98	3.24	3.15	3.12	3.17	3.42	3.09	3.23	3.56	3.00	3.08	3.11	2.64	2.51	2.08	2.76
FeO	8.33	8.26	8.56	8.22	8.18	7.60	8.26	8.90	8.70	8.19	8.24	8.86	8.70	9.13	8.97	19.45	9.37	8.68	8.54	10.43	9.77	9.56	9.54
MnO	0.22	0.27	0.30	0.28	0.28	0.27	0.35	0.12	0.27	0.20	0.08	0.11	0.26	0.27	0.14	0.32	0.20	0.27	0.20	0.17	0.34	0.23	0.26
MgO	14.07	14.62	14.21	14.12	14.39	14.13	14.19	14.61	14.43	14.40	14.70	14.21	14.03	14.31	14.50	13.67	14.54	14.73	14.46	14.69	14.22	14.81	14.32
CaO	21.57	21.23	21.31	21.28	21.60	21.77	21.30	21.45	20.61	20.33	20.20	20.27	20.01	20.49	20.59	16.11	20.34	20.99	20.27	20.04	20.36	19.60	20.35
Na_2O	0.38	0.40	0.39	0.36	0.37	0.42	0.41	0.45	0.40	0.33	0.29	0.30	0.45	0.34	0.36	0.72	0.34	0.44	0.36	0.34	0.41	0.34	0.32
Total	99.64	99.21	99.31	98.95	99.87	99.35	98.54	101.07	99.46	97.90	98.37	98.13	98.68	98.54	100.04	99.53	99.66	100.26	98.48	100.89	100.21	99.01	99.44
Si^{4+}	1.903	1.894	1.888	1.903	1.910	1.917	1.888	1.896	1.895	1.908	1.908	1.903	1.907	1.884	1.904	1.726	1.901	1.896	1.906	1.911	1.925	1.933	1.910
Ti^{4+}	0.037	0.033	0.034	0.034	0.030	0.033	0.031	0.035	0.033	0.026	0.031	0.028	0.033	0.035	0.029	0.030	0.032	0.029	0.029	0.030	0.029	0.030	0.030
Al^{3+}	0.133	0.127	0.141	0.133	0.123	0.125	0.137	0.130	0.144	0.141	0.139	0.142	0.152	0.139	0.142	0.170	0.133	0.136	0.139	0.116	0.110	0.092	0.123
Fe^{2+}	0.261	0.261	0.270	0.259	0.256	0.238	0.263	0.276	0.274	0.261	0.260	0.282	0.275	0.291	0.280	0.660	0.294	0.271	0.271	0.324	0.305	0.301	0.301
Mn^{2+}	0.007	0.009	0.010	0.009	0.009	0.009	0.011	0.004	0.009	0.006	0.003	0.004	0.008	0.009	0.004	0.011	0.006	0.009	0.006	0.005	0.011	0.007	0.008
Mg^{2+}	0.785	0.822	0.799	0.794	0.802	0.788	0.805	0.806	0.809	0.817	0.828	0.807	0.790	0.813	0.807	0.827	0.814	0.820	0.816	0.814	0.791	0.831	0.804
Ca^{2+}	0.866	0.859	0.862	0.860	0.865	0.873	0.869	0.851	0.831	0.829	0.818	0.828	0.810	0.837	0.824	0.701	0.818	0.840	0.823	0.798	0.814	0.791	0.821
Na^{+}	0.028	0.029	0.029	0.026	0.027	0.030	0.030	0.032	0.029	0.024	0.021	0.022	0.033	0.025	0.026	0.057	0.025	0.032	0.026	0.025	0.030	0.025	0.023
Sum	4.019	4.034	4.032	4.019	4.022	4.013	4.036	4.033	4.025	4.015	4.010	4.016	4.009	4.033	4.018	4.191	4.023	4.033	4.017	4.024	4.016	4.013	4.019
En	40.9	42.2	41.2	41.3	41.5	41.3	41.3	41.6	42.1	42.7	43.4	42.0	41.9	41.7	42.1	37.6	42.1	42.3	42.6	41.9	41.2	43.1	41.6
Fs	14.0	13.8	14.4	14.0	13.7	12.9	14.1	14.4	14.7	14.0	13.8	14.9	15.0	15.4	14.9	30.5	15.6	14.4	14.5	17.0	16.4	16.0	16.0
Wo	45.1	44.0	44.4	44.7	44.8	45.8	44.6	43.9	43.2	43.3	42.9	43.1	43.0	42.9	43.0	31.9	42.3	43.3	42.9	41.1	42.4	41.0	42.5

Complex	Ambohitrosy																		
Sample	AB26B	AB26B	AB26B	AB26B	AB26B	AB26B	AB26B	AB26B	95-05	95-05	95-05	95-05	AB10	AB10	AB10	AB10	AB10	AB10	AB10
SiO_2	52.03	51.49	52.08	51.62	51.94	51.92	49.85	50.61	51.79	52.31	50.34	51.25	51.42	53.24	51.17	50.89	51.27	51.36	51.44
TiO_2	0.49	0.47	0.46	0.46	0.50	0.43	0.93	0.90	0.54	0.56	0.67	0.77	0.13	0.72	0.73	0.03	0.27	0.32	0.56
Al_2O_3	1.43	1.47	1.53	1.31	1.71	1.38	3.02	2.84	1.96	1.82	2.64	1.74	0.22	1.71	1.72	0.15	0.34	0.76	1.42
FeO	8.99	9.54	9.34	9.50	8.83	9.32	9.66	9.99	10.47	11.41	9.46	12.27	16.77	13.70	13.24	17.79	19.21	16.58	13.81
MnO	0.26	0.23	0.30	0.39	0.29	0.32	0.19	0.27	0.30	0.37	0.30	0.33	0.70	0.65	0.51	0.56	0.68	0.52	0.63
MgO	14.67	14.52	14.80	14.72	14.62	14.61	14.31	13.56	15.81	17.24	15.28	15.60	9.04	12.49	12.09	8.38	9.55	11.00	12.94
CaO	21.36	20.72	20.63	20.93	21.15	20.52	20.46	20.86	17.96	16.17	19.91	17.01	20.86	19.18	19.91	21.10	18.56	19.19	19.27
Na_2O	0.38	0.35	0.34	0.34	0.33	0.35	0.30	0.36	0.27	0.24	0.32	0.27	0.33	0.46	0.41	0.26	0.34	0.50	0.44
Total	99.87	99.13	99.72	99.62	99.62	99.04	99.07	99.64	99.28	100.40	99.41	99.50	99.53	102.25	99.96	99.25	100.35	100.50	100.88
Si^{4+}	1.949	1.947	1.951	1.945	1.947	1.958	1.890	1.909	1.943	1.940	1.900	1.933	2.001	1.969	1.946	1.998	1.989	1.972	1.945
Ti^{4+}	0.016	0.016	0.015	0.015	0.017	0.014	0.031	0.030	0.018	0.019	0.022	0.026	0.004	0.024	0.024	0.001	0.009	0.010	0.019
Al^{3+}	0.063	0.066	0.068	0.058	0.076	0.061	0.135	0.126	0.087	0.080	0.117	0.077	0.010	0.075	0.077	0.007	0.016	0.034	0.063
Fe^{2+}	0.282	0.302	0.293	0.299	0.277	0.294	0.306	0.315	0.329	0.354	0.299	0.387	0.546	0.424	0.421	0.584	0.623	0.532	0.437
Mn^{2+}	0.008	0.007	0.010	0.012	0.009	0.010	0.006	0.009	0.010	0.012	0.010	0.011	0.023	0.020	0.016	0.019	0.022	0.017	0.020
Mg^{2+}	0.819	0.818	0.826	0.827	0.817	0.821	0.809	0.762	0.884	0.953	0.860	0.877	0.524	0.688	0.685	0.490	0.552	0.629	0.729
Ca^{2+}	0.857	0.840	0.828	0.845	0.849	0.829	0.831	0.843	0.722	0.642	0.805	0.688	0.870	0.760	0.811	0.888	0.772	0.789	0.781
Na^{+}	0.028	0.026	0.025	0.025	0.024	0.026	0.022	0.026	0.020	0.017	0.023	0.020	0.025	0.033	0.030	0.020	0.026	0.037	0.032
Sum	4.023	4.023	4.017	4.028	4.017	4.015	4.031	4.021	4.011	4.017	4.037	4.021	4.003	3.995	4.013	4.008	4.009	4.022	4.027
En	41.7	41.6	42.2	41.7	41.8	42.0	41.4	39.5	45.5	48.6	43.6	44.7	26.7	36.4	35.4	24.8	28.0	32.0	37.1
Fs	14.7	15.7	15.4	15.7	14.7	15.6	16.0	16.8	17.4	18.6	15.6	20.3	29.0	23.5	22.6	30.4	32.8	27.9	23.2
Wo	43.6	42.7	42.3	42.6	43.5	42.4	42.6	43.7	37.1	32.8	40.8	35.0	44.3	40.2	42.0	44.8	39.2	40.1	39.7

Table A2.4: Clinopyroxene compositions for the Maningoza Suite

Complex	Berevo																					
Sample	PF06017	PF06017	PF06017	PF06017	PF06017	PF06017	PF06017	PF06017	PF06017	PF06017	PF06017	PF06017	PF06020	PF06020	PF06020	PF06020	PF06020	PF06020	PF06020	PF06020	PF06020	PF06020
SiO_2	37.72	37.71	37.59	37.31	37.73	37.55	37.51	37.40	37.31	37.75	37.76	37.29	37.45	37.60	37.45	37.17	37.21	37.42	53.44	37.69	37.61	37.51
FeO	26.69	26.42	27.06	26.98	26.12	26.85	25.04	26.61	26.76	26.69	26.39	26.85	25.75	26.17	25.79	25.70	25.84	25.97	16.11	26.72	26.23	26.53
MnO	0.50	0.44	0.46	0.49	0.46	0.46	0.51	0.46	0.46	0.46	0.55	0.47	0.56	0.48	0.47	0.44	0.47	0.52	0.43	0.51	0.53	0.51
MgO	35.57	35.68	35.50	35.19	35.91	35.69	37.01	35.83	35.79	35.79	36.16	35.72	36.12	35.73	35.75	35.53	35.85	35.83	25.89	35.90	35.91	35.88
CaO	0.08	0.09	0.11	0.09	0.08	0.08	0.03	0.07	0.07	0.10	0.04	0.09	0.05	0.07	0.09	0.09	0.08	0.08	1.94	0.10	0.06	0.08
Total	100.59	100.38	100.81	100.17	100.38	100.66	100.21	100.44	100.39	100.86	100.92	100.49	100.00	100.07	99.59	99.05	99.51	99.88	99.54	100.98	100.40	100.60
Si^{4+}	0.997	0.998	0.993	0.993	0.997	0.993	0.989	0.991	0.990	0.995	0.994	0.989	0.993	0.997	0.997	0.995	0.992	0.994	1.301	0.993	0.994	0.992
Fe^{2+}	0.590	0.585	0.598	0.600	0.577	0.594	0.552	0.589	0.594	0.589	0.581	0.595	0.571	0.580	0.574	0.575	0.576	0.577	0.328	0.589	0.580	0.587
Mn^{2+}	0.011	0.010	0.010	0.011	0.010	0.010	0.011	0.010	0.010	0.010	0.012	0.011	0.013	0.011	0.011	0.010	0.011	0.012	0.009	0.011	0.012	0.011
Mg^{2+}	1.401	1.407	1.398	1.396	1.414	1.407	1.454	1.414	1.415	1.406	1.418	1.411	1.427	1.412	1.418	1.418	1.425	1.419	0.939	1.409	1.415	1.414
Ca^{2+}	0.002	0.003	0.003	0.003	0.002	0.002	0.001	0.002	0.002	0.003	0.001	0.003	0.002	0.002	0.002	0.003	0.002	0.002	0.051	0.003	0.002	0.002
Sum	3.003	3.002	3.006	3.006	3.002	3.007	3.010	3.009	3.010	3.004	3.006	3.011	3.007	3.003	3.003	3.004	3.007	3.005	2.680	3.006	3.005	3.008
Fo	70.0	70.3	69.7	69.5	70.7	70.0	72.1	70.2	70.1	70.1	70.5	70.0	71.0	70.5	70.8	70.8	70.8	70.7	73.6	70.1	70.5	70.3

Complex	Ambereny																Dyke				
Sample	MI06014	MI06014	MI06014	MI06014	MI06014	MI06014	MI06014	MI06014	MI06019	MI06019	MI06019	MI06019	MI06019	MI06019	MI06019	MI06019	PF06138	PF06138	PF06138	PF06138	PF06138
SiO_2	39.80	38.26	39.71	39.35	39.75	39.57	39.68	40.67	40.01	40.09	39.95	39.95	40.47	40.12	40.05	39.85	37.61	38.93	37.50	38.37	38.85
FeO	28.90	28.80	28.77	28.99	28.87	28.70	29.00	28.07	26.60	26.52	26.42	26.42	25.97	26.09	26.37	26.47	43.74	36.68	44.92	39.48	34.28
MnO	0.45	0.45	0.45	0.44	0.46	0.40	0.46	0.44	0.48	0.48	0.44	0.45	0.42	0.44	0.44	0.44	0.82	0.61	0.88	0.71	0.59
MgO	33.40	33.57	33.63	33.24	33.03	33.20	32.83	31.78	34.77	34.53	34.86	35.06	35.01	34.93	35.31	35.29	21.83	26.83	21.18	25.52	28.81
CaO	0.05	0.04	0.05	0.05	0.04	0.05	0.04	0.30	0.06	0.05	0.06	0.07	0.05	0.04	0.05	0.06	0.36	0.39	0.36	0.39	0.36
Total	102.78	101.29	102.75	102.29	102.29	102.11	102.17	101.58	102.03	101.79	101.97	102.12	102.12	101.78	102.34	102.26	104.57	103.60	104.96	104.61	103.06
Si^{4+}	1.033	1.012	1.031	1.028	1.037	1.034	1.037	1.062	1.035	1.039	1.034	1.032	1.042	1.038	1.032	1.029	1.033	1.041	1.032	1.030	1.034
Fe^{2+}	0.627	0.637	0.625	0.634	0.630	0.627	0.634	0.613	0.576	0.575	0.572	0.571	0.559	0.564	0.568	0.572	1.004	0.820	1.033	0.887	0.763
Mn^{2+}	0.010	0.010	0.010	0.010	0.010	0.009	0.010	0.010	0.010	0.010	0.010	0.010	0.009	0.010	0.010	0.010	0.019	0.014	0.020	0.016	0.013
Mg^{2+}	1.292	1.324	1.301	1.295	1.284	1.292	1.279	1.236	1.341	1.334	1.344	1.350	1.343	1.347	1.356	1.358	0.893	1.069	0.868	1.021	1.143
Ca^{2+}	0.001	0.001	0.001	0.001	0.001	0.001	0.001	0.008	0.002	0.001	0.002	0.002	0.001	0.001	0.001	0.002	0.011	0.011	0.010	0.011	0.010
Sum	2.966	2.987	2.969	2.970	2.963	2.966	2.962	2.935	2.965	2.961	2.965	2.967	2.957	2.961	2.968	2.971	2.965	2.958	2.967	2.968	2.965
Fo	67.0	67.2	67.2	66.8	66.7	67.0	66.5	66.5	69.6	69.5	69.8	69.9	70.3	70.1	70.1	70.0	46.6	56.2	45.2	53.1	59.5

Complex	Ambohitrosy																			
Sample	AB-15	AB-15	AB-26A	AB-26A	AB-26A	AB-26A	AB-26A	AB-26A	AB-26A	AB-26A	AB-07	AB-07	AB-07	AB-07	AB-07	AB-07	AB-07	AB-07	AB-07	AB-07
SiO_2	38.36	38.60	37.32	37.36	36.95	36.50	35.80	37.05	37.05	37.35	37.94	37.71	37.27	37.66	37.73	37.53	37.44	37.47	37.54	37.99
FeO	24.55	25.10	30.38	30.75	30.07	30.82	30.79	31.24	31.15	30.19	29.11	28.73	28.65	28.85	28.43	28.22	28.88	28.23	28.13	27.93
MnO	0.34	0.30	0.49	0.64	0.54	0.63	0.54	0.70	0.50	0.57	0.55	0.53	0.53	0.56	0.53	0.55	0.48	0.50	0.50	0.52
MgO	37.86	37.67	31.90	31.60	31.98	31.28	31.08	31.54	31.10	31.72	34.14	34.45	34.43	34.25	33.67	33.59	33.43	34.10	34.52	34.18
CaO	0.05	0.02	0.11	0.12	0.14	0.18	0.08	0.08	0.18	0.11	0.07	0.10	0.14	0.12	0.06	0.10	0.05	0.06	0.10	0.07
Total	101.39	101.81	100.32	100.71	99.74	99.52	98.46	100.74	100.37	100.15	101.92	101.66	101.17	101.47	100.64	100.37	100.50	100.60	100.95	100.85
Si^{4+}	0.996	0.999	1.007	1.007	1.003	0.998	0.992	1.001	1.005	1.010	1.000	0.996	0.990	0.997	1.006	1.003	1.002	1.000	0.996	1.007
Fe^{2+}	0.533	0.543	0.686	0.693	0.682	0.705	0.714	0.706	0.707	0.682	0.642	0.635	0.637	0.639	0.634	0.631	0.647	0.630	0.624	0.619
Mn^{2+}	0.007	0.007	0.011	0.015	0.012	0.015	0.013	0.016	0.011	0.013	0.012	0.012	0.012	0.013	0.012	0.012	0.011	0.011	0.011	0.012
Mg^{2+}	1.465	1.452	1.283	1.269	1.293	1.275	1.284	1.270	1.258	1.278	1.341	1.356	1.363	1.351	1.338	1.339	1.334	1.356	1.365	1.351
Ca^{2+}	0.001	0.001	0.003	0.003	0.004	0.005	0.002	0.002	0.005	0.003	0.002	0.003	0.004	0.003	0.002	0.003	0.001	0.002	0.003	0.002
Sum	3.004	3.001	2.992	2.997	2.997	3.001	3.007	2.999	2.995	2.989	3.000	3.003	3.010	3.003	2.994	2.996	2.998	3.001	3.003	2.994
Fo	73.0	72.5	64.8	64.2	65.1	63.9	63.9	63.8	63.6	64.8	67.2	67.7	67.8	67.5	67.4	67.5	67.0	67.9	68.2	68.2

Table A3.1: Olivine compositions for the Maningoza Suite

Formation	Antanetilava						Ankibobozaka		Berevo									Fonjay	
Sample	PF06130	PF06129	PF06132	PF06148	PF06148	PF06153	PF06004	PF06004	PF06017	PF06017	PF06020	PF06020	PF06027	PF06018	PF06018	PF06018	PF06018	MI06010	
TiO_2	14.44	0.04	18.07	10.86	11.58	20.49	1.77	11.83	1.25	1.81	3.35	2.47	0.03	2.68	18.25	13.05	20.42	10.24	45.11
Al_2O_3	1.82	0.04	5.05	1.70	1.49	1.16	1.74	0.47	2.51	3.40	2.97	3.55		0.27	0.32	0.89	1.06	5.73	0.56
FeO (T)	72.62	94.19	72.10	79.11	76.53	67.80	89.65	76.35	89.04	87.33	86.51	87.37	80.79	91.36	73.85	76.70	69.42	81.21	52.80
MnO	1.04	0.64	0.23	0.46	0.77	2.95	0.05	1.21	0.13	0.11	0.21	0.16		0.49	2.45	1.85	3.72	0.46	1.12
MgO	0.04	0.07	0.03		0.02	0.03	0.04	0.07	0.62	1.06	0.69	0.86		0.07	0.01	0.02	0.05	1.25	1.56
Cr_2O_3																			0.17
Total	89.96	94.98	95.48	92.13	90.39	92.43	93.25	89.93	93.55	93.71	93.73	94.41	80.82	94.87	94.88	92.51	94.67	98.89	101.32
Ti^{4+}	0.436	0.001	0.509	0.319	0.348	0.608	0.051	0.359	0.036	0.051	0.095	0.069	0.001	0.076	0.528	0.384	0.592	0.273	0.826
Al^{3+}	0.086	0.002	0.223	0.078	0.070	0.054	0.078	0.022	0.112	0.150	0.132	0.156	0.000	0.012	0.015	0.041	0.048	0.239	0.016
Fe^{3+}	1.041	1.996	0.759	1.283	1.234	0.730	1.820	1.260	1.817	1.748	1.678	1.706	1.998	1.835	0.929	1.190	0.769	1.214	0.329
Fe^{2+}	1.399	0.977	1.500	1.304	1.321	1.508	1.047	1.313	0.996	0.988	1.050	1.016	1.001	1.057	1.448	1.322	1.467	1.193	0.746
Mn^{2+}	0.035	0.020	0.007	0.015	0.026	0.099	0.002	0.041	0.004	0.003	0.007	0.005	0.000	0.016	0.080	0.061	0.121	0.014	0.023
Mg^{2+}	0.002	0.004	0.002	0.000	0.001	0.002	0.002	0.004	0.035	0.059	0.039	0.048	0.000	0.004	0.001	0.001	0.003	0.066	0.057
Cr^{3+}																			0.003
Sum	3.000	3.000	3.000	3.000	3.000	3.000	3.000	3.000	3.000	3.000	3.000	3.000	3.000	3.000	3.000	3.000	3.000	3.000	2.000
Fe_2O_3	22.1	50.5	15.9	28.3	27.0	14.7	45.3	27.4	46.8	45.7	42.3	44.0	49.9	44.8	19.0	25.9	15.7	29.3	9.5
FeO	59.4	49.4	62.8	57.6	57.8	60.8	52.1	57.0	51.3	51.7	52.9	52.4	50.0	51.5	59.3	57.4	60.1	57.5	43.0
TiO_2	18.5	0.1	21.3	14.1	15.2	24.5	2.5	15.6	1.8	2.7	4.8	3.6	0.1	3.7	21.6	16.7	24.2	13.2	47.6

Formation	Dyke								Ambereny									
Sample	PF06071	PF06071	PF06071	PF06071	PF06071	PF06138	PF06138	PF06138	MI06014	MI06014	MI06015	MI06015	MI06015	MI06016	MI06016	MI06016	MI06019	MI06019
TiO_2	22.17	25.04	24.84	24.61	25.41	22.04	24.33	22.85	9.50	6.39	4.17	6.14	3.92	9.83	28.17	14.80	28.92	26.55
Al_2O_3	0.97	1.86	1.96	2.17	1.99	2.41	2.43	2.70	6.59	5.15	2.12	0.71	0.99	0.50	0.40	0.42	8.01	5.28
FeO (T)	72.60	64.60	66.71	65.47	65.00	71.94	67.24	71.04	78.27	83.63	82.53	87.59	88.62	83.86	63.75	78.45	60.70	64.90
MnO	0.81	0.85	0.85	0.83	0.89	1.23	1.07	1.22	0.46	0.29	0.64	0.56	0.56	1.41	3.78	1.39	2.22	1.93
MgO	0.10	0.43	0.28	0.37	0.27	0.07	0.16	0.25	1.17	0.59	1.82	0.02	0.00	0.02	0.02	0.05	0.61	0.60
Cr_2O_3																		
Total	96.65	92.78	94.64	93.45	93.56	97.69	95.23	98.06	95.99	96.04	91.28	95.02	94.10	95.61	96.12	95.11	100.45	99.25
Ti^{4+}	0.630	0.740	0.719	0.721	0.745	0.616	0.699	0.635	0.260	0.176	0.121	0.175	0.112	0.280	0.813	0.426	0.770	0.722
Al^{3+}	0.043	0.086	0.089	0.100	0.091	0.106	0.109	0.118	0.282	0.222	0.096	0.032	0.045	0.022	0.018	0.019	0.334	0.225
Fe^{3+}	0.696	0.435	0.472	0.459	0.419	0.662	0.492	0.612	1.198	1.426	1.662	1.619	1.731	1.419	0.356	1.130	0.125	0.331
Fe^{2+}	1.599	1.686	1.676	1.672	1.700	1.574	1.655	1.583	1.182	1.135	0.995	1.155	1.094	1.234	1.689	1.378	1.672	1.631
Mn^{2+}	0.026	0.028	0.028	0.027	0.029	0.039	0.035	0.038	0.014	0.009	0.021	0.018	0.018	0.045	0.123	0.045	0.067	0.059
Mg^{2+}	0.006	0.025	0.016	0.021	0.016	0.004	0.009	0.014	0.063	0.032	0.104	0.001	0.000	0.001	0.001	0.003	0.032	0.032
Cr^{3+}																		
Sum	3.000	3.000	3.000	3.000	3.000	3.000	3.000	3.000	3.000	3.000	3.000	3.000	3.000	3.000	3.000	3.000	3.000	3.000
Fe_2O_3	13.5	8.2	9.0	8.8	7.9	13.1	9.5	12.1	29.3	35.2	42.7	37.8	41.8	31.9	6.6	23.9	2.5	6.6
FeO	62.0	63.8	63.7	63.8	64.1	62.4	63.7	62.7	57.9	56.1	51.1	54.0	52.8	55.5	63.0	58.2	66.8	64.8
TiO_2	24.5	28.0	27.3	27.5	28.1	24.4	26.9	25.2	12.7	8.7	6.2	8.2	5.4	12.6	30.3	18.0	30.7	28.7

Table A4.1: Oxide compositions for the Maningoza Suite

Bulk-Rock Chemistry Data for the Maningoza Suite

The complete major and trace element (including REE) dataset for the Maningoza Suite is presented in Tables A5.1 to A5.4. The major and REE data for the Ambohitrosy Complex taken from Rasolofomanana (1998) is presented in Table A5.5.

Formation	Ambolodia												Sambao										
Sample	PF06115	PF06116	PF06118	PF06117	PF06119	PF06120	PF06121	PF06122	PF06126	PF06127	PF06128	PF06136	BY6F090	BY6F098	BY6F101	BY6F113	BY6F154	BY6F091	BY6F102	BY6F103	BY6F151	BY6F098B	BY6F148	BY6F106
wt. %																								
SiO_2	68.19	68.10	67.96	47.71	60.80	56.82	48.30	48.04	61.45	47.78	57.52	51.77	47.20	52.99	48.03	50.96	51.98	47.38	45.42	59.23	52.54	70.34	74.92	69.38
TiO_2	0.66	0.64	0.64	1.51	1.34	1.53	1.38	1.39	1.20	1.12	1.58	1.69	1.41	1.97	1.39	2.01	1.47	1.62	2.74	1.25	2.42	0.31	0.06	0.26
Al_2O_3	12.66	12.32	12.39	13.35	12.43	13.03	14.06	13.74	12.52	13.01	12.15	12.95	14.21	12.18	15.87	12.76	13.62	13.87	15.31	12.35	12.37	11.87	12.84	11.23
Fe_2O_3	4.64	4.51	4.69	14.01	10.38	12.01	13.23	13.41	9.01	12.70	13.72	14.60	12.47	15.41	11.86	16.07	11.07	14.60	16.19	7.52	13.86	4.03	1.24	3.08
MnO	0.10	0.11	0.11	0.21	0.17	0.19	0.20	0.19	0.14	0.19	0.20	0.20	0.19	0.30	0.16	0.20	0.16	0.21	0.17	0.17	0.20	0.06	0.04	0.07
MgO	0.79	0.78	1.01	6.44	1.73	2.44	6.15	6.12	1.81	6.60	2.03	4.49	7.57	2.12	7.47	4.07	4.96	6.58	4.99	1.18	3.41	0.47	0.16	0.40
CaO	1.97	2.39	2.06	12.11	3.91	5.46	10.79	10.77	4.38	11.12	5.08	8.57	13.05	6.18	9.96	8.20	7.07	12.40	7.72	6.87	7.19	1.66	0.14	3.98
Na_2O	3.57	3.84	3.21	2.29	2.95	2.99	2.93	2.70	3.16	2.56	3.73	2.68	2.24	3.56	2.84	3.25	2.83	2.57	3.83	2.47	2.97	2.41	4.26	2.58
K_2O	5.19	4.13	4.55	0.28	3.89	2.31	0.50	0.46	3.20	0.33	2.67	1.33	0.17	1.48	0.60	0.99	2.17	0.15	0.42	2.88	1.16	6.00	4.82	1.11
P_2O_5	0.16	0.16	0.17	0.13	0.40	0.34	0.17	0.18	0.30	0.11	0.41	0.27	0.12	0.78	0.23	0.26	0.29	0.13	0.48	0.25	0.67	0.04	0.01	0.01
LOI	1.09	2.18	2.28	0.81	1.22	1.90	1.42	2.28	2.32	3.46	0.45	1.04	0.24	0.97	0.59	0.27	3.00	-0.23	1.53	4.75	1.58	1.58	0.53	5.29
Total	99.40	99.65	99.76	99.28	100.11	100.06	99.45	99.92	99.95	99.52	99.90	99.96	99.25	99.05	99.31	99.47	99.13	99.51	99.32	99.45	99.97	99.36	99.30	99.61
ppm																								
Sc	8.1	8.1	7.5		15.	22.	43.		16.	42.		32.	43.	24.	28.	36.	32.	42.	17.	20.	32.	4.4	0.5	3.2
V	26.	25.	26.		34.	220.	363.		114.	385.		436.	176.	7.4	132.	234.	126.	210.	91.	75.	154.	7.9	0.47	1.7
Co	4.8	4.9	5.5		14.	28.	49.		17.	53.		46.	81.	28.	56.	82.	49.	73.	57.	22.	50.	44.	96.	48.
Cr	6.9	6.4	6.3		3.6	13.	107.		16.	108.		24.												
Cu	15.	79.	16.		10.	25.	184.		43.	165.		128.												
Ni	3.7	3.4	3.7		1.9	10.	53.		10.	46.		25.	121.	1.4	168.	19.	54.	71.	49.	13.	19.	4.5	2.2	1.0
Rb[a]	114.	87.	101.	2.28	76.	49.	12.	4.66	71.	3.27	61.	20.	<1.7	32.	4.18	25.	30.	<1.7	1.76	52.	16.	86.	227.	36.
Rb[b]	115.	87.	100.		80.	51.	14.		73.	5.8		22.	2.1	28.	6.3	24.	30.	1.9	4.2	47.	16.	78.	199.	36.
Sr[a]	105.	114.	106.	165.	229.	227.	229.	234	151.	297.	272.	338.	175.	311.	406.	372.	315.	174.	503.	218.	484.	90.	4.15	342.
Sr[b]	117.	127.	115.		220.	230.	229.		158.	286.		319.	158.	269.	360.	331.	293.	155.	426.	207.	424.	86.	5.0	324.
Y[a]	59.	57.	63.	44.	53.	45.	30.	30	60.	22.	57.	35.	25.	59.	27.	33.	44.	31.	39.	49.	57.	108.	27.	52.
Y[b]	43.	47.	45.		40.	41.	28.		47.	23.		33.	23.	51.	24.	29.	40.	27.	33.	41.	51.	90.	12.	45.
Zr[a]	462.	450.	444.	102.	303.	246.	104.	107.	383.	81.	290.	200.	80.	239.	145.	166.	221.	91.	228.	366.	456.	422.	123.	501.
Zr[b]	194.	198.	271.		256.	226.	71.		269.	72.		181.	72.	203.	124.	136.	189.	87.	193.	332.	286.	175.	119.	344.
Nb[a]	22.	20.	20.	7.95	16.	13.	8.33	8.33	19.	7.45	14.	11.	7.46	16.	12.	11.	14.	7.47	15.	19.	24.	51.	102.	23.
Nb[b]	17.	17.	14.		10.	8.6	2.9		12.	1.9		7.0	1.8	10.	5.1	4.6	8.1	2.0	8.6	13.	19.	45.	89.	16.
Cs	0.57	0.42	0.41		0.42	0.23	0.34		0.19	2.53		0.70												
Ba	993.	834.	873.		853.	648.	168.		635.	152.		465.	41.	381.	235.	435.	488.	37.	176.	660.	1050.	789.	20.	1064.
La	48.	48.	48.		32.	26.	6.8		37.	4.9		19.	2.7	20.	12.	16.	23.	2.9	12.	41.	42.	144.	1.2	55.
Ce	100.	99.	96.		70.	57.	17.		79.	12.		43.	8.6	47.	27.	35.	47.	9.7	33.	86.	94.	305.	2.7	115.
Pr	12.	12.	12.		8.8	7.3	2.5		9.9	1.9		5.8	1.7	7.2	3.8	5.0	6.2	1.8	5.4	10.8	12.4	37.6	0.38	14.1
Nd	41.	41.	42.		33.	27.	11.		37.	8.5		22.	8.7	33.	17.	21.	25.	10.0	25.	41.	50.	133.	1.6	51.
Sm	8.1	8.2	8.4		7.3	6.3	3.3		8.3	2.5		5.1	3.1	9.4	4.3	5.5	6.0	3.6	6.7	8.9	11.	24.	0.67	11.
Eu	1.5	1.6	1.6		2.1	1.9	1.3		1.9	1.0		1.7	1.2	3.3	1.5	1.9	1.8	1.4	2.4	2.3	3.4	2.3	0.08	1.7
Gd	7.8	8.0	8.3		7.7	7.0	4.3		8.7	3.4		5.4	4.0	11.	4.8	6.0	7.0	4.7	7.2	8.6	11.	20.	1.1	9.2
Tb	1.4	1.4	1.5		1.3	1.2	0.80		1.6	0.64		0.99	0.72	1.8	0.78	0.98	1.2	0.84	1.1	1.4	1.7	3.2	0.27	1.5
Dy	7.5	7.7	8.3		7.6	6.8	4.6		9.0	3.7		5.5	4.4	11.	4.7	5.6	7.1	5.2	6.5	7.9	10.	18.	2.2	8.6
Ho	1.7	1.7	1.8		1.7	1.6	1.1		2.0	0.87		1.3	0.94	2.2	0.98	1.2	1.5	1.1	1.3	1.7	2.1	3.8	0.58	1.8
Er	3.9	4.1	4.5		4.2	3.8	2.7		5.0	2.2		3.1	2.6	5.7	2.6	3.2	4.2	3.0	3.5	4.5	5.8	10.	2.1	5.0
Tm	0.59	0.66	0.72		0.67	0.62	0.43		0.81	0.35		0.50	0.38	0.84	0.39	0.49	0.64	0.46	0.52	0.69	0.86	1.6	0.41	0.76
Yb	3.2	3.8	4.2		3.8	3.4	2.4		4.7	1.9		2.7	2.3	5.1	2.3	2.9	3.8	2.8	3.2	4.3	5.4	9.6	3.2	4.7
Lu	0.51	0.55	0.63		0.63	0.56	0.40		0.74	0.32		0.47	0.34	0.76	0.35	0.43	0.58	0.41	0.47	0.65	0.83	1.4	0.51	0.70
Hf	4.1	4.3	6.7		6.4	5.1	1.8		6.8	1.7		4.0	2.04	5.19	2.99	3.72	4.55	2.39	4.52	8.14	9.0	6.5	9.2	9.2
Ta	0.75	0.70	0.65		0.52	0.39	0.08		0.57	*n.d.*		0.22	0.12	0.58	0.29	0.24	0.43	0.14	0.48	0.65	0.96	2.36	7.77	0.77
Pb	13.	14.	11.		12.	13.	1.5		11.1	1.1		5.3	0.85	4.51	2.24	5.30	7.74	0.61	1.73	12.20	7.4	26.	46.	19.
Th	5.2	5.6	5.9		4.6	3.5	0.46		5.1	0.30		1.7	0.15	1.54	0.48	0.88	1.64	0.14	0.44	4.7	1.8	5.1	5.4	5.9
U	0.75	0.76	0.97		1.2	0.94	0.08		1.0	0.06		0.39	0.05	0.36	0.13	0.18	0.39	0.04	0.15	1.04	0.42	1.4	2.8	0.97

Table A5.1: Bulk-rock compositions for the Maningoza Suite

Formation	Antanetilava																			
Sample	PF06131	PF06133	PF06134	PF06142	PF06143	PF06144	PF06147	PF06149	PF06151	PF06154	PF06152	PF06130	PF06135	PF06145	PF06146	PF06148	PF06150	PF06153	PF06129	PF06132
wt. %																				
SiO_2	67.92	68.14	68.23	65.01	59.35	68.67	69.23	66.49	68.66	68.45	68.72	49.11	49.28	47.32	47.71	49.03	50.53	49.15	46.60	45.88
TiO_2	0.86	0.86	0.83	1.01	1.36	0.83	0.86	0.85	0.85	0.86	0.85	1.23	1.42	1.11	1.31	1.46	1.60	1.72	0.59	0.50
Al_2O_3	12.20	12.25	12.44	13.04	12.86	12.45	12.54	12.58	12.84	12.60	12.87	13.85	15.08	15.13	14.76	14.85	13.93	14.30	20.28	23.50
Fe_2O_3	5.28	5.19	5.22	6.87	10.01	5.27	4.93	5.77	4.52	5.25	5.38	12.60	11.13	11.75	12.01	12.11	13.04	13.38	7.27	6.48
MnO	0.11	0.11	0.11	0.12	0.16	0.15	0.07	0.12	0.08	0.10	0.09	0.19	0.16	0.17	0.19	0.16	0.19	0.17	0.13	0.10
MgO	0.90	0.94	0.98	1.32	2.38	0.96	0.60	1.27	0.74	0.92	0.72	6.04	6.11	10.53	8.08	5.89	5.22	5.29	4.73	4.36
CaO	2.69	2.06	2.14	2.82	4.72	2.10	1.35	2.35	1.54	2.03	1.27	10.27	8.48	9.92	8.55	8.44	9.69	8.31	15.21	15.33
Na_2O	3.19	3.64	3.65	4.01	3.25	3.43	3.24	3.37	3.17	3.73	3.36	3.11	3.01	2.51	3.33	3.42	2.86	3.19	1.92	1.62
K_2O	4.43	4.54	4.36	3.57	2.95	4.46	4.72	4.27	5.28	4.08	4.36	0.31	1.74	0.40	0.56	1.35	1.16	1.46	0.36	0.15
P_2O_5	0.25	0.26	0.25	0.30	0.30	0.24	0.23	0.26	0.26	0.25	0.23	0.16	0.31	0.17	0.21	0.32	0.29	0.34	0.05	0.04
LOI	1.38	1.28	1.00	0.75	1.37	0.90	1.35	1.53	0.98	0.83	1.56	2.12	2.09	-0.01	2.57	2.26	0.91	2.12	2.22	1.43
Total	99.67	99.76	99.49	99.23	99.34	99.83	99.86	99.55	99.60	99.39	100.18	99.47	99.65	99.24	99.80	99.68	99.76	99.70	99.76	99.72
ppm																				
Sc	11.	12.	12.	12.	19.	10.	11.	12.	11.	11.	10.	38.	25.	28.	29.	26.	33.	28.	23.	
V	46.	46.	47.	79.	178.	46.	46.	54.	46.	47.	42.	366.	319.	285.	228.	351.	386.	375.	210.	
Co	5.3	5.0	4.8	9.8	22.	7.2	6.9	6.5	6.2	5.0	6.5	52.	42.	61.	55.	46.	44.	49.	35.	
Cr	7.0	8.1	6.2	9.8	10.	8.4	8.9	8.1	11.	7.8	5.2	178.	143.	431.	278.	59.	146.	46.	210.	
Cu	6.7	5.4	5.5	20.	39.	13.	6.6	4.8	7.8	6.3	5.5	131.	100.	107.	95.	100.	120.	87.	67.	
Ni	3.0	2.7	2.9	5.8	9.8	4.7	5.9	4.1	5.3	3.4	3.6	50.	114.	283.	192.	111.	52.	60.	51.	
Rb^a	93.	98.	93.	70.	65.	93.	131.	88.	110.	87.	147.	3.9	21.	2.8	8.4	20.	13.	17.	6.1	<1.7
Rb^b	94.	100.	95.	74.	65.	95.	130.	90.	107.	88.	138.	6.0	26.	5.9	11.	23.	17.	23.	8.6	
Sr^a	197.	221.	232.	238.	302.	202.	148.	200.	212.	206.	182.	329.	508.	291.	470.	494.	375.	484.	240.	295.
Sr^b	196.	230.	240.	221.	277.	198.	155.	210.	212.	202.	168.	299.	447.	266.	415.	430.	321.	419.	252.	
Y^a	47.	51.	46.	50.	45.	45.	48.	49.	47.	46.	48.	24.	27.	22.	25.	29.	32.	32.	13.	13.
Y^b	35.	44.	40.	37.	35.	32.	30.	41.	38.	34.	30.	20.	26.	18.	21.	27.	26.	26.	12.	
Zr^a	392.	388.	398.	451.	336.	388.	387.	411.	406.	391.	407.	109.	188.	93.	132.	191.	181.	212.	41.	35.
Zr^b	335.	360.	366.	323.	277.	290.	249.	343.	353.	317.	328.	82.	173.	60.	48.	39.	141.	141.	33.	
Nb^a	20.	20.	20.	22.	18.	20.	19.	20.	21.	20.	20.	8.5	13.	8.8	9.1	12.	12.	15.	6.1	5.8
Nb^b	13.	15.	16.	15.	11.	13.	13.	16.	15.	13.	14.	2.7	7.9	2.7	3.8	7.8	5.8	7.5	0.8	
Cs	0.65	1.2	0.75	0.32	0.34	0.40	0.47	0.50	0.59	0.53	0.52	0.42	0.19	0.84	0.43	0.32	0.13	0.23	1.5	
Ba	1397.	1201.	1170.	1076.	869.	1163.	1209.	1297.	1357.	1145.	1220.	242.	724.	156.	400.	655.	521.	660.	54.	
La	44.	50.	46.	46.	35.	44.	42.	47.	47.	46.	37.	8.0	23.	7.0	9.8	23.	19.	24.	1.7	
Ce	91.	101.	98.	93.	75.	88.	84.	99.	98.	94.	74.	19.	51.	17.	24.	50.	43.	54.	4.8	
Pr	11.	12.	12.	12.	9.	11.	11.	12.	12.	11.	9.5	2.8	6.5	2.6	3.4	6.5	5.6	6.9	0.80	
Nd	39.	43.	40.	42.	34.	38.	38.	41.	40.	40.	33.	12.	23.	11.	14.	24.	22.	26.	3.8	
Sm	7.4	7.9	7.6	8.2	7.0	7.1	7.2	7.8	7.5	7.5	6.3	3.1	4.8	2.9	3.5	4.9	4.8	5.5	1.3	
Eu	1.7	1.8	1.8	2.0	1.9	1.6	1.6	1.8	1.7	1.7	1.5	1.1	1.5	1.1	1.2	1.6	1.6	1.7	0.57	
Gd	7.1	7.5	6.8	7.7	6.9	6.6	6.7	7.2	6.8	6.9	5.9	3.8	4.7	3.4	4.0	4.9	5.2	5.4	1.7	
Tb	1.2	1.3	1.2	1.3	1.2	1.1	1.1	1.3	1.2	1.2	1.0	0.70	0.80	0.60	0.70	0.82	0.90	0.93	0.34	
Dy	6.7	7.0	6.5	7.4	6.8	6.3	6.4	6.7	6.2	6.5	5.8	3.9	4.3	3.5	4.0	4.4	5.0	5.2	2.0	
Ho	1.5	1.6	1.5	1.6	1.5	1.4	1.4	1.5	1.4	1.5	1.3	0.88	0.98	0.79	0.91	1.02	1.14	1.12	0.46	
Er	3.7	3.9	3.6	4.0	3.7	3.4	3.3	3.7	3.4	3.6	3.3	2.3	2.4	2.0	2.2	2.4	2.7	2.8	1.2	
Tm	0.60	0.64	0.61	0.64	0.61	0.55	0.53	0.61	0.57	0.59	0.52	0.35	0.37	0.31	0.36	0.38	0.43	0.44	0.18	
Yb	3.5	3.6	3.5	3.7	3.5	3.2	3.2	3.7	3.2	3.4	3.2	2.0	2.1	1.8	2.0	2.1	2.5	2.4	1.0	
Lu	0.57	0.60	0.57	0.59	0.57	0.52	0.47	0.54	0.52	0.55	0.52	0.33	0.34	0.30	0.33	0.35	0.41	0.38	0.16	
Hf	7.9	8.1	8.2	7.6	6.6	7.2	6.5	7.5	7.5	7.8	7.8	2.2	3.6	1.5	1.4	1.1	3.5	3.6	0.8	
Ta	0.66	0.70	0.71	0.74	0.53	0.69	0.63	0.68	0.64	0.67	0.67	0.15	0.26	0.11	0.13	0.21	0.20	0.30	n.d.	
Pb	15.	16.	16.	15.	11.	16.	12.	14.	15.	17.	15.	2.2	4.3	1.5	3.4	4.3	4.6	5.1	1.1	
Th	6.5	6.7	6.5	5.3	4.3	6.5	6.3	5.9	6.0	6.6	6.0	0.58	1.1	0.22	0.31	0.79	1.0	1.3	0.10	
U	1.4	1.4	1.4	1.1	0.93	1.4	1.5	1.2	1.3	1.4	1.3	0.12	0.21	0.05	0.06	0.13	0.20	0.23	0.03	

Table A5.2: Bulk-rock compositions for the Maningoza Suite

Complex	Ankibobozaka						Berevo															
Sample	PF06004	PF06001	PF06002	PF06003	PF06005	PF06006	PF06008	PF06011	PF06024	PF06030	PF06013	PF06017	PF06020	PF06021	PF06027	PF06032	PF06022	PF06018	PF06019	PF06026	PF06015	PF06016
wt. %																						
SiO_2	47.34	50.93	68.99	69.72	68.48	69.98	49.62	53.17	47.75	48.98	48.35	46.80	46.28	46.43	45.45	52.23	65.94	71.79	71.58	72.49	71.88	72.05
TiO_2	1.22	1.76	0.43	0.45	0.44	0.46	2.12	1.61	1.35	1.65	1.24	0.28	0.70	0.31	0.51	1.48	0.73	0.70	0.69	0.69	0.68	0.70
Al_2O_3	13.74	13.21	12.64	12.97	12.76	12.78	12.77	13.18	13.70	12.78	16.36	23.62	17.71	19.97	23.00	12.78	12.56	11.60	11.42	11.76	11.57	11.37
Fe_2O_3	12.96	13.30	4.31	4.62	4.54	4.69	15.20	13.67	13.35	14.80	9.98	6.46	10.30	8.58	6.12	13.95	6.40	4.31	4.34	4.43	4.20	4.26
MnO	0.20	0.19	0.11	0.14	0.12	0.13	0.23	0.20	0.20	0.21	0.15	0.09	0.15	0.12	0.11	0.20	0.14	0.10	0.09	0.09	0.09	0.08
MgO	7.85	5.24	0.32	0.28	0.21	0.30	4.68	5.16	7.09	5.80	5.92	6.02	9.30	10.21	3.38	4.52	0.69	0.67	0.69	0.70	0.63	0.60
CaO	12.20	7.98	1.25	1.18	1.57	1.41	8.76	9.50	12.35	10.10	12.86	13.31	12.15	11.77	14.76	8.45	2.23	1.80	1.91	2.01	1.89	1.87
Na_2O	1.87	3.28	4.70	4.60	4.75	4.55	2.25	2.85	2.44	3.06	2.82	1.98	1.96	1.84	1.87	3.17	4.21	2.88	2.90	2.85	2.80	2.81
K_2O	0.58	1.50	4.42	4.50	4.41	4.38	1.50	0.76	0.26	0.38	0.40	0.15	0.17	0.15	0.30	1.06	3.76	4.49	4.50	4.36	4.45	4.44
P_2O_5	0.10	0.29	0.04	0.05	0.04	0.05	0.24	0.20	0.14	0.16	0.11	0.03	0.06	0.02	0.04	0.16	0.18	0.13	0.13	0.14	0.13	0.13
LOI	1.65	1.41	1.69	0.39	1.65	0.65	2.22	0.46	0.58	0.52	0.80	0.60	0.61	0.48	2.93	1.01	2.19	0.75	1.04	0.27	0.62	0.76
Total	100.10	100.14	99.42	99.26	99.48	99.76	99.99	100.98	99.41	99.50	99.19	99.55	99.71	100.13	99.09	99.49	99.33	99.43	99.73	99.95	99.18	99.42
ppm																						
Sc	48.	35.	6.4	6.7	8.7	7.3	35.	37.	46.	41.	40.	6.6	25.	11.	17.	34.	11.	7.9	8.1	8.6	8.5	8.3
V	400.	400.	3.1	3.0	2.8	3.1	466.	418.	401.	492.	426.	66.	235.	78.	163.	418.	9.5	33.	29.	32.	31.	31.
Co	51.	42.	0.75	1.3	0.78	0.76	43.	45.	55.	52.	39.	39.	58.	57.	27.	46.	4.1	4.4	4.2	4.8	4.3	4.1
Cr	245.	46.	11.	10.	9.2	11.	37.	88.	236.	39.	330.	175.	597.	210.	154.	18.	11.	14.	15.	16.	14.	14.
Cu	171.	142.	5.5	5.2	4.2	4.5	86.	186.	216.	193.	115.	29.	145.	88.	75.	99.	6.1	8.1	8.9	12.	6.3	6.2
Ni	92.	35.	4.2	5.2	3.3	3.8	32.	52.	79.	52.	87.	129.	234.	260.	33.	29.	3.7	5.0	5.8	6.4	4.7	4.5
Rb^a	18.	21.	81.	85.	78.	82.	27.	9.5	2.5	6.15	<1.7	<1.7	<1.7	<1.7	11.	21.	78.	108.	111.	102.	103.	108.
Rb^b	17.	20.	73.	78.	72.	76.	25.	10.	4.3	8.2	4.6	1.1	1.3	0.7	11.	23.	71.	97.	98.	94.	94.	96.
Sr^a	137.	333.	126.	110.	118.	123.	262.	277.	249.	305.	364.	367.	352.	376.	257.	302.	213.	141.	131.	147.	147.	154.
Sr^b	139.	300.	133.	123.	133.	135.	244.	252.	230.	274.	323.	326.	309.	332.	240.	275.	205.	149.	139.	151.	155.	157.
Y^a	31.	37.	73.	67.	61.	64.	46.	34.	25.	32.	21.	5.17	10	3.32	9.72	35.	70.	48.	50.	53.	50.	48.
Y^b	25.	28.	48.	47.	43.	44.	38.	28.	21.	26.	17.	4.0	8.6	3.0	8.1	28.	52.	35.	36.	37.	36.	36.
Zr^a	75.	224.	612.	544.	516.	551.	179.	157.	84.	110.	70.	30.	42.	22.	39.	140.	515.	393.	391.	375.	397.	400.
Zr^b	43.	138.	134.	120.	142.	110.	158.	20.	14.	22.	51.	13.	27.	10.	19.	92.	77.	131.	140.	64.	228.	170.
Nb^a	6.59	13.	26.	24.	24.	25.	12.	10.	8.05	8.73	7.14	6.12	6.89	4.73	5.87	9.76	21.55	19.99	20.	20.	20.	21.
Nb^b	1.8	6.3	18.	18.	17.	18.	5.9	5.1	2.2	2.9	2.0	0.59	1.2	0.33	0.64	4.0	16.	14.	14.	14.	14.	14.
Cs	0.54	0.03	0.38	0.28	0.21	0.62	0.02	0.14	0.24	0.20	0.06	0.03	0.02	0.03	1.1	0.60	0.34	2.7	1.7	2.4	1.8	2.2
Ba	87.	585.	1366.	1475.	1488.	1465.	362.	230.	103.	156.	131.	62.	74.	56.	41.	365.	1316.	756.	853.	808.	785.	754.
La	3.9	20.	62.	67.	61.	63.	15.	12.	4.8	7.0	4.9	1.7	2.7	1.3	2.1	13.	55.	45.	43.	44.	47.	46.
Ce	9.2	45.	124.	125.	123.	125.	34.	30.	13.	18.	13.	4.3	7.0	3.2	5.4	29.	109.	95.	93.	93.	97.	94.
Pr	1.6	5.9	15.	17.	15.	16.	4.6	4.2	2.2	2.8	2.0	0.63	1.1	0.45	0.82	4.0	14.	11.	11.	11.	12.	12.
Nd	7.7	23.	52.	56.	52.	53.	20.	17.	9.8	13.	8.9	2.8	4.7	2.0	3.6	15.	48.	39.	39.	39.	39.	39.
Sm	2.7	5.2	9.8	11.	10.	10.	5.2	4.5	3.0	3.7	2.5	0.68	1.3	0.51	1.1	4.0	9.8	7.6	7.5	7.7	7.7	7.6
Eu	1.0	1.7	1.9	2.4	2.2	2.1	1.8	1.5	1.2	1.4	1.0	0.47	0.63	0.40	0.50	1.4	2.5	1.3	1.3	1.3	1.4	1.3
Gd	3.9	5.5	9.2	10.0	9.2	9.2	6.6	5.2	3.8	4.7	3.0	0.81	1.6	0.59	1.4	4.8	9.9	7.0	7.2	7.2	7.0	7.0
Tb	0.74	0.99	1.6	1.7	1.7	1.6	1.2	0.94	0.71	0.85	0.56	0.14	0.29	0.10	0.28	0.92	1.8	1.2	1.2	1.2	1.3	1.2
Dy	4.5	5.5	8.8	9.1	8.7	8.5	7.0	5.3	3.9	4.9	3.3	0.78	1.6	0.60	1.6	5.0	9.8	6.7	6.8	6.9	6.7	6.7
Ho	1.0	1.2	1.9	2.0	1.9	1.9	1.6	1.2	0.91	1.1	0.74	0.17	0.38	0.13	0.37	1.2	2.2	1.5	1.5	1.5	1.5	1.5
Er	2.6	3.0	4.4	4.7	4.4	4.3	4.1	3.0	2.2	2.8	1.9	0.44	0.90	0.33	0.85	2.9	5.3	3.5	3.7	3.7	3.7	3.7
Tm	0.41	0.48	0.65	0.70	0.69	0.67	0.64	0.46	0.35	0.43	0.28	0.07	0.14	0.05	0.14	0.46	0.85	0.56	0.59	0.57	0.62	0.60
Yb	2.4	2.8	3.5	3.7	3.8	3.7	3.7	2.5	1.9	2.4	1.6	0.38	0.81	0.29	0.73	2.8	4.5	3.3	3.4	3.2	3.4	3.2
Lu	0.37	0.44	0.57	0.59	0.62	0.60	0.61	0.41	0.30	0.38	0.25	0.07	0.14	0.05	0.12	0.422165	0.74	0.50	0.51	0.50	0.57	0.54
Hf	1.4	3.6	3.8	3.6	4.2	3.7	4.0	0.74	0.62	0.77	1.3	0.32	0.74	0.26	0.47	2.6	2.4	3.3	3.6	1.8	5.7	4.2
Ta	0.13	0.31	0.85	0.45	0.34	0.39	0.34	0.03	n.d.	0.13	0.10	0.02	n.d.	n.d.	n.d.	n.d.	0.34	0.81	0.79	0.77	0.38	0.37
Pb	4.0	4.8	15.	13.	15.	13.	4.3	3.6	1.7	2.3	1.3	0.89	0.75	0.41	1.6	2.9	15.	20.	18.	18.	18.	18.
Th	0.24	1.0	4.1	3.9	3.8	4.3	1.4	1.3	0.18	0.53	0.18	0.05	0.09	0.03	0.14	1.1	5.3	7.9	7.9	7.6	8.3	8.1
U	0.04	0.19	0.34	0.45	0.42	0.46	0.28	0.21	0.05	0.08	0.04	0.01	0.03	n.d.	0.04	0.21	0.53	1.3	1.5	1.3	1.6	1.3

Table A5.3: Bulk-rock compositions for the Maningoza Suite

Complex	Fonjay						Ambereny						Dykes											
Sample	MI06004A	MI06006	MI06008	MI06010	MI06011	MI06013	MI06014	MI06017	MI06018	MI06019	MI06021	MI06016	PF06071	PF06138	MI06034	PF06023	PF06028	PF06009	PF06012	PF06014	PF06123	PF06124	PF06125	BYF6107	BY6F086
wt. %																									
SiO_2	44.31	48.73	56.48	46.59	46.52	46.00	47.40	48.08	48.12	48.40	50.16	73.70	51.73	47.03	69.78	67.19	68.73	64.29	61.01	54.85	72.89	48.16	50.14	46.56	46.44
TiO_2	1.31	0.46	1.02	1.00	0.13	0.09	0.27	0.56	0.75	0.34	1.85	0.32	1.70	1.24	0.38	0.78	0.53	0.85	1.34	1.99	0.43	1.36	1.33	2.18	0.87
Al_2O_3	14.21	15.91	15.10	19.98	26.89	25.96	21.32	18.85	16.81	18.95	14.35	11.81	13.53	14.62	13.78	12.88	12.21	14.98	12.60	12.63	11.58	13.52	13.10	16.32	12.93
Fe_2O_3	11.86	6.67	11.20	9.07	3.33	3.73	5.75	7.42	8.90	9.12	14.17	3.45	13.69	12.93	2.25	6.70	5.39	5.75	9.67	13.55	4.01	13.73	13.35	15.18	10.47
MnO	0.18	0.11	0.29	0.14	0.05	0.05	0.10	0.12	0.14	0.13	0.23	0.07	0.18	0.19	0.06	0.15	0.14	0.19	0.16	0.21	0.07	0.20	0.19	0.20	0.16
MgO	8.83	8.77	1.05	5.58	5.40	7.21	6.80	6.42	7.45	9.86	5.39	0.31	4.76	7.99	0.45	0.70	0.39	0.75	2.50	3.02	0.44	6.73	5.67	5.61	11.10
CaO	11.77	16.54	5.38	14.40	15.71	14.93	15.35	14.99	14.53	10.06	9.87	0.86	8.12	13.12	0.26	2.25	1.27	1.72	5.12	5.47	1.44	11.48	10.61	8.04	11.56
Na_2O	1.67	1.65	6.40	1.90	1.32	1.28	1.81	1.86	1.89	2.50	2.78	3.46	3.12	2.07	3.62	4.42	3.44	5.27	3.35	3.87	2.70	2.57	2.65	3.97	1.61
K_2O	0.11	0.06	1.01	0.30	0.04	0.02	0.06	0.14	0.14	0.27	0.40	5.52	1.23	0.10	6.95	3.78	4.91	4.68	2.85	2.33	5.95	0.49	0.55	0.31	0.10
P_2O_5	0.11	0.00	0.32	0.07	0.00	0.00	0.01	0.03	0.06	0.03	0.33	0.03	0.26	0.09	0.04	0.18	0.07	0.30	0.35	0.56	0.06	0.12	0.15	0.32	0.10
LOI	4.09	0.15	0.85	-0.02	0.22	0.28	0.17	0.33	0.38	0.97	-0.73	0.18	0.55	0.15	1.02	0.45	1.57	0.37	0.12	1.05	0.17	1.51	1.64	0.49	2.76
Total	99.12	99.36	99.58	99.18	99.82	99.85	99.18	99.01	99.39	100.85	99.26	100.18	99.55	99.91	99.26	99.69	99.15	99.42	99.26	99.94	100.17	100.24	99.90	99.56	99.35
ppm																									
Sc	37.	43.	16.	29.	4.0	5.2	30.	38.	45.	9.3	36.	4.9		40.	4.6	11.	12.	11.	20.	31.	4.8	46.	38.	19.	38.
V	159.	88.	0.58	119.	7.9	12.	51.	95.	116.	36.	188.	4.0		373.	5.6	9.4	2.8	7.8	227.	244.	30.	439.	378.	106.	126.
Co	56.	55.	34.	57.	62.	45.	59.	52.	57.	69.	101.	231.		58.	18.	4.0	1.7	1.6	22.	29.	3.3	52.	50.	69.	66.
Cr														290.		11.	6.1	5.9	23.	6.0	10.	171.	58.		
Cu														171.		5.8	10.0	4.4	31.	18.	21.	215.	159.		
Ni	172.	132.	1.4	73.	231.	130.	114.	85.	94.	195.	49.	13.		111.	3.2	4.4	2.6	2.7	16.	6.5	4.6	73.	49.	40.	286.
Rb[a]	3.6	<1.7	15.16	8.6	<1.7	<1.7	<1.7	<1.7	3.2	<1.7	6.1	178.	19.74	<1.7	142.	77.	98.	86.	50.	38.	119.	9.3	11.	<1.7	<1.7
Rb[b]	4.9	0.32	17.	10.	0.21	0.42	0.77	2.5	3.9	1.2	9.7	152.		1.3	127.	71.	91.	78.	47.	36.	117.	9.8	12.	2.6	2.1
Sr[a]	251.	201.	204.	222.	231.	266.	223.	174.	208.	584.	398.	56.	421.	166.	31.	205.	234.	277.	262.	337.	91.	229.	211.	496.	179.
Sr[b]	232.	176.	189.	206.	213.	244.	212.	164.	192.	503.	360.	52.		164.	31.	200.	227.	257.	244.	301.	99.	233.	211.	435.	168.
Y[a]	22.	7.9	72.	19.	<1.3	<1.3	6.3	14.	16.	4.5	34.	85.	33.	24.	79.	72.	44.	75.	45.	48.	59.	28.	32.	34.	20.
Y[b]	20.	6.3	60.	16.	0.57	0.98	5.3	12.	15.	3.5	31.	63.		19.	63.	53.	32.	57.	36.	40.	44.	25.	29.	30.	18.
Zr[a]	80.	14.	222.	66.	7.0	11.	15.	34.	44.	37.	199.	326.	197.	67.	715.	522.	308.	747.	300.	262.	502.	89.	138.	179.	61.
Zr[b]	70.	10.	96.	37.	1.5	2.2	8.6	27.	23.	10.	29.	84.		65.	595.	51.	269.	586.	122.	217.	173.	37.	80.	149.	57.
Nb[a]	10.	5.1	20.	9.1	4.8	5.9	5.6	6.4	6.0	5.5	13.	23.	12.	8.14	60.	23.	16.	38.	15.	15.	22.	7.2	9.8	12.	7.6
Nb[b]	4.5	0.11	14.	2.8	0.03	0.04	0.09	0.47	0.72	0.35	7.2	17.		1.3	52.	16.	9.6	30.	8.7	9.9	18.	2.3	3.9	5.8	2.1
Cs														0.41		0.31	0.53	0.49	0.41	0.02	0.31	0.24	0.10		
Ba	63.	28.	259.	57.	6.	13.	21.	27.	52.	136.	323.	876.		125.	282.	1346.	1347.	1921.	754.	888.	1365.	135.	187.	134.	75.
La	3.7	0.76	12.	2.7	0.23	0.39	0.49	1.3	2.2	2.3	19.	67.		2.0	164.	53.	36.	74.	34.	35.	55.	5.5	11.	9.3	4.6
Ce	9.6	2.2	34.	7.2	0.50	0.91	1.3	3.4	5.5	4.9	41.	110.		7.1	278.	108.	75.	151.	74.	75.	111.	13.	24.	26.	12.
Pr	1.6	0.39	6.0	1.3	0.08	0.13	0.23	0.62	0.90	0.68	5.8	15.		1.3	40.	13.	9.0	19.	9.2	9.7	13.	2.1	3.4	4.1	1.8
Nd	8.4	2.2	31.	6.5	0.36	0.63	1.3	3.4	4.8	2.9	24.	55.		7.1	136.	48.	32.	68.	34.	36.	45.	9.3	14.	19.	8.1
Sm	2.9	0.83	10.0	2.2	0.09	0.18	0.56	1.3	1.8	0.68	5.9	11.		2.5	24.	10.	6.3	13.	7.2	7.9	8.3	3.0	3.7	5.4	2.4
Eu	1.2	0.47	5.5	0.98	0.15	0.22	0.39	0.63	0.78	0.50	2.2	1.3		1.00	3.8	2.4	1.8	3.6	1.7	2.6	1.1	1.2	1.2	2.1	0.91
Gd	3.8	1.2	13.	3.0	0.12	0.21	0.88	1.9	2.6	0.74	6.3	12.		3.4	18.	10.	6.2	11.	7.4	8.1	7.7	3.9	4.6	6.2	3.1
Tb	0.64	0.21	2.1	0.51	0.02	0.03	0.16	0.35	0.46	0.11	1.0	1.9		0.64	2.6	1.8	1.1	1.9	1.3	1.4	1.4	0.74	0.84	1.0	0.52
Dy	4.1	1.3	13.	3.2	0.11	0.20	1.0	2.3	2.9	0.70	6.1	12.		3.7	15.	10.	6.2	11.	7.1	7.5	7.4	4.3	4.7	6.1	3.4
Ho	0.85	0.27	2.6	0.67	0.02	0.04	0.22	0.51	0.65	0.14	1.3	2.5		0.85	2.8	2.2	1.4	2.4	1.6	1.7	1.7	1.0	1.1	1.3	0.75
Er	2.3	0.72	7.2	1.8	0.06	0.10	0.57	1.3	1.7	0.37	3.4	6.8		2.2	7.5	5.6	3.4	6.0	3.8	4.2	4.0	2.5	2.8	3.3	2.1
Tm	0.34	0.10	1.1	0.26	0.01	0.01	0.09	0.20	0.26	0.06	0.51	1.0		0.33	1.2	0.87	0.56	0.97	0.61	0.65	0.64	0.40	0.44	0.50	0.33
Yb	2.0	0.55	7.1	1.6	0.05	0.09	0.51	1.2	1.6	0.33	3.0	6.0		1.9	7.2	4.9	3.4	5.8	3.6	3.7	3.5	2.1	2.4	3.0	2.0
Lu	0.30	0.08	1.2	0.24	0.01	0.01	0.08	0.18	0.24	0.05	0.46	0.88		0.30	1.1	0.76	0.55	0.92	0.53	0.62	0.52	0.33	0.40	0.45	0.30
Hf	1.9	0.36	2.7	1.1	0.03	0.07	0.29	0.81	0.73	0.29	1.1	3.9		1.6	16.	1.8	6.7	13.	3.6	5.6	4.2	1.2	2.3	3.7	1.5
Ta	0.31	0.01	0.82	0.19	0.00	0.00	0.00	0.02	0.03	0.00	0.39	1.2		0.02	2.5	0.80	0.49	1.4	0.45	0.13	0.66	0.03	0.10	0.34	0.09
Pb	1.2	0.47	2.0	2.5	0.11	0.22	0.51	0.57	0.86	0.90	6.7	24.		0.39	24.	13.	13.	20.	10.	8.2	11.	2.7	4.2	1.5	1.1
Th	0.41	0	1.2	0.31	0.00	0.00	0.02	0.16	0.32	0.01	1.6	17.		0.09	10.0	5.2	4.0	5.9	2.5	3.3	5.0	0.30	1.1	0.31	0.17
U	0.11	0.01	0.26	0.09	0.00	0.00	0.01	0.06	0.08	0.01	0.30	3.3		0.03	1.8	0.50	0.81	1.2	0.56	0.59	0.78	0.05	0.21	0.10	0.04

Table A5.4: Bulk-rock compositions for the Maningoza Suite

Complex	Ambohitrosy																				
Sample	95.15	AB.26b	AB07	95.16	9513b	AB.02	95.01a	AB.06	AB.17	AB.16	95.09	AB.26a	95.02	AB.15	AB26n	AB.12	95.03	95.01b	95.05b	95.06	AB.05
wt. %																					
SiO_2	42.29	43.27	45.58	46.29	46.88	46.87	46.95	47.15	47.53	47.61	48.10	48.70	48.82	50.30	51.36	54.39	52.00	52.25	53.00	53.48	53.80
TiO_2	4.00	2.69	1.66	1.99	1.43	0.84	1.13	1.47	1.74	1.83	1.15	0.73	1.23	0.81	0.48	0.62	1.70	1.22	1.76	1.00	1.93
Al_2O_3	11.21	11.97	13.61	14.55	14.33	11.80	14.25	13.54	13.62	13.42	15.00	13..2	14.43	23.83	22.36	21.70	13.51	14.20	13.24	14.25	12.84
Fe_2O_3	20.74	20.44	13.25	14.35	12.47	11.90	11.32	13.17	12.58	15.00	11.25	10.55	12.00	6.29	5.20	5.43	13.61	11.00	14.00	10.00	13.00
MnO	0.28	0.21	0.17	0.23	0.19	0.18	0.17	0.19	0.20	0.22	0.22	0.18	0.19	0.09	0.09	0.14	0.22	0.17	0.21	0.16	0.21
MgO	6.01	7.04	8.04	7.14	6.90	16.87	7.94	6.80	6.98	6.64	8.53	10.08	6.58	2.40	3.30	1.26	5.28	6.20	4.76	6.59	3.05
CaO	12.02	13.17	14.30	11.14	12.31	8.00	13.76	12.20	11.60	11.00	12.93	14.26	12.53	13.64	14.24	9.78	9.29	11.70	8.79	11.35	6.20
Na_2O	2.59	1.70	1.93	2.90	2.68	1.64	2.30	2.17	2.83	2.22	2.21	1.60	2.67	2.88	2.75	4.29	3.37	2.43	3.37	2.98	3.69
K_2O	0.55	0.24	0.22	0.58	0.37	0.39	0.48	0.31	0.58	0.05	0.21	0.41	0.55	0.49	0.57	1.21	0.87	0.77	1.04	0.88	1.49
LOI	0.53	0.04	0.00	1.63	1.80	2.21	2.52	0.59	1.39	0.57	1.22	1.09	1.59	0.39	0.80	0.57	1.04	0.84	0.71	0.02	1.84
Total	100.22	100.77	98.76	100.80	99.36	100.70	100.82	97.59	99.05	98.56	100.82	87.60	100.59	101.12	101.15	99.39	100.89	100.78	100.88	100.71	98.05
ppm																					
La									7.5	13.	4.3	3.8		2.5		15.	11.				24.
Ce									18.	11.	11.	8.5		5.3		37.	25.				47.
Pr																					
Nd									13.	21.	7.7	5.6		4.6		24.	17.				33.
Sm									4.3	6.6	2.3	1.7		1.8		7.6	4.7				9.7
Eu									1.7	2.3	0.97	0.7		0.73		2.1	1.5				2.8
Gd									6.5	9.6	3.2	2.3		2.7		9.3	5.7				14.
Tb																					
Dy									6.9	10.	3.2	2.4		3.0		10.	5.7				13.
Ho																					
Er									4.0	6.2	1.9	1.4		1.7		6.1	3.2				8.2
Tm																					
Yb									3.8	6.2	1.7	1.4		1.5		5.6	3.1				6.4
Lu									0.60	0.99	0.24	0.21		0.23		0.90	0.49				1.0

Complex	Ambohitrosy																			
Sample	AB 10	AB.19	95.20b	AB 14	95.20a	AB 13	95.14	AB 18	AB 9	AB 13a	95.21	AB 27	AB.08	AB 24	AB 20	95.18	AB 22	ABF079	95.1	95.04
wt. %																				
SiO_2	57.80	60.11	61.95	62.80	64.61	65.00	65.05	65.10	65.40	65.80	67.29	67.40	68.90	69.10	70.50	73.58	73.70	73.15	63.96	67.70
TiO_2	1.33	1.37	0.88	0.63	0.70	0.39	0.90	0.54	0.81	0.43	0.48	0.50	0.63	0.51	0.51	0.20	0.33	0.36	0.81	0.72
Al_2O_3	13.70	14.14	14.57	14.20	14.46	14.40	14.38	14.10	12.80	14.30	13.10	9.20	10.00	10.85	11.10	14.00	9.40	10.16	12.65	12.64
Fe_2O_3	11.20	9.02	8.29	7.38	7.81	5.72	7.78	7.24	7.46	5.85	7.05	10.30	0.08	6.85	5.70	2.48	5.60	6.41	5.90	4.72
MnO	0.19	0.18	0.34	0.21	0.22	0.09	0.21	0.21	0.23	0.10	0.16	0.31	0.08	0.25	0.15	0.04	0.11	0.14	0.09	0.08
MgO	2.39	2.47	0.78	0.26	0.57	0.10	0.20	0.36	0.39	0.09	0.68	0.12	0.07	0.28	0.14	0.14	0.09	0.06	2.42	2.17
CaO	5.24	5.54	1.03	1.30	1.38	0.19	1.29	1.72	1.59	0.14	1.25	0.54	0.26	0.64	0.48	0.47	0.26	0.16	6.22	4.43
Na_2O	5.30	4.70	6.83	7.47	6.75	6.91	7.65	7.30	6.43	7.00	6.12	5.90	5.49	5.25	3.78	4.60	4.86	4.97	3.18	2.79
K_2O	2.60	2.30	3.29	4.38	3.98	4.98	2.90	3.90	3.96	4.90	4.21	3.90	4.60	4.23	4.56	4.66	4.33	4.41	2.40	3.64
LOI	0.09	0.29	0.78	1.41	0.13	1.11	0.21	0.24	0.32	1.11	0.21	0.78	0.91	0.86	0.53	0.50	0.59	0.40	1.80	1.61
Total	99.84	100.12	98.74	100.04	100.61	98.89	100.57	100.71	99.39	99.72	100.55	98.95	91.02	98.82	97.45	100.67	99.27	100.22	99.43	100.50
ppm																				
La	27.		91.		30.											61.				
Ce	64.		98.		67.											139.				
Pr																				
Nd	39.		134.		40.											61.				
Sm	12.		39.		11.											15.				
Eu	2.8		9.5		2.7											1.5				
Gd	15.		58.		13.											16.				
Tb																				
Dy	20.		65.		16.											19.				
Ho																				
Er	13.		42.		10.0											12.				
Tm																				
Yb	13.		45.		12.											13.				
Lu	2.0		8.3		2.3											2.1				

Table A5.5: Bulk-rock compositions for the Ambohitrosy Complex. Data from Rasolofomanana (1998).

Petrographic Descriptions for the Maningoza Suite

PF06001 – Ankibobozaka

Grain size(mm)	Modal %	Mineral	Description
0.5	60	Plagioclase	An_{15} = oligoclase, subhedral, lamellar twinning
0.5	20	Opaques	Anhedral, magnetite
<0.5	10	Chlorite	Secondary, anhedral
<0.5	10	Clinopyroxene	Clear in colour, subhedral

Texture: The rock is fine grained and has an equigranular texture. The plagioclase grains are bladed and exhibit a brown staining due to alteration. The presence of the secondary mineral chlorite is an indication that the rock has undergone alteration.

Rock type: Dolerite/basalt

PF06002 – Ankibobozaka

Grain size(mm)	Modal %	Mineral	Description
<4.0	55	Alkali-feldspar	Anhedral,
<2.0	20	Quartz	Euhedral to subhedral
<1.0	10	Opaques	Anhedral, magnetite
<3.0	10	Plagioclase	Anhedral
<1.0	<5	Calcite	Euhedral to subhedral
<0.5	Tr.	Amphibole	Green in colour, anhedral
<0.2	Tr.	Zircon	Anhedral

Texture: The rock is medium grained and has an inequigranular texture. The plagioclase and alkali-feldspar grains are tabular in shape and range in grain size. The rock has a granophyric texture with an intergrowth of quartz in alkali-feldspar.

Rock type: Granophyre

PF06003 – Ankibobozaka

Grain size(mm)	Modal %	Mineral	Description
<2.0	60	Alkali-feldspar	Subhedral to anhedral
<2.0	20	Quartz	Anhedral
<2.0	10	Plagioclase	Subhedral to anhedral
0.5-3.0	10	Opaques	Anhedral, magnetite
<0.5	Tr.	Amphibole	Green to brown, anhedral

Texture: The rock is medium grained and has an equigranular texture. The plagioclase and alkali-feldspar grains are tabular in shape and range in grain size. The rock has a granophyric texture with an intergrowth of quartz in alkali-feldspar.

Rock type: Granophyre

PF06004 – Ankibobozaka

Grain size(mm)	Modal %	Mineral	Description
0.5-3.0	50	Clinopyroxene	Light brown colour, subhedral, 2V angle = 35°, optic sign = +ve, composition = augite
<2.0	40	Plagioclase	Subhedral, extinction angle = 15°, An_{29} = oligoclase, lamellar twinning
<0.5	<5	Chlorite	Subhedral
0.1-0.5	5	Opaque	Subhedral, magnetite

Texture: The medium grained rock has an equigranular texture. The rock also has bladed randomly orientated plagioclase grains that are embedded by blocky clinopyroxene grains forming a poikilitic texture. The plagioclase laths penetrate beyond augite crystals forming a subophitic texture.

Rock type: Dolerite – microgabbro

PF06005 – Ankibobozaka

Grain size(mm)	Modal %	Mineral	Description
<4.0	70	Alkali-feldspar	Anhedral
0.5-2.0	20	Quartz	Subhedral
<3.0	10	Plagioclase	Anhedral, cross-hatched twinning
0.5-1.5	5	Opaques	Anhedral, magnetite
0.5-2.0	<5	Calcite	Subhedral to anhedral
0.1-0.5	Tr.	Biotite	Anhedral
<0.5	Tr.	Amphibole	Brown in colour, anhedral

Texture: The medium grained rock is inequigranular in texture and contains plagioclase and alkali-feldspar that are tabular and range in grain size. The rock has a granophyric texture with an intergrowth of quartz in alkali-feldspar.

Rock type: Granophyre

PF06006 – Ankibobozaka

Grain size(mm)	Modal %	Mineral	Description
<3.0	60	Alkali-feldspar	Subhedral to anhedral
<2.0	20	Quartz	Subhedral to anhedral
0.5-1.0	<5	Clinopyroxene	Subhedral to anhedral
1.0-2.0	<5	Amphibole	Subhedral
<3.0	<1	Calcite	Subhedral
0.5-1.5	5	Opaque	Anhedral, magnetite
1.0-2.0	5	Biotite	Anhedral

Texture: The rock is medium grained and has an inequigranular texture. The rock contains alkali-feldspar with a tabular crystal shape. There is also a granophyric texture present with intergrowths of quartz in alkali-feldspar.

Rock type: Granophyre

PF06008 – Berevo

Grain size(mm)	Modal %	Mineral	Description
0.2-1.0	45	Plagioclase	Anhedral, lamellar twinning
0.1-0.5	35	Clinopyroxene	Light brown colour, Subhedral to anhedral
0.2-1.0	10	Opaques	Anhedral, hematite, magnetite
0.5-1.0	5	Chlorite	Subhedral
1.0	5	Orthopyroxene	Subhedral to anhedral

Texture: The medium to fine grained rock has an equigranular texture. The plagioclase crystals are bladed and have a random orientation. The pyroxene crystals are blocky in shape and show no intergrowth.

Rock type: Microgabbro

PF06009 – Berevo

Grain size(mm)	Modal %	Mineral	Description
<0.2	15	Opaque	Anhedral, magnetite, hematite
<0.2	<5	Biotite	Anhedral
<0.2	70	Feldspar	Anhedral
<0.2	10	Quartz	Anhedral, secondary

Texture: The rock is fine grained and has an equigranular texture with the crystals being aphanitic. There is also secondary quartz veining present in he rock.

Rock type: Trachyte

PF06011 – Berevo

Grain size(mm)	Modal %	Mineral	Description
0.5-1.5	68	Plagioclase	Subhedral, extinction angle 45°, An_{95} = anorthite, lamellar twinning
<0.5	2	Alkali-feldspar	Subhedral to anhedral
<1.0	25	Clinopyroxene	Dark brown colour, Anhedral
0.2-0.4	5	Opaques	Subhedral to anhedral, magnetite, hematite

Texture: The rock is medium grained with an inequigranular texture. The plagioclase crystals are bladed and are randomly orientated.

Rock type: Microgabbro

PF06012 – Berevo

Grain size(mm)	Modal %	Mineral	Description
<0.2	40	Opaque	Anhedral, magnetite, hematite
<0.2	60	Plagioclase	Anhedral

Texture: The rock is fine grained and has an equigranular texture. There is no orientation or layering observed. The crystals are aphanitic.

Rock type: Basalt

PF06013 – Berevo

Grain size(mm)	Modal %	Mineral	Description
2.0-4.0	60	Plagioclase	Euhedral to subhedral, extinction angle = 30°, An_{55} = labrodorite, lamellar twinning
0.5-2.0	30	Clinopyroxene	Light brown colour, euhedral to subhedral, 2V angle = 45°, optic sign = +ve, composition = augite
0.5-1.0	10	Opaques	Euhedral to subhedral, magnetite
0.5-1.0	<1	Serpentine	Anhedral, secondary
0.3-0.8	<1	Calcite	Anhedral, secondary

Texture: The rock is medium grained and has an inequigranular texture. The plagioclase crystals are bladed and are randomly orientated. The clinopyroxene crystals are blocky. The rock has been subjected to very little or no alteration.

Rock type: Gabbro

PF06014 – Berevo

Grain size(mm)	Modal %	Mineral	Description
0.2-1.0	50	Plagioclase	Subhedral to anhedral
0.2-1.0	20	Clinopyroxene	Brown in colour, subhedral to anhedral
<0.2	20	Opaque	Subhedral, magnetite, hematite
0.5	10	Chlorite	Subhedral, secondary

Texture: The rock is fine- to medium-grained and has an inequigranular texture. The plagioclase crystals are bladed and have a random orientation. The presence of the secondary mineral chlorite indicates that the rock has undergone some alteration.

Rock type: Dolerite

PF06015 – Berevo

Grain size(mm)	Modal %	Mineral	Description
1.0-2.0	30	Alkali-feldspar	Subhedral-anhedral
0.1-1.0	20	Quartz	Subhedral-anhedral
1.0-2.0	30	Plagioclase	Subhedral-anhedral
0.5-1.0	5	Amphibole	Subhedral, green in colour
0.1-0.5	10	Opaque	Subhedral, magnetite
0.1-0.5	Tr.	Epidote	Subhedral-anhedral, secondary
0.5-1.0	<5	Chlorite	Secondary, subhedral
0.5	Tr.	Calcite	Secondary, subhedral
0.5-1.0	Tr.	Clinopyroxene	Light brown, anhedral

Texture: The rock has a fine to medium grain size and is inequigranular in texture. The plagioclase and alkali-feldspar crystals are tabular and range in grain size. The rock has a granophyric texture with an intergrowth of quartz in alkali-feldspar.

Rock type: Granophyre

PF06016 – Berevo

Grain size(mm)	Modal %	Mineral	Description
<1.0	30	Quartz	Subhedral
<1.5	30	Alkali-feldspar	Subhedral to anhedral
<1.5	20	Plagioclase	Subhedral to anhedral
0.2-1.0	10	Chlorite	Secondary, anhedral
<0.5	5	Epidote	Secondary
0.1-0.7	15	Opaques	Subhedral, magnetite, hematite
<0.5	Tr.	Amphibole	Anhedral, green in colour

Texture: The rock is medium grained and has an inequigranular texture. The plagioclase and alkali-feldspar crystals are tabular as well as the quartz crystals. The rock has a granophyric texture with an intergrowth of quartz in alkali-feldspar.

Rock type: Granophyre

PF06017 – Berevo

Grain size(mm)	Modal %	Mineral	Description
4.0	30	Olivine	Subhedral to anhedral, reaction rim
1.0-4.0	60	Plagioclase	Euhedral to subhedral, extinction angle = 20°, An_{38} = andesine, repeated lamellar twinning
<1.5	7	Clinopyroxene	Brown in colour, Anhedral
0.5	3	Opaques	Subhedral, magnetite
0.5-1.0	<1	Epidote	Secondary, subhedral
<0.5	<1	Serpentine	Secondary, anheral

Texture: The rock is medium to coarse grained and has inequigranular texture. The plagioclase crystals are bladed and are randomly orientated. The clinopyroxene and olivine crystals are blocky in shape. Some of the olivine crystals show a reaction to serpentine on their rims.

Rock type: Olivine gabbro

PF06018 – Berevo

Grain size(mm)	Modal %	Mineral	Description
<1.0	20	Quartz	Subhedral to anhedral
1.0-2.0	30	Alkali-feldspar	Anhedral
1.0-2.0	30	Plagioclase	Anhedral
<0.5	<5	Opques	Anhedral, hematite
<0.5	<5	Epidote	Secondary, anhedral
<1.0	<10	Chlorite	Secondary, anhedral
<0.5	Tr.	Amphibole	Anhedral, green in colour

Texture: The rock is medium grained and has equigranular texture. The alkali-feldspar and plagioclase crystals are tabular in shape. The rock has a granophyric texture with an intergrowth of quartz in alkali-feldspar.

Rock type: Granophyre

PF06019 – Berevo

Grain size(mm)	Modal %	Mineral	Description
<1.0	20	Alkali-feldspar	Anhedral
<1.0	30	Quartz	Subhedral to anhedral
<1.0	30	Plagioclase	Anhedral
0.1-0.5	10	Opaque	Anhedral, hematite
<0.5	5-10	Chlorite	Secondary, anhedral
<0.5	Tr.	Epidote	Secondary, anhedral
<0.5	Tr.	Amphibole	Anhedral, green in colour

Texture: The rock is medium to fine grained and has an equigranular texture. The plagioclase and alkali-feldspar crystals are tabular in shape. The rock has a granophyric texture with an intergrowth of quartz in alkali-feldspar.

Rock type: Granophyre

PF06020 – Berevo

Grain size(mm)	Modal %	Mineral	Description
2.0-4.0	35	Clinopyroxene	Light brown colour, euhedral, 2V angle = 45°, optic sign = +ve, composition = augite
2.0-3.0	40	Plagioclase	Euhedral, extinction angle = 10°, An_{27} = oligoclase, lamellar twinning
1.0-2.0	10	Olivine	Subhedral
<1.0	<10	Opaques	Euhedral, magnetite
<0.5	<3	Epidote	Anhedral, secondary
<0.5	<2	Serpentine	Anhedral secondary

Texture: The rock is medium to coarse grained and has an equigranular texture. The olivine and clinopyroxene have a poikilitic texture with the olivine embedded within the clinopyroxene. The plagioclase crystals are bladed and have a random orientation. The plagioclase laths are embedded with the clinopyroxene forming a ophitic and in some cases subophitic texture. Plagioclase and olivine both show signs of alteration to secondary minerals epidote and serpentine, respectively.

Rock type: Gabbro

PF06021 – Berevo

Grain size(mm)	Modal %	Mineral	Description
Phenocryst	*40*		
>5.0	40	Clinopyroxene	Light brown colour, euhedral, 2V angle = 45°, optic sign = +ve, composition = augite
Matrix	*60*		
<3.0	15	Olivine	Subhedral
<2.0	40	Plagioclase	Euhedral, extinction angle = -5°, An_0 = albite, repeated lamellar twinning
0.2-0.5	5	Opaques	Euhedral, magnetite
<0.2	<1	Serpentine	Anhedral, secondary

Texture: The rock is medium to coarse grained and has an inequigranular (seriate) texture. The smaller plagioclase laths are embedded in the larger clinopyroxene grains giving an ophtic and subophitic texture. The plagioclase crystals are bladed and have a random orientation. The olivine grains are embedded with the clinopyroxene forming a poikilitic texture. The rock classifies as a pyroxene porphyry due to the large amount of phenocrysts of pyroxene.

Rock type: Gabbro

PF06022 – Berevo

Grain size(mm)	Modal %	Mineral	Description
<2.0	30	Quartz	Subhedral to anhedral
<1.0	10	Opaque	Subhedral to anhedral, magnetite
<4.0	30	Alkali-feldspar	Anhedral
<4.0	30	Plagioclase	Anhedral
<0.2	<1	Amphibole	Subhedral, green to brown in colour
0.2	<1	Calcite	Secondary, subhedral

Texture: The rock is medium grained with an inequigranular texture. The alkali-feldspar and plagioclase crystals are tabular in shape. The rock has a granophyric texture with an intergrowth of quartz in alkali-feldspar.

Rock type: Granophyre

PF06023 – Berevo

Grain size(mm)	Modal %	Mineral	Description
Phenocrysts	*45*		
<1.0	30	Alkali-feldspar	Subhedral to anhedral
<1.0	15	Plagioclase	Subhedral to anhedral, lamellar twinning
Matrix	*55*		
<0.5	45	Quartz	Anhedral
0.5	<1	Amphibole	Subhedral to anhedral, green in colour
0.1-0.5	<10	Opaques	Anhedral, magnetite, hematite
<0.5	<1	Epidote	Subhedral

Texture: The rock is medium to fine grained and is inequigranular (porphyritic) in texture. The alkali-feldspar and plagioclase crystals are both tabular in shape. The rock has a granophyric texture with an intergrowth of quartz in alkali-feldspar.

Rock type: Granophyre

PF06024 – Berevo

Grain size(mm)	Modal %	Mineral	Description
<4.0	55	Plagioclase	Euhedral to subhedral, lamellar twinning
<1.5	30	Clinopyroxene	Brown in colour, euhedral to subhedral
<2.0	10	Opaques	Subhedral, magnetite
0.5	<5	Chlorite	Anhedral, secondary

Texture: The rock is medium grained and has an inequigranular texture. The plagioclase crystals are bladed and have a random orientation. In some cases the plagioclase and clinopyroxene grains are enclosed by one another forming a poikilitic and subophitic texture.

Rock type: Dolerite

PF06026 – Berevo

Grain size(mm)	Modal %	Mineral	Description
<1.0	40	Quartz	Subhedral to anhedral
0.5	20	Alkali-feldspar	Subhedral to anhedral
0.5	30	Plagioclase	Subhedral to anhedral, lamellar twinning
0.5	5	Amphibole	Brown in colour, subhedral
0.1-0.5	5	Opaque	Subhedral, hematite

Texture: The rock is fine to medium grained with an equigranular texture. The plagioclase and alkali-feldspar crystals are tabular and show a brown alteration texture. The rock has a granophyric texture with an intergrowth of quartz in alkali-feldspar.

Rock type: Granophyre

PF06027 – Berevo

Grain size(mm)	Modal %	Mineral	Description
Phenocrysts	*75*		
>5.0	60	Plagioclase	Euhedral, extinction angle = 40°, An_{78} = bytownite, repeated lamellar twinning, zoning
Matrix	*25*		
1.0-3.0	10	Plagioclase	Euhedral, extinction angle = 40°, An_{78} = bytownite
3.0	10	Clinopyroxene	Light brown to clear in colour, euhedral, 2V angle = 45°, optic sign = +ve, composition = augite
3.0-4.0	<5	Amphibole	Subhedral
0.5	<5	Opaques	Subhedral, magnetite
0.5	<5	Chlorite	Secondary, anhedral

Texture: The rock is coarse grained and is inequigranular (porphyritic) in texture. The plagioclase crystals are bladed and are tabular in shape. There is also a small amount of subophitic texture where smaller plagioclase crystals are embedded in clinopyroxene crystals. The rock is plagioclase porphyry due the large composition of porphyritic plagioclase crystals.

Rock type: Gabbro

PF06028 – Berevo dyke

Grain size(mm)	Modal %	Mineral	Description
Phenocrysts	*<5*		
1.0-3.0	<5	Alkali-feldspar	Subhedral
Matrix	*95*		
<0.3	30	Plagioclase	Anhedral
<0.3	35	Alkali-feldspar	Anhedral
<0.5	30	Quartz	Anhedral
0.2	Tr.	Carbonate	Anhedral
<0.3	Tr.	Amphibole	Anhedral, brown in colour

Texture: The rock is fine grained and has an equigranular texture but has a small amount of alkali-feldspar phenocrysts. The plagioclase and alkali-feldspar crystals are tabular in shape and show an alteration texture.

Rock type: Trachyte

PF06030 – Berevo

Grain size(mm)	Modal %	Mineral	Description
0.5-3.0	50	Plagioclase	Euhedral, extinction angle = 5°, An_{24} = oligoclase, lamellar twinning
1.0	35	Clinopyroxene	Euhedral to subhedral, brown in colour, 2V angle = 50°, optic sign = +ve, composition = augite
0.5	10	Opaques	Subhedral, magnetite
0.5	5	Chlorite	Anhedral, secondary

Texture: The rock is medium grained and has an inequigranular texture. The plagioclase crystals are bladed in shape and penetrate the blocky clinopyroxene crystals forming a subophitic texture. The presence of the secondary mineral chlorite indicates that alteration has occurred in the rock.

Rock type: Microgabbro

PF06032 – Berevo

Grain size(mm)	Modal %	Mineral	Description
1.0-3.0	50	Plagioclase	Euhedral to subhedral, extinction angle = 0°, An_{18} = oligoclase, lamellar twinning
0.5-1.5	35	Clinopyroxene	Brown and green in colour, subhedral
1.0	<10	Opaques	Euhedral, magnetite
0.5	<10	Chlorite	Secondary, anhedral
<0.5	Tr.	Quartz	Subhedral
<0.5	Tr.	Amphibole	Subhedral, green in colour

Texture: The rock is medium grained and has an inequigranular texture. The plagioclase crystals are bladed in shape with a random orientation and the clinopyroxene crystals are blocky in shape. The presence of the secondary mineral chlorite is an indication of alteration.

Rock type: Microgabbro

PF06071 – Dyke

Grain size(mm)	Modal %	Mineral	Description
<1.0	50	Plagioclase	Euhedral to subhedral, extinction angle = 10°, An_{18} = oligoclase, lamellar twinning
<0.5	35	Clinopyroxene	Brown in colour, subhedral
<0.5	10	Opaques	Euhedral to subhedral, magnetite
<0.5	5	Chlorite	Secondary, subhedral

Texture: The rock is fine- to medium-grained with an equigranular texture. The plagioclase crystals are bladed in shape with random orientation and the clinopyroxene crystals are blocky in shape. The presence of chlorite is an indication of alteration

Rock type: Dolerite/basalt

PF06115 – Ambolodia

Grain size(mm)	Modal %	Mineral	Description
0.5-2.0	50	Plagioclase	Subhedral to anhedral, lamellar twinning
0.1-0.4	10	Opaques	Subhedral, magnetite
0.2-0.5	<10	Clinopyroxene	Brown colour, anhedral
0.5	20	Alkali-feldspar	Subhedral to anhedral
0.4-0.7	10	Quartz	Anhedral
0.2	Tr.	Amphibole	Anhedral, brown in colour

Texture: The rock is fine to medium grained and has an inequigranular texture. The Plagioclase crystals are bladed and tabular in shape. The alkali-feldspar crystals are tabular in shape. Both plagioclase and alkali-feldspar show a brown alteration texture. In some cases the larger plagioclase grains enclose the smaller clinopyroxene grains forming a poikilitic texture.

Rock type: Feldspar trachyte

PF06116 – Ambolodia

Grain size(mm)	Modal %	Mineral	Description
0.5-2.5	50	Plagioclase	Subhedral
0.3-1.0	20	Quartz	
0.4-0.7	10	Opaques	Subhedral to anhedral, magnetite
0.2	<10	Epidote	Secondary, anhedral
0.3-0.7	5	Calcite	Secondary, subhedral
0.4-1.0	5	Chlorite	Secondary, anhedral

Texture: The rock is fine grained and has an inequigranular texture. The plagioclase and alkali-feldspar show a brown alteration texture. The larger plagioclase grains have undergone alteration to calcite and epidote. The 20 percent modal proportions of secondary minerals indicate a large amount of alteration.

Rock type: Feldspar dacite

PF06117 – Ambolodia

Grain size(mm)	Modal %	Mineral	Description
0.2	40	Plagioclase	Subhedral, lamellar twinning
0.1-0.3	30	Clinopyroxene	Brown colour, anhedral
0.2-0.4	20	Opaques	Subhedral, magnetite
0.2-0.5	10	Chlorite	Secondary, anhedral

Texture: The rock is fine grained and has an equigranular texture. The plagioclase and clinopyroxene grains do not enclose each other and forms no poikilitic texture. The plagioclase grains also show a brown alteration texture. The plagioclase crystals are bladed in shape and the clinopyroxene crystals have a blocky shape. The presence of chlorite is an indication of alteration.

Rock type: Basalt

PF06118 – Ambolodia

Grain size(mm)	Modal %	Mineral	Description
<0.1-1.0	40	Plagioclase	Subhedral to anhedral
0.1-0.5	35	Quartz	Anhedral
0.2-0.6	<10	Opaques	Subhedral, magnetite
0.4-1.2	10	Chlorite	Secondary, subhedral
0.2-0.4	<5	Calcite	Secondary, subhedral

Texture: The rock is fine grained and an inequigranular texture. The larger plagioclase grains have undergone some alteration to calcite and chlorite. The plagioclase and quartz crystals are tabular in shape. The plagioclase grains also show a brown alteration type texture. The presence of secondary minerals is an indication of alteration.

Rock type: Feldspar dacite

PF06119 – Ambolodia

Grain size(mm)	Modal %	Mineral	Description
0.5-2.5	50	Plagioclase	Subhedral to anhedral
0.2-0.4	35	Opaques	Subhedral to anhedral, magnetite
0.3-0.7	5	Clinopyroxene	Light brown colour, subhedral
0.4	5	Chlorite	Secondary, subhedral to anhedral
0.2-0.4	<5	Quartz	Anhedral

Texture: The rock is fine grained and has an inequigranular texture. The larger plagioclase grains have undergone some alteration to chlorite and in some cases enclose the smaller clinopyroxene grains. The plagioclase crystals are tabular in shape and show a brown alteration texture. The presence of secondary minerals is an indication of alteration.

Rock type: Trachy-andesite

PF06120 – Ambolodia

Grain size(mm)	Modal %	Mineral	Description
<2.5	35	Plagioclase	Subhedral
0.1-0.3	15	Clinopyroxene	Brown in colour, anhedral
0.2-0.5	15	Opaques	Subhedral, magnetite
0.4	15	Epidote	Secondary, anhedral
<1.4	<10	Chlorite	Secondary, anhedral
<1.0	10	Quartz	Anhedral
<0.2	Tr.	Amphibole	Hornblende

Texture: The rock is fine grained and has an inequigranular texture. The plagioclase crystals are bladed in shape and have a brown alteration texture. The substantial amounts of secondary minerals suggest the rock has undergone alteration.

Rock type: Basaltic-andesite

PF06121 – Ambolodia

Grain size(mm)	Modal %	Mineral	Description
<1.5	45	Plagioclase	Subhedral to anhedral, lamellar twinning
0.2-0.3	35	Clinopyroxene	Light brown in colour, anhedral
0.3-0.5	10	Opaques	Subhedral, magnetite, hematite
0.2-0.4	5	Chlorite	Secondary, subhedral to anhedral
0.2-0.4	5	Epidote	Secondary, subhedral to anhedral

Texture: The rock is fine grained and has an inequigranular texture. The plagioclase grains are mostly bladed in shape and the pyroxene grains have a blocky shape. The 10 percent modal proportions of secondary mineral suggest the rock has undergone alteration.

Rock type: Basalt

PF06122 – Ambolodia olodia

Grain size(mm)	Modal %	Mineral	Description
<0.5-1.0	45	Plagioclase	Euhedral-subhedral
0.2-0.4	35	Clinopyroxene	Light brown colour, anhedral
0.2-0.5	10	Opaques	Subhedral, magnetite
0.2-0.8	5	Chlorite	Secondary, subhedral to anhedral
0.5	5	Epidote	Secondary, subhedral to anhedral

Texture: The rock is fine grained and has an equigranular texture. The plagioclase crystals have a bladed shape and are randomly orientated. The clinopyroxene crystals have a blocky shape and in a very small amount the larger plagioclase grains enclose the smaller pyroxene grains forming a poikilitic texture. The presence of secondary mineral indicates the rock has undergone alteration. In some cases the secondary minerals occur as round filled in vesicles.

Rock type: Basalt

PF06123 – Maningoza dyke swarm

Grain size(mm)	Modal %	Mineral	Description
Phenocryst	*70*		
0.5-2.0	70	Feldspar	Subhedral
Matrix	*30*		
0.3-0.7	20	Quartz	Anhedral
0.2-1.0	5	Opaques	Subhedral, magnetite, hematite
0.4-0.6	5	Epidote	Secondary, subhedral to anhedral

Texture: The rock is fine grained with an inequigranular (porphyritic) texture. The feldspars exhibit a brown alteration type texture. The presence of the secondary epidote is an indication of alteration.

Rock type: Rhyolite

PF060124 – Maningoza dyke swarm

Grain size(mm)	Modal %	Mineral	Description
1.0-2.5	45	Plagioclase	Euhedral-subhedral, extinction angle = 5°, An_{12} = oligoclase, lamellar twinning
<0.5	35	Clinopyroxene	Light brown colour, subhedral, 2V angle = 60°, sign = +ve, composition = augite/diopside
0.4-0.8	20	Opaques	Subhedral, magnetite, hematite
<0.5	<1	Epidote	Secondary, yellow-green pleochroism

Texture: The rock is fine to medium grained with an inequigranular texture. The plagioclase crystals are bladed in shape and are randomly orientated. The clinopyroxene grains are blocky in shape. There is a small amount of plagioclase laths penetrating clinopyroxene grains to form a subophitic texture.

Rock type: Dolerite

PF06125 – Maningoza dyke swarm

Grain size(mm)	Modal %	Mineral	Description
0.5-1.2	60	Plagioclase	Euhedral to subhedral, extinction angle = 15°, An_{22} = oligoclase, lamellar twinning
0.2-0.4	20	Opaques	Subhedral to anhedral, magnetite
0.3-0.7	15	Clinopyroxene	Light brown colour, subhedral, 2V angle = 35°, sign = +ve, composition = augite
0.4-0.6	<5	Chlorite	Secondary, anhedral

Texture: The rock is fine to medium grained and has an inequigranular texture. The plagioclase grains are bladed in shape and have a random orientation. The pyroxene grains have a blocky shape. The plagioclase laths and clinopyroxene grains do not enclose one another and form no poikilitic texture. The plagioclase laths also seem to create a spherulite texture. The presence of the secondary mineral chlorite is an indication of alteration.

Rock type: Dolerite

PF06126 – Ambolodia

Grain size(mm)	Modal %	Mineral	Description
<2.5	60	Plagioclase	Subhedral to anhedral, lamellar twinning
0.3-0.6	20	Clinopyroxene	Anhedral, light brown colour
0.3-0.5	10	Epidote	Subhedral to anhedral
0.2-0.4	5	Opaque	Anhedral, magnetite, hematite
0.3-0.7	<5	Chlorite	Subhedral to anhedral
0.2	Tr.	Amphibole	Anhedral, light green in colour

Texture: The rock is fine grained and has an inequigranular texture. The plagioclase crystals are bladed in shape and have a random orientation. The clinopyroxene grains are blocky in shape. The plagioclase and clinopyroxene do not enclose one another and form no poikilitic texture. The presence of secondary minerals indicates that the rock has undergone alteration.

Rock type: Andesite

PF06127 – Ambolodia

Grain size(mm)	Modal %	Mineral	Description
<0.3	40	Plagioclase	Anhedral
<0.2	30	Clinopyroxene	Light brown colour, anhedral
0.2-0.4	15	Opaques	Subhedral to anhedral, magnetite
0.4-0.6	5	Chlorite	Secondary, anhedral
0.3-0.6	10	Epidote	Secondary, subhedral

Texture: The rock is fine grained and has an inequigranular texture. The plagioclase crystals have a bladed shape and have a random orientation. The clinopyroxene grains are blocky in shape. The plagioclase and clinopyroxene show no poikilitic texture. The presence of secondary minerals indicates that the rock has undergone alteration. The chlorite grains sometimes occur as filled in spherical vesicles forming an amygdaloidal texture.

Rock type: Basalt

PF06128 – Ambolodia

Grain size(mm)	Modal %	Mineral	Description
0.5-1.3	60	Plagioclase	Subhedral, lamellar twinning
<0.5	20	Opaques	Subhedral, magnetite
0.3-0.8	20	Clinopyroxene	Brown in colour, subhedral
0.4	<1	Chlorite	Secondary, anhedral

Texture: The rock is fine grained and an equigranular texture. The plagioclase crystals are bladed in shape and have a random orientation. The clinopyroxene crystals have a blocky shape.

Rock type: Andesite

PF06129 – Antanetilava

Grain size(mm)	Modal %	Mineral	Description
Phenocryst	*20*		
>5	20	Plagioclase	Euhedral to subhedral, extinction angle = 40°, An_{78} = bytownite, lamellar twinning
Matrix	*80*		
0.5-1.0	20	Plagioclase	Euhedral to subhedral, extinction angle = 40°, An_{78} = bytownite, lamellar twinning
0.6-1.4	40	Clinopyroxene	Green to brown in colour, euhedral to subhedral, 2V angle = 30° sign = +ve, composition = augite
0.4-0.6	7	Opaques	Subhedral, magnetite
0.8	6	Epidote	Secondary, subhedral
1.2	7	Chlorite	Secondary, anhedral

Texture: The rock is fine to medium grained and has an inequigranular (seriate) texture. The plagioclase occurs as large phenocrysts and as smaller bladed crystals with random orientation. The clinopyroxene grains are blocky in shape. The phenocrysts of plagioclase enclose the smaller clinopyroxene grains forming a ophitic texture. The presence of the secondary minerals is an indication of alteration.

Rock type: Feldspar basalt

PF06130 – Antanetilava

Grain size(mm)	Modal %	Mineral	Description
Phenocryst	*45*		
>3.0	45	Clinopyroxene	Green to brown in colour, euhedral, 2V angle = 45°, sign = +ve, composition = augite
Matrix	*55*		
1.0-1.5	35	Plagioclase	Euhedral to subhedral, extinction angle = 0°, An_{12} = oligoclase, lamellar twinning
0.5-2.0	15	Chlorite	Secondary, subhedral
1.0	5	Opaques	Euhedral to subhedral, magnetite

Texture: The rock is medium grained and has an inequigranular (seriate) texture. The clinopyroxene grains occur as phenocrysts and enclose the smaller plagioclase grains forming an ophitic and subophitic texture. The plagioclase grains are bladed in shape and have a random orientation. The clinopyroxene grains are blocky in shape. The substantial presence of chlorite indicates that the rock has undergone alteration.

Rock type: Dolerite

PF06131 – Antanetilava

Grain size(mm)	Modal %	Mineral	Description
<0.5	40	Plagioclase	Anhedral
0.3-0.6	20	Opaques	Subhedral, magnetite, hematite
0.4-0.6	<20	Quartz	Anhedral
0.5-0.6	8	Amphibole	Clear in colour, anhedral
0.5	<6	Epidote	Secondary, subhedral
0.5	<6	Chlorite	Secondary, anhedral
0.4	<1	Calcite	Secondary, subhedral

Texture: The rock is fine grained with an inequigranular texture. The plagioclase shows a brown alteration type texture. The presence of secondary minerals is an indication of alteration.

Rock type: Dacite

PF06132 – Antanetilava

Grain size(mm)	Modal %	Mineral	Description
Phenocryst	*55*		
>5.0	55	Plagioclase	Euhedral, repeated lamellar twinning
Matrix	*45*		
0.4-1.2	15	Plagioclase	Euhedral, lamellar twinning
1.0-2.0	15	Clinopyroxene	Euhedral, brown in colour
0.4-0.7	10	Opaques	Subhedral, magnetite
0.5-0.8	5	Chlorite	Secondary, anhedral

Texture: The rock is medium grained and has an inequigranular (seriate) texture showing plagioclase porphyry. The phenocrysts of plagioclase enclose smaller clinopyroxene grains showing a poikilitic texture and clinopyroxenes in the matrix enclose smaller plagioclase grains showing an ophitic and subophitic texture. The plagioclase crystals are bladed and tabular and the clinopyroxene crystals are blocky in shape. The presence of the secondary mineral chlorite is an indication of alteration.

Rock type: Feldspar basalt

PF06133 – Antanetilava

Grain size(mm)	Modal %	Mineral	Description
Phenocrysts	*20*		
0.5-1.2	8	Plagioclase	Euhedral
0.3-0.6	7	Opaques	Subhedral to anhedral, hematite
0.2-0.5	5	Amphibole	Euhedral, light brown to green in colour
0.5	<1	Chlorite	Subhedral, secondary
Matrix	*80*		
<0.4	30	Plagioclase	Anhedral
<0.4	30	Quartz	Anhedral
<0.4	20	Alkali-feldspar	Anhedral

Texture: The rock is fine grained with an inequigranular (porphyritic) texture. The phenocrysts of plagioclase enclose the phenocrysts of clinopyroxene giving a poikilitic type texture. The plagioclase and alkali-feldspar in the matrix show a brown alteration type of texture. The presence of the secondary mineral chlorite is an indication of alteration.

Rock type: Rhyolite

PF06134 – Antanetilava

Grain size(mm)	Modal %	Mineral	Description
Phenocryst	*5*		
0.5-1.0	<2	Alkali-feldspar	Subhedral
0.5-1.0	Tr.	Amphibole	Subhedral-anhedral, brown to green in colour
0.2-0.5	<3	Opaques	Anhedral, hematite
0.5	Tr.	Chlorite	Anhedral, secondary
Matrix	*95*		
<0.1	35	Alkali-feldspar	Anhedral
<0.1	30	Plagioclase	Anhedral
<0.2	30	Quartz	Subhedral to anhedral

Texture: The rock is fine grained and has an inequigranular (porphyritic) texture. The plagioclase and alkali-feldspar both have a brown alteration type texture and the phenocrysts grains are tabular in shape.

Rock type: Rhyolite

PF06135 – Antanetilava

Grain size(mm)	Modal %	Mineral	Description
0.2-0.7	40	Plagioclase	Euhedral to subhedral, lamellar twinning
<1.3	30	Clinopyroxene	Brown in colour, euhedral to subhedral
<0.3	20	Opaques	Subhedral, magnetite, hematite
0.2-0.4	10	Chlorite	Secondary, euhedral to subhedral

Texture: The rock is fine grained and has an equigranular texture. The plagioclase grains are bladed in shape and have a random orientation. The plagioclase grains and are embedded within the blocky clinopyroxene grains to form an ophtitc and subophitic texture. The presence of the secondary mineral chlorite is an indication of alteration.

Rock type: Basalt

PF06136 - Ambolodia

Grain size(mm)	Modal %	Mineral	Description
<0.5	40	Plagioclase	Subhedral, lamellar twinning
<0.3	30	Clinopyroxene	Subhedral to anhedral, brown in colour
0.5	20	Opaques	Subhedral, magnetite
0.2-0.5	10	Chlorite	Anhedral
0.2-0.6	1	Quartz	Veins, anhedral

Texture: The rock is fine grained and has an equigranular texture. The plagioclase grains are bladed in shape and have a random orientation. The clinopyroxene grains are blocky in shape and do not enclose the plagioclase laths (nor do the plagioclase grains enclose the clinopyroxene grains) forming no poikilitic texture. There is a small amount quartz veining present in the rock. The presence of secondary chlorite is an indication of alteration.

Rock type: Basalt

PF06138 – Dyke

Grain size(mm)	Modal %	Mineral	Description
0.5-2.0	50	Plagioclase	Subhedral, extinction angle = 30°, An_{43} = andesine, lamellar twinning
0.5-1.0	40	Clinopyroxene	Subhedral to anhedral, light brown colour, 2V angle = 0°, sign = +ve, composition = pigeonite
0.3-0.7	4	Opaques	Subhedral, magnetite
0.5	3	Chlorite	Subhedral, secondary
0.4-0.6	3	Olivine	Subhedral to anhedral

Texture: The rock is fine to medium grained and has an equigranular texture. The plagioclase grains are bladed in shape and are randomly orientated. The clinopyroxene grains are blocky in shape and do not enclose the plagioclase laths (nor do the plagioclase laths enclose the clinopyroxene grains) forming no poikilitic texture. The presence of the secondary mineral chlorite is an indication of alteration.

Rock type: Olivine dolerite

PF06142 – Antanetilava

Grain size(mm)	Modal %	Mineral	Description
<0.1-1.0	30	Alkali-feldspar	Subhedral to anhedral
<0.1-0.5	25	Quartz	Anhedral
<0.1-1.0	20	Plagioclase	Anhedral
<1.0	10	Clinopyroxene	Light brown in colour, anhedral
0.5-1.0	5	Chlorite	Anhedral
0.4-0.7	10	Opaque	Subhedral to anhedral, magnetite
0.2-0.3	Tr.	Amphibole	Anhedral, green to brown in colour

Texture: The rock is fine grained and has an equigranular texture. The plagioclase and alkali-feldspar grains are tabular in shape and show a brown alteration type texture. The clinopyroxene grains are blocky in shape do not enclose any plagioclase grains (nor do the plagioclase grains enclose the clinopyroxene grains) showing no poikilitic texture. The presence on secondary mineral chlorite is an indication of alteration.

Rock type: Trachyte

PF06143 – Antanetilava

Grain size(mm)	Modal %	Mineral	Description
0.5-1.5	50	Plagioclase	Subhedral, lamellar twinning
0.5-1.0	20	Clinopyroxene	Light brown in colour, Subhedral to anhedral
0.3-0.9	20	Opaques	Subhedral, magnetite
0.2-0.5	5	Chlorite	Subhedral to anhedral
0.2-0.4	5	Amphibole	Subhedral, light brown to green in colour

Texture: The rock is fine to medium grained and has an equigranular texture. The plagioclase grains are bladed in shape and have a random orientation. The plagioclase grains show a brown alteration texture and in some cases are enclosed by the blocky clinopyroxene grains forming a subophitic texture. The presence of chlorite is an indication of alteration.

Rock type: Andesite

PF06144 – Antanetilava

Grain size(mm)	Modal %	Mineral	Description
0.5-1.0	15	Alkali-feldspar	Euhedral to subhedral
0.5-1.0	50	Plagioclase	Euhedral to subhedral
0.2-0.5	20	Quartz	Subhedral
0.5	5	Chlorite	Subhedral to anhedral
0.2	<1	Epidote	Anhedral
0.5	10	Opaques	Subhedral, magnetite
0.2-0.4	Tr.	Amphibole	Anhedral, green in colour

Texture: The rock is fine grained and has an equigranular texture. The rock has a quenched texture observed by the plagioclase and alkali-feldspar grains. The plagioclase grains are prismatic and the alkali-feldspar grains are tabular in shape and both show a brown alteration type texture. The presence of secondary minerals is an indication of alteration.

Rock type: Rhyolite

PF06145 – Antanetilava

Grain size(mm)	Modal %	Mineral	Description
0.5-0.8	50	Plagioclase	Euhedral, extinction angle = -5°, An_{14} = oligoclase, lamellar twinning
0.6-1.0	40	Clinopyroxene	Light brown in colour, Euhedral to subhedral, 2V angle = 60°, sign = +ve, composition = augite/diopside
0.4-0.8	5	Opaques	Subhedral, magnetite
0.2-1.0	5	Olivine	Subhedral

Texture: The rock is fine grained and has an equigranular texture. The plagioclase grains are bladed in shape and have a random orientation. The clinopyroxene grains are blocky in shape and enclose some of the plagioclase grains forming a subophitic and ophitic texture. There is little or no evidence of alteration in this rock.

Rock type: Olivine basalt

PF06146 – Antanetilava

Grain size(mm)	Modal %	Mineral	Description
0.4-0.8	60	Plagioclase	Subhedral to anhedral, lamellar twinning
0.2-0.5	30	Opaques	Anhedral, magnetite, hematite
0.2-0.6	10	Clinopyroxene	Brown in colour, subhedral to anhedral
0.2-0.4	<1	Chlorite	Subhedral to anhedral, secondary

Texture: The rock is fine grained and has an equigranular texture. The plagioclase grains are bladed in shape and have a random orientation. The plagioclase grains also show a brown alteration type texture. The clinopyroxene grains are blocky in shape and do not enclose the plagioclase laths (nor do the plagioclase laths enclose the clinopyroxene grains) forming no poikilitic texture. The rock is an agglomerate of two different rock types of roughly the same composition and similar textures.

Rock type: Basalt breccia

PF06147 – Antanetilava

Grain size(mm)	Modal %	Mineral	Description
0.5	30	Quartz	Anhedral
0.5-1.5	35	Plagioclase	Euhedral to subhedral
0.5-1.5	20	Alkali-feldspar	Subhedral
0.4-0.7	5	Opaques	Subhedral to anhedral, magnetite
0.3	5	Chlorite	Secondary, anhedral
0.7	5	Epidote	Secondary, anhedral
0.3	Tr.	Biotite	Anhedral

Texture: The rock is fine grained and has an equigranular texture. The rock also has a quenched texture observed by the plagioclase grains. The plagioclase grains are bladed and prismatic in shape and have an orientation relating to the quenched texture. The plagioclase grains and the tabular alkali-feldspar grains both have a brown alteration type texture. The presence of secondary minerals is an indication of alteration.

Rock type: Rhyolite

PF06148 – Antanetilava

Grain size(mm)	Modal %	Mineral	Description
Phenocrysts	*40*		
2.0-5.0	40	Clinopyroxene	Light brown in colour, subhedral
Matrix	*60*		
0.5-1.0	50	Plagioclase	Subhedral to anhedral, lamellar twinning
0.4-0.8	10	Opaques	Subhedral, magnetite
0.3-0.6	<1	Chlorite	Subhedral to anhedral, secondary

Texture: The rock is medium grained and has an inequigranular (porphyritic) texture. The plagioclase grains are bladed and have a random orientation. The blocky clinopyroxene grains enclose the plagioclase grains showing an ophitic and subophitic texture. The plagioclase grains also exhibit some brown alteration staining.

Rock type: Dolerite

PF06149 – Antanetilava

Grain size(mm)	Modal %	Mineral	Description
0.4-0.8	30	Plagioclase	Anhedral
0.2-0.8	20	Quartz	Subhedral to anhedral
0.2-0.4	10	Opaques	Subhedral, magnetite, hematite
0.1-0.4	5	Amphibole	Light brown in colour, anhedral
0.4-0.8	30	Alkali-feldspar	Anhedral
0.1-0.3	<2	Chlorite	Secondary, anhedral
0.1-0.3	3	Epidote	Secondary, anhedral

Texture: The rock is fine grained and is equigranular. The plagioclase and alkali-feldspar grains both have an alteration type texture. The clinopyroxene and plagioclase grains are small and neither encloses the other forming no poikilitic texture. The presence of secondary minerals is an indication of alteration.

Rock type: Rhyolite

PF06150 – Antanetilava

Grain size(mm)	Modal %	Mineral	Description
0.3-0.5	55	Plagioclase	Subhedral to anhedral
0.1-0.3	35	Clinopyroxene	Brown in colour, anhedral
0.3-08	10	Opaques	Subhedral, magnetite
0.3-0.5	<1	Chlorite	Secondary, anhedral

Texture: The rock is fine grained and has an equigranular texture. The plagioclase grains are bladed in shape and have a random orientation. The blocky clinopyroxene grains and plagioclase grains are small and neither encloses the other forming no poikilitic texture.

Rock type: Basalt

PF06151 – Antanetilava

Grain size(mm)	Modal %	Mineral	Description
<0.2	35	Plagioclase	Anhedral
<0.4	30	Quartz	Anhedral
<0.2	25	Alkali-feldspar	Anhedral
0.3-0.7	5	Opaques	Subhedral, magnetite
0.3-0.6	<5	Chlorite	Secondary, subhedral
0.2-0.4	Tr.	Amphibole	Light brown in colour, Anhedral

Texture: The rock is fine grained and has equigranular texture. The alkali-feldspar and plagioclase both have a brown alteration type texture. The presence of the secondary mineral chlorite is an indication of alteration.

Rock type: Rhyolite

PF06152 – Antanetilava

Grain size(mm)	Modal %	Mineral	Description
<0.3	30	Plagioclase	Anhedral
<0.3	30	Alkali-feldspar	Anhedral
<0.4	30	Quartz	Anhedral
0.3-0.8	10	Opaques	Subhedral, magnetite
0.3-0.5	Tr.	Amphibole	Light brown in colour, anhedral
0.5	Tr.	Biotite	Brown pleochroic, Subhedral to anhedral

Texture: The rock is fine grained and has an equigranular texture. The rock has a Lapilli texture with diameters ranging from 2mm to 20mm. The plagioclase and alkali-feldspar both have a brown alteration type texture.

Rock type: Rhyolite

PF06153 – Antanetilava

Grain size(mm)	Modal %	Mineral	Description
Phenocryst	*30*		
<3.0	30	Clinopyroxene	Light brown in colour, Subhedral
Matrix	*70*		
<0.6	30	Plagioclase	Subhedral
0.4-0.7	20	Opaques	Subhedral, magnetite, hematite
0.4-0.8	20	Chlorite	Secondary, anhedral

Texture: The rock is medium grained and has an inequigranular (porphyritic) texture. The plagioclase grains are bladed in shape and have a random orientation. The blocky shaped clinopyroxene grains enclose the plagioclase grains forming a subophitic and ophitic texture. The large amount of secondary chlorite indicates a high level of alteration.

Rock type: Dolerite/basalt

PF06154 – Antanetilava

Grain size(mm)	Modal %	Mineral	Description
<0.5	35	Plagioclase	Anhedral
<0.4	30	Quartz	Subhedral to anhedral
<0.5	30	Alkali-feldspar	Anhedral
0.2-0.6	<1	Amphibole	Light brown colour, Anhedral
0.3-0.5	<1	Chlorite	Anhedral, secondary
0.3-0.8	<5	Opaques	Subhedral, magnetite

Texture: The rock is fine grained and has an equigranular texture. The plagioclase and alkali-feldspar both have a brown alteration type texture. The clinopyroxene grains and feldspar grains do not enclose each other and form no poikilitic texture.

Rock type: Rhyolite

ABF052 – Ambohitrosy

Grain size(mm)	Modal %	Mineral	Description
Phenocrysts	*10*		
<1.0	7	Epidote	Secondary, subhedral
<1.5	3	Chlorite	Secondary, subhedral to anhedral
Matrix	*90*		
<0.2	40	Chlorite	Secondary, subhedral
<0.2	30	Epidote	Secondary, subhedral
<0.2	15	Opaques	Subhedral to anhedral, magnetite
<0.2	5	Plagioclase	Subhedral to anhedral

Texture: The rock is fine grained with an overall inequigranular (porphyritic) texture. The minerals in the matrix are equigranular in texture. The secondary minerals make up most of the rock showing that the rock has undergone a large amount of alteration.

Rock type: Basalt

ABF057 – Ambohitrosy

Grain size(mm)	Modal %	Mineral	Description
Phenocrysts	*10*		
>5.0	10	Clinopyroxene	Brown in colour, euhedral, 2V angle = 30°, optic sign = +ve, composition = augite
Matrix	*90*		
1.0-3.0	70	Plagioclase	Euhedral, extinction angle = 40°, An_{78} = bytownite, repeated lamellar twinning
1.0-2.0	5	Clinopyroxene	Brown in colour, euhedral, 2V angle = 30°, optic sign = +ve, composition = augite
1.0-1.5	10	Opaques	Euhedral, magnetite
<1.0	5	Chlorite	Secondary, subhedral

Texture: The rock is coarse grained with an inequigranular (porphyritic) texture. The plagioclase grains are bladed in shape and have a random orientation. Zoning also occurs in certain plagioclase grains. The clinopyroxene grains are blocky in shape and enclose the plagioclase grains forming an ophitic and subophitic texture. The presence of the secondary mineral chlorite is an indication of alteration.

Rock type: Feldspar gabbro

ABF058 – Ambohitrosy

Grain size(mm)	Modal %	Mineral	Description
Phenocrysts	*30*		
>4.0	30	Clinopyroxene	Brown in colour, subhedral, 2V angle = 30°, optic sign = +ve, composition = augite
Matrix	*70*		
1.0-1.5	30	Plagioclase	Euhedral to subhedral, extinction angle = 40°, An_{78} = bytownite, lamellar twinning
1.0-1.5	25	Clinopyroxene	Brown in colour, subhedral, 2V angle = 30°, optic sign = +ve, composition = augite
0.5-1.3	10	Opaques	Euhedral to subhedral, magnetite
0.5-1.0	5	Chlorite	Secondary, anhedral
0.5	Tr.	Biotite	Brown pleochroic, anhedral

Texture: The rock is coarse grained and has an inequigranular (porphyritic) texture with phenocrysts of clinopyroxene. The plagioclase grains and clinopyroxene grains do not enclose one another forming no poikilitic texture. The plagioclase grains are bladed and have a random orientation. The presence of chlorite indicates that the rock has undergone alteration.

Rock type: Gabbro

ABF060 – Ambohitrosy

Grain size(mm)	Modal %	Mineral	Description
>1.0	80	Alkali-feldspar	Euhedral to subhedral, reaction rims
1.0-2.0	15	Opaques	Euhedral to subhedral, magnetite
1.0-3.0	5	Plagioclase	Euhedral to subhedral

Texture: The rock is coarse grained and is equigranular in texture. The alkali-feldspar grains are tabular in shape and show a small amount of brown alteration.

Rock type: Syenite

ABF063 – Ambohitrosy

Grain size(mm)	Modal %	Mineral	Description
<0.2	40	Plagioclase	Subhedral, lamellar twinning
<0.2	30	Clinopyroxene	Brown in colour, subhedral
<0.2	10	Opaques	Subhedral, magnetite
<0.2	20	Chlorite	Secondary, subhedral

Texture: The rock is fine grained and has an equigranular texture. The plagioclase grains are bladed in shape and have a random orientation. There is no poikilitic texture with the blocky shaped clinopyroxene. The presence of the secondary mineral chlorite indicates that the rock has undergone alteration.

Rock type: Basalt

ABF066 – Ambohitrosy

Grain size(mm)	Modal %	Mineral	Description
Phenocrysts	*10*		
1.0-1.5	10	Opaques	Euhedral, magnetite
Matrix	*90*		
<0.2	40	Plagioclase	Subhedral
<0.2	30	Quartz	Subhedral
<0.2	20	Alkali-feldspar	Subhedral

Texture: The rock is fine grained and has an inequigranular (porphyritic) texture. The plagioclase grains are prismatic in shape and show a quenched type of texture. The alkali-feldspar grains are tabular and both feldspars show a brown alteration type texture.

Rock type: Rhyolite

ABF074 – Ambohitrosy

Grain size(mm)	Modal %	Mineral	Description
1.0-3.0	40	Plagioclase	Subhedral, perthite texture
1.0-2.5	30	Quartz	Subhedral
1.0-3.0	20	Alkali-feldspar	Subhedral, perthite texture
0.5-2.0	6	Amphibole	Euhedral, green pleochroic
0.5-2.0	4	Chlorite	Euhedral, secondary

Texture: The rock is coarse grained with an equigranular texture. The plagioclase grains and alkali-feldspar grains are tabular in shape. The presence of the secondary mineral chlorite is an indication that the rock has undergone alteration.

Rock type: Granite

ABF075 – Ambohitrosy

Grain size(mm)	Modal %	Mineral	Description
1.5-2.5	25	Plagioclase	Subhedral to anhedral, reaction rims
1.0-2.0	30	Quartz	Subhedral
1.5-2.5	30	Alkali-feldspar	Subhedral to anhedral, reaction rims
0.3-0.8	7	Opaques	Anhedral
0.4-0.8	5	Amphibole	Subhedral, green to yellow in colour
0.4-0.9	3	Chlorite	Anhedral, secondary

Texture: The rock is coarse grained with an equigranular texture. The plagioclase and alkali-feldspar grains are tabular in shape. The presence of the secondary mineral chlorite indicates that the rock has undergone alteration.

Rock type: Granite

ABF076 – Ambohitrosy

Grain size(mm)	Modal %	Mineral	Description
1.0-4.0	30	Alkali-feldspar	Euhedral to subhedral
0.5-2.0	30	Quartz	Euhedral to subhedral
1.0-4.0	20	Plagioclase	Euhedral to subhedral
0.5-2.0	10	Amphibole	Subhedral, green pleochroic
<0.5	<5	Opaques	Anhedral
0.5-2.0	5	Chlorite	Secondary, subhedral

Texture: The rock is coarse grained and has an equigranular texture. The plagioclase and alkali-feldspar grains both a tabular shape. The presence of the secondary mineral chlorite indicates that the rock has undergone alteration.

Rock type: Granite

BY6F091 – Sambao

Grain size(mm)	Modal %	Mineral	Description
Phenocrysts	*15*		
08-1.2	8	Plagioclase	Subhedral to anhedral, extinction angle = 15°, An_{31} = andesine, zoning, lamellar twinning
07-1.0	5	Clinopyroxene	Light brown colour, subhedral to anhedral
0.8-1.1	2	Olivine	Subhedral to anhedral
0.5-0.7	Tr.	Chlorite	Anhedral, secondary
Matrix	*85*		
<0.2	35	Plagioclase	Anhedral, extinction angle = 15°, An_{31} = andesine
<0.2	35	Clinopyroxene	Light brown colour, anhedral
<0.2	10	Opaques	Subhedral, magnetite

Texture: The rock is fine grained and has an inequigranular (porphyritic) texture. The plagioclase grains are bladed in shape and have a random orientation. The plagioclase and the blocky shaped clinopyroxene grains do not enclose one another forming no poikilitic texture.

Rock type: Olivine basalt

BY6F 098B – Sambao

Grain size(mm)	Modal %	Mineral	Description
Phenocrysts	*40*		
>3.0	15	Plagioclase	Subhedral to anhedral, reaction rims, perthite texture, cross-hatch twinning
>3.0	15	Alkali-feldspar	Subhedral to anhedral, reaction rims, perthite texture,
1.0-2.0	10	Quartz	Anhedral
Matrix	*60*		
<0.2	15	Plagioclase	Subhedral
<0.2	20	Alkali-feldspar	Subhedral
<0.2	10	Quartz	Subhedral
<0.3	10	Opaques	Subhedral, magnetite, hematite
<0.5	5	Chlorite	Secondary, anhedral

Texture: The rock is fine grained and has an inequigranular (porphyry) texture. The plagioclase and alkali-feldspar grains are tabular in shape and show an alteration texture. The presence of the secondary mineral chlorite is an indication of alteration.

Rock type: Feldspar rhyolite

BY6F102 – Sambao

Grain size(mm)	Modal %	Mineral	Description
0.9-1.5	40	Plagioclase	Euhedral to subhedral, extinction angle = 0°, An_{21} = oligoclase, lamellar twinning
0.4-1.0	30	Clinopyroxene	Brownish red in colour, subhedral, 2V angle = 0°, sign = +ve, composition = pigeonite
0.5-0.7	13	Chlorite	Secondary , anhedral
0.3-0.6	10	Opaques	Euhedral to subhedral, magnetite
0.2-0.8	7	Olivine	Subhedral

Texture: The rock is fine to medium grained and has an equigranular texture. The plagioclase grains are bladed in shape and have a random orientation. The plagioclase grains enclose some of the blocky shaped clinopyroxene grains forming a poikilitic texture. The large amount of the secondary mineral chlorite indicates alteration has taken place.

Rock type: Olivine basalt

BY6F103 – Sambao

Grain size(mm)	Modal %	Mineral	Description
Phenocryst	*6*		
1.0-1.5	5	Plagioclase	Subhedral, lamellar twinning
0.8-1.2	1	Calcite	Anhedral, secondary
Matrix	*94*		
<0.2	50	Plagioclase	Subhedral to anhedral
<0.2	29	Calcite	Secondary, anhedral
<0.2	15	Opaques	Subhedral, magnetite

Texture: The rock is fine grained and has an inequigranular (porphyritic) texture. The plagioclase grains are bladed in shape and have a random orientation. The large amount of the secondary mineral calcite indicates a high level of alteration.

Rock type: Basalt

BY6F106 – Sambao

Grain size(mm)	Modal %	Mineral	Description
Phenocrysts	*15*		
0.5-1.5	5	Quartz	Anhedral, rounded
0.5-4.0	5	Alkali-feldspar	Anhedral
0.5-3.5	5	Plagioclase	Anhedral, lamellar twinning
Matrix	*85*		
n/a	85	Glass/obsidian	Yellowy brown in colour

Texture: The rock is very fine grained and has an inequigranular (vitrophyric) texture.

Rock type: Glass/obsidian

BY6F107 – Sambao

Grain size(mm)	Modal %	Mineral	Description
0.5-2.0	50	Plagioclase	Subhedral, extinction angle = 10°, An_{26} = oligoclase, lamellar twinning
0.6-1.0	25	Clinopyroxene	Reddish brown colour, subhedral
0.3-0.5	10	Olivine	Subhedral to anhedral
0.3-0.5	8	Opaques	Subhedral, magnetite
0.4-0.6	7	Chlorite	Anhedral, secondary

Texture: The rock is fine grained and has an equigranular texture. The plagioclase grains are bladed in shape and have a random orientation. The blocky shaped clinopyroxene grains and the plagioclase laths do not enclose each other forming no poikilitic texture. The presence of the secondary mineral chlorite indicates alteration.

Rock type: Olivine basalt

MI06004A – Cretaceous dyke

Grain size(mm)	Modal %	Mineral	Description
0.2-2.4	40	Plagioclase	An_{67} = labradorite; subhedral
0.2-1.2	30	Clinopyroxene	Augite; anhedral; brown; simple twinning
<0.2-0.4	20	Calcite	Anhedral; vesicular in places
<0.02	<5	Quartz	Subhedral to anhedral; undulose extinction (strain shadows)
<0.2	5	Opaques	Anhedral; magnetite, ilmenite

Texture: The fine- to medium-grained (0.2-0.4 mm), inequigranular interlobate rock has randomly oriented “spiky” plagioclase laths (infrequently phenocrystic) embedded in anhedral augite. Augite and/or plagioclase possibly alters to calcite. Vesicles of well-cleaved rhombohedral calcite are surrounded by rims of calcite aggregates.

Rock type: Quartz dolerite

MI06006 – Fonjay

Grain size(mm)	Modal %	Mineral	Description
0.2-2.4	50	Plagioclase	An_{67} = labradorite; subhedral to anhedral; albite & carlsbad twins, rare pericline twins
0.2-3.6	42	Clinopyroxene	Augite; anhedral; colourless to pale brown; simple twinning
0.2-1.2	<5	Opaques	Magnetite, ilmenite, pyrite/chalcopyrite, pyrrhotite?
<0.01	<3	Quartz	Anhedral to subhedral; strain shadows

Texture: This rock is medium-grained (1.0-1.5 mm) and display a granoblastic (granitic) texture in which labradorite and augite are intergrown. Augite rims commonly are altered to

calcite and equigranular opaques encloses other grains. Where plagioclase and augite alters to calcite, these grains form a granophyric intergrowth with opaque minerals.

Rock type: Quartz gabbro

MI06007A – Fonjay

Grain size(mm)	Modal %	Mineral	Description
<0.2-1.0	44	Plagioclase	An_{55} = labradorite; subhedral to anhedral; albite & carlsbad twins
0.2-4.0	30	Clinopyroxene	Augite; subhedral to anhedral; colourless to grey; untwinned; zoned
<0.1-0.4	14	Olivine	Intermediate Fe-Mg composition; subhedral to anhedral
<0.1-1.2	10	Opaques	Anhedral
<0.1	<1	Chlorite	Subhedral to anhedral; high relief; high birefringence
<0.1	<1	Biotite	Subhedral; alteration product?

Texture: The inequigranular rock is fine- to medium-grained (0.5-1.5 mm). Aggregates of granoblastic labradorite are vesicle-shaped with coarser grains surrounded by a fine groundmass of plagioclase. Plagioclase grains tend to be coarser where clinopyroxene is absent. Augite mostly forms phenocrysts (porphyroblastic) and is surrounded by fine aggregates of olivine and plagioclase.

Rock type: Olivine gabbro

MI06007B – Fonjay

Grain size(mm)	Modal %	Mineral	Description
<0.1-1.0	45	Plagioclase	An_{57} = labradorite; subhedral to anhedral; mostly albite twins, rare carlsbad twins; granoblastic
<0.1-1.0	25	Clinopyroxene	Augite; anhedral; weakly pleochroic brown; untwinned
<0.1	15	Olivine	Subhedral to anhedral; high relief; high birefringence
<0.1-0.4	10	Opaques	Anhedral; probably ilmenite, magnetite
<0.1	<5	Biotite	Orange-brown; no cleavage; present with augite

Texture: This rock is inequigranular and fine-grained (0.2-0.4 mm). Labradorite forms “spiky“ laths in a matrix of augite and olivine. Areas dominated by fine aggregates of olivine are close in contact with augite and notably devoid of plagioclase. Both augite and labradorite are porphyroblastic in places.

Rock type: Olivine dolerite (microgabbro)

MI06008 – Fonjay

Grain size(mm)	Modal %	Mineral	Description
0.1-12.0	42	Plagioclase	An_{75} = bytownite; subhedral to euhedral; combination of albite, carlsbad & pericline twins; granoblastic
0.5-12.0	32	Clinopyroxene	Augite; subhedral to anhedral; pale green to pink pleochroic
<0.5-2.0	<5	Orthopyroxene	Enstatite; subhedral to anhedral; red-brown
<0.1-0.4	13	Chlorite,Sericite	Subhedral to anhedral; aggregates
<0.1-1.0	5	Opaques	Magnetite, ilmenite
<0.8	<2	Calcite	Subhedral to anhedral
<0.4	<1	Quartz	Anhedral

Texture: The rock is medium-grained (2.5-3.0 mm) and has a blocky texture. Plagioclase show zoning (oscillatory twinning) and alters to calcite. Pyroxene alters to aggregates of chlorite and sericite.

Rock type: Orthopyroxene gabbro

MI06009 – Fonjay

Grain size(mm)	Modal %	Mineral	Description
0.5-12.0	50	Plagioclase	An_{80} = bytownite; euhedral to subhedral; combination of albite, carlsbad & pericline twins; zoned
0.5-3.0	20	Orthopyroxene	Enstatite; subhedral to anhedral; pale yellow-brown
<0.1-1.0	10	Chlorite	Subhedral to anhedral
<0.1-2.0	10	Opaques	Magnetite, ilmenite; anhedral
0.5-4.0	7	Clinopyroxene	
0.1-0.8	<3	Biotite	

Texture: The inequigranular rock is medium-grained (1.0-1.5 mm) and has a interlobate to polygonal texture. Complex twins are in plagioclase. Plagioclase grains are zoned and display oscillatory twinning with an euhedral core. Augite alters mainly to chlorite. The pyroxene formed as an interstitial last phase.

Rock type: Gabbronorite

MI06010 – Fonjay

Grain size(mm)	Modal %	Mineral	Description
<0.1-3.0	45	Plagioclase	An_{62} = labradorite; euhedral to subhedral; complex albite, carlsbad & pericline twins
0.1-4.0	25	Clinopyroxene	Augite; subhedral to anhedral; rare twins
<0.1-0.2	20	Olivine	Anhedral; interstitial
<0.5	10	Opaques	Magnetite, ilmenite, pyrite, pyrrhotite?; anhedral

Texture: The medium-grained (1.0 mm) rock is inequigranular and has a interlobate to polygonal texture. Plagioclase grains display complex twins and larger euhedral phenocrysts are set in a matrix of randomly oriented plagioclase and interstitial augite and olivine.

Rock type: Olivine gabbro

MI06011 – Fonjay

Grain size(mm)	Modal %	Mineral	Description
0.4-3.0	70	Plagioclase	An_{77} = bytownite; euhedral to subhedral; combination of albite, carlsbad & pericline twins
0.2-5.0	20	Clinopyroxene	Augite; anhedral; multiple twins; colourless to grey
<0.1	<5	Chlorite,Calcite	Subhedral to anhedral; rims augite
<0.1	<5	Opaques	Subhedral to anhedral; magnetite (2%), ilmenite (2%), pyrrhotite?, pyrite (1%)

Texture: The inequigranular rock is medium-grained (1.5-2.0 mm) and has a interlobate to polygonal texture. Larger plagioclase phenocrysts are set in a matrix of plagioclase and augite Plagioclase grains are granoblastic in places. Augite alters to chlorite and calcite which forms a rim around the pyroxene and also fills cracks and the parting cleavage of the pyroxene.

Rock type: Gabbro

MI06012 – Fonjay

Grain size(mm)	Modal %	Mineral	Description
0.4-3.0	78	Plagioclase	Labradorite, bytownite & rare anorthite; euhedral to subhedral; complex albite, carlsbad & pericline twins
0.2-3.0	12	Clinopyroxene	Augite; subhedral to anhedral; colourless to grey
<0.3	<3	Orthopyroxene	Enstatite; subhedral to anhedral; higher relief than clinopyroxene
<0.1	<5	Chlorite,Calcite	Subhedral to anhedral
<0.1	<2	Opaques	Ilmenite; anhedral

Texture: The rock is medium-grained (1.0 mm) and has an inequigranular interlobate to polygonal texture. Augite alters to chlorite and calcite which forms a rim around the pyroxene. Plagioclase grains are granoblastic in places and display complex twinning. Multiple twins are present in pyroxene.

Rock type: Orthopyroxene gabbro

MI06013 – Fonjay

Grain size(mm)	Modal %	Mineral	Description
0.2-4.0	77	Plagioclase	An_{67} = labradorite; euhedral to subhedral; combination of albite, carlsbad & pericline twins
0.2-3.0	17	Clinopyroxene	Augite; anhedral; multiple twins; colourless to pale brown; well cleaved
0.4-2.0	3	Orthopyroxene	Enstatite; anhedral; colourless; higher relief than clinopyroxene
<0.1	2	Chlorite	Subhedral to anhedral; pleochroic brown
<0.1	1	Opaques	Pyrite/chalcopyrite; anhedral

Texture: The medium-grained (1.0-1.5 mm) rock is inequigranular and has a interlobate to polygonal texture. Plagioclase grains display complex twins and plagioclase inclusions are common in augite. Clinopyroxene tends to surround orthopyroxene. Enstatite alters to chlorite

Rock type: Orthopyroxene gabbro

MI06014 – Ambereny

Grain size(mm)	Modal %	Mineral	Description
0.1-10.0	67	Plagioclase	An_{67} = labradorite; subhedral to anhedral; mostly albite twins, lesser pericline twins
<0.1-0.5	20	Clinopyroxene	Augite; subhedral to anhedral
<0.1-0.4	10	Orthopyroxene	Enstatite; subhedral to anhedral; lower birefringence and higher relief than clinopyroxene
<0.1-.04	3	Opaques	Magnetite, ilmenite; subhedral to anhedral

Texture: This rock is inequigranular, fine- to medium-grained (0.2-1.5 mm) and forms an interlobate to polygonal texture. Porphyritic phenocrysts of subhedral labradorite is set in an equigranular granoblastic matrix of pyroxene and plagioclase. Large phenocrysts of plagioclase display undulatory extinction.

Rock type: Gabbronorite

MI06015 – Ambereny

Grain size(mm)	Modal %	Mineral	Description
0.1-1.4	45	Plagioclase	Subhedral to anhedral; albite & pericline twins, compositionally zoned
0.1-1.5	35	Quartz	Subhedral to anhedral
0.1-1.5	10	Hornblende	Subhedral to anhedral; pleochroic green-brown to green
0.1-1.0	<5	K-feldspar	Subhedral to anhedral; core of zoned plagioclase
<0.1-0.4	<4	Opaques	Magnetite; anhedral
<0.1	<1	Biotite	Subhedral

Texture: The inequigranular rock is fine- to medium-grained (0.1-1.5 mm) and has an interlobate and granophyric texture. Intergrown plagioclase and quartz forms vermicular grains/blebs. Hornblende alters to biotite.

Rock type: Tonalite

MI06016 – Ambereny

Grain size(mm)	Modal %	Mineral	Description
0.1-1.4	45	Plagioclase	Subhedral to anhedral; albite & pericline twins
0.1-1.5	35	Quartz	Subhedral to anhedral
0.1-1.5	10	K-feldspar	Subhedral to anhedral; core of zoned plagioclase
0.1-1.0	5	Hornblende	Subhedral to anhedral
<0.1-0.4	<3	Opaques	Magnetite; anhedral
<0.1	<2	Biotite	Subhedral to anhedral

Texture: The fine- to medium-grained (0.1-1.5 mm) inequigranular rock has an interlobate texture. Hornblende alters to biotite.

Rock type: Granodiorite/Tonalite

MI06017 – Ambereny

Grain size(mm)	Modal %	Mineral	Description
0.2-10.0	45	Plagioclase	An_{60} = labradorite; subhedral; combination of albite, carlsbad & pericline twins; compositionally zoned
0.2-3.0	35	Clinopyroxene	Augite; anhedral; pale brown
0.2-1.5	10	Orthopyroxene	Enstatite; anhedral; pale brown; higher relief than clinopyroxene
<0.1-2.0	5	Opaques	Magnetite, ilmenite, pyrrhotite?, pyrite/chalcopyrite; subhedral to anhedral
<0.2	3	Chlorite	Subhedral; clusters/aggregates
<0.2	2	Biotite	Rare; associated with chlorite

Texture: The rock is fine- to medium-grained (0.2-1.5 mm) and has an inequigranular interlobate to polygonal and porphyritic texture. Large phenocrysts of plagioclase are set in a groundmass of pyroxene and plagioclase. Enstatite alters to chlorite and biotite which replaces the orthopyroxene crystals. Interstitial pyroxene (especially clinopyroxene) are in the labradorite and augite. The plagioclase grains have a lath-like habit.

Rock type: Gabbronorite

MI06018 – Ambereny

Grain size(mm)	Modal %	Mineral	Description
0.2-4.0	50	Plagioclase	An_{62} = labradorite; subhedral; complex albite, carlsbad & pericline twins
0.4-2.0	36	Clinopyroxene	Augite; anhedral; pale brown; simple twins
0.2-2.0	7	Orthopyroxene	Enstatite; anhedral; pale brown
<0.1-2.0	3	Opaques	Magnetite, ilmenite?; subhedral to anhedral
<0.2	3	Chlorite	Subhedral; clusters/aggregates
<0.2	1	Biotite	Rare; associated with chlorite

Texture: The rock is fine- to medium-grained (0.2-1.0 mm) and has an inequigranular interlobate to polygonal and porphyritic texture. Large phenocrysts of plagioclase are set in a groundmass of pyroxene and plagioclase. Enstatite alters to chlorite and biotite.

Rock type: Gabbronorite

MI06019 – Ambereny

Grain size(mm)	Modal %	Mineral	Description
0.4-4.0	50	Plagioclase	An_{60} = labradorite; euhedral to subhedral; combination of albite, carlsbad & pericline twins; compositionally zoned
0.5-3.0	40	Olivine	Anhedral
0.2-1.0	2	Clinopyroxene	Augite?; subhedral to anhedral; pale brown
0.4-1.0	2	Orthopyroxene	Enstatite?; subhedral to anhedral; pale brown
<0.1	3	Chlorite	Subhedral; clusters/aggregates
<0.1-1.0	3	Opaques	Magnetite, ilmenite, pyrite/chalcopyrite, pyrrhotite?; anhedral; interstitial

Texture: This fine- to medium-grained (0.5-2.0 mm) rock is inequigranular and has an polygonal to interlobate texture. Roughly aligned tabular plagioclase are platy in habit and form a mosaic of interlocking grains. Orthopyroxene alters to chlorite and lesser calcite which replaces the orthopyroxene crystals. Olivine alters to serpentinite and carbonates which forms a rims around the anhedral crystal of olivine.

Rock type: Troctolite

MI06020A – Ambereny

Grain size(mm)	Modal %	Mineral	Description
0.4-2.0	45	Plagioclase	An_{60} = labradorite; euhedral to subhedral; albite & carlsbad twins, compositionally zoned; porphyritic
<0.1-2.7	35	Quartz	Anhedral
0.2-0.5	8	K-feldspar	Euhedral to subhedral; core of zoned plagioclase
0.2-2.0	7	Hornblende	Subhedral to anhedral; pleochroic green; poor cleavage; simple twins
<0.1-0.7	5	Opaques	Magnetite; anhedral to subhedral

Texture: The inequigranular rock is fine- to medium-grained (0.2-2.0 mm) and has a polygonal to interlobate and granophyric texture. Intergrown plagioclase and quartz forms vermicular grains/blebs. Large phenocrysts of plagioclase and amphibole are set in a equigranular groundmass of plagioclase, amphibole and quartz. Plagioclase is highly altered/weathered to sericite and hornblende to chlorite. In places randomly oriented needles comprise labradorite.

Rock type: Tonalite

MI06020B – Ambereny

Grain size(mm)	Modal %	Mineral	Description
<0.1	55	Plagioclase	Anhedral to subhedral; lath-like habit
<0.1	15	Opaques	Anhedral to thin streaks, needle-like
<0.1	20	Quartz	Anhedral
<0.1	10	Chlorite,Sericite	Anhedral to subhedral; core of zoned plagioclase

Texture: This microcrystalline rock is inequigranular, very fine-grained (<0.1 mm) and has a spiky texture. Acicular needles of plagioclase and opaque minerals are set in a groundmass of plagioclase, chlorite, sericite and quartz. Chlorite is probably derived from clinopyroxene.

Rock type: Microgabbro

MI06020C – Ambereny

Grain size(mm)	Modal %	Mineral	Description
0.4-1.5	45	Plagioclase	Subhedral to anhedral; albite twins; lath-like; very weathered
0.1-0.4	35	Quartz	Subhedral to anhedral; rare triple points; undulose extinction
0.1-0.5	7	Chlorite	Subhedral to anhedral; lath-like or clusters
<0.1-0.4	5	Opaques	Anhedral to subhedral
0.1-0.4	<5	K-feldspar	Anhedral; very weathered (saussuritized); altered
0.1-0.3	3	Biotite	Subhedral to anhedral; lath-like

Texture: The inequigranular rock is fine- to medium-grained (0.2-1.5 mm) and has an interlobate to amoeboid and granophyric (radial) texture. Chlorite is probably derived from clinopyroxene and the biotite from hornblende. Biotite is closely associated with the opaque minerals.

Rock type: Tonalite

MI06021 – Ambereny

Grain size(mm)	Modal %	Mineral	Description
0.2-1.5	50	Plagioclase	An_{65} = labradorite; euhedral to subhedral; albite & carlsbad twins; lath-shaped
<0.1-0.8	30	Clinopyroxene	Augite; anhedral; colourless to pale brown
<0.1	10	Opaques	Anhedral
<0.1-0.2	8	Biotite	Subhedral to anhedral; pleochroic brown
0.1-0.2	<2	Quartz	Anhedral; strain shadows

Texture: This fine- to medium-grained (0.2-1.5 mm) rock is inequigranular and has an polygonal to interlobate and porphyritic texture. Acicular needles of plagioclase are set in a equigranular and microcrystalline groundmass of pyroxene, plagioclase and biotite. Larger lath-shaped labradorite phenocrysts form a spiky texture.

Rock type: Microgabbro

MI06022 – Cretaceous dyke

Grain size(mm)	Modal %	Mineral	Description
0.1-1.5	45	Plagioclase	An_{65} = labradorite; euhedral to subhedral; albite & carlsbad twins; lath-shaped
0.2-0.4	38	Clinopyroxene	Augite; subhedral to anhedral; pale brown
<0.1-0.4	10	Opaques	Anhedral
0.1-0.2	<5	Quartz	Anhedral
<0.1	2	Chlorite	Subhedral; clusters/aggregates

Texture: This fine- to medium-grained (0.3-1.5 mm) rock is inequigranular and has an polygonal to interlobate and porphyritic texture. Acicular needles of plagioclase are set in a equigranular and microcrystalline groundmass of pyroxene, plagioclase and chlorite. Larger lath-shaped labradorite phenocrysts form a spiky texture. Chlorite is replacing augite.

Rock type: Dolerite

MI06034 – Cretaceous dyke

Grain size(mm)	Modal %	Mineral	Description
<.01-0.4	55	Feldspar	Alkali feldspar and plagioclase; subhedral
<0.1-4.0	20	Quartz	Subhedral to anhedral
0.1-2.0	5	Biotite	Subhedral; pleochroic brown
<0.1-0.4	20	Opaques	Magnetite?; euhedral to anhedral

Texture: The inequigranular rock is very fine-grained (<0.1 mm). Larger phenocrysts of quartz, opaques and biotite (porphyritic texture) is set in a very fine-grained (microcrystalline) matrix of feldspar, quartz and possibly volcanic glass. Microcrystalline feldspars are aligned parallel to flow banding and also arranged parallel to the phenocryst edges.

Rock type: Rhyolite